SUMMARY OF RESEARCH ON

CONCRETE-FILLED STRUCTURAL STEEL TUBE COLUMN SYSTEM CARRIED OUT UNDER

THE US-JAPAN COOPERATIVE RESEARCH PROGRAM ON

COMPOSITE AND HYBRID STRUCTURES

by

Isao Nishiyama, Shosuke Morino, Kenji Sakino, Hiroyuki Nakahara, Toshiaki Fujimoto, Akiyoshi Mukai,

Eiichi Inai, Makoto Kai, Hiroyoshi Tokinoya, Toshiyuki Fukumoto, Koji Mori, Kenzo Yoshioka,

Osamu Mori, Kenji Yonezawa, Mizuaki Uchikoshi and Yukio Hayashi

FORWARD

From the fiscal year of 1993, a five-year research project on concrete-filled structural steel tube (CFT) column system was carried out as part of the fifth phase of the US-Japan Cooperative Earthquake Research Program on Composite and Hybrid Structures.   At the beginning of the project, a number of topics related to research issues were raised and prioritized by cooperation work of the researchers and practitioners involved in the project.   In those days, a structural system having concrete-filled structural steel tube used for columns had just come to be used in real buildings in Japan.   Thus, the CFT column system was selectively studied on the Japanese side, since expansion of the application scope beyond previous work would be very useful for practitioners.   Namely, the studies were performed in case of larger width (diameter)-to-thickness ratio of steel tubes and higher concrete / structural steel strengths. This paper presents a summary of the research completed on the Japanese side. I believe that the results are of great use and importance for practitioners.

Other research projects on 1) New materials, elements and systems, 2) Reinforced concrete (RC) column / steel beam system, and 3) RC / SRC (steel reinforced concrete) wall system were also carried out in parallel to the research project on CFT column system under the same phase of the US-Japan Cooperative Research Program. Summaries on those research projects will be presented in different opportunity. Lists of the individual technical papers are included in Appendix for the advanced use by the researchers and practitioners.

January 2002
Hiroyuki YAMANOUCHI
Chief Executive
Building Research Institute

TABLES OF CONTENTS

SUMMARY OF RESEARCH ON

CONCRETE-FILLED STRUCTURAL STEEL TUBE COLUMN SYSTEM CARRIED OUT UNDER

THE US-JAPAN COOPERATIVE RESEARCH PROGRAM ON

COMPOSITE AND HYBRID STRUCTURES

Editors: Isao NISHIYAMA *1 and Shosuke MORINO *2

ABSTRACT

The US-Japan Cooperative Earthquake Research Program began in 1979 following the recommendations as outlined in the final report of the US-Japan Planning Group for the program ["Recommendations for a US-Japan Cooperative Research Program utilizing Large-Scale Testing Facilities", Report No. UCB/EERC 79-26, September 1979]. First four phases of the program have been implemented on 1) Reinforce Concrete, 2) Structural Steel, 3) Masonry, and 4) Precast / Prestressed Concrete. Phase 5 of the US-Japan Cooperative Research Program on Composite and Hybrid Structures was carried out from the fiscal year of 1993 as a five-year research program. In this phase of research program, the following four research topics were executed: 1) New materials, elements and systems, 2) Concrete-filled structural steel tube column system, 3) Reinforced concrete column and structural steel beam system, and 4) Reinforced concrete and steel reinforced concrete wall system.

In this paper, the technical research results conducted in the Japanese side related to the research topic of the concrete-filled structural steel system is overviewed and summarized. It includes experimental results (columns, beam-columns and beam-to-column assemblies), proposed constitutive model for steel and concrete considering synergistic action, analytical results, and design implication study. Draft of the manuscripts was shared among the researchers directly involved in the research project, and it was summarized in this research paper by the editors.

As for the research results on the other three topics, summary paper has not yet been completed. The available technical papers, which cover a part of the research topics, are listed in the appendix for the reference to the readers.

_____

*1 Advanced Research Engineer, Department of Construction Engineering, Building Research Institute

*2 Professor, Dept. of Architecture, Faculty of Engineering, Mie University

LIST OF TABLES

LIST OF FIGURES

CHAPTER 1: INTRODUCTION AND OVERVIEW OF RESEARCH

1.1 Introduction

It is widely recognized that innovative uses of two or more different materials in a structure generally lead to a more efficient system for resisting seismic force. Use of such structural system has increased in the US and in Japan during the past ten years. Despite the amount of research and development work, especially by Japanese construction companies, not enough was known regarding their seismic behavior or performance. Design procedures and codes for their usage in typical design offices were non-existent. Therefore, a five-year research program on such structural systems was initiated as the fifth phase of the US-Japan Cooperative Research Program, which originally started in 1979 following the recommendations outlined in the final report of the US-Japan Planning Group for the program [1.1]. Because of the diverse and broad scope of the subject area, it was recommended that the research program in the fifth phase should be organized into the following four groups: 1) New materials, elements and systems, 2) Concrete-filled structural steel tube (CFT) column system, 3) Reinforced concrete (RC) column / steel beam system, and 4) RC / SRC (steel reinforced concrete) wall system.

The project aimed at developing design guidelines (for a unified code development) through cooperative studies to determine the relationship among full-scale tests, small-scale tests, component tests, and related analytical and design implication studies. Because the CFT column system was becoming popular in Japan at the beginning of the project, research topics, thought to be useful in expanding the practical application scope, were selectively studied. These include research on larger width (diameter)-to-thickness ratio of structural steel tube, higher strength concrete than normal concrete and higher strength steel than normal structural steel. In this paper, summary of the research done in Japan on CFT column system is presented.

Sharing of the manuscript of each chapter is as follows.

Chapter 1: I. Nishiyama*1, S. Morino*2

Chapter 2: K. Sakino*3, H. Nakahara*4

Chapter 3: T. Fujimoto*5, A. Mukai*1, I. Nishiyama, K. Sakino

Chapter 4: E. Inai*6, A. Mukai, M. Kai*7, H. Tokinoya*8, T. Fukumoto*9, K. Mori*10

Chapter 5: K. Yoshioka*11, T. Fujimoto, M. Kai, K. Mori, O. Mori*12, E. Inai, A. Mukai, K. Yonezawa*8, T. Fukumoto

Chapter 6: K. Sakino, E. Inai

Chapter 7: M. Uchikoshi*13, Y. Hayashi*14, S. Morino

*1: Advanced Research Engineer, Building Research Institute

*2: Professor, Department of Architecture, Faculty of Engineering, Mie University

*3: Professor, Faculty of Human-Environmental Studies, Kyusyu University

*4: Lecturer, Department of Architecture, Faculty of Engineering, Kagoshima University

*5: Research Engineer, Research Center, ANDO Corporation

*6: Associate Professor, Faculty of Engineering, Yamaguchi University

*7: Research Engineer, Technical Research Institute, Matsumura Corporation

*8: Research Engineer, Technical Research Institute, Obayashi Corporation

*9: Senior Research Engineer, Technical Research Institute, Kajima Corporation

*10: Research Engineer, Technical Research Institute, Asanuma Corporation

*11: Professor, Department of Architectural Engineering, Dai-Ichi University

*12: Research Engineer, Technical Research Institute, Toyo Corporation

*13: Senior Engineer, Structural Engineering Department, KUME SEKKEI Co. Ltd.

*14: General Manager, Structural Engineering Department, Kajima Corporation

Members of the Technical Sub-Committee on CFT column system (refer to the overall research organization in section 1.5) are listed below. Affiliations are those at the time of the project.

Chairman: S. Morino (Mie University)

Members: K. Sakino (Kyusyu University)

K. Yoshioka (dispatched from Building Contractors Society)

T. Fukumoto (dispatched from Building Contractors Society)

A. Tomita (dispatched from Building Contractors Society)

E. Inai (dispatched from Building Contractors Society)

T. Fujimoto (dispatched from Building Contractors Society)

S. Gokan (dispatched from Japan Structural Consultants Association)

Y. Hayashi (dispatched from Japan Structural Consultants Association)

M. Uchikoshi (dispatched from Japan Structural Consultants Association)

F. Ohsugi (dispatched from Japan Structural Consultants Association)

T. Nakamura (dispatched from Japan Structural Consultants Association)

H. Sawada (dispatched from Japan Structural Consultants Association)

I. Nishiyama (Building Research Institute)

A. Mukai (Building Research Institute)

1.2 Definition of Composite and Hybrid Structures and Concrete-Filled Structural Steel Tube Column System

Recently in the field of building construction in Japan, it has become the goal to develop new types of structural systems combining existing and / or new materials in better coordination to add structural and architectural advantages, which were difficult to be attained by traditional structural systems. These types of new structural systems are called "Composite and Hybrid Structures (CHS)". Among possible variations of CHS, the most frequently investigated and practically feasible one is the combination of RC and structural steel.

The advantages of CHS include attaining better "structural functions" and "productability and constructability", which are very difficult to be achieved by the existing structural systems. For example, largely flexible space

from longer span beams, reduction of story and / or building height because of shallower floor systems, and improvement of habitability by an increase in lateral stiffness are some advantages in structural functions. The advantages in productability and constructability include the freedom of structural planning, and the shortening of construction periods and quality improvements due to the shift to prefabrication.

From the viewpoint of structural technology, the control of failure modes of structures in seismic design and the rational uses of structural members in a structure are easily achieved with CHS systems. In short, the structural system can be made clearer in the mechanical viewpoint.

The CHS system can be classified into three categories according to their geometry as shown schematically in Figure 1.1. These three categories correspond to 1-D, 2-D and 3-D CHS systems. The first category is the composite and hybrid member. Single members such as beams and columns are composed of different materials. CFT, fiber reinforced concrete and SRC members are typical examples of this category. The second category is the composite and hybrid frame. Even if the individual members such as the beam or column are not composite members, the combination of different types of single members makes a composite and hybrid structure. The RC column and steel beam system is an example in this category. The third category is a structure made of different materials and members, combined three-dimensionally. A typical example of this category is the RC core wall with an exterior steel frame system, or a RC frame in the lower stories with a steel frame in the upper stories. The CFT column system presented in this paper is in the category of a 1-D CHS system.

1.3 Status of CFT Column System in Japan

CFT has been used for columns carrying large axial force since it was first used in Great Britain for the construction of road bridges in the late 1870's. In Japan, the first design recommendations for CFT column were established in 1967 by the Architectural Institute of Japan (AIJ). Then it was revised in 1981 [1.2]. In these recommendations, CFT columns were considered a kind of SRC column because of their similarity in usage and mechanical characteristics. The recommendations made it possible to utilize CFT columns in practice. However, the limit of the width (diameter)-to-thickness ratio for structural steel tubes was not relaxed in comparison with the ratio for bare structural steel tube. Also, the filled concrete strength was not increased in the estimate of actual strength even though it was confined by a steel tube and was under tri-axial stress conditions. Moreover, the CFT column without concrete cover could not be used practically without a special approval. The Building Standard Law in Japan [1.3] said that covering concrete for a CFT column was only an assumption to be considered to be a SRC column. Thus, the diffusion of CFT column into real constructions was quite slow. This situation has not changed even after the design method for CFT was included in the current AIJ-SRC standards revised in 1987 [1.4], in which both the width (diameter)-to-thickness ratio and the strength of the confined concrete were improved reflecting the real behavior verified by further studies.

In the "New-Urban Housing Project" organized in 1985 by the Ministry of Construction, very broad research and development (R&D) were conducted. In particular, quantitative estimation of the strength and ductility of CFT beam-columns brought by the synergistic action of structural steel tube and filled concrete was studied and formulated into design formulas. The mixture of filling concrete and the casting methods were also investigated. The fire resistance of CFT columns was also extensively examined to study the possibility of the omission of

covering concrete considering thermal capacity of filled concrete. However, the research results were monopolized only by the private companies involved in this R&D.

Based on this current status of CFT column systems, standardized design method usable for ordinary practitioners is strongly required. This covers not only the general results by the New-Urban Housing Project, but also much larger width (diameter)-to-thickness ratios and material strengths. Figure 1.2 shows a typical CFT column system and concrete filling.

1.4 Prioritized Research Topics Recommended in US-Japan Joint Workshop

Prior to the initiation of the fifth phase of the research, a Joint Planning Workshop [1.5] was held to identify research issues. A number of topics related to research issues of CFT column system were raised and discussed, some of which were interrelated and others were ultimately divided into more specific issues. As a consequence of the discussions, a number of prioritized (high, medium, or low) research topics were recommended as follows.

(1) High Priority Research Topics

    The topics are summarized in Table 1.1.

1) Beam-Columns

    Determination of the effect of confinement vs. composite action.

    Determination of methods of evaluating axial, shear, and flexural stiffness, ductility and resistance under monotonic and cyclic loading.

    Determination of bond stress and shear transfer mechanisms between the structural steel tube and the concrete.

2) Columns

    Evaluation of creep and shrinkage effects on CFT columns of high-rise buildings.

3) Connections

    Determination of force and moment transfer mechanisms and design models for FR, PR and pinned connections for connections between braces, beams, and columns.

    Determination of the effect of panel zone deformation on the seismic performance of CFT columns.

4) Frames

    Analytical studies combining the above connection and member behavior to evaluate the seismic performance of moment resisting frames and braced frames with CFT columns. This work should include hysteretic behavior, damping, and dynamic characteristics of the structural system. It should evaluate factors such as weak column - strong beam behavior and strong column - weak beam behavior, and be directed toward determination of Ds and Rw factors and the seismic design forces.

5) Very High Strength Concrete

    This is a general research topic related to all composite or hybrid structures, but it also has impact on CFT columns.

6) Literature Review

    Literature review related to CFT construction with a complete list of publications, brief abstracts of individual papers and reports to facilitate the exchange of information between the US and Japan.

(2) Medium Priority Research Topics

These topics are summarized in Table 1.2.

1) Columns

Determination of the buckling behavior of CFT columns.

2) Nontraditional Connection Design

Development of nontraditional connections for CFT construction through the research for innovation initiative.

3) Construction Practice

Development of rules and guidelines for casting of concrete in CFT structures.

Establish the differences between as-built vs. design of practical CFT structures.

Determination of the effect of construction loads on CFT structures.

4) Frames

Evaluation of the relative merits of designing for composite action only, for confinement only, and for combined composite action and confinement.

(3) Low Priority Research Topics

1) Repair and Retrofit

Establish methods and guidelines for repairing or retrofitting CFT composite and structures.

1.5 Japanese Research Program: Items Plan and Organization

The overall research operation system is shown in Figure 1.3. Domestic cooperative research by the Building Research Institute, the Building Contractors Society, the Japan Structural Consultants Association, the Kozai Club, and the Building Center of Japan was organized with research collaboration from universities. The Technical Coordinating Committee (chaired by Dr. H. Aoyama : Professor Emeritus of Univ. of Tokyo) played the role of the decision of the domestic research and the research adjustment with the US side. In the Technical Sub-committee on CFT column systems (chaired by Dr. S. Morino: Professor of Mie Univ.), the detailed research plan and its execution were carried out.

As mentioned in Section 1.3, the previous research in Japan was biased to the experimental research on beam-columns and the strength and ductility were empirically estimated. Therefore, much basic study on the section behavior of CFT columns required further investigation for applicability. The usable material strength in the field of building construction was increasing both in structural steel and concrete. Therefore, the research result applicable to them was strongly desired. The confinement effect of the structural steel tube for filled concrete was thought to be extraordinary large. Hence, the usage of thin structural steel tubes was the trend in CFT column system. Therefore, the possibility of utilization of thin structural steel tube was an important issue. Finally, the dissemination of research result to the practitioners should be accelerated by giving design examples and rational usage of this system. Considering the above, the following four items were stressed in determining the research plan of the Japanese side.

1) More fundamental experimental / analytical studies
2) Larger material strength (S_u = 400~780MPa, Fc = 20~90MPa)

3) More slender steel tube section (B/t = 19~74, D/t = 17~152; B = width of square steel tube, D = diameter of steel tube, t = thickness of steel tube)

4) Trial design for practitioners

1.5.1 Experimental / Analytical Investigations

Four series of tests were planned as shown in Figure 1.4: a) centrally loaded stub columns, b) eccentrically loaded stub columns, c) beam-columns, and d) beam-to-column connections. The objectives of these testing were to clarify the synergistic interaction between structural steel tube and filled concrete and the stress transfer mechanism, and to derive methods to evaluate stiffness, strength and ductility of CFT column system.

Study parameters were as follows: 1) tube shapes (square and circular); 2) nominal tensile strength of steel tube (400, 590 and 780MPa); 3) width (diameter)-to-thickness ratio B/t (D/t) of steel tube; 4) design standard strength of concrete (20, 40, 80 and 90 MPa); 5) axial load ratio n = N/No (N = axial load, and No = squash load of CFT section); and vi) connection details. The width (diameter)-to-thickness ratio was classified into three ranks (FA, FC and FD) from the viewpoint of energy dissipation capacity of plastic hinges forming in hollow structural steel tubes. In determining the range of parameters, the emphasis was placed on obtaining a wide range of test data usable to establish a design method for CFT column systems. Structural steel tubes were cold-formed, and the value of B/t or D/t was controlled by changing the size of the tube.

Actual mechanical properties of steel and concrete are different from the corresponding nominal and design values. In this paper, actual or nominal/design values are used case by case in each section.

(1) Centrally Loaded Stub Columns

The main objective of the centrally loaded stub column tests was to clarify the confining effect of the structural steel tube on the concrete strength and the restraining effect of filled concrete on local buckling of the steel tube, and to establish the constitutive laws for steel and concrete which can be used for the analysis of CFT members. Table 1.3 summarizes the test program of centrally loaded stub columns.

The constitutive laws for concrete and steel in a CFT column were established from the test results of concrete cylinders, CFT stub columns, and hollow structural steel tube stub columns. The following phenomena were taken into account: 1) increase in concrete strength due to confinement, 2) scale effect on concrete strength, 3) strain softening in concrete, 4) increase in tension strength and decrease in compression strength of steel tube due to ring tension stress, 5) local buckling of steel tube, 6) effect of concrete restraining the progress of local buckling deformation, and 7) strain hardening of steel.

(2) Eccentrically Loaded Stub Columns

The main objective of the eccentrically loaded stub column tests was 1) to check the accuracy of the moment vs. curvature relation numerically calculated on the basis of the proposed constitutive laws for steel and concrete, and 2) to derive the formula to evaluate the ultimate strength of the cross section subjected to combined axial force and bending moment. Test program of eccentrically loaded stub columns is summarized in Table 1.3.

(3) Tests of CFT Beam-Columns

Tests of CFT beam-columns were conducted with the main objectives of 1) checking the accuracy of the method of analysis based on the proposed constitutive laws for steel and concrete, 2) deriving formulas to evaluate the rotation capacity, and 3) developing a model for the restoring force characteristics used in the dynamic response analysis of CFT column systems. In this test series, some of the beam-columns were loaded under varying axial force so as to increase the verification accuracy of the proposed analytical methods, which were rarely tested previously. Table 1.4 summarizes the test program of CFT beam-columns.

(4) Tests of Beam-to-Column Connections

In order to clarify the performance of beam and column subassemblages in which the connection panel fails in shear, and to develop the design formulas for the connection, several connection tests were carried out. In the test, a constant vertical load on the column and cyclic shear force at the beam ends was applied. Table 1.5 summarizes the test program of beam-to-column connections.

1.5.2 Trial Design

Structural designs of 10, 24 and 40-story CFT moment frame buildings were carried out on the theme structure which was 38.4m in X-direction (6 spans) and 35.2m in Y-direction (3 spans) shown in Figure 1.5. In these structural design, allowable stress design, ultimate strength design and dynamic analysis of designed frame were performed. The buildings with the same floor plans were also designed as pure steel frames. The total amount of structural steel is an index for estimating the economy of buildings. The amount of structural steel used for CFT buildings was compared with that used for pure steel buildings. In this comparison, CFT system showed advantages over pure steel especially for higher buildings. The detailed discussion will be made in Chapter 7.

CHAPTER 2: BEHAVIOR OF CENTRALLY LOADED SHORT COLUMNS

This chapter presents the ultimate loads and load vs. deformation relationships of centrally loaded CFT (concrete-filled structural steel tube) short columns.

2.1 Experimental Investigation

2.1.1 Specimens, Parameters and Test Procedure

A total of 90 specimens was fabricated and tested in the first phase of experimental investigations on centrally loaded hollow and CFT short columns. The objectives of these tests were to investigate confining effect of steel tube on concrete strength and restraining effect of filled concrete on local buckling of steel tube, and to derive methods to evaluate ultimate loads and load vs. deformation relationships. In order to confirm the observations obtained from the first phase tests, a total of 24 specimens with square section was tested in the second phase of experiments.

Study parameters for the first phase tests are as follows: 1) tube shapes (circular and square), 2) nominal tube tensile strength (400, 590, 780MPa), 3) tube diameter (width)-to-thickness ratio (rank FA, FC, FD) and 4) design concrete strength (20, 40, 80MPa). The diameter (width)-to-thickness ratios D/t (or B/t) were classified into three ranks (FA, FC, FD) from a viewpoint of energy dissipation capacity of plastic hinges formed in hollow steel tubes. Hollow steel tube with rank FA is supposed to possess the ductility factor of 4 under pure compression, and that of rank FC the ductility factor of 1, which means that the tube locally buckles at the yield stress. Hollow steel tube with rank FD buckles elastically. In determining the range of parameters, the emphasis was placed on obtaining a wide range of test data usable to establish a generally applicable design method of CFT column systems. Steel tubes were cold-formed with three different nominal wall thickness: 3.0, 4.5 and 6.0mm. The value of D/t ratio was controlled by the diameter of circular tube (122~450mm). The B/t ratio was controlled by the width of square tube (120~324mm). Both ends of steel tube were welded to the end plates with the thickness of 20mm for centrally loaded columns. Ratio of the clear height of specimens to D (or B) was 3.0. The details of a typical specimen are shown in Figure 2.1. Material properties of steel tubes were obtained from tensile tests of coupons taken from each steel plate before tube-forming. Yield ratio of the steel plates, which is defined as the ratio of the yield stress to the tensile strength, strongly depends on the steel grades: 0.64~0.69 for grade 400MPa steel; 0.9 for 590MPa; and 0.95 for 780MPa. Specimens with the same concrete strength were filled from one batch of a ready mixed concrete plant, and the tests were conducted about three months after concrete casting. Properties of all specimens are summarized in Table 2.1, 2.2(a) and 2.2(b).

The test setup shown in Figure 2.1 was used to apply the axial load. Averaged longitudinal strains were obtained from axial shortenings between two end plates measured by four LVDT's, and strains in steel tubes were measured by two-element rosette strain gauges mounted on outer steel tube surface.

2.1.2 Test Results

(1) Hollow Steel Tube Columns

The compressive stress $_s S_{su}$ at the maximum axial load of hollow steel tube columns is given in Table 2.1,

which includes the compressive yield stress $\boldsymbol{s}_{scy}$ defined as the stress corresponding to an offset strain of 0.2%, as well as the tensile yield stress $\boldsymbol{s}_{sy}$ obtained from tensile coupon tests. The compressive yield stress is available for all the circular columns except for specimen CC4-D-0. In many cases of square columns with B/t ratio of rank FC or FD, however, compressive yield stress was not obtained from tests, because an abrupt drop in axial load due to the local buckling occurred before yielding.

(2) Concrete Filled Steel Tube Columns

The maximum axial loads N_u of circular and square CFT columns are summarized in Table 2.2(a) and 2.2(b), respectively. The non-dimensional maximum axial loads in the form of N_u / N_o ($N_{\exp}$ is used instead of N_u in Tables 2.2(a) and 2.2(b)) are also given in Tables, where N_o is the nominal squash load given by Equation 2.1.

$$N_o = N_{so} + N_{co} = A_s \cdot \boldsymbol{s}_{sy} + A_c \cdot \boldsymbol{s}_{cp} = A_s \cdot \boldsymbol{s}_{sy} + A_c \cdot \boldsymbol{g}_U \cdot f_c' \qquad .....(2.1)$$

where A_s and A_c are cross sectional area of steel tube and filled concrete, respectively, and $\boldsymbol{s}_{cp}$ is the compressive strength of filled concrete which is estimated by multiplying the compressive strength of $10\phi \times 20$cm cylinder f_c' by $\boldsymbol{g}_U$. $\boldsymbol{g}_U$ is a reduction factor introduced to take a scale effect into consideration, and it will be discussed in detail later. In the case of circular CFT columns, the value of the compressive yield stress $\boldsymbol{s}_{scy}$ given in Table 2.1 was used to evaluate N_o in Equation 2.1, instead of $\boldsymbol{s}_{sy}$. The value of $\boldsymbol{s}_{scy}$ of specimen CC4-D, for which $\boldsymbol{s}_{scy}$ is not available as mentioned before, was assumed to be equal to that of specimen CC4-C fabricated by using the same steel plate as CC4-D. In the case of square CFT columns, the tensile yield stress given in Table 2.1 is used as the yield stress because of the following two reasons: 1) the compressive yield stress is not available for many CFT columns with B/t ratio of rank FC or FD, and 2) an effect of cold-forming during fabrication of steel tubes is expected to be relatively small in square steel tubes.

As shown in Table 2.2(a), the maximum axial load N_u is greater than the nominal squash load N_o in most of the circular CFT columns. A main reason for this augmentation of axial load capacity is attributed to a confinement effect of steel tube on the concrete strength. On the other hand, the maximum load is less than the nominal squash load in the square CFT columns with B/t ratio of rank FD as shown in Table 2.2(b). A main reason for this reduction of axial load capacity is attributed to the local buckling of steel tube. Methods to estimate the ultimate axial load will be discussed in the following section after discussing the scale effect on the concrete strength.

(3) Scale Effect

One of the most important parameters in the experimental program is the D/t (or B/t) ratio of the steel tube as mentioned previously. Steel tubes were cold-formed from the steel plate with the same thickness for each grade of steel. The values of D/t and B/t ratio were controlled by the outside diameter of circular steel tube and the width of square steel tube. This resulted in the great differences in diameter or width of specimens as shown in Figure 2.2. As expected from Figure 2.2, it seemed to be necessary to take a scale effect on the compressive strength of concrete into consideration. Based on the careful investigations, we have reached a conclusion that

the concrete compressive cylinder strength should be modified according to the test results obtained by Blanks et al. [2.1], which is shown in Figure 2.3. Symbols "A" to "D" in Figure 2.3 denote the diameter (or width) and sectional shape (circular or square) of CFT stub column specimens shown by corresponding symbols of "A" to "D" in Figure 2.2. Figure 2.3 shows that the concrete compressive strength of the largest specimen shown by the symbol "A" should be considered to be about 85% of that of the smallest specimen whose size is almost the same as concrete cylinder with 4 inches in diameter and 8 inches in height. Although the conclusion on the scale effect shown in Figure 2.3 was limited within circular columns, we applied Blanks' result to the square CFT columns by replacing them into the equivalent circular columns.

2.2 Analytical Investigation

In the next phase of the study, analytical models to estimate the ultimate strength of CFT short columns have been developed. Based on these models, stress vs. strain relations for filled concrete and steel tube have been proposed independently, so that the proposed stress vs. strain relations can be applicable to a moment vs. curvature analysis of CFT columns.

2.2.1 Ultimate Strength of Centrally Loaded Short Columns
(1) Circular Columns

In the initial stages of loading of the circular CFT columns subjected to concentric axial load, Poisson's ratio for the concrete is lower than that for steel. Therefore, a separation between steel tube and concrete core takes place provided that the adhesive bond between the steel and concrete does not work. As the load increases furthermore and the longitudinal strain reaches to a certain critical strain, the lateral deformations of the concrete catch up with those of the steel tube. When the load increases furthermore, the hoop stress in the steel tube becomes in tension, and the concrete core is subjected to triaxial compression. This phenomenon results in the increase of axial compressive load of concrete. The equation for axial compressive load capacity is obtained by the following procedure:

First, the strength formula for concrete is assumed by Equation 2.2.

$$\sigma_{ccB} = \gamma_U \, f_c' \, k \, \sigma_r \qquad\qquad .....(2.2)$$

where, σ_{ccB} = confined concrete strength,

γ_U = strength reduction factor for concrete = $1.67 D_c^{-0.112}$,

D_c = diameter of concrete core (in mm),

f_c' = concrete cylinder strength,

k = confinement coefficient = 4.1 [2.2], and

σ_r = confining stress (lateral pressure).

The hoop stress σ_{sq} and axial stress σ_{sz} of the steel tube at ultimate load are assumed by Equation 2.3.

$$\sigma_{sq} = \alpha_u \cdot \sigma_{sy}, \; \sigma_{sz} = \beta_{uc} \cdot \sigma_{sy} \qquad\qquad .....(2.3)$$

where, a_u, b_{uc} = coefficients determined based on experimental results, assumed to be independent of material properties and dimensions of columns.

Referring to Figure 2.4, the relation between the hoop stress $\sigma_{s\theta}$ and the lateral pressure σ_r is given by Equation 2.4.

$$\sigma_r = \frac{-2t}{D-2t} \cdot \sigma_{s\theta} \qquad .....(2.4)$$

In the course of the evaluation of confining effect on concrete strength, it is assumed that the difference between the ultimate strength N_u and the nominal squash load N_o is provided by the confining effect on concrete strength, and this gain depends upon the tube strength N_{so}.

$$N_u - N_o = \lambda \cdot N_{so}; \qquad \frac{N_u}{N_o} = 1.0 + \lambda \frac{N_{so}}{N_o} \qquad .....(2.5)$$

where, N_{so} = axial yield strength of steel tube (= $A_s \cdot \sigma_{sy}$), and
λ = augmentation factor.

From Equations 2.2 and 2.3, N_u is given as follow.

$$N_u = A_s \cdot \sigma_{sz} + A_c \cdot \sigma_{ccB} \qquad .....(2.6)$$

Substituting Equations 2.2, 2.3 and 2.4 into Equation 2.6, and using Equation 2.1 leads to Equation 2.7.

$$N_u - N_o = A_s \cdot b_{uc} \cdot \sigma_{sy} + A_c \left(\gamma_U \cdot f_c' + k \cdot \sigma_r \right) - A_s \cdot \sigma_{sy} - A_c \cdot \gamma_U \cdot f_c'$$
$$= A_s \cdot \sigma_{sy} (b_{uc} - 1) - A_c \cdot k \cdot \frac{2t}{D-2t} \cdot \sigma_{s\theta}$$
$$= A_s \cdot \sigma_{sy} \left(b_{uc} - 1 - \frac{A_c}{A_s} \cdot k \cdot \frac{2t}{D-2t} \cdot a_u \right) \qquad .....(2.7)$$

Comparing Equation 2.7 with Equation 2.5, the factor λ is given by Equation 2.8.

$$\lambda = \frac{N_u - N_o}{N_{so}} = b_{uc} - 1 - \frac{(D-2t)}{2(D-t)} \cdot k \cdot a_u \qquad .....(2.8)$$

Equation 2.8 shows that the value of λ becomes constant if the values of coefficients k, a_u and b_{uc} are constant. The value of λ defines the normalized axial compressive load capacity N_u / N_o as a linear function of the parameter N_{so} / N_o. The value of λ was determined by a regression analysis based on

- 11 -

available experimental data as described below. The relation between the coefficients a_u and b_{uc} is obtained from the assumption that steel stresses at the ultimate stage given by Equation 2.3 satisfy the von Mises' yield criterion given by Equation 2.9.

$$s_{sz}^2 - s_{sz} \cdot s_{sq} + s_{sq}^2 = s_{sy}^2 \qquad\qquad\qquad .....(2.9)$$

where, s_{sz} = axial stress of steel tube under yield condition, and

s_{sq} = hoop stress of steel tube under yield condition, and thus

$$a_u^2 - a_u \cdot b_{uc} + b_{uc}^2 = 1 \qquad\qquad\qquad .....(2.10)$$

Once the value of l is fixed, the values of a_u and b_{uc} are determined by solving Equations 2.8 and 2.10, where $k = 4.1$ as described before, and D/t = 50 as a representative to avoid dependency of the values of a_u and b_{uc} on D/t ratio.

Figure 2.5 shows the relationships between experimental axial load capacity N_u of CFT columns and yield load of steel tube N_{so}, both divided by nominal squash load N_o. The open circles show the existing experimental results obtained elsewhere in Japan. The design formula recommended in the "Recommendations for Design and Construction of Concrete Filled Steel Tubular Structures" [2.3] was proposed based on the open circled data, where the slope of the dotted line l is defined as 0.27 in Equation 2.5. The solid circles show the results presented in this chapter (US-Japan data). The slope of the solid line based on the US-Japan data is slightly lower than that of dotted line. However, it is concluded that the design formula already recommended is not necessary to be revised. The value of l equal to 0.27 gives the values to the coefficients a_u and b_{uc} as -0.19 and 0.89 respectively, from Equations 2.8 and 2.10.

Figure 2.6 shows the comparisons between experimental results on axial load capacity of the circular CFT stub columns and calculated capacities by Equation 2.11 which is obtained from the above procedure.

$$N_u = N_o + l \cdot N_{so} = N_o + 0.27 N_{so} \qquad\qquad\qquad .....(2.11)$$

(2) Square Columns

In the case of square columns, it is necessary to take into consideration a capacity reduction due to the local buckling of steel tube of the column with large B/t ratio rather than the confinement effect of the steel tube. Figure 2.7 shows the relationships between the axial load capacity factor of the steel tube S and the normalized width-to-thickness ratio $(B/t)\sqrt{s_{sy}/E_s}$, where S denotes the ultimate compressive strength divided by the yield axial strength of steel tube. The axial load capacity factor of the hollow steel tube stub columns and the steel tube in CFT stub columns shown in Figure 2.7 are given by Equations 2.12, 2.13 and 2.14, where N_{su} is the axial compression strength of square steel tube portion.

$$N_{su} = A_s \cdot s_{scr}, \quad s_{scr} = \min\left(s_{sy}, S \cdot s_{sy}\right) \qquad\qquad\qquad .....(2.12)$$

where, $\dfrac{1}{S} = 0.698 + 0.128\left(\dfrac{B}{t}\right)^2 \cdot \dfrac{\boldsymbol{s}_{sy}}{E_s}$ for hollow steel tube stub columns   .....(2.13)

$$\dfrac{1}{S} = 0.698 + 0.128\left(\dfrac{B}{t}\right)^2 \cdot \dfrac{\boldsymbol{s}_{sy}}{E_s} \times \dfrac{4.00}{6.97}$$ for steel tube in CFT stub columns   .....(2.14)

Equation 2.13 was obtained by a regression analysis using the experimental results of the hollow steel tube stub columns, and modified into Equation 2.14 by multiplying 4.00/6.97. This modification is based on an elastic buckling theory by considering the difference in boundary conditions (or buckling modes) between the hollow steel tube (simply-supported plate) and steel tube in CFT columns (clamped plate) shown in Figure 2.7.

The axial load capacity of CFT short columns can be estimated by Equation 2.15.

$$N_u = N_{su} + N_{co} = A_s \cdot \boldsymbol{s}_{scr} + A_c \cdot \boldsymbol{g}_U \cdot f_c^{'}$$ .....(2.15)

Figure 28 shows the comparisons between experimental results on axial load capacity of the square CFT stub columns and calculated capacities obtained by Equation 2.15 which gives a slightly conservative value to the columns with small B/t ratio. The reason for this is considered to be a strain-hardening effect of steel tubes rather than the confinement effect.

2.2.2 Stress vs. Strain Models for Filled Concrete

To predict the load vs. deformation relationships of centrally loaded CFT columns, a stress vs. strain curve model of confined concrete is necessary. Sakino and Sun [2.4] have proposed a unified stress vs. strain model for concrete confined by steel tube and / or conventional rectilinear hoop. This model is expressed by Equation 2.16.

$$Y = \dfrac{VX + (W-1)X^2}{1 + (V-2)X + WX^2}$$ .....(2.16)

where, X and Y are concrete stress ($\boldsymbol{s}_c$) and strain ($\boldsymbol{e}_c$) normalized by corresponding peak values $\boldsymbol{s}_{ccB}$ and $\boldsymbol{e}_{cco}$, respectively.

The stress vs. strain curve can be determined if the strengths of unconfined (plain) and confined concrete are given, which can be seen from Table 2.3. "Original" model in Table 2.3 [2.4] has been expanded for confined concrete in circular or square CFT column by Narahara et al. [2.5]. In the case of circular CFT columns, the strength enhancement factor K defined as $\boldsymbol{s}_{ccB}/\boldsymbol{s}_{cp}$ ($\boldsymbol{s}_{cp}$ is the strength of unconfined concrete, and assumed to be $\boldsymbol{g}_U f_c^{'}$) is given by Equation 2.17 which is obtained from Equations 2.2 and 2.4.

$$K = 1.0 - k \cdot \dfrac{2t}{(D-2t)} \cdot \dfrac{\boldsymbol{s}_{sq}}{\boldsymbol{s}_{cp}}$$ .....(2.17)

Once the values of k and $\boldsymbol{s}_{sq}$ are fixed as 4.1 and $-0.19\boldsymbol{s}_{sy}$ as described before, Equation 2.17 can be transformed into Equation 2.18 where D/t=50 as a representative for the simplicity.

$$K = 1.0 + 0.032 \frac{\boldsymbol{s}_{sy}}{\boldsymbol{s}_{cp}} \qquad .....(2.18)$$

In the case of square CFT columns, the value of K factor should be 1.0 from the viewpoint of axial load capacity of centrally loaded short columns, in other words the confinement effect on ultimate axial load cannot be expected. It is expected, however, that the axial load deformation capacity of filled concrete after reaching ultimate axial load can be improved by confinement effect of square steel tubes in CFT columns as observed in many experimental results. A slope of falling branch of stress vs. strain curve for the confined concrete is governed by the constant W in Equation 2.16, which is the function of $\boldsymbol{s}_{cp}$ and effective lateral pressure index $\boldsymbol{s}_{re}$ defined in Table 2.3. The empirical formula to estimate the value of W for a square steel tube acting only as the transverse reinforcement (referred to as the steel jacket) has also been proposed by Sakino and Sun [2.4], and is shown in Table 2.3 as "Original" model. In this paper, it is assumed that the value of W for the square steel tube in CFT column is equal to that for the square steel jacket. Table 2.3 gives all the information to obtain stress vs. strain curves for concrete confined by square steel jackets and steel tubes in circular and square CFT columns. Figure 2.9 shows these stress vs. strain curves along with the curve for unconfined concrete. The unconfined concrete strength and the yield strength of circular (D/t=60) and square (B/t=60) steel tubes shown in Figure 2.9 are 20MPa and 300MPa, respectively.

2.2.3 Stress vs. Strain Models for Steel Tube

For the circular CFT columns, the stress vs. strain relationship of the steel tube is developed as elastic-perfectly plastic relation model as shown in Figure 2.10. The maximum stress of the steel tube is $0.89\boldsymbol{s}_{sy}$ as described before. In the case of square CFT columns, the stress vs. strain models for steel tube in CFT columns are proposed as shown in Figure 2.11. The three types of multi-linear model are described in the figure, where Type-1 is the model for steel tube with small B/t ratio of which maximum stress is expected to be larger than the yield stress due to the strain-hardening effect, while the maximum stress of the steel tube with large B/t ratio (Type-3) does not reach the yield stress due to the local buckling. In the case of the steel tube with the medium B/t ratio (Type-2), the maximum stress of the steel tube is defined as the yield stress. The classification for the modeling is according to the value of generalized B/t ratio, $\sqrt{\boldsymbol{a}_s}$ as shown in Figure 2.7. The specific values of $\boldsymbol{s}_{sB}$, $\boldsymbol{e}_{sB}$, $\boldsymbol{e}_{sE}$, $\boldsymbol{s}_{sT}$, $\boldsymbol{e}_{sT}$ are calculated by using the equations summarized in Table 2.4 for each type. In the table, $\boldsymbol{s}_{sB}$ and $\boldsymbol{e}_{sB}$ are the stress and strain at the local buckling, respectively, and $\boldsymbol{e}_{sE}$ is strain at elastic limit. In the case of Type-2 and Type-3, $\boldsymbol{e}_{sE}$ is the same as $\boldsymbol{e}_{sB}$, and $\boldsymbol{s}_{sT}$ and $\boldsymbol{e}_{sT}$ are the stress and strain at the termination point of falling branch.

2.3 Comparisons of the Experiments and Analytical Models

The proposed analytical load vs. deformation curves are compared with six experimental results for each shape of CFT columns in Figure 2.12 and in Figure 2.13. These figures show the relations between experimental or calculated axial load of CFT columns divided by the nominal squash load N_o and longitudinal strain. The

thick solid lines with experimental plots show experimental results and the thin solid lines show the analytical curves. The dashed line and chained line show calculated loads of the filled concrete and steel tube, respectively. In each figure, specimens with different D/t or B/t ratio are shown together for comparisons. Good agreement is observed between the predicted and experimental behavior.

CHAPTER 3: BEHAVIOR OF ECCENTRICALLY LOADED SHORT COLUMNS

This chapter presents the results of experimental investigation and analytical simulation of the behavior of CFT stub columns subjected to eccentric axial load.

3.1 Experimental Investigation

3.1.1 Specimens and Parameters

The details of a typical specimen are shown in Figure 3.1. Circular tube was cold-formed by press-bending and welding. Square tube was fabricated by welding together two pieces of channel section, which were cold-formed from flat plate. Both ends of steel tube were butt-welded with backing plates to the end plates of 40mm in thickness. Holes only for anchor bolts subjected to tension force were opened in the end plates, and a hole for concrete casting was opened in the top end plate. Ratio of the clear height of specimen to diameter or width was 3.0.

A total of sixty-five specimens was tested: thirty-three circular and thirty-two square CFT specimens. The test parameters were selected as follows: 1) nominal tensile strength of steel tube s_u (400, 590, 780MPa), 2) design concrete strength Fc (20, 40, 80MPa), 3) diameter (width)-to-thickness ratio of steel tube D/t or B/t (rank FA, FC, FD), and 4) axial force ratio. The diameter (width)-to-thickness ratio is classified into four ranks (FA~FD) in the Japanese design practice from a viewpoint of deformation capacity of plastic hinges forming in hollow steel tubes. The ductility factor of 4 is guaranteed in the rank FA, 1 in the rank FC, and the elastic local buckling occurs in the rank FD with strength deterioration. Steel tubes were cold-formed with three different nominal wall thickness: 3.0, 4.5 and 6.0mm. The value of D/t (B/t) ratio was controlled by the outside diameter of circular tube (122~450mm) or the width of square tube (120~324mm). Although three different loading schemes were used in the tests which are explained later in this chapter, the eccentricity of the axial load or the ratio of the end moment to the axial load was determined in such a way that the ultimate strength of the specimen would hit a certain point selected on the M-N interaction curve which was calculated beforehand.

Table 3.1 shows the dimensions of the tubes, material strengths and axial load ratios. More detailed information on the material properties of steel tube and concrete is summarized in Tables 3.2 and 3.3, respectively, in which the values are the average of 3 tensile coupon tests for steel and 3 cylinder compression tests for concrete. Material properties of steel tubes were obtained from tensile coupon tests taken from each steel plate before manufacture. Yield ratio of steel plates, which is defined as the ratio of the yield stress to the tensile strength, strongly depends on the steel grades: 0.64~0.69 for grade 400MPa steel, 0.90~0.92 for 590MPa, and 0.95 for 780MPa. Specimens with the same concrete strength were filled from one batch of a ready mixed concrete plant, and the eccentric stub column tests were conducted about three months after concrete casting.

3.1.2 Loading Condition

Monotonic loading tests were carried out at three research institutes, so the loading conditions were not identical.

Circular columns were tested under the loading condition shown in Figure 3.2(a), and square columns were tested under the conditions shown in Figures 3.2(b) and 3.2(c). In the case of loading conditions shown in Figures 3.2(a) and 3.2(c), the magnitude of axial force in the column was maintained constant during the test. In the case of the condition shown in Figure 3.2(b), however, the axial force and bending moment were increased proportionally. Average curvature was obtained by measuring relative rotation between two sections, which were apart by the distance of two times the outside diameter for circular columns and three times the width for square columns. Longitudinal and lateral displacements and curvature were measured by LVDTs, and longitudinal and transverse strains of steel tubes were measured by wire strain gages.

3.1.3 Test Results

The test results are shown in Table 3.4. Figure 3.3 shows the moment M vs. curvature f relationships of the specimens, where M and f denote bending moment at the mid-height of the specimen and average curvature obtained by the rotation measurements, respectively. In the value of M, Pd moment evaluated at the mid-height is included. In some of the specimens made of grade 590 or 780MPa steel, crack in the welds between the end plate and steel tube was observed at the instance marked by "x" in Figure 3.3, and the test was terminated. This failure occurred not only in the circular but also in the square CFT specimens. Reliable data on the ultimate moment were not available for 9 specimens of circular columns and 8 square columns failing in premature crack in the welds, of which maximum values of bending moment obtained in the tests are indicated in the parentheses in Table 3.4.

Figure 3.3(a) shows the moment vs. curvature relationships of the circular CFT columns. Each specimen shows stable moment vs. curvature relation with large ductility, except for those fracturing at the weld, and four specimens in the lower two figures using grade 400MPa steel in Figure 3.3(a). These four specimens showed severe strength deterioration after the maximum strength reached, since the specimen with D/t = 101 and Fc = 80MPa were subjected to large axial load but confining effect was not much expected from the steel tube of 400MPa grade steel, and D/t ratio was too large and the effect of local buckling clearly appeared in the case of specimens with D/t = 152 and Fc = 40MPa. It must be careful to use the high strength concrete combined with the low strength steel tube. It is generally understood that the usage of the high strength concrete causes the reduction in the deformation capacity. While, the deformation capacity is improved by using high strength steel tube.

Figure 3.3(b) shows the moment vs. curvature relationships of the square CFT columns. In each graph, experimental $M - f$ relations of two or three specimens with different axial force ratio of N/N_o are shown, and they are quite similar, although the maximum strength is clearly affected by N/N_o ratio. The strength reduction due to local buckling is more or less observed in each specimen except for those in the top two graphs, but the reduction is not very large. In some cases, the crashed concrete filled the gap between locally deformed steel tube and concrete, and the load increased again, as observed in the specimen with B/t = 33, Fc = 20MPa and grade 590MPa steel (s_{sy} = 618MPa). Severe strength deterioration observed in the specimen with grade 780MPa steel (s_{sy} = 835MPa) was mainly caused by Pd effect. Effects of the concrete strength on the column behavior are not clear.

3.2 Analytical Investigation

3.2.1 Moment-Thrust-Curvature Relation

Moment-thrust-curvature relation of a CFT column was numerically derived by the fiber analysis based on the stress vs. strain relations of concrete and steel.

The stress vs. strain relations of concrete are discussed in Chapter 2 and are shown schematically in Figure 3.4, where the confining effect of circular steel tube is considered in the strength increase and the behavior after the maximum strength for circular section, while it is only considered in the descending behavior after the maximum strength in the case of square section, and the tensile strength of concrete is ignored. The mathematical expressions of the stress vs. strain relation of concrete are shown below following Chapter 2 [3.1, 3.2]:

$$Y = \frac{VX + (W-1)X^2}{1 + (V-2)X + WX^2} \qquad\qquad .....(3.1)$$

$$X = \varepsilon_c / \varepsilon_{cco} \qquad\qquad \text{for circular CFT} \qquad\qquad .....(3.2\text{-a})$$

$$X = \varepsilon_c / \varepsilon_{co} \qquad\qquad \text{for square CFT} \qquad\qquad ..... (3.2\text{-b})$$

$$Y = \sigma_c / \sigma_{ccB} \qquad\qquad \text{for circular CFT} \qquad\qquad ..... (3.3\text{-a})$$

$$Y = \sigma_c / \sigma_{cp} \qquad\qquad \text{for square CFT} \qquad\qquad ..... (3.3\text{-b})$$

$$V = E_c \cdot \varepsilon_{cco} / \sigma_{ccB} \qquad\qquad \text{for circular CFT} \qquad\qquad ..... (3.4\text{-a})$$

$$V = E_c \cdot \varepsilon_{co} / \sigma_{cp} \qquad\qquad \text{for square CFT} \qquad\qquad ..... (3.4\text{-b})$$

$$W = 1.5 - 17.1\sigma_{cp} \times 10^{-3} + 2.39\sqrt{\sigma_{re}} \qquad\qquad ..... (3.5)$$

$$\sigma_{ccB} = \sigma_{cp} + k \cdot \sigma_r \qquad\qquad ..... (3.6)$$

$$K = \sigma_{ccB} / \sigma_{cp} \qquad\qquad ..... (3.7)$$

$$\sigma_{cp} = f_c' \times \gamma_U , \quad \gamma_U = 1.67 D_c^{-0.112} \qquad\qquad ..... (3.8)$$

$$\frac{\varepsilon_{cco}}{\varepsilon_{co}} = \begin{cases} 1 + 4.7(K-1) & K \le 1.5 \\ 3.35 + 20(K-1.5) & K > 1.5 \end{cases} \qquad\qquad ..... (3.9)$$

$$E_c = \left(6.90 + 3.32\sqrt{\sigma_{cp}}\right) \times 10^3 \qquad\qquad ..... (3.10)$$

$$e_{co} = 0.94 \left(s_{cp} \right)^{1/4} \times 10^{-3}$$ ..... (3.11)

$$s_r = \frac{2t \cdot 0.19 \cdot s_{sy}}{D - 2t}$$ ..... (3.12)

$$s_{re} = \frac{k}{k_e} s_r , \quad k = 4.1, \quad k_e = 23 \quad \text{for circular CFT}$$ ..... (3.13-a)

$$s_{re} = \frac{1}{2} r_h \cdot s_{sy} \left(\frac{t}{b} \right) \qquad \text{for square CFT}$$ ..... (3.13-b)

where, s_c : axial stress of concrete,

e_c : axial strain of concrete,

s_{ccB} : compressive strength of confined concrete,

e_{cco} : axial strain at the maximum strength of confined concrete,

s_{cp} : compressive strength of plain concrete = $g_U \cdot f_c'$,

f_c' : compressive strength of concrete cylinder,

e_{co} : axial strain at the maximum strength of plain concrete,

E_c : Young's modulus of concrete,

k : confinement coefficient,

s_{sy} : yield strength of steel tube,

g_U : factor for scale effect,

D : diameter of steel tube,

t : thickness of steel tube,

s_r : confining stress,

r_h : volumetric ratio of steel tube ($r_h = 4(B-t)/b^2$)

B : Outside width of steel tube , and

b : inner width of steel tube.

Fundamental discussions on the stress vs. strain relations of steel tube are also made in Chapter 2. Here, the stress vs. strain relations used for the analysis are shown schematically in Figure 3.5. The steel tube resists axial load and bending moment, as well as it provides confinement. Therefore, the tube is subjected to both axial stress and transverse stress. In order to take this effect of the biaxial stress state into account in the fiber analysis of a circular CFT, it was assumed that the biaxial stresses at the initial yield satisfied the von Mises' yield criterion, and the compressive yield stress was reduced to $0.91 s_{sy}$ and the tensile yield stress was increased to $1.08 s_{sy}$, where s_{sy} denotes the yield stress obtained from the material coupon tests. Finally, bi-linear stress vs. strain relation considering the strain-hardening effect was shown in Figure 3.5(a), where the local buckling is not considered. The slope in the region of the strain-hardening can be chosen from the material tests.

On the other hand, the effect of local buckling is more pronounced in the case of a square tube, and the model shown in Figure 3.5(b) was used for a square steel tube. The compression stress of the tube with small B/t ratio

(rank FA) increases to the value larger than s_{sy} due to strain-hardening, and then the local buckling occurs with strength deterioration. It is assumed that the local buckling of the tube with medium B/t ratio (rank FC) occurs at the stress just reaching s_{sy}, and that of the tube with larger B/t ratio occurs at the elastic buckling stress given by the following formula.

$$s_{scr} = \frac{\pi^2 k_c E_s}{12(1-\nu^2)}\left(\frac{t}{B}\right)^2 \qquad .....(3.14)$$

where, E_s and ν denote the Young's modulus and Poisson's ratio of steel, and

k_c is the plate buckling coefficient.

It is assumed that k_c=6.97, since the shape of the cross section of a buckled square CFT was observed to be similar to the clamped plate. In every case of ranks FA, FC and FD, the compressive stress reaches the stable part in the range of large strain. The bi-linear relation is assumed for the tensile stress vs. strain relation with nominal yield stress equal to $1.1s_{sy}$, considering confining effect similar to circular CFT and strain-hardening in a simple manner.

The mathematical expressions of the stress vs. strain relations of circular and square tubes are given below [3.1, 3.3]:

a) Circular CFT

$$-0.91e_{sy} < e < 1.08e_{sy} \quad (-0.91s_{sy} < s < 1.08s_{sy})$$

$$s = E_s \cdot e \qquad .....(3.15)$$

where, e_{sy} : yield strain of steel tube($= s_{sy}/E_s$),

e : strain of steel tube,

s_{sy} : yield stress of steel tube,

s : stress of steel tube, and

E_s : Young's modulus.

$$e < -0.91e_{sy} \quad (s < -0.91s_{sy})$$

$$s = \frac{(s_{st} - s_{sy})}{(e_{su} - e_{sy})} \cdot (e + 0.91e_{sy}) - 0.91E_s \cdot e \qquad .....(3.16)$$

where, s_{st} : tensile stress of steel tube, and

e_{su} : strain at the tensile stress.

$$1.08e_{sy} < e \quad (1.08s_{sy} < s)$$

$$s = \frac{(s_{st} - s_{sy})}{(e_{su} - e_{sy})} \cdot (e - 1.08e_{sy}) + 1.08E_s \cdot e \qquad \text{.....(3.17)}$$

b) Square CFT

b-1) The tensile stress vs. strain relation

$$e < 1.1e_{sy} \quad (s < 1.1s_{sy})$$

$$s = E_s \cdot e \qquad \text{.....(3.18)}$$

$$1.1e_{sy} < e \quad (1.1s_{sy} < s)$$

$$s = 1.1 \cdot s_{sy} \qquad \text{.....(3.19)}$$

b-2) The compressive stress vs. strain relation

- rank FA ($\sqrt{e_{sy}} \cdot \dfrac{B}{t} \leq 1.54$)   ..... Type-1 in Table 2.4 and Figure 2.7

$$-e_{sy} < e$$

$$s = E_s \cdot e$$

$$-e_{sB} < e < -e_{sy}$$

$$s = s_{sy} \left\{ \frac{(1-S)}{(e_{sy} - e_{sB})} (e + e_{sy}) - 1 \right\} \qquad \text{.....(3.20)}$$

$$\text{where,} \quad e_{sB} = e_{sy} \left(\frac{6.06}{a_s^2} - \frac{0.801}{a_s} + 1.10 \right) \qquad \text{.....(3.21)}$$

$$S = 1/(0.698 + 0.128 \cdot a_s) \qquad \text{.....(3.22)}$$

$$a_s = e_{sy} \left(\frac{B}{t} \right)^2 \qquad \text{.....(3.23)}$$

$$-e_{sT} < e < -e_{sB}$$

- 21 -

$$s = \frac{\left(s_{sT} - S \cdot s_{sy}\right)}{\left(e_{sT} - e_{sB}\right)}(e + e_{sB}) - S \cdot s_{sy} \qquad \qquad .....(3.24)$$

where, $\quad e_{sT} = 3.59e_{sy} + e_{sB}$ $\qquad \qquad .....(3.25)$

$$s_{sT} = s_{sy}\left(1.19 - 0.207\sqrt{a_s}\right) \qquad \qquad .....(3.26)$$

$e < -e_{sT}$

$$s = -s_{sT} \qquad \qquad .....(3.27)$$

- rank FC $(1.54 \le \sqrt{e_{sy}} \cdot \dfrac{B}{t} \le 2.03$)   ..... Type-2 in Table 2.4 and Figure 2.7

$-e_{sy} < e$

$$s = E_s \cdot e$$

$-e_{sT} < e < -e_{sy}$

$$s = \frac{\left(s_{sT} - s_{sy}\right)}{\left(e_{sT} - e_{sy}\right)}(e + e_{sy}) - s_{sy} \qquad \qquad ..... (3.28)$$

where, $\quad e_{sT} = 4.59e_{sy}$ $\qquad \qquad ..... (3.29)$

$e < -e_{sT}$

$$s = -s_{sT}$$

- rank FD $(2.03 \le \sqrt{e_{sy}} \cdot \dfrac{B}{t}$)   ..... Type-3 in Table 2.4 and Figure 2.7

$-Se_{sy} < e$

$$s = E_s \cdot e$$

where, $\quad S = 1 \Big/ \left(0.698 + 0.128 \cdot \dfrac{4.00}{6.97}a_s \right) \qquad \qquad .....(3.30)$

$-e_{sT} < e < -Se_{sy}$

$$s = \frac{\left(s_{sT} - S \cdot s_{sy}\right)}{\left(e_{sT} - S \cdot e_{sy}\right)}\left(e + e_{sB}\right) - S \cdot s_{sy} \qquad \qquad \text{.....(3.31)}$$

where, $e_{sT} = 4.59 S \cdot e_{sy}$ $\qquad \qquad \text{.....(3.32)}$

$e < -e_{sT}$

$s = -s_{sT}$

Figures 3.6(a) and 3.6(b) show the comparisons between the moment vs. curvature relations obtained from the tests and the analyses of circular and square CFT specimens, respectively. In Figure 3.6(a) for circular CFT specimens, it is observed that the theoretical initial elastic stiffness quite well agrees with the test results in all cases. In some cases, the analysis gives unsafe side estimate to the maximum strength obtained in the tests, and in some other cases, the strength deterioration after the maximum strength attained is more pronounced in the analyses than in the tests. However, the analysis generally well traces the experimental behavior. It seems that the $M - f$ relation of a circular CFT column is strongly affected by the stress vs. strain relation of concrete, rather than that of steel tube.

On the contrary to those observations made for circular CFT columns, it is observed in Figure 3.6(b) for square CFT columns that the analysis gives too conservative estimate to the maximum strength of specimens with grade 780MPa steel (s_{sy}=835MPa), and in these specimens the strength deterioration after the maximum strength is much severer in the experiments. This may be attributed to the analysis in which the effect of work-hardening of the cold-formed square steel tube was not considered. In general, the flexural behavior of square CFT column obtained by the analysis was strongly affected by the stress vs. strain relation of the steel tube, which in contrary to the case of a circular CFT column.

3.2.2 Ultimate Bending Strength

Table 3.4 shows the value of the ultimate moment, where M_u denotes the test result, and $M_{cal.1}$, $M_{cal.2}$, and $M_{cal.3}$ denote theoretical ultimate moments. The value of $M_{cal.1}$ was calculated from the rectangular stress blocks assumed for both steel and concrete shown in Figure 3.7, where neither the confining effect on concrete strength nor the local buckling of steel tube were considered. The value of $M_{cal.2}$ was calculated in the same way, but the reduction of the concrete strength due to scale effect is considered as shown in Equation 3.8. The value of $M_{cal.3}$ was obtained from the peak point of the moment vs. curvature relation, which was determined by the fiber analysis, based on the stress vs. strain relations given by Equations 3.1 and 3.15 - 3.32.

Comparison between the ratio of experimental ultimate moment M_u to theoretical full plastic moment $M_{cal.1}$ and D/t (or B/t) ratio is shown in Figure 3.8 for all specimens except for those failed in premature failure due to cracking. In the case of circular CFT columns shown in Figure 3.8(a), the effect of confined

concrete and strain-hardening of steel are more pronounced in the specimens with D/t ratio smaller than 75, and thus $M_u / M_{cal.1}$ exceeds 1.0, while it cannot reach 1.0 in the specimen with D/t ratio larger than 75 due to the scale effect on concrete. The average of $M_u / M_{cal.1}$ of all circular specimens was 1.087 with the coefficient of variation equal to 0.04. On the other hand, the value of $M_u / M_{cal.1}$ is less than 1.0 in most square specimens due to the scale effect and the local buckling, as shown in Figure 3.8(b). A few specimens with small B/t ratio show the value of $M_u / M_{cal.1}$ larger than 1.0, but it is much smaller than those of circular specimens with small D/t ratio, and thus the increase in bending strength due to the confined concrete is not expected in square CFT columns. The average of $M_u / M_{cal.1}$ of all square specimens was 0.908 with the coefficient of variation equal to 0.014.

In Figure 3.9, the ultimate moment data are plotted by changing the theoretical ultimate moment to $M_{cal.2}$. The scale effect on concrete strength is considered in the calculation of $M_{cal.2}$. The difference in the data distributions in Figures 3.8(a) and 3.9(a), both for circular CFT columns, is quite clear; the value of $M_u / M_{cal.2}$ is larger than or equal to 1.0 except for one or two specimens, and it may be said that the safe side evaluation of the strength is improved by taking the scale effect into account. The average and coefficient of variation of $M_u / M_{cal.2}$ became 1.164 and 0.035, respectively. However, Figures 3.8(b) and 3.9(b) for square CFT columns show almost the same data distributions, although a little improvement of the strength evaluation is observed; the average and coefficient of variation of $M_u / M_{cal.2}$ became 0.949 and 0.011, respectively. The reduction of the ultimate strength is thus mainly caused by the local buckling in the case of square CFT columns.

Comparison between the ratio of experimental ultimate moment M_u to calculated moment $M_{cal.3}$ and D/t (or B/t) ratio is shown in Figure 3.10. In the calculation of $M_{cal.3}$, the following factors were considered: 1) scale effect on concrete strength; 2) confinement effect on concrete strength and change in nominal compressive and tensile yield stress of steel tube due to biaxial state of stress, both for a circular CFT columns; and 3) reduction in nominal compressive yield stress of square steel tube due to local buckling. Much better accuracy is observed in Figure 3.10, compared with Figures 3.8 and 3.9. The average and the coefficient of variation of $M_u / M_{cal.3}$ are as follows: 0.998 and 0.008 for circular CFT columns; and 1.079 and 0.015 for square CFT columns.

CHAPTER 4: BEHAVIOR OF BEAM-COLUMNS

This chapter presents the behavior of interior beam-columns subjected to constant axial load. It also presents exterior beam-columns subjected to a variable axial load, or a tensile axial load, that may be caused by the overturning moment during severe earthquakes, and the behavior of square beam-columns subjected to the two-dimensional lateral loads, whose significance has been revealed by recent earthquakes. A total of thirty-three beam-column specimens was tested for these purposes. This chapter also presents the results of the simulations based on the stress vs. strain relationships proposed in the preceding chapters.

4.1 Experimental Investigation

4.1.1 Specimens and Parameters

Table 4.1 gives a summary of the specimens. The test parameters were steel tube shape (circular and square), material strength of steel tube and concrete, width (diameter)-to-thickness ratio of steel tube, axial loading condition (constant and variable) and lateral loading direction for the square specimens. Steel plates with the tensile strength of grade 400MPa, 590MPa, and 780MPa were used for steel tubes. The results of coupon tests and stub column tests of steel tubes are listed in Table 4.2, where the compressive yield stress was obtained from the 0.2% offset method. Two classes of FA and FC were selected on the width (diameter)-to-thickness ratio of the steel tube, based on the classification of hollow steel tubes by Japanese design practice [4.1]. A plate element with the width (diameter)-to-thickness ratio in FA class is supposed to possess the ductility factor of 4 under the pure compression, while that in FC class the ductility factor of 1, that is, the local buckling occurs when the compression stress just reaches the yield stress. Concrete with the design strength (Fc) of either 40 or 90MPa was used to fill the steel tubes. The actual cylinder strengths are listed in Table 4.3.

A constant compressive axial load of 40% of nominal compressive strength, N_o $(= A_s \cdot \pmb{s}_{scy} + A_c \cdot f_c')$, was applied on interior column specimens, where A_s and A_c are sectional area of steel tube and concrete, respectively; $\pmb{s}_{scy}$ is the compressive yield stress of steel tube; f_c' is cylinder strength of concrete. This value was considered as the maximum of the long-term axial load in a practical design. A variable axial load with a range of 30% tension of nominal yield strength of steel tube, N_s $(= A_s \cdot \pmb{s}_{scy})$, to 70% compression of N_o was applied on exterior column specimens. The lateral loading in the direction with an angle of 22.5 or 45.0 degrees to the principal axis was applied to four square interior column specimens. The total number of circular specimens was thirteen, and the total number of square specimens was twenty.

As illustrated in Figure 4.1, the specimen had the footing and top stub at both column ends. The clear column length was six times the column depth or diameter in all specimens. The steel tube run through the footing and top stub and welded there. Square steel tubes were fabricated by welding two pieces of channel sections together, which were cold-formed from flat plates. Circular steel tubes were cold-formed from press bending. Concrete was cast into all specimens on the same day by filling it from the hole on the top of stub. Concrete was also cast into the footing and top stub to obtain the sufficient stiffness. The loading tests were started after three months from concrete casting. The cylinder strength of each specimen at the test age is listed in Table 4.4.

4.1.2 Test Setup and Procedure

Figure 4.2 illustrates the test setup and the loading condition of specimen. The test setup was designed to subject specimen to an axial load and horizontal displacement reversals in a double curvature condition with the point of inflection occurring at the middle height. The footing and top stub were fixed to the reaction floor and the loading beam using the tension rods, respectively. Two vertical hydraulic actuators applied an axial load, and held the top stub in parallel with the footing at the same time. A horizontal hydraulic actuator applied horizontal load by controlling the displacement. The history of rotation angle q shown in Figure 4.3 was applied to all specimens. Figure 4.4 illustrates rules on the axial force loading. During horizontal loading, the axial compressive load of 40% of N_o was maintained constant for the interior column specimens. For the exterior column specimens, the axial compressive load of 70% of N_o was maintained constant in a half cycle of the positive horizontal loading, while the axial tension load of 30% of N_s was maintained constant in the other half cycle of the negative horizontal loading. The axial load was changed when the horizontal load became zero, permitting the horizontal drift of specimen during changing of axial load. The applied forces were measured using the calibrated load cells. The specimens were instrumented to obtain the horizontal and axial deformations.

4.1.3 Test Results

Table 4.4 gives the measured column depth (diameter) and thickness of steel tube, the actual width (diameter)-to-thickness ratio, the material strengths, the applied axial load (N), and the actual axial load ratio (N / N_o or N / N_s) of each specimen. The experimental flexural strengths (M_{ue}) are also listed there, compared with the calculated flexural strength (M_{uc}) and the analytical flexural strength (M_{ua}). M_{uc} is the full plastic moment based on the compressive yield stress s_{scy} of steel tube and the cylinder strength f_c'. M_{ua} was obtained from the simulations described in the following section. Moment (M) vs. rotation angle (q) relationships and axial strain (e) vs. rotation angle (q) relationships of the specimens are shown in Figures 4.5 through 4.9. The moment M is the end moment in the loading direction, including the Pd moment. The rotation angle q is the chord rotation angle, and is obtained from dividing the measured horizontal drift by column length. The axial strain e expresses the average axial strain over the column length. The symbols of square, triangle and circle in Figures 4.5 through 4.9 denote the first local buckling of the steel tube, the first crack or fracture of steel and the maximum flexural strength, in each loading direction, respectively.

(1) Circular Interior Column Specimens

As seen in Figure 4.5, all specimens reached the maximum strength after local buckling occurred in the compressive flange. The specimens with grade 780MPa steel (s_{sy}=771~820MPa) tube showed a moment reduction in the loading cycle of $q = \pm 4\%$ due to the crack occurring in the heat affected zone of welding at the column end. The other specimens showed a very ductile behavior, even after the local buckling occurred. The experimental flexural strength is 1.16~1.60 times the calculated strength.

(2) Circular Exterior Column Specimens

A fracture of the tensile flange at the column ends occurred in the loading cycle under the axial tension in all

specimens as shown in Figure 4.6. The specimens with grade 590MPa steel tube (s_{sy}=482~504MPa) showed a significant moment reduction due to the fracture in the loading cycle of $q = \pm 3 \quad \pm 4\%$, after local buckling occurred and progressed at the compressive flange in the loading cycle under the axial compression. The specimens with grade 780MPa steel tube also showed a reduction in moment resistance due to the fracture in the loading cycle of $q = \pm 2\%$, without the progress of the local buckling. The experimental flexural strength is 0.91~1.59 times the calculated strength in the loading cycle under the axial compression, and 0.94~1.40 times in the loading cycle under the axial tension.

(3) Square Interior Column Specimens

The ultimate moment was observed after the local buckling occurred in the compressive flange, followed by cyclic deterioration in moment resistance in all specimens as shown in Figure 4.7. A crack was not observed in steel tube. The rotation angle at the ultimate moment q_{max} was 1.0~1.5% in the specimens with grade 400MPa steel tube (s_{sy}=276~295MPa), 1.5~2.0% in the specimens with grade 590MPa steel tubes (s_{sy}=537~540MPa) and 2.0~3.0% in the specimens with grade 780MPa steel tube (s_{sy}=824~825MPa). The q_{max} of the specimen with FA class steel tube was clearly greater than that of specimen with FC class steel tube. The axial deformation tended to accumulate in compression, especially after local buckling occurred. The amount of the axial shortening was much larger than that of circular specimens. The experimental flexural strength is 0.95~1.29 times the calculated strength.

(4) Square Interior Column Specimens Subjected to Biaxial Bending

As shown in Figure 4.8, the behavior of the specimen was very similar to that of the specimen loaded laterally in the principle direction up to the ultimate moment stage, then slightly larger moment deterioration was observed. A crack was observed at the corner of square steel tube near the column end, however a drastic reduction in moment resistance due to the crack was not observed. The experimental flexural strength is 0.95~1.20 times the calculated strength.

(5) Square Exterior Column Specimens

Local buckling of the compressive flange was observed at the early deformation stage in the loading direction of axial compression, then a fracture of the tensile flange at the column end occurred on the loading direction of axial tension in the loading cycle of $q = \pm 2\%$, which is shown in Figure 4.9. The experimental flexural strength is 0.75~1.19 times the calculated strength in the loading cycle under the axial compression, and 1.01~1.09 times in the loading cycle under the axial tension.

4.2 Discussion on the Test Results

4.2.1 Effect of Sectional Shape

Circular steel tubes have the advantage of restraining local buckling and confining filled concrete, compared with square steel tubes. Under the constant axial compressive load, the flexural strength and ductility of circular specimens are superior to those of square specimens, as shown in Figures 4.10 and 4.11. The square specimens showed a remarkable axial shortening and deterioration in moment resistance after the local buckling, while the circular specimens showed no or a little strength reduction and smaller axial shortening even after the local

buckling occurred. This indicates that larger tensile strain occurred at the tension flange of circular specimens in the large deformation stage. This causes the crack and fracture of circular steel tubes, in particular grade 780MPa steel tubes, which results in without sufficient elongation ability. Furthermore, the tensile stresses occurring in the hoop direction of circular tubes seem to promote the crack and fracture.

4.2.2 Effect of Width (Diameter)-to-Thickness Ratio

Local buckling generally occurs at the earlier deformation stage with the larger width (diameter)-to-thickness ratio. The ductility of the square columns becomes smaller as this ratio is larger, while this ratio has a little influence on the ductility of circular columns, within the range of test program.

4.2.3 Effect of Material Strength

Figure 4.10 gives relationships between the q_{max} and the material strengths of the interior column specimens. The ductility becomes larger as the steel strength becomes higher. It generally becomes smaller as the concrete strength becomes higher, but concrete strength has a little influence on the behavior in case of the specimens with high strength steel tube. This tendency indicates that high strength steel tube is effective to improve brittle behavior of high strength concrete, and that the restraining effect of the filled concrete against the local buckling of steel tube dose not depend on concrete strength.

Figure 4.11 gives relationships between the moment enhancement ratio M_{ue}/M_{uc} which are denoted by the symbols of   and   , and the material strengths of the steel tube of the interior specimens. The moment enhancement ratios of the circular specimens are greater than those of square specimens. The confinement effect in the circular columns is clearly recognized, especially in the specimens with high strength steel tube. The symbol of   in the Figure 4.11(a) denotes the ratio of M_{ue}/M_{ucc}, where M_{ucc} is the calculated flexural strength considering the confinement effect by steel tube obtained from the method prescribed in the AIJ-CFT Recommendations [4.2]. In this case, the moment enhancement ratio becomes the same level as that of square specimens, and is nearly 1.2 over the strength. From the test results of eccentrically loaded square CFT short columns, it was concluded in Fujimoto et al. [4.3] that the moment enhancement by the confinement effect from the steel tube could not be expected in square CFT columns. This indicates that the other factors, such as the strain-hardening of steel tube, the extra confinement from the stiff footing and top stub under the compressive axial load, provides the moment enhancement of about 1.2 for the circular and square specimens equally.

4.2.4 Effect of Variable Axial Load

The compressive flange under the axial compression became the tensile flange under the axial tension. Therefore, the flange was cyclically strained with large amplitude under the variable axial load. This causes local buckling at the early deformation stage and the fracture of steel tube. Consequently, the ductility of beam-columns reduces under the variable axial load.

4.2.5 Effect of Biaxial Bending

The crack occurring at the corner of square tubes was observed in the square specimens loaded laterally in the

direction with the angle of 22.5 or 45 degrees to the principal axis. This is because the maximum tensile strain occurs at the corner, which has experienced the plastic tensile strain during the cold-forming process. Figure 4.12 gives relationships between the experimental flexural strengths and the loading directions. This indicates that square beam-columns have almost the same performance even if the loading direction is changed, as in the case of circular columns.

4.3 Analytical Investigation

4.3.1 Analytical Model

Figure 4.13 illustrates a column model used in the computer simulations with the curvature and axial strain distributions assumed in the model. To represent the plastic deformation, the model has hinging portions with a certain length near the column ends, where inelastic curvature and axial strain of the critical section uniformly distribute. The behavior of the column model including the elastic shear deformation can be expressed in the following incremental form.

$$\begin{Bmatrix} \Delta \boldsymbol{q}_x(i) \\ \Delta \boldsymbol{q}_x(j) \end{Bmatrix} = \begin{bmatrix} \dfrac{2L}{6EI} + \dfrac{1}{GAL} & \dfrac{-L}{6EI} + \dfrac{1}{GAL} \\ \dfrac{-L}{6EI} + \dfrac{1}{GAL} & \dfrac{2L}{6EI} + \dfrac{1}{GAL} \end{bmatrix} \begin{Bmatrix} \Delta M_x(i) \\ \Delta M_x(j) \end{Bmatrix} + L_p \begin{Bmatrix} \Delta \boldsymbol{f}_{x,p}(i) \\ \Delta \boldsymbol{f}_{x,p}(j) \end{Bmatrix} \quad \dots\dots(4.1)$$

$$\begin{Bmatrix} \Delta \boldsymbol{q}_y(i) \\ \Delta \boldsymbol{q}_y(j) \end{Bmatrix} = \begin{bmatrix} \dfrac{2L}{6EI} + \dfrac{1}{GAL} & \dfrac{-L}{6EI} + \dfrac{1}{GAL} \\ \dfrac{-L}{6EI} + \dfrac{1}{GAL} & \dfrac{2L}{6EI} + \dfrac{1}{GAL} \end{bmatrix} \begin{Bmatrix} \Delta M_y(i) \\ \Delta M_y(j) \end{Bmatrix} + L_p \begin{Bmatrix} \Delta \boldsymbol{f}_{y,p}(i) \\ \Delta \boldsymbol{f}_{y,p}(j) \end{Bmatrix} \quad \dots\dots(4.2)$$

$$\Delta \boldsymbol{d}_a = \Delta N / EA + L_p \left(\Delta \boldsymbol{e}_{a,p}(i) + \Delta \boldsymbol{e}_{a,p}(j) \right) \quad \dots\dots(4.3)$$

where, the variables with a subscript of (i) or (j) express those related to the end i or j; $\Delta \boldsymbol{q}_x$ and $\Delta \boldsymbol{q}_y$ are the increments of end rotation angle in the x- and y-directions, respectively; $\Delta \boldsymbol{d}_a$ is the increment of axial deformation; ΔM_x and ΔM_y are the increments of moment at column end in the x and y-directions, respectively; ΔN is the increment of axial force; EI, GA and EA are the flexural, shear and axial stiffness in the elastic range, respectively; L is column length; L_p is the length of hinging portion and assumed to be column depth or diameter in the simulations; $\Delta \boldsymbol{f}_{x,p} = \Delta \boldsymbol{f}_x - \Delta \boldsymbol{f}_{x,e}$; $\Delta \boldsymbol{f}_{y,p} = \Delta \boldsymbol{f}_y - \Delta \boldsymbol{f}_{y,e}$; $\Delta \boldsymbol{e}_{a,p} = \Delta \boldsymbol{e}_a - \Delta \boldsymbol{e}_{a,e}$; $\Delta \boldsymbol{f}_x$ and $\Delta \boldsymbol{f}_y$ are the increments of curvature at the critical section in the x- and y-directions, respectively; $\Delta \boldsymbol{e}_a$ is the increment of axial strain at the critical section; $\Delta \boldsymbol{f}_{x,e}$, $\Delta \boldsymbol{f}_{y,e}$ and $\Delta \boldsymbol{e}_{a,e}$ are the elastic components of $\Delta \boldsymbol{f}_x$, $\Delta \boldsymbol{f}_y$ and $\Delta \boldsymbol{e}_a$, and equal to $\Delta M_x / EI$, $\Delta M_y / EI$ and $\Delta N / EA$, respectively; $\Delta \boldsymbol{f}_{x,p}$, $\Delta \boldsymbol{f}_{y,p}$ and $\Delta \boldsymbol{e}_{a,p}$ are the inelastic components of $\Delta \boldsymbol{f}_x$, $\Delta \boldsymbol{f}_y$ and $\Delta \boldsymbol{e}_a$, respectively.

The first component of the right hand side of Equations 4.1 through 4.3 represents the increment of elastic deformation of the column, and the second one represents the increment of inelastic deformation. Developing

these equations, the incremental strain vectors $\{\Delta \boldsymbol{f}_x, \Delta \boldsymbol{f}_y, \Delta \boldsymbol{e}_a\}$ at the critical sections related to i and j ends can be expressed by the incremental deformation vector $\{\Delta \boldsymbol{q}_x(i), \Delta \boldsymbol{q}_x(j), \Delta \boldsymbol{q}_y(i), \Delta \boldsymbol{q}_y(j), \Delta \boldsymbol{d}_a\}$. Therefore, the force vector $\{M_x(i), M_x(j), M_y(i), M_y(j), N\}$ can be obtained step by step from the ordinary sectional analysis for the moment vs. curvature relationships, following the idealized stress vs. strain relationships.

In the simulation for specimens, the double curvature condition with the inflection point occurring at the middle height was assumed, and thus $\boldsymbol{q}_x(i) = \boldsymbol{q}_x(j)$ and $\boldsymbol{q}_y(i) = \boldsymbol{q}_y(j)$. The concrete and steel elements as illustrated in Figure 4.14 were used. In order to fit the elastic stiffness to the test result, elastic rotational and axial springs were added at both column ends, which represent the local deformations of the fixed ends observed during testing. Furthermore, to take the moment enhancement caused by the confinement effect from the footing and top stub under the axial compressive load into consideration, the critical section is assumed to move inward from the column end corresponding to the development of hinging under the axial compression, and finally be located at the position with the distance of $L_p / 2$ from the column end at the ultimate stage. Considering the axial loading condition of the specimens, this modification of the end moment was conducted as follows:

$$M_{end} = M_{cr}\left(1 + \boldsymbol{b} \cdot H\right) \qquad\qquad\qquad\qquad .....(4.4)$$

$$H = \left(1 - K_t / K_e\right)^{6.0} \qquad\qquad\qquad\qquad .....(4.5)$$

$$\boldsymbol{b} = L_p / \left(L - L_p\right) \qquad \text{for the deformation range under the constant axial compressive load}$$

$$.....(4.6a)$$

$$\boldsymbol{b} = 0 \qquad\qquad \text{for the deformation range under the constant axial tensile load, or while the axial}$$
$$\text{load is changed} \qquad\qquad .....(4.6b)$$

where, M_{end} is the moment at the column end; M_{cr} is the moment at the critical section, which is determined by the stresses of the elements; H is a irreversible index of the development of hinging with a range of 0 to 1, but does not progress while $\boldsymbol{b}$ is zero; K_e and K_t are the elastic and instantaneous flexural stiffness at the critical section, respectively; and $\boldsymbol{b}$ expressed in Equation 4.6a is a geometric constant.

M_{end} is equal to M_{cr} in the elastic range. However, it becomes $L/\left(L - L_p\right)$ times M_{cr} after the hinge is fully developed under the axial compression. The value of $L/\left(L - L_p\right)$ is 1.2 in this simulation because all specimens have L of six times column depth and L_p is assumed to be column depth. Note that this modification of the end moment was conducted in the x- and y-directions, independently.

The stress vs. strain relationships of concrete and steel in circular and square CFT columns have been formulated based on the test results of centrally loaded short columns in Chapter 2. However, these models were based on the average axial strain between the measurement length of three times the column depth or diameter.

The slope of the descending branch of the stress vs. strain relationships is generally sensitive to the measurement lengths because the failure region is limited within a certain length. In the simulation, the failure length was assumed to be the column depth or diameter, and a modification was conducted with multiplying the slope of the descending branch of the formulated stress vs. strain relationships of both concrete and steel by a coefficient of 1/3. The hysteretic rules proposed by Fujii et al. [4.4] and Meng et al. [4.5] were used for concrete and steel, respectively. Typical hysteretic stress vs. strain relationships are shown in Figure 4.15. Note that the strength of 52MPa was used in modeling 40MPa concrete whose actual cylinder strength was 36~42MPa. The reason for this is that the test results of centrally loaded short columns with the same materials as the beam-column specimens indicated that the concrete had a much higher strength than 40MPa. Characteristics after yielding including the strain-hardening based on the coupon tests were used in modeling steel tubes. Further details concerning the analytical model and the used assumptions were discussed in Inai et al. [4.6].

4.3.2 Analytical Results and Discussion

Figures 4.16 to 4.20 give the analytical $M - q$ relationships and $e - q$ relationships of specimens. The analytical flexural strengths (M_{ua}) are listed in Table 4.4, compared with the experimental flexural strengths (M_{ue}).

(1) Circular Specimens

The analytical $M - q$ relationships show good agreement with the test results of the interior column specimens while there is a little difference in the $e - q$ relationships, which is seen from the comparison of Figures 4.16 and 4.17. For the exterior column specimens with grade 780MPa steel tube, the analytical results are also in good agreement with the test results. However, the analytical results can not represent the behavior after the local buckling observed in the exterior column specimens with grade 590MPa steel tube, since the influence of the local buckling is not considered in the used stress vs. strain curve and hysteretic rules of steel tubes. The ratio of M_{ue} / M_{ua} of the specimens is 0.90~1.19, except for the exterior specimens with grade 590MPa steel tube. The presented analytical model can represent the hysteretic behavior of circular CFT beam-columns, except for the behavior after the local buckling under the high axial compression.

(2) Square Specimens

Figures 4.18 through 4.20 show analytical $M - q$ and $e - q$ relations of square specimens. The analytical $M - q$ relationships show good agreement with the test results of all specimens, including the behavior after the local buckling, and represent the effects of test parameters on the behavior. A little difference in the $e - q$ relationships is observed in the interior column specimens. However, the tendency of axial shortening after the local buckling is well represented. The ratio of M_{ue} / M_{ua} of all specimens is 0.89~1.09. The presented analytical model can represent the hysteretic behavior of square CFT beam-columns very well.

CHAPTER 5: BEHAVIOR OF BEAM-TO-COLUMN SUBASSEMBLADGES

Shear panels are considered having very high reservation of ultimate strength comparing with other critical sections such as beams and columns as the concrete panel is highly confined by steel tube. Therefore, small concern was paid to such an element to the present and there have been not so many experimental researches on the beam-to-column subassemblies. Recently the strength of steel and concrete become very high, but the experimental studies on such connections are very few. This chapter presents the results of the experimental investigation on CFT column - steel beam subassemblies using high strength materials, which were made as weak shear panel so as to investigate the failure pattern, shear force carrying capacity, shear force transfer mechanism in the panel and the effect of confinement.

5.1 Experimental Investigation

5.1.1 Specimens and Test Program

Figure 5.1 shows the illustration of subassemblies and Figure 5.2 shows the details of panel zone. Table 5.1 shows the dimensions and materials of eleven specimens. Ten specimens were plane subassemblies to which reversed lateral load from one direction and column axial force were applied. One specimen was a stereo subassembly to which reversed lateral forces from two directions and constant column axial force were applied. There were two types of connections in the plane specimens. Eight were of interior and two were of exterior subassemblies. Additional one had a shape of exterior but subjected to constant axial force. The column sections were rectangular or circular. The specimens were about one third scaled models of actual CFT system, and they were all planned to fail at shear panel zone. To make shear panel weak, the thickness of steel tube in the panel was reduced to be about one third of that of column tube except for specimen C3. The thickness of steel tube in the panel of C3 was around one half of that of column steel tube. The variables of the test programs were the loading direction of lateral force, the types of subassemblies such as interior or exterior, the shapes of steel tube column and the combinations of the strength of concrete and steel. Diaphragms in the panel zone were made continuously to beam flange to avoid fracture in the welds at the junction of the panel and the beam flange. The specimen R4 is only a subassembly of which diaphragm was welded around the steel tube of the column (so-called exterior diaphragm) as shown in Figure 5.2.

High strength concrete around 90MPa and high strength steel around 590 or 780MPa were used for specimens. Rectangular specimen R1 and circular specimen C1 were standard specimens in this test program, of which concrete strength was around 90MPa and steel strength was around 590MPa. For specimens R2 and C2, the steel strength was the same as R1 and C1, but the concrete strength was reduced to around 40MPa. For specimens R3 and C3, the concrete strength was the same as R1 and C1 and the steel strength was around 780MPa. Specimen R4 had the exterior diaphragm which differed from R1, but the strength of steel and concrete was the same as R1. Specimen R6 was a stereo subassembly which had basically the same details with specimen R1. Specimens R5, R5' and C4 were the exterior subassemblies with the same material strength of R1 and C1.

Execution of the tests was shared at several research institutes. So, the dimensions of the specimens were determined according to the capacity of testing setup of each research institute. For example, the length of beams of circular specimen C3 was 3000 mm which differ from C1, C2. Therefore, the experimental results of the yield and ultimate strength, the story drifts and so on of the specimens were evaluated and compared using the normalized values. Properties of the concrete and steel are shown in Table 5.2

5.1.2 Test Setup and Procedure

Figure 5.3 and 5.4 show the test setup of specimen R1 and that of R6.

Figure 5.5 shows reversed loading procedure of interior specimens. Each cycle was controlled by the story drift angle. Constant compressive axial force equivalent to 0.2 $_pN_o$ was applied to the interior specimens and was kept through the test. Varying axial force from compression to tension was applied to the exterior specimens. Figure 5.6 shows the applying rule of varying axial force. Compressive axial force equivalent to 0.7 $_pN_o$ was applied before the beginning of the positive cycle of loading. Then, just before negative loading after positive one, the compressive axial force was replaced by the tensile axial force equivalent to 0.3 $_pN_{so}$. Here, the $_pN_o$ is the nominal squash load in the panel zone and $_pN_{so}$ is the axial yielded strength of steel tube in the panel zone.

An example of instruments to measure the story drift and the deflection of the shear panel is illustrated in Figure 5.7. Strain measurements were carried out so as to know the yielding process of the shear panel, beams and columns,

5.1.3 Test Results

5.1.3.1 Two dimensional Specimens

(1) Progress of Damage

The test results are shown in Tables 5.3(a) and 5.3(b). All specimens failed in the shear panel, as they were scheduled. At first, local yielding in the shear panel occurred and it spreads to overall panel. Then, local yielding occurred in the beam flange and the steel tube column, which did not spread widely as the moment carrying capacity of the beam and the column were planned being much stronger than the shear capacity of the panel as shown in Tables 5.3(a) and 5.3(b) .

At the final stage of experiment, small expansion of shear panel zone was observed, but buckling or cracking of steel tube in the panel was not observed. Figure 5.8 shows the crack pattern of the filled concrete in the panel zone after test, where the steel tube was cut and taken off.

(2) Story Shear Force vs. Story Drift Angle Relationships

The story shear force vs. story drift angle relationships of the specimens are shown in Figures 5.9(a) and 5.9(b). In these figures, $_pQ_u$ and $_pQ_y$ are the ultimate and yield panel shear strengths converted to story shear force. All specimens showed ductile behavior with large energy absorption. After maximum strength, rapid loss of shear force carrying capacity was not observed and gradual strength reduction occurred. For exterior

subassemblies R5 and C4, the plastic zone in the panel expanded little by little in consequence of the increased loading cycles. The formation of a plastic hinge in the panel made the specimens unstable, as the specimens were unsymmetrical. Therefore in the final stage of experiment, the bending deformation of the specimens occurred at the panel zone when axial compressive force of 0.7 $_pN_o$ was applied to the column prior to the beginning of the positive loading cycle. This is the reason why the flow of story drift angle occurred on the zero line of story shear force as shown in the relationships of specimen R5 and C4 in Figures 5.9(a) and 5.9(b).

(3) Behavior of Panels, Beams and Columns

Figures 5.10(a) and 5.10(b) show the shear force vs. shear deflection angle relationships of panels. The shear deflection was measured as shown in Figure 5.7. Every shear panel showed very ductile performance. Figures 5.10(a) and 5.10(b) also show the relationships of story shear force and deflection angle of beams or columns. These figures indicated that the beams and columns were still almost elastic even though local yielding had occurred.

Contributions of each elements, panel, beam and column, in the overall displacement of each subassembly are showed in Figures 5.11(a) and 5.11(b). Percentage of contribution of shear panel in overall displacement became greater in consequence of the increase of overall displacement. In the case of R5 and C4, different contributions of each element were observed in negative loading cycle subjected to tensile axial force. Filled concrete in shear panel decreases the contribution in proportion to the increase of overall displacement. Therefore the stress vs. strain relationships of specimen R5, R5' and C4 showed a little greater inelastic hysteresis comparing with other interior subassemblies subjected to constant compressive axial force as shown in Figures 5.10(a) and 5.10(b).

5.1.3.2 Three Dimensional Specimens
(1) Progress of Damage and Behavior of Subassembly

Test results of stereo specimen R6 are also shown in Table 5.3(a). The values about Specimen R6 in the table are expressed as of 45-degree direction. Figure 5.12 shows shear force vs. story drift angle relationship. The values of this figure are also converted to the values of 45-degree direction. Elastic rigidity was almost the same as the calculation. First yield of panel occurred at R=1.5% in the story drift angle. Up to R=3.0%, overall shear panel had yielded. Story drift angle at the maximum strength was R=3.0%, in both positive and negative loading cycle. At this time no sign of failure of the joint panel was observed except for yielding. Afterward, the gradual expansion of steel in the panel began. At last half cycle, cracks occurred at the corner of the panel and the welded boundary with diaphragm. The shear force carrying capacity of the joint panel was gradually decreased after the maximum strength. However, the specimen indicated large ductility.

(2) Behavior of Panel, Beam and Column

Figure 5.13 shows the relations of shear force of panel and shear deflection angle of shear panel in x- and y-directions respectively. The figures show very ductile behavior of the shear panel. Figure 5.l3 also shows the relationships of the story shear and the deflection angle of the beam and column. These figures indicated almost elastic behavior of the beam and column and the elastic rigidities were almost the same with the calculation. Shear panel, beam and column showed approximately the same hysteresis in both x- and y-directions.

Figure 5.14 shows the contribution of the each elements, panel, beam and column, in the overall story drift angle. The percentage of story drift angle by panel was very small at first, though, finally it exceeded 70% of overall drift angle.

5.1.3.3 Discussions on Test Results

Figure 5.15 shows the relationships of normalized shear force of panel and normalized story drift angle so as to compare the effects of different test variables.

(1) Effect of Material Strength

Figure 5.15(a) shows the comparison of behavior of rectangular subassemblies Rl, R2 and R3 and circular subassemblies C1, C2 and C3.

In these figures, the envelope curves of R1 vs. R2 and C1 vs. C2 show the comparison of the behavior of the specimens made of the same steel strength and different concrete strength. Much difference did not observed between them. However, R1 and C1, of which concrete strength were higher, showed slightly steeper degradation of strength after the maximum strength.

The envelope curves of R1 vs. R3 and C1 vs. C3 show the behavior of the specimens with the same concrete strength and different steel strength. Both specimens R3 and C3, of which steel strength were higher, showed rather steeper strength degradation and small ductility.

Circular subassemblies showed higher shear force carrying capacity than rectangular subassemblies.

(2) Effect of Axial Load

Figure 5.15(b) shows the envelope curves of normalized shear strength of the shear panel and story drift angle relationships of specimens R1 and R5 to know the effect of axial force. In the positive lateral loading side, specimen R5 subjected to higher axial load of $0.7 \, _pN_o$ showed smaller ductility than R1 subjected to constant axial load of $0.2 \, _pN_o$. In the negative lateral loading side, the rigidity of R5 did not decrease so much even though the specimen subjected to tensile axial load of $0.3 \, _pN_{so}$. Both specimens showed ductile performance.

(3) Effect of Diaphragm

Figure 5.15(c) shows the envelope curves of specimens R1 and R4, which have different types of diaphragms. Rigidity and strength of specimen R4 with exterior (outer) diaphragm was smaller than those of R1 with interior (through) diaphragm. Exterior diaphragm of R4 was partially yielded near the corner of the steel tube column, however it remained being elastic at the center portion of the diaphragm during the test.

(4) Effect of Loading Directions

Figure 5.15(d) shows the envelope curves of specimens R1 and R6. R6 was the three-dimensional specimen loaded simultaneously in x- and y-directions to give lateral force in 45-degree direction. The shear force carrying capacity of the panel of R6 in 45-degree direction was a little greater than that of specimen R1.

(5) Yield / Ultimate Shear Strength of Shear Panel

Figure 5.16 shows the yield strength and ultimate strength of shear panel compared with the design strengths calculated by AIJ-SRC Standards [5.1] as the short-term allowable strength and the ultimate strength. Only specimen R4 with exterior diaphragm showed a little smaller yield strength than AIJ-SRC Standard. The ultimate strength was given as 1.2 times of the short-term allowable strength in the AIJ-SRC Standard.

Figure 5.17 shows the yield and ultimate shear strengths of specimen R6 compared with R1. In this figure, the yield and ultimate shear strengths were normalized by the short-term allowable shear strength by AIJ-SRC Standards. It can be seen that the shear panel subjected to the 45-degree directional loading showed a little higher ultimate strength that R1 and it showed much higher reserved strength in the yield strength.

5.2 Analytical Investigation

5.2.1 Model for the Restoring Force Characteristics of Shear Panels

The discussion of this section is limited to rectangular specimens. The relationships of shear force and shear deflection angle of steel tube and concrete are assumed to be presented by tri-linear curve as shown in Figure 5.18 [5.2].

(1) Shear Strength vs. Shear Deflection Angle of Steel Panel

The shear behavior of the steel panel is given by tri-linear curve, of which the yielding point, the softening point and the maximum point are given by the following equations.

1) yielding point

$$_{ps}Q_y = \frac{8}{9}{_w}A\frac{\sqrt{{_w}\boldsymbol{s}_y^2 - {_s}\boldsymbol{s}_o^2}}{\sqrt{3}} \qquad .....(5.1)$$

$$_{ps}\boldsymbol{g}_y = k\frac{_{ps}Q_y}{{_w}A \cdot {_s}G} \qquad .....(5.2)$$

2) softening point

$$_{ps}Q_r = {_w}A\frac{\sqrt{{_w}\boldsymbol{s}_r^2 - {_s}\boldsymbol{s}_o^2}}{\sqrt{3}} \qquad .....(5.3)$$

$$_{ps}\boldsymbol{g}_r = \frac{\left(_{ps}Q_r - _{ps}Q_y\right)}{{_w}A \cdot {_s}G^{'}} + _{ps}\boldsymbol{g}_y \qquad .....(5.4)$$

3) maximum point

$$_{ps}Q_m = {_w}A\frac{\sqrt{{_w}S_B^2 - {_s}S_o^2}}{\sqrt{3}} \qquad \qquad .....(5.5)$$

$$_{ps}g_m = \frac{\left({_{ps}}Q_m - {_{ps}}Q_r\right)}{{_w}A \cdot {_s}G^{''}} + {_{ps}}g_r \qquad \qquad .....(5.6)$$

where, $_wA = 2 \cdot {_w}B \cdot {_w}t$,

$_wB$: width of shear panel,

$_sG$: elastic shear rigidity of steel,

$_sG^{'}, {_s}G^{''}$: the second and the third rigidity of the relationship of shear stress and shear deflection angle determined by Prandtle-Ruess' stress vs. strain relationship,

$_wt$: thickness of web plate of steel tube,

$_sS_o$: axial stress of steel tube,

$_wS_y$: yield point of web plate of steel tube,

$_wS_r = 0.8 \times \left({_w}S_B - {_w}S_y\right) + {_w}S_y$: intermediate stiffness degradation point stress of web plate of steel tube,

$_wS_B$: tensile stress of web plate of steel tube, and

k : shear stress coefficient of steel box section.

(2) Shear Strength vs. Shear Deflection Angle of Filled Concrete

It was assumed that concrete was elastic up to shear cracking and concrete continued to keep the same strength after the maximum strength. The points of shear cracking and the maximum strength was expressed by the following equations.

1) shear cracking point

Shear cracking strength and corresponding displacement angle are calculated by the equation of the principal stress of concrete.

$$_{pc}Q_c = {_c}A\sqrt{{_c}S_t\left({_c}S_t + {_c}S_0\right)} \qquad \qquad .....(5.7)$$

$$_{pc}g_c = 1.2\frac{_{pc}Q_c}{{_c}A \cdot {_c}G} \qquad \qquad .....(5.8)$$

where, $_cS_t = 0.5\sqrt{f_c^{'}}$,

$_cA$: sectional area of concrete,

$_cG$: elastic shear rigidity coefficient of concrete,

$_cS_o$: axial stress of concrete, and

$f_c^{'}$: compressive strength of concrete.

2) maximum strength point

- 37 -

Maximum strength of concrete is calculated by using the arch mechanism in the panel zone surrounded by steel tube and diaphragm as shown in Figure 5.19.

$$_{pc}Q_m = \left(\frac{_cB}{2} \cdot \tan q + \sqrt[4]{\frac{_fM_{pc}}{_ct \cdot f_c'} \sin q} \right) {_ct \cdot f_c'} \qquad .....(5.9)$$

$$_{pc}g_m = \frac{_{pc}Q_m}{_ca_m \cdot {_cA} \cdot G/1.2} \qquad .....(5.10)$$

where, $q = \tan^{-1}\left(\sqrt{1 + \left(\frac{H}{_cB}\right)^2} - \frac{H}{_cB} \right)$,

$_ca_m = 0.00158 f_c' + 0.0411 \frac{H}{_cB} + 0.086$,

$_cB$: width of concrete in panel,

H : height of concrete in panel,

q : declined angle of concrete arch mechanism in panel,

$_fM_{pc}$: plastic moment of flange plate of steel tube $= \left(_cB \cdot _f t^2 \right)_f S_y$,

$_f t$: thickness of flange plate in panel,

$_f S_y$; yield point of flange plate of steel tube, and

$_c t$: thickness of concrete.

The estimated skeleton curves for specimens Rl, R2, R3, R4 and R5 are plotted in Figure 5.20 with experimental ones. Specimen R5 is the exterior subassembly with varying column axial force in the positive and negative loading cycles. Thus, the skeleton curves are shown separately in the figure.

Calculated skeleton curves show almost the same characteristics with experiments, especially in the yield strength of shear panels. However, the calculations are apt to evaluate the smaller maximum shear force carrying capacities than experiments.

5.2.2 Three Dimensional FEM Analysis
5.2.2.1 Analyzed Specimens

It is clear that the consideration of the confinement of filled concrete by steel tube is inevitable so as to understand the inelastic behavior of columns, beam-columns and beam-to-column connections of CFT system. A three dimensional finite element analysis is an appropriate tool to precisely simulate this effect. Therefore, nine specimens, R1, R2, R3, R5 and R5' from rectangular specimens and C1, C2, C3 and C4 from circular specimens, were analyzed by the three dimensional FEM method and compared with test results.

5.2.2.2 Analytical Procedure

1) Idealization of Specimens

The halves of the specimens were idealized into three dimensional finite elements using symmetrical conditions as shown in Figure 5.21. The computer code "FINAL" [5.3, 5.4] developed by Obayashi Corporation was used for this study.

2) Constitutive Relations

Isoparametric solid elements with eight nodes were used for concrete, and isoparametric shell elements with four nodes were used for steel plates. The constitutive equations of the concrete elements were based on an orthotropic hypoelastic model based on the equivalent uniaxial strain concept. Willam-Warnke's five-parameter model [5.5] was applied to determine the failure criteria of concrete surface under an triaxial stress condition, and actual values of five-parameters were given by Ohnuma and Aoyagi's coefficients [5.6]. Stress vs. strain relationship of steel was expressed by an elasto-plastic relation, which is based on von Mises' yield criterion.

3) Stress vs. Strain Relationship of Concrete

It's well recognized that concrete confined by a steel tube increases the ultimate strength and ductility. Empirical equations to evaluate the confinement effect were proposed on the basis of the test results of short CFT columns. However, cracks might be produced in the CFT panel when shear stress exceeded a critical stress level. It was questionable whether the empirical equations are applicable to the analysis in such case. Therefore in this analysis, two kinds of stress vs. strain relationships for concrete are prepared so as to take into account the ductile characteristics of confined concrete as shown in Figure 5.22.

　　Case 1: whole stress vs. strain, including both ascending and degrading zone, was expressed by a modified Ahmad model [5.7]

　　Case 2: relation of the ascending zone up to the maximum stress was expressed by the Ahmad model and the degrading zone after the maximum stress was expressed by Sakino's model [5.8]

4) Bond Transfer

In the panel zone, a perfect bond was assumed between the concrete and steel. It was because the concrete was surrounded and highly confined by a steel tube and diaphragms. For the column, a film element was inserted between the concrete and steel tube to permit the bond slip on the contact surfaces.

5.2.2.3 Analytical Results

Figure 5.23 shows the story shear force vs. story drift angle relationships of specimens obtained by experiment and analysis. The analysis of case 2 gave good simulations with experiments of all specimens. The analysis by case 1 gave a little smaller shear force carrying capacity than the experimental and showed rapid loss of shear strength in the case of specimens R1 and C1.

Figure 5.24 shows the relationships of shear force ($_pQ_c$) transferred by concrete and shear deflection angle ($\boldsymbol{g}$)

in the panel obtained from the analysis. $_pQ_c$ was calculated from the stresses of integral points of the concrete elements. In this figure, $_pQ_c$ is normalized by A_c (sectional area of concrete) and $f_c^{'}$ (the maximum strength of concrete). Figure 5.25 shows the relationship of shear force ($_pQ_s$) transferred by the steel plate and the shear deflection angle ($\boldsymbol{g}$) in the panels. It is observed that the maximum shear stress of the rectangular panel is around $0.3f_c^{'}$ for the concrete strength of 100MPa, and is around $0.35f_c^{'}$ for 50MPa concrete strength. The maximum shear stresses of the circular panel is around $0.35f_c^{'}$ for the concrete strength of 100MPa, and is around $0.4f_c^{'}$ for 50MPa concrete strength. The maximum shear stresses of both rectangular and circular panels are not in proportion to the concrete strengths of the panel. In Figure 5.25, bi-linear relationships of $_pQ_s - \boldsymbol{g}$ calculated by the following equations are also given. The values of $_sQ_p$ obtained from the FEM analysis, which included the frame-work contribution carried by the flanges of steel tube and diaphragms in the panel, are almost the same with the bi-linear line or a little greater.

$$G_s = \frac{E_s}{2(1+\boldsymbol{n}_s)}A_s \qquad\qquad .....(5.11)$$

$$_pQ_{sy} = \frac{\sqrt{\boldsymbol{s}_{sy}^{2} - \boldsymbol{s}_o^{2}}}{\sqrt{3}} \cdot A_s \qquad\qquad ..... (5.12)$$

where, G_s : elastic shear rigidity,

E_s : Young's modulus of steel,

$_pQ_{sy}$: shear yield strength of panel,

A_s : effective sectional area to transfer shear stress, and

for rectangular tube $\quad A_s$ = the area of web

for circular tube $\qquad A_s$ = half area of whole sectional area

$\boldsymbol{s}_{sy}$: yield point of steel, $\quad \boldsymbol{s}_o$: axial stress of steel, and $\boldsymbol{n}_s$: Poisson's ratio.

Figure 5.26 shows the contour of the minimum principal stress of concrete and the flow of the principal stresses in the rectangular and circular panels. The principal stress flows seems to be wider compared with RC joint panels. It is because that the steel tube of the CFT column in the joint panel contributes to the confining of the concrete.

5.3 Examples of Numerical Simulations

So as to grasp the effect of column depth to beam depth ratio and declivity coefficient D' in the softening zone of concrete on the shear force transfer by concrete panel, imaginary column-to-beam assemblies shown in Table 5.4 were analyzed. The analytical results on imaginary assemblies are summarized in Table 5.5 together with those on tested assemblies. In Figure 5.27, normalized concrete shear force ($_pQ_c / A_c / f_c^{'}$) is plotted against the column depth to beam depth ratio (H/Dc), which indicates that smaller H/Dc gives larger $_pQ_c / A_c / f_c^{'}$. Figure 5.28 shows the effect of declivity coefficient D' on the $_pQ_c / A_c / f_c^{'}$.

Notes

1) Equations on CFT Shear Panel of AIJ-SRC Standards [5.1]

(a) Short-Term Allowable Shear Strength of Shear Panel

$$_pQ_y = \left(2\cdot {}_jf_s\cdot {}_j\boldsymbol{b}\cdot {}_cV + {}_sf_s\cdot {}_sV\right)/{}_{sB}d$$

where, $_jf_s$: short-term shear strength of concrete (kgf/cm^2) ,

$$= 1.5\times \min\left(f_c'/30, 5 + f_c'/100\right)$$

$_sf_s$: short-term shear strength of steel (kgf/cm^2) $= F_y/\sqrt{3}$,

$$_j\boldsymbol{b} := \min\left(2\cdot {}_sD/{}_{sB}d, 4.0\right) \qquad \text{for circular column;}$$

$$= \min\left(2.5\cdot {}_sD/{}_{sB}d, 4.0\right) \qquad \text{for rectangular column,}$$

$_sD$: diameter of steel tube (outer diameter for circular tube and outer width for square tube),

$_cV$: effective volume of concrete in the joint panel zone $= {}_cA\cdot {}_{sB}d$

$_sV$: effective shear volume of steel in the joint panel zone $= {}_sA\cdot {}_{sB}d/2$

$_{sB}d$: distance of central axis between upper and lower flanges of steel beam.

(b) Ultimate Shear Strength of Shear Panel

$$_pQ_u = 1.2\times_pQ_y$$

2) Modified Ahmad Model and Sakino's Model for Concrete [5.7], [5.8]

$$\boldsymbol{s} = \left\{A\cdot X + \left(D'-1\right)X^2\right\}\cdot \boldsymbol{s}_p/\left\{1 + \left(A-2\right)\cdot X + D'\cdot X^2\right\}$$

$$A = E/E_o,\ \ E_p = \boldsymbol{s}_p/\boldsymbol{e}_p$$

(a) Softening Zone in Ahmad model

$$X = \left\{1 + \left(\boldsymbol{e}-\boldsymbol{e}_p\right)/\boldsymbol{e}_p\right\}^n,\ \ n = 0.9 + 3.4\left(f_c'/1000\right)^2$$

$$D' = 1 + 1800\cdot \left\{\left(\boldsymbol{s}_p/f_c'\right)-1\right\}^2/f_c'$$

(b) Softening Zone in Sakino's model

a) rectangular tubular column

$$X = \boldsymbol{e}/\boldsymbol{e}_p,\ \ \boldsymbol{s}_p = f_c' + 23\boldsymbol{s}_{re}$$

$$D' = 1.5 - 1.68\times 10^{-3} f_c' + 0.75\sqrt{\boldsymbol{s}_{re}}$$

$$\boldsymbol{s}_{re} = 0.5\boldsymbol{r}_h\cdot \boldsymbol{s}_{hs}\left(d''/C\right)\cdot \left\{1 - s/(2D_c)\right\}$$

b) circular tubular column

$$X = \boldsymbol{e}/\boldsymbol{e}_p,\ \ \boldsymbol{s}_p = f_c' + \left\{0.625\cdot 2\cdot t/\left(D_c - 2t\right)^3\right\}\cdot \boldsymbol{s}_{sh}$$

$$D' = 1.5 - 1.68\times 10^{-3} f_c' + 0.75\left\{\left(K-1\right)\cdot f_c'/23\right\}^{0.5}$$

$$K = \boldsymbol{s}_p/f_c'$$

where, $\boldsymbol{s}_p$, $\boldsymbol{e}_p$: the maximum stress and the corresponding strain,

$\boldsymbol{s}$, $\boldsymbol{e}$: stress and strain,

E_o : elastic rigidity,

f_c' : uniaxial compressive strength,

d'' : thickness of tube,

$\boldsymbol{s}_{sh}$: yield point of steel,: volume ratio of steel tube,

r_h : volume ratio of steel tube,

C : interior width of steel tube, and

s : pitch of lateral reinforcements (in the case of CFT s=0).

CHAPTER 6: PROPOSED DESIGN FORMULAS FOR COLUMNS AND BEAM-COLUMNS

6.1 General

The Architectural Institute of Japan (AIJ) recently edited "Recommendations for Design and Construction of Concrete Filled Steel Tubular Structures" [6.1] (referred to as AIJ-CFT Recommendations). The AIJ-CFT Recommendations have following features from the viewpoint of design formulas for load carrying capacities of CFT columns and beam-columns. The first one is that they have new design formulas for slender columns (column curves). The second one is that the design formulas for circular CFT columns take into consideration of confinement effect which has been taken into consideration in Chinese Code [6.2], British Code [6.3] and Euro Code [6.4], but has been ignored for a long time in the "Standards for Structural Calculation of Steel Reinforced Concrete Structures" [6.5] (referred to as AIJ-SRC Standards) as well as ACI Codes [6.6]. The contents of AIJ-CFT Recommendations are expected to be included near future in the AIJ-SRC Standards, which deal with the structures composed of concrete-encased steel members including CFT members.

The AIJ-CFT Recommendations, however, have following limitations of application concerning material strength and thickness of steel tube wall.

Material Strength:

Compressive strength of concrete $\qquad F_c \le 60 MPa$

Tensile strength of steel $\qquad s_u \le 590 MPa$

Diameter (or width)-to-thickness ratio D/t (or B/t) of steel tubes:

Circular section $\qquad \dfrac{D}{t} \le \dfrac{2.35 \times 10^4}{F} \times 1.5 \qquad$ .....(6.1)

Square section $\qquad \dfrac{B}{t} \le \dfrac{7.3 \times 10^2}{\sqrt{F}} \times 1.5 \qquad$ .....(6.2)

where, F is a standard value to determine allowable stress of steel (in MPa), and is taken as smaller value of nominal yield stress s_y, or 70% of nominal tensile strength s_u.

The main objective of the five-year research project on CFT column system carried out as a part of the fifth phase of the US-Japan Cooperative Earthquake Research Program was widening these limitations by an experimental work as mentioned in Chapter 1. The tests of centrally and eccentrically loaded stub columns and beam-columns subjected to combined axial load and bending moment were planned and conducted. The design formulas for ultimate axial load and ultimate bending moment have been proposed based on those data, which covered the following ranges of experimental parameters:

Material strength:

Compressive strength of concrete $\qquad 20MPa \le F_c \le 90MPa$

Tensile strength of steel $\qquad 400MPa \le s_u \le 780MPa$

Diameter (or width)-to-thickness ratio D/t (or B/t) of steel tubes:

$D/t \le 152$, $B/t \le 74$ $\qquad$ for grade 400MPa steel

$D/t \le 75$, $B/t \le 50$ $\qquad$ for grade 590MPa steel

$D/t \le 52$, $B/t \le 41$ $\qquad$ for grade 780MPa steel

The design formulas for ultimate bending moment were proved to be applicable to estimate the ultimate load carrying capacity of beam-columns obtained by experiments subjected to combined axial load, bending moment and shear. This chapter summarizes the design formulas for load carrying capacities of CFT columns based on experimental investigations described in the previous chapters. The emphasis is placed on the capacities of the CFT columns with thinner steel tube walls and / or high strength material which does not satisfy the limitations of AIJ-CFT Recommendations. Note that in this chapter the soil mechanics sign convention for stress and strain is followed. Namely, compressive stresses and strains are positive.

6.2 Ultimate Strength Formulas for Centrally Loaded Short Columns
6.2.1 Circular Columns

An ultimate axial load of centrally loaded circular CFT short columns is given by Equation 6.3.

$$N_u = N_o + 1 \cdot N_{so} \qquad\qquad .....(6.3)$$

where, $\quad N_o = $ nominal squash load $= N_{so} + N_{co} = A_s \cdot s_{sy} + A_c \cdot g_U \cdot f_c' \qquad .....(6.4)$

$\quad 1 = $ augmentation factor to take confinement effect on concrete strength into consideration $= 0.27$,

$\quad f_c' = $ cylinder strength of concrete,

$\quad A_s = $ cross sectional area of steel tube,

$\quad A_c = $ cross sectional area of filled concrete,

$\quad s_{sy} = $ yield point stress of steel tube,

$\quad g_U = 1.67 D_c^{-0.112}$ (for small scale test specimens) $\qquad .....(6.5)$

$\qquad = 0.85$ (for actual design), and

$\quad D_c : $ diameter of concrete core, in mm.

The value of 1 in Equation 6.3 was obtained as 0.27 by the regression analysis of the test data of centrally loaded CFT stub columns. Based on the analytical procedure in which yield criteria for the steel and concrete are assumed to be ones proposed by von Mises and Richart [6.7], respectively, the value of $1 = 0.27$ gives the biaxial stress state of the steel tube shown in Figure 6.1, i.e. a magnitude of axial stress s_{sz} is $0.89 s_{sy}$, and that of hoop tensile stress is $-0.19 s_{sy}$. A reduction factor g_U for concrete strength, which has been

introduced as the coefficient to take into consideration a scale effect [6.8] in the original empirical formula, is assumed to be a constant of 0.85 for the actual design. Figures 6.2(a) and 6.2(b) show comparisons between ultimate axial loads calculated by Equation 6.3 and experimental results obtained in the US-Japan Research Program and those in database which were collected from the proceedings of Annual Meeting of Architectural Institute of Japan published in 1977 through 1989. As observed in Figure 6.2, the design formula given by Equation 6.3 has reasonable accuracy.

6.2.2 Square Columns

An ultimate axial load of centrally loaded square CFT short columns is given by Equation 6.6.

$$N_u = N_{su} + N_{co} = A_s \cdot \boldsymbol{s}_{scr} + A_c \cdot \boldsymbol{g}_U \cdot f_c^{'} \qquad\qquad .....(6.6)$$

$$\boldsymbol{s}_{scr} = \min\left(\boldsymbol{s}_{sy}, S \cdot \boldsymbol{s}_{sy}\right) \qquad\qquad .....(6.7)$$

$$\frac{1}{S} = 0.698 + 0.128\left(\frac{B}{t}\right)^2 \frac{\boldsymbol{s}_{sy}}{E_s} \times \frac{4.00}{6.97} \qquad\qquad .....(6.8)$$

The confinement effect of square steel tube on compressive strength of concrete is ignored in Equation 6.6, but the restraining effect of filled concrete on local buckling of steel tube wall is taken into consideration through the factor S given by Equation 6.8. The factor S is a reduction factor due to the local buckling of the steel tube. The formula for S was first empirically derived from the test data of centrally loaded stub column of hollow square tube, and then modified to the reduction factor applicable to the steel tube in a CFT column by multiplying 400/6.97, considering the difference in the mode of bcal buckling shown in Figure 6.3. The numbers 4.00 and 6.97 are coefficients for plate buckling corresponding to the modes shown in Figures 6.3(a) and 6.3(b), respectively. Figures 6.4(a) and 6.4(b) show comparisons between ultimate axial loads calculated by Equation 6.6 and experimental results obtained in the US-Japan Research Program and those in database which were collected from the proceedings of Annual Meetings of AIJ of 1977 through 1989. As observed in Figure 6.4, the formula given by Equation 6.6 results in slightly conservative estimation for ultimate strength

6.3 Ultimate Strength Formula for Eccentrically Loaded Short Columns

The ultimate strength for eccentrically loaded short columns is presented by an interaction curve between axial load and ultimate moment. The AIJ-CFT Recommendations prescribe that the ultimate moment of columns under axial load be estimated as a full plastic moment. In other words, both of the concrete and steel tube are assumed to be a perfectly plastic material. On the other hand, according to stress vs. strain models for filled concrete of circular and square CFT columns proposed based on test results of centrally loaded CFT columns, the specific stress vs. strain curves for filled concrete of circular CFT column with D/t ratio of 100 and square CFT column with B/t ratio of 75 are rather brittle as shown in Figure 6.5, where the concrete compressive strength and yield stress of steel tube are assumed to be 80MPa and 300MPa, respectively. Then, it is necessary to introduce an ultimate (usable) strain and shape factors for concrete stress block for the evaluation of the strength of CFT columns composed of high-strength concrete and thin-walled steel tube, which the AIJ-CFT

Recommendations cannot be applied to.

6.3.1 Circular Columns

The AIJ-CFT Recommendations prescribe that ultimate moments of circular CFT columns be calculated by using stress blocks for filled concrete and steel tube shown in Figure 6.6. Nominal yield stress is assumed to be $0.89s_{sy}$ and $-1.08s_{sy}$ in compression and tension, respectively. These values were derived from the experimental data, and based on the assumption that stress in the steel tube confining the concrete satisfy von Mises' yield criterion with the presence of hoop tension s_{sq} equal to $-0.19s_{sy}$ as shown in Figure 6.1. The magnitude of compressive strength of concrete is given by Equation 6.9 which has been proposed by Richart et al. [6.7].

$$s_{ccB} = g_U \cdot f_c^{'} + k \cdot s_r = 0.85 \cdot f_c^{'} + 4.1 \frac{2t}{D-2t}(0.19)s_{sy} \qquad .....(6.9)$$

where, g_U =0.85 taking the scale effect into consideration as described in 6.2.1, and k=4.1 recommended

by Richart et al.

The confining stress (lateral pressure) s_r is caused by the confinement provided by the steel tube, and related to the hoop stress s_{sq}. The relation between s_r and s_{sq} depends on the D/t ratio, but the relation for D/t=50 is used here as a representative, for the simplicity in the design practice. Finally, the concrete strength for circular CFT column is given by Equation 6.10.

$$s_{ccB} = 0.85 f_c^{'} + 0.032 s_{sy} \qquad .....(6.10)$$

The use of high-strength concrete and / or very thin-walled steel tube results in rather brittle stress vs. strain curve for filled concrete as shown in Figure 6.5. Sun and Sakino [6.9] have proposed the ultimate strain and shape factors for stress block shown in Figure 6.7 and Table 6.1 for concrete confined by the circular steel tube, instead of the block shown in Figure 6.6(a) recommended in AIJ-CFT Recommendations.

The ultimate moment theory, in which the ultimate strain is introduced as prescribed in ACI Code [6.6], needs rather complicated computation procedure, because there exists an elastic part in the web of steel tube near the neutral axis. The full plastic moment of steel tube, however, can be used as approximate estimation of ultimate moment under such complicated stress distribution, because the contribution of thin-walled steel web to the ultimate moment of the CFT column is relatively small. In that ease, the ultimate strain is not necessary to calculate the ultimate moment. It should be kept in mind, however, that the shape factors of concrete stress block shown in Table 6.1 are formulated based on the assumed ultimate strain.

Figure 6.8 shows the comparisons between the experimental ultimate moments of specimens tested in the US-Japan Research Program and calculated ones based on the stress blocks for steel tube and filled concrete shown in Figures 6.6(b) and 6.7, respectively. As observed in Figure 6.8, the design formula has reasonable accuracy. In the case of CFT columns whose material strength and D/t ratio are within the applicable limitations of the AIJ-CFT Recommendations, the difference between the ultimate moment calculated by the proposed method and method prescribed in the AIJ-CFT Recommendations is very small, because the confinement effect of steel tube with relatively thick steel tube brings very ductile behavior of filled concrete. Then the proposed method to calculate the ultimate moment of circular CFT columns based on stress blocks shown in Figures 6.6(b) and 6.7 can be used in wide range as described in the section 6.1.

6.3.2 Square Columns

The AIJ-CFT Recommendations prescribe that the ultimate moment of square CFT columns can be estimated as a full plastic moment calculated by using stress block for concrete and steel shown in Figures 6.9(a) and 6.9(b), respectively. In the case of CFT columns using steel tube with large B/t ratio, however, the reduced compressive stress block of steel should be introduced to take the effect of local buckling of steel tube into consideration. Moreover, the use of high-strength concrete and / or thin-walled steel tube results in rather brittle stress vs. strain curve for concrete, then the ultimate strain and shape factors for stress block of concrete should be introduced in the similar manner as the case of circular CFT columns.

Based on the consideration described above, it is proposed that the stress block for concrete and steel tube shown in Figures 6.10(a) and 6.10(b) be used to estimate the ultimate moment of the square CFT columns with high-strength concrete and / or thin-walled steel tube. For those columns, the confinement effect of steel tube on the ductility of filled concrete is very small and negligible, then the stress block shown in Figure 6.10(a) and Table 6.2 for plain concrete proposed by Sun et al. [6.10] can be used. The magnitude of compressive stress in stress block for steel tube is the local buckling strength s_{scr} discussed in preceding section and given by Equations 6.7 and 6.8. The effect of the elastic part in the web of square steel tube near the neutral axis is ignored as shown in Figure 6.10(b) because of the same reason described in preceding section for the circular CFT columns. This results in a slight overestimation of the ultimate moment of steel tube, which is compensated by an underestimation of that of concrete due to ignoring the confinement effect of steel tube on the ductility of concrete described before. It is noteworthy that the stress block shown in Figure 6.10 should be used only for CFT columns with high-strength concrete and / or thin-walled steel tube which are out of applicable limitations in AIJ-CFT Recommendations. Figure 6.11 shows the comparisons between the experimental ultimate moments of columns subjected to axial load and bending moment and calculated ones based on the stress block in Figure 6.9 or 6.10. As observed in Figure 6.11, the design formula has reasonable accuracy.

6.4 Design Formulas for Beam-Columns under Combined Compression, Bending and Shear

In order to establish a seismic design method for the CFT column systems, it is necessary to investigate a behavior of CFT columns subjected to combined forces and deformed in a double curvature pattern shown in Figure 6.12. The maximum shear Q_{max} and the limit rotation angle R_u, which are defined in Figure 6.13 as

indices of load carrying and deformation capacities of columns, will be discussed in this section.

6.4.1 Ultimate Bending Strength

The ultimate horizontal load of the columns shown in Figure 6.12 are dominated by their flexural capacity except for the extremely short columns such as the columns with an aspect ratio, $h/D \leq 3.0$ or $h/B \leq 3.0$. The design formulas for ultimate moment discussed in the preceding section, which are proposed based on the behavior of eccentrically loaded CFT columns, might be used to estimate the ultimate moment at a critical section of the columns shown in Figure 6.12. The comparison between the experimental ultimate moments and theoretical ones calculated by the method discussed in the preceding section is shown in Figures 6.14(a) and 6.14(b). The experimental ultimate moments are defined as the column end moments at the maximum shear of the envelope curve of hysteresis loops of shear force vs. rotation angle of columns subjected to cyclic shear force under constant axial load. The column end moment includes a secondary moment due to axial load and lateral displacement, so-called Pd moment. As observed in Figure 6.14, the experimental ultimate moments are larger than theoretical ones. The main reason for the discrepancies between the experimental and theoretical ultimate moments is that the additional confinement provided by the stiff loading stub adjacent to the critical section would shift the critical section away from the end section to a section carrying smaller moment. The other reason can be attributed to a strain-hardening effect of the steel tube. It can be said that the theoretical prediction has a comfortable margin to the actual ultimate moment even though some part of this margin is canceled by the Pd moment which is usually ignored in the actual design procedure.

The column end moment at the maximum shear is taken as the experimental ultimate load carrying capacity of columns and is plotted in Figures 6.14(a) and 6.14(b). The alternative definitions of ultimate load carrying capacity can be made according to a performance-based design procedure. For example, if the maximum column end moment attained within a rotation angle limitation of 0.01 radian is taken as the experimental ultimate moment, Figures 6.14(a) and 6.14(b) are replaced by Figures 6.15(a) and 6.15(b). Following remarks can be made from Figures 6.15(a) and 6.15(b).

1) The ultimate moments of specimens with circular and square sections using high-strength steel (grade 780MPa) tube cannot reach the theoretical moment due to the larger yield strain of high-strength steel.
2) The ultimate moments of specimens with circular section hardly reach the theoretical moment except for the specimens using mild steel (grade 400MPa). The reason for this is that the confinement effect of steel tube cannot be fully developed within the rotation angle of 0.01 in radian.

In order to design the CFT columns using high-strength steel tube according to the performance-based design procedure, it is necessary to conduct further investigations on lateral load carrying capacity of the CFT columns under loading condition shown in Figure 6.12 especially for columns with circular section.

6.4.2 Limit Rotation Angle

The limit rotation angle R_u of CFT columns discussed in this section is a characteristic point on the envelope

curve of hysteresis loops of shear force vs. rotation angle, and is defined as the rotation angle at which 95% of the maximum shear is maintained after reaching the maximum shear as shown in Figure 6.13. The design formulas for R_u given by Equations 6.11 and 6.12 have been established for both of circular and square CFT columns by regression analysis using the experimental results tested in the US-Japan Research Program and those in the database described before. The comparisons between experimental limit rotation angles and those predicted by Equations 6.11 and 6.12 are shown in Figure 6.16 for circular columns and in Figure 6.17 for square columns.

For circular columns:

$$R_u(\%) = 8.8 - 6.7\frac{N}{N_o} - 0.04\frac{D}{t} - 0.012 f_c^{'} \qquad \qquad .....(6.11)$$

For square columns:

$$R_u(\%) = \frac{100}{0.15 \quad 3.79\frac{N}{N_0}}\frac{t}{B}\boldsymbol{b} \qquad \qquad .....(6.12)$$

$$\boldsymbol{b} = 1.0 - \frac{f_c^{'} - 40.3}{566} \le 1.0$$

where, the value of $f_c^{'}$ is given in MPa.

The Japanese Building Standard Law prescribes that the ultimate state seismic demand used in the capacity design procedure can be decreased in accordance with a structural characteristic factor D_s which is similar to the R factor in NEHRP Provisions [6.11]. The D_s factor depends on the deformation capacity and energy absorption capacity of the structures. The value of D_s factor is between 0.3~0.55 for so-called steel reinforced concrete (SRC) structures. The Japanese Building Standard Law prescribes the D_s factor of each story according to the structural system and member ductility. The members are classified in a design practice into four classes from the viewpoint of ductility, i.e. FA (very ductile), FB (ductile), FC (semi ductile) and FD (semi brittle). Table 6.3 is proposed to classify the CFT columns into these four categories according to their limit rotation angles given by Equation 6.11 or 6.12.

6.4.2 Hysteretic Model for Behavior of CFT Beam-Columns
(1) Tri-linear Skeleton Model
As illustrated in Figure 6.18, the moment vs. rotation angle relationship of CFT beam-columns subjected to cyclic lateral loading and a constant axial load can be expressed by a tri-linear skeleton model. This model is defined by the following five parameters: 1) the elastic stiffness Ke; 2) the first bending point moment My; 3) the stiffness degrading ratio at the second bending point ay; 4) the second bending point moment Mu; and 5) the ultimate rotation angle Ru. The behavior of CFT beam-columns is assumed to be elastic until the first bending point. My is given by the short-term allowable flexural strength prescribed in the AIJ-SRC Standards [6.5]. Mu

is given by the ultimate flexural strength of beam-columns discussed in the preceding sections in this chapter. Ru can be estimated from Equations 6.11 or 6.12. ay can be determined by statistical analysis of the experimental data.

(2) Stiffness degrading Ratio ay

Figure 6.19 gives the definition of the experimental stiffness degrading ratio ay, which was given by the ratio of K2 to K1, where K2 was the secant stiffness at the point of 85% of the maximum flexural strength Mmax, and K1 was the experimental initial stiffness and assumed to be the secant stiffness at the point of 33% of Mmax. The moment of 85% of Mmax was considered to correspond to the ultimate flexural strength proposed in this paper. The effects of structural parameters (D/t, B/t, $_s S_y$, $_c S_B$ and N/No) on ay were statistically investigated using the experimental data shown in Table 6.4. As a result, it was concluded that no or very weak correlations existed between the structural parameters and ay. 80% of experimental ay were distributed within the range from 0.4 to 0.9 as shown in Figures 6.20 and 6.21. Accordingly, the following average values of the experimental data were proposed as ay to be used in modeling.

$$_y = 0.65 \quad \text{for circular CFT beam-columns} \qquad\qquad\qquad ….. (6.13)$$

$$_y = 0.7 \quad \text{for square CFT beam-columns} \qquad\qquad\qquad …. (6.14)$$

(3) Comparisons between Proposed Hysteretic Model and Experimental Results

Figure 6.22 shows comparisons between the proposed trilinear skeleton model and the test results of the specimens in the US-Japan Cooperative Research Program. The proposed model underestimates the ultimate moment. This is because the ultimate flexural strength proposed in this paper gives average value for eccentrically loaded or pure bended CFT columns, and because moment enhancement by the extra confinement from the loading stubs is frequently observed in the tests of beam-column specimens with stiff loading stubs. This moment enhancement is considered as a safety margin in practical structural design. Figure 6.23 shows comparisons of the hysteretic behavior, where the normal trilinear hysteretic rule is applied in the model. The model can give a good prediction for rotation angles within about 1%, which covers the deformation range expected in the ordinary design of buildings, while it overestimates the hysteretic energy for drift angles over 1% because of the difference of the stiffness on unloading.

Recently, more precise analysis is required to show the performance of building structures, which frequently requires the inelastic dynamic analysis of building structures. The proposed hysteretic model for CFT beam-columns can be used with high reliability based on experimental verification.

CHAPTER 7: TRIAL DESIGN AND MERITS OF CFT COLUMN SYSTEM

An actual merit of the CFT column system in a real building structure has not yet been clearly proved. It is very important to define the merit of CFT system in comparison with structural steel system, when it is applied to a real building structure. From this perspective, trial design of CFT theme structures based on the design formulas presented in the preceding chapters have been performed in an attempt to achieve this objective.

7.1 Theme Structures
7.1.1 Geometry

Theme structures treated here are 10, 24 and 40-story unbraced building frames made of CFT or structural steel system as shown in Figure 7.1, and they have a typical framing floor plan as shown in Figure 7.2 [7.1]. CFT or structural steel is used for columns and H-shaped structural steel member is used for beams.

All frames were designed according to the current Japanese practice [7.2], that is, the allowable stress design against the seismic shear force under moderate earthquake, and the check for the ultimate horizontal strength of the designed frame against severe earthquake. The story shear used in the allowable stress design is given by the following design formulas [7.3].

$$Q_i = C_i \cdot \sum_{j=j+1}^{n} W_j \qquad \qquad .....(7.1)$$

$$C_i = R_t \cdot Z \cdot A_i \cdot C_o \qquad \qquad .....(7.2)$$

$$A_i = 1 + \frac{1}{\sqrt{a_i}} \cdot a_i \cdot \frac{2T}{1+3T} \qquad \qquad .....(7.3)$$

where, W_j : weight of the j-th story,

R_t : $\qquad R_t = 1.0$ when $T < T_c$

$\qquad \qquad R_t = 1.0 - 0.2(T/T_c - 1)^2$ when $T_c \le T < 2T_c$

$\qquad \qquad R_t = 1.6T_c/T$ when $2T_c \le T$,

T : first natural period of the building,,

T_c : natural period of the ground below the building with the value of 0.4, 0.6 or 0.8 according to the kind of ground,

Z : factor of seismic zone with the value of 0.7, 0.8, 0.9 or 1.0 according to the seismic map of Japan, and

a_i : ratio of the weight supported by the i-th story to the whole building weight above the ground level.

It was assumed that $R_t = 1.0$ for 10-story frame, 0.6 for 24-story frame, 0.5 for 40-story frame, $Z = 1.0$, and $C_o = 0.2$. Here, the value of R_t for 24-story and 40-story frames were not calculated directly by the equation described above, and were selected by the experienced design value for each height of building, because the height of them exceed the capable range of the equation in the current Japanese practice.

The ultimate horizontal strength was calculated by the pushover analysis, and it was verified that the strength of each story exceeded D_s and F_{es} times Q_i given by Equation 7.1 with $C_o = 1.0$, where D_s is the structural characteristic value and was taken equal to 0.25, and F_{es} is the building shape factor and was taken equal to 1.0. Table 7.1 shows the characteristics of each theme structure used in the trial design and kinds of analysis performed. In the trial design, plastic hinges mainly formed in beams, and the columns remain elastic until mechanism state, except for a few cases such as the column bases in the 1st story. Executed were elastic static and dynamic analyses using full stiffness matrix of an entire structure, pushover analysis to obtain $Q - d$ relation of each story, and elasto-plastic dynamic analyses. Elasto-plastic dynamic analysis was performed only for 24-story frames.

7.1.2 Load Conditions

Table 7.2 shows the intensities of gravity loads, which are normally employed in the design practice of a typical office building in Japan. The intensity of live load is different for the design under the long-term gravity load, and for the design under the short-term seismic load. Table 7.3 shows the intensity of gravity load calculated for each story indicated, which is used for the seismic design. The value per unit floor area is approximately 8.8 kN/m^2. Shear force acting in each story Q_i was calculated from Equations 7.1 to 7.3.

7.2 Trial Design

7.2.1 Design Conditions

The objective of the trial design is to find merits of CFT system in a common design, by investigating the difference between the behavior of CFT and structural steel systems. In a common seismic design of a building structure, the concept of weak beam and strong column has been adopted to avoid energy concentration to a specific story. Thus, the following design conditions were adopted in this study.

1) The ratio of the stress in the column caused by the design load to the allowable stress was kept as near to 0.8 as possible, and that of the beam as near to 1.0 as possible.
2) Story drift angles were kept within 1/200 under the design load in the allowable stress design.
3) The collapse mechanism at the ultimate state was the overall frame mechanism in which the plastic hinges formed only in beams, and all columns remained elastic except for the specific part such as the bottom ends of columns at the lowest story.

Table 7.4 shows the list of members for 40-story frames proportioned by the design conditions.

7.2.2 Analysis of Designed Frame

(1) Elastic Stress Analysis

The following treatments and assumptions were made for the model of elastic stress analysis, which was to obtain design stresses. These were basically applied to other analyses described later in this paper.

1) Bending, shear and axial deformations were considered for columns.

2) Bending and shear deformations were considered for beams.

3) The floor of each story was assumed as a rigid horizontal diaphragm.

4) Stiffness of CFT columns was calculated as a simple sum of stiffness of steel and concrete.

5) Multiplying factor to take the effect of slabs on the stiffness of beams was assumed 1.5 for one side slab and 2.0 for both side slabs.

3-dimensional analysis by stiffness matrix method was used for elastic stress analysis.

(2) Elastic Dynamic Analysis

Lumped mass model with 3 degrees of freedom was used for elastic dynamic analysis. The stiffness in each story was determined by diminishing the full stiffness matrix used in the elastic stress analysis. Newmark's b method for integration with time interval of 0.01 second was adopted for the analysis, and damping constant was assumed to be 0.02 for critical damping, which was proportional to the stiffness. Input seismic ground motions shown in Table 7.5, with maximum velocity level scaled to 25cm/sec and time interval of 0.01 second, were adopted for the analysis.

(3) Pushover Analysis

The following treatments and assumptions were made for the model of pushover analysis in addition to those adopted in the elastic stress analysis.

1) $M - q$ relation assumed for beam ends was normal bilinear, which changed the stiffness at the full plastic moment, having the second stiffness equal to 1/100 of the first.

2) Columns were assumed to remain elastic until the end of analysis since the plastic hinge formed only in beams.

3-dimensional analysis by stiffness matrix method was used for elasto-plastic pushover analysis. Yielding in beams was considered by using the model of rigid-plastic rotational spring at the member ends in the analysis.

(4) Elasto-Plastic Dynamic Analysis

Elasto-plastic dynamic analysis was performed by using one frame model in Y-direction extracted from the 24-story frames, to consider the hysteresis of each member directly in the analysis at every step. Shear deformations at beam-to-column connections were considered in addition to the deformations considered in the elastic stress analysis. Input seismic ground motions shown in Table 7.5, with maximum velocity level scaled to 50cm/sec and time interval of 0.005 second, were adopted for the analysis. Hysteresis models adopted for

columns and beams are shown in Table 7.6.

7.2.3 Results of Analysis

All results of trial design are shown in the form of comparison between CFT and structural steel.

(1) Results of Elastic Stress Analysis

The weight and stiffness of 40-story frames are shown in Table 7.7, which reveals the following characteristics.

1) The weight of CFT column is 2.1 to 3.3 times larger than that of structural steel column.

2) The cross sectional axial stiffness of CFT column is 1.5 to 2.2 times larger than that of structural steel column.

3) The cross sectional bending stiffness of CFT column is 1.1 to 1.5 times larger than that of structural steel column.

4) The story weight of CFT system is 1.1 to 1.16 times larger than that of structural steel system.

5) The story shear stiffness of CFT system is 1.1 to 1.3 times larger than that of structural steel system.

The story drifts of 40-story frames under the design load are shown in Table 7.8. The story drifts of CFT frame in lower stories are larger than those of structural steel frame, while the former becomes smaller than the latter in upper stories. Figure 7.3 shows each story displacement of CFT frames and components caused by the bending and shear deformations of beams and the bending, shear and axial deformations of columns. The story displacements caused by beam deformation d_B and column axial deformation d_C were calculated by the following equations.

$$d_B = d_0 - d_1$$
$$d_C = d_0 - d_2$$

where,

d_0 : Total story displacement,

d_1 : Story displacement obtained from the analysis with making the bending and shear stiffness of beams 10000 times larger than the designed values, and

d_2 : Story displacement obtained from the analysis with making the axial stiffness of columns 10000 times larger than the designed values.

It is observed from Figure 7.3 that 60 to 70% of the total story displacement is caused by beam deformation and the rest is caused by column deformation in all cases of 3 frames analyzed. The proportion of axial deformation of the column to the total story displacement increases as the number of story increases, and it becomes as large as 30% in the case of 40-story frame.

(2) Results of Elastic Dynamic Analysis

Figure 7.4 shows examples of vibration mode shapes and Table 7.9 shows the 1st natural period of vibration.

There's only 2% difference between CFT and structural steel.

Figure 7.5 shows the maximum response of the shear coefficients caused by El Centro. No significant difference is observed between CFT and structural steel systems.

(3) Results of Pushover Analysis

Figure 7.6 shows $Q - d$ relations of 2nd and 9th floors of 40-story frames. Table 7.10 shows the energy absorbed until the drift angle reaches 1/100, which is the area enclosed by the $Q - d$ curve, the horizontal axis and the vertical line at the drift angle of 1/100. The following observations are made.

1) Yield story shear forces of CFT and structural steel systems are almost the same, because the overall frame mechanism with beam hinges is adopted.

2) The energy absorbed in one story of CFT system at drift angle of 1/100 is larger by 4 to 8% than that of structural steel system.

(4) Results of Elasto-Plastic Dynamic Analysis

Table 7.11 and Figure 7.7 show maximum responses. From these results the following features can be observed.

1) The maximum story shear coefficient of CFT system is smaller by 5 to 8% than that of structural steel system.

2) The maximum overturning moment of CFT system is larger by 2 to 8% than that of structural steel system. The difference may be caused mainly by the difference of mass of each system.

3) No significant difference regarding the maximum story drift can be found between CFT and structural steel systems.

Figure 7.8 shows maximum response of ductility factors of beams and columns, and Figure 7.9 shows the plastic hinge formation in beams and columns. From these results the following features can be observed.

1) Ductility factors of beams stay within 3.0 at all stories, which are within the supposed performance of beams of 4.0. Ductility factors of CFT and structural steel columns measured in comparison with elastic deformation corresponding to M_p stay within 0.6 at all stories.

2) Yielding occurred at the bottom of columns at the 1st story of CFT system, and no hinges are generated in any columns in structural steel system. This is derived from the difference of the definition of the first yielding between two systems, that is, the first yielding point is defined by M_y for CFT and M_p for structural steel columns. The pattern of hinge generation in beams is very similar between two systems.

7.2.4 Amount of Steel and Cost Estimation

Figure 7.10 shows the comparison of steel amount per unit floor area used for CFT and structural steel systems, and its ratio. Total steel amount includes steel used for columns, beams and sub-beams for entire building. Plates and bolts for connections and reinforcing bars for floor slabs, foundation beams and footings are not included,

which may be almost the same in both CFT and structural steel systems. The total steel amounts per unit floor area of 3 structural steel frames are 105 kg/m^2 for 10-story frame, 143 kg/m^2 for 24-story frame and 189 kg/m^2 for 40-story frame. These numbers are within a reasonable comparable range compared with those in the existing buildings. The steel amount of CFT columns is less by about 25% than that of structural steel columns, and the total steel amount of CFT system is less by about 10% than that of structural steel system.

Table 7.12 shows a cost estimation of main frames including columns, beams and sub-beams. The unit cost is assumed to be 250,000 yen per ton for structural steel, and 35,000 yen per cubic meters for concrete. These unit costs include materials, fabrications, transportation, and constructions. The cost of main frames for CFT system is lower by 5 to 7% than that of structural steel system. The total building cost for CFT system would be lower by 1% than that of structural steel system, if the cost of main frame structure is assumed to occupy 15% of the total building cost. As the number of stories increases, the cost merit of CFT system becomes larger

CHAPTER 8: SUMMARIES AND FUTURE RESEARCH NEEDS

8.1 Summary of Each Chapter

(1) Summary of Chapter 1

The overview of the research on the Japanese side on concrete-filled structural steel tube (CFT) column system was presented in Chapter 1. It includes the definition of the composite and hybrid structures, in which CFT column system is positioned. The status of CFT column system in Japan is next briefly summarized. As for the research on CFT column system, various research issues on this topic are raised and they are prioritized. Finally, the concrete research plan is summarized. The concrete research plan includes both experimental and analytical investigations and design implication study through trial design is also included.

(2) Summary of Chapter 2

The ultimate strength and load vs. deformation relationships of the CFT columns with circular and square sections are investigated based on the experimental results of 114 centrally loaded stub columns. The following conclusions are reached on the bases of the study.

1) As for the ultimate strength of circular CFT columns, the difference between the ultimate strength and the nominal squash load, which is provided by the confining effect on concrete strength, can be estimated as a linear function of the tube yield strength. The biaxial stress state of the circular steel tube at the ultimate strength is estimated based on the analytical procedure in which yield criteria for the steel and concrete are assumed to be ones proposed by Mises and Richart, respectively.

2) Formula for a capacity reduction factor due to the local buckling of the steel tube was first empirically derived from the test data of centrally loaded steel columns of thin-walled hollow square tube. Then, it is modified to the reduction factor applicable to the steel tube in a CFT column by considering restraining effect of filled concrete on the local buckling of steel tube. This enables the estimation of ultimate strength of square CFT columns with thin-walled steel tube, which is smaller than the nominal squash load due to the local buckling of the steel tube.

3) Stress vs. strain models for concrete in CFT columns are formulated based on Sakino-Sun's model which has been proposed for concrete confined by a square steel tube acting only as the transverse reinforcement so-called as a steel jacket.

4) Stress vs. strain model for a square steel tube is formulated based on the experimental results.

(3) Summary of Chapter 3

The ultimate strength and load vs. deformation relationships of the CFT columns with circular and square sections were investigated based on the experimental results of 65 eccentrically loaded stub columns. The followings are observed from the study.

1) Bending strength of eccentrically loaded circular CFT columns exceeded the superposed strength due to the confinement effect regardless of the combination of material strength of steel tube and filling

concrete.

2) Use of the high strength concrete generally caused the reduction of ductility of a circular CFT column. However, it was made clear that such a non-ductile flexural behavior was improved by confining the concrete with high strength steel tube.

3) Increase in bending strength due to the confinement effect could not be expected in the case of square CFT columns. Moreover, the effect of local buckling must be considered.

4) Fiber analysis generally well traced the flexural behavior of eccentrically loaded CFT columns, and estimated well the ultimate strength obtained in the tests. Here, the scale effect on concrete strength, confinement effect on concrete strength and change in nominal yield stress of a circular CFT columns, and the reduction in nominal compressive yield stress of square steel tube due to local buckling are included in the analytical models.

(4) Summary of Chapter 4

The ultimate strength and load vs. deformation relationships of the CFT beam-columns with circular and square sections were investigated based on the experimental results of 33 beam-columns. The main findings are summarized in the followings.

1) Circular CFT beam-columns show superior ductility than square ones.

2) Ductility becomes larger as the steel tube strength becomes higher, and it generally becomes smaller as the filled concrete strength becomes higher. However, concrete strength has a little influence in the case of the CFT beam-columns with high strength steel tube. To utilize high strength concrete, use of high strength steel tube is effective.

3) Ductility of CFT beam-columns reduces under the variable axial load. It is because the damage produced by the combined action of the lateral and axial loads concentrates on one of the flanges of the beam-columns both in the positive and negative loadings.

4) Enhancement in moment resisting capacity by the confinement effect from steel tube can be expected in circular CFT beam-columns, while it cannot be expected in square CFT beam-columns. Extra confinement from the footing and top stub of the specimens is admitted in both circular and square CFT beam-columns.

5) Square CFT beam-columns show almost identical structural performance independent to the loading directions.

6) The proposed analytical models in Chapters 2 and 3 are effective to represent the hysteretic behavior of CFT beam-columns, except for the behavior after local buckling in the circular CFT beam-columns under the high compressive axial load.

(5) Summary of Chapter 5

The ultimate strength and load vs. deformation relationships of the CFT beam-to-column subassembladges are studied based on the experimental results of 11 beam-to-column specimens. The main findings are summarized in the followings.

1) All subassemblies yielded at the shear panel, showing very good performance in elasto-plastic region and indicated very ductile behavior. The gradual failure of panel occurred and no rapid loss of strength was observed The intense buckling of steel tube and the crash of concrete also did not occurred Circular subassemblies showed more ductile performance than rectangular subassemblies.

2) The shear panel contributed to share a large part of displacement in the overall displacement of . subassemblies in plastic stage. Beams and columns preserved being almost elastic through testing. However, when the exterior specimens subjected to tensile axial force, the contribution of shear panel decrease the share in overall displacement as the cracks of the concrete in the panel zone had occurred

3) Combination of strength of steel tube and filled concrete affected the maximum strength and the behavior of specimens. Subassemblies of which the tube of panel was made of higher strength steel showed the higher maximum strength. However, the specimens showed a little bit steeper degradation of shear force carrying capacity after the maximum strength. This was true for both rectangular and circular subassemblies,

4) The yield and ultimate strength of specimens were greater than the shut-term allowable strength and the ultimate strength of shear panel by SRC code of AIJ

5) The skeleton curves of the relationships between shear force and shear deflection angle of panels of rectangular subassemblies were discussed on the basis of arch mechanism in the shear panel. The confinement effect of the filled concrete in the shear panel was considered in the calculation The obtained skeleton curves gave nearly good expressions with the actual relationships of specimens

6) Three dimensional FEM analysis simulated well the behavior and the ultimate strength of both rectangular and circular subassemblies. The appropriate idealization of softening zone in concrete stress-strain relationship after the maximum strength gave good simulations with the experimental results. Confining concrete by a steel tube and diaphragms did not contribute to increase in strength. but did contribute to increase the ductility of panels

7) Shear force transferred by concrete and steel in panel obtained by the three dimensional FEM analysis on actual specimens and by the numerical simulation. Shear force transferred by steel in elastic to plastic zone was evaluated with the bi-linear relation Shear force transferred by concrete almost proportionally decreased with the decrease of beam depth - column depth ratios.

(6) Summary of Chapter 6

The design formulas for axial compressive load capacity, ultimate moment and deformation capacity of the CFT columns with circular and square sections are proposed based on experimental results of specimens which were planned to obtain a wide range of test data usable to establish a generally applicable design methods of CFT column systems. The proposed design formulas have following features.

1) The confinement effect in circular CFT columns, which has been ignored for a long time in AIJ Standards for structural calculation of SRC structures as well as ACI Code, is taken into consideration by assuming that a magnitude of hoop tension in steel tube at the ultimate state is $-0.19{}_{s}s_{sy}$. The ultimate moment of steel tube is estimated as the full plastic moment of the steel tube with the hoop

tension of $-0.19s_{sy}$, and that of the concrete is estimated based on the ultimate strain and shape factors of stress block of concrete confined by the steel tube with the hoop tension of $-0.19s_{sy}$.

2) The capacity reduction due to the effect of the local buckling of steel tube is introduced to design formulas of square CFT columns with large B/t ratio. Thus, the ultimate moment of square CFT columns within the applicable limitations of AIJ Standards for structural calculations of SRC structures is estimated as the full plastic moment, and that of the columns out of the applicable limitations can be estimated by the proposed method in which the ultimate strain and shape factors of stress block for plain concrete and the effect of the local buckling of steel tube are taken into considerations.

3) The design formulas for the limit rotation angle R_u of the CFT columns with circular and square sections are proposed as an index of deformation capacity of the columns. The estimation of R_u makes it possible to classify the CFT columns into four from the viewpoint of ductility demand according to the Japanese Building Standard Law.

(7) Summary of Chapter 7

From the studies of the trial design, the characteristics and merits of CFT column systems are summarized as follows.

1) The lateral story stiffness of CFT column system is larger than that of structural steel system. The story weight of CFT column system becomes larger than structural steel system, too. This leads to the similar vibration characteristic of CFT and structural steel systems.

2) No major difference in natural periods and elastic responses was observed between CFT and structural steel systems.

3) No significant difference in the energy absorption capability and the elasto-plastic behavior was observed between CFT and structural steel systems, as far as the overall frame mechanism was adopted.

4) Total steel consumption of CFT column system for entire building was less by about 10% than that of structural steel system.

5) Within the assumption of the unit costs of steel and concrete, the cost of main frame structure became lower by about 6% than that of structural steel system.

To sum up, cost merit was found in CFT column system compared to structural steel system. However, no significant merits of CFT column system could be found in terms of static and dynamic behavior within the range of small story drift of 1/100, considered in a common structural design, compared to structural steel system. It may be said that the robustness of CFT column system beyond the range of the story drift of 1/100 supposed in a common design is higher than that of structural steel system. However, to prove the robustness of CFT column system in terms of bearing capacity and ductility, collapse analysis into the range of large story drift beyond the maximum bearing capacity, allowing the plastic hinge formation in columns, will be needed.

8.2 Future Research Needs

This series of research could not cover the verification by large frame tests. Therefore, further investigation of

large frames is necessary. The concrete filling into structural steel tubes is important in securing the structural performance of CFT column system although it cannot be inspected by the current methodology. This should also be examined in the future. The damage to CFT columns initiates from the crash of filled concrete which is not observable, and thus the evaluation of such damage is a significant issue to be solved.

ACKNOWLEDGEMENTS

REFERENCES

1.1) "Recommendations for a U.S.-Japan Cooperative Research Program utilizing Large-Scale Testing Facilities", Report No.UCB/EERC 79-26, September 1979

1.2) Architectural Institute of Japan (AIJ): "Standards for Structural Calculation of Steel Reinforced Concrete Structures", 1967 & 1981 revision

1.3) Building Standard Law of Japan

1.4) Architectural Institute of Japan (AIJ): "Standards for Structural Calculation of Steel Reinforced Concrete Structures", 1987 revision, June 20, 1987 (in Japanese)

1.5) U.S.-Japan Planning Groups Joint Planning Workshop: "Recommendations for U.S.-Japan Cooperative Research Program -Phase 5 Composite and Hybrid Structures", UMCEE92-29, 1992.11.

2.1) Blanks, R. F. and McNamara, C. C.: "Mass Concrete Tests in Large Cylinders", ACI Journal, Vol. 31, January - February, 1935, pp.280-303

2.2) Richart, F. E., Brandtzaeg, A and Brown R. L.: "The Failure of Plain and Spirally Reinforced Columns in Compression", Bulletin No.190, University of Illinois, Engineering Experimental Station, Urbana, 1929

2.3) Architectural Institute of Japan (AIJ): "Recommendations for Design and Construction of Concrete Filled Steel Tubular Structures", October 20, 1997 (in Japanese)

2.4) Sakino, K. and Sun, Y.: "Stress-Strain Curve of Concrete Confined by Rectilinear Hoop", Journal of Structural Construction Engineering of AIJ, No.461, July, 1994, pp.95-l04 (in Japanese)

2.5) Nakahara, H., Sakino, K., and Inai, E.: "Analytical Model for Axial Compressive Behavior of Concrete Filled Square Steel Tubular Columns", Proceedings of the Japan Concrete Institute, Vol.20, No.3, 1998, pp.817-822 (in Japanese)

3.1) Sakino, K., Ninakawa, T., and Matsumoto, M.: "US-Japan Cooperative Research Project on Composite and Hybrid Structures (CFT-17) Axial Compressive Behavior of Concrete Filled Circular Steel Tubular Columns", Summaries of Technical Papers of Annual Meeting of AIJ, Structures III, 1997, pp.917-918 (in Japanese)

3.2) Nakahara, H., Sakino, K., and Inai, E.: "Analytical Model for Axial Compressive Behavior of Concrete Filled Square Steel Tubular Columns", Proceedings of the Japan Concrete Institute, Vol.20, No.3, 1998, pp.171-178 (in Japanese)

3.3) Nakahara, H., and Sakino, K.: "Behavior of Concrete Filled Square Steel Tubular Columns under a Constant Gravity Load and Cyclic Bending Moment", Summaries of Technical Papers of Annual Meeting of AIJ, Structures III, 1999, pp.1241-1242 (in Japanese)

4.1) Housing Guidance Division of Ministry of Land, Infrastructure and Transport (MLIT), Japan Building Officials Conference, Building Center of Japan: "Technical Standard Manuals for Structural Regulations of Buildings", March 15, 2001 (in Japanese)

4.2) Architectural Institute of Japan (AIJ): "Recommendations for Design and Construction of Concrete Filled Steel Tubular Structures", October 20, 1997 (in Japanese)

4.3) Fujimoto, T., Mukai, A., Nishiyama, I., Noguchi, T., Baba, T., Sakino, K, and Morino, S. :"Eccentric compression test of concrete filled square steel tubular stub columns using high strength materials", Journal of Structural Construction Engineering (Transactions of AIJ), No.501, 1997, pp.173-180 (in Japanese)

4.4) Fujii, S., Aoyama, H., and Umemura, H.: "Analytical moment-curvature relationship of reinforced concrete sections based on the material characteristics", Summaries of Technical Papers of Annual Meeting of AIJ, 1973, pp.1261-1262

4.5) Meng, L., Ohi, K., and Takanashi, K.: "A simplified model of steel structural members with strength deterioration used for earthquake response analysis", Journal of Structural Construction Engineering (Transactions of AIJ), No.437, 1992, pp.115-124

4.6) Inai, E., Nishiyama, I., and Sakino, K.: "Simulation of shear-flexural behavior of concrete filled steel tubular columns, Part 1 on the analytical method", Summaries of Technical Papers of Annual Meeting of AIJ, Structures III, 1997, pp.921-922

5.1) Architectural Institute of Japan (AIJ): "Standards for Structural Calculation of Steel Reinforced Concrete Structures", 1987 revision, June 20, 1987 (in Japanese)

5.2) Fukumoto, T., Sawamoto, Y., and Morita, K.: "Connection between High-Strength Concrete-Filled Square Tubular Steel Column and Steel Beam Reinforced with Internal Diaphragm", Journal of Structural and Construction Engineering (Transactions of A IJ), No.507, May, 1998, pp.171-178 (in Japanese)

5.3) Naganuma, H.: " Stress-Strain Relationship For Concrete Under Triaxial Compression", Journal of Structural and Construction Engineering (Transactions of AIJ), No.474, August, 1995, pp.163-170 (in Japanese)

5.4) Naganuma, H.: "Orthotropic Constitutive Relationship For Concrete Considering Nonlinear Poisson: Effect Under Triaxial Stress", Journal of Structural and Construction Engineering (Transactions of AJJ), No.485, July, 1996, pp.109-116 (in Japanese)

5.5) William, K. J., and Warnke, E. P.: "Constitutive Model for the Triaxial Behavior of Concrete", Proceedings of International Association for Bridge and Structural Engineering, Vol.19, 1975

5.6) Ohnuma, H. and Aoyagi, M.: "Ultimate Strength Property of Concrete under Triaxial Compressive Stresses", Report of CRIElPI, No.381021, Dec., 1981 (in Japanese)

5.7) Yonezawa, K., Yoshioka, K. et al.: "US-Japan Cooperative Structural Research Project on Composite and Hybrid Structures (CFT-22)", AIJ Annual Convention C-1, September, 1997, pp.927-928 (in Japanese)

5.8) Sakino, K. et al.: "US-Japan Cooperative Structural Research Project on Composite and Hybrid Structures (CFT-17)", AIJ Annual Convention C-1, September, 1997, pp.917-918 (in Japanese)

6.1) Architectural Institute of Japan (AIJ): "Recommendations for Design and Construction of Concrete Filled Steel Tubular Structures", October 20, 1997 (in Japanese)

6.2) Harbin University of Civil Engineering and Architecture: "Design Code of Concrete Filled Steel Tubes (DL5099-1997)"

6.3) British Standards Institution: "BS5400,Part 5, Concrete and Composite Bridges," 1979

6.4) European Committee for Standardization: "Eurocode 4: Design of Composite Steel and Concrete Structures," 1992

6.5) Architectural Institute of Japan (AIJ): "Standards for Structural Calculation of Steel Reinforced Concrete Structures", 1987 revision, June 20, 1987 (in Japanese)

6.6) American Concrete Institute: "Building Code Requirements of Structural Concrete-ACI 318-95", 1995

6.7) Richart, F. E., Brandtzaeg, A and Brown R. L.: "The Failure of Plain and Spirally Reinforced Columns in Compression", Bulletin No.190, University of Illinois, Engineering Experimental Station, Urbana, 1929

6.8) Blanks, R. F. and McNamara, C. C.: "Mass Concrete Tests in Large Cylinders", ACI Journal, Vol. 31, January - February, 1935, pp.280-303

6.9) Sun, Y. P. and Sakino, K.: "Assessment of Ultimate Strength and Deformability of an RC Column Retrofitted by Circular Steel Tube", Proceedings of the 2nd International RILEM/CSIRO/ACRA Conference, September 21-23, 1998, pp.229-245

6.10) Sun, Y. P., Sakino, K, Aklan, A. M. and Ikenono, Y. : "Ultimate strength and Deformability of RC Column Retrofitted by Square Steel Tube", Proceedings of the 2nd International RILEM/CSIRO/ACRA Conference, September 21-23, 1998, pp.619-632

6.11) NEHRP Provisions (1994 Edition), NEHRP Recommended Provisions For Seismic Regulations For New Buildings, Part 1 – Provisions, Building Seismic Safety Council, Washington, D.C. 1994

7.1) U.S.-Japan Planning Groups Joint Planning Workshop: Recommendations for U.S.-Japan Cooperative Research Program -Phase 5 Composite and Hybrid Structures, UMCEE92-29, 1992.11.

7.2) Housing Guidance Division of Ministry of Land, Infrastructure and Transport (MLIT), Japan Building Officials Conference, Building Center of Japan: "Technical Standard Manuals for Structural Regulations of Buildings", March 15, 2001 (in Japanese)

7.3) Building Standard Law of Japan

Table 1.1 High Priority Research Topics Recommended in the Joint Planning Workshop [1.5]

HIGH PRIORITY RESEARCH TOPICS

Research Topic	Experimental and Analytical Basic Studies				Experimental Subassemblies		Experimental Structures			Analytical Studies of Structural Bodies		Design Studies	
	Materials	Interation of Materials	Components	Scale effects; Rate of Loading, etc.	2-D	3-D	Quasi-static	Shaking Table	Field	Modeling of Behavior	Parametric and Design Studies	Design Studies	Design Guidelines
Beam-Columns: Effect of Confinement vs. Composite		E	E							E	E		
Method of Evaluation		E	E	E						E	E		M
Bond and Shear Transfer		E	E	E						E	E		M
Columns: Creep, Shrinkage (High Rise)	M	M	M	M									M
Connections: Force & Moment Transfer			E		E	?				E	E	E	E
Panel Zone behavior										M	M	M	M
Frames: Analytical Studies Combining Above							L	?	?	L	L	L	L
Analysis of Braced Frames							L	?	?	L	L	L	L
Very High Strength Concrete	E	E	E										M
Literature Survey		E or M	E or M										

E, M and L identify topics which should be done early, intermediate or late in the proposed five year research program, respectively.

Some categories are noted with a (?), and these identify areas which are desirable if funds are available.

Table 1.2 Medium Priority Research Topics Recommended in the Joint Planning Workshop [1.5]

MEDIUM PRIORITY RESEARCH TOPICS

Research Topic	Experimental and Analytical Basic Studies				Experimental Subassemblies		Experimental Structures			Analytial Studies of Strucrtural Bodies		Design Studies	
	Materials	Interation of Materials	Components	Scale effects; Rate of Loaidng, etc.	2-D	3-D	Quasi-static	Shaking Table	Field	Modeling of Behavior	Parametric and Design Studies	Design Studies	Desing Guidelines
Columns: Buckling	M	M	M	-	-	-	-	-	-	M	M	-	M
Non-Traditional Connection Design	*	*	*	*	*	-	-	-	-	*	*	*	-
Construction: Placement of Concrete & As Built vs. Design	M	-	M	-	?	-	-	-	-	-	-	-	M
Construction Loads	-	-	-	-	-	-	-	-	-	M	-	-	M
Frames: Composite, Confinement only, or Both	-	-	-	-	-	-	-	-	-	L	L	L	L

Some categories are noted with a (*), and these identify areas which can not be classified into H, M or L in the workshop.

Table 1.3 Test Program of Centrally and Eccentrically Loaded Stub Columns

Shape	Steel[1]	Rank	B, D (mm)	t (mm)	B/t D/t	Concrete	Number of specimens	
							CLSC	ELSC
	400	FA	148		34	0 (void) Fc20 Fc40 Fc80	23[2]	11
		FC	216	4.38	49			
		FD	324		74			
	590	FA	144		23	0 (void) Fc20 Fc40 Fc80	23[2]	11
		FC	211	6.36	33			
		FD	318		50			
	780	FA	120		19	0 (void) Fc20 Fc40 Fc80	23[2]	10
		FC	175	6.47	27			
		FD	264		41			
	400	FA	149		50	0 (void) Fc20 Fc40 Fc80	15	11
		FC	300	2.96	101			
		FD	450		152			
	590	FA	122		27	0 (void) Fc20 Fc40 Fc80	15	11
		FC	238	4.54	52			
		FD	360		79			
	780	FA	108		17	0 (void) Fc20 Fc40 Fc80	15	11
		FC	222	6.47	34			
		FD	336		52			

CLSC: centrally-loaded stub column

ELSC: eccentrically-loaded stub column

[1] Nominal tensile strength of steel, S_u, in MPa.

[2] Eight specimens among 23 are additionally conducted specimens, so they have different B, D and t from standard ones. Detailed dimensions of these specimens are in Table 2.1 and Table 2.2(b).

Table 1.4 Test Program of CFT Beam-Columns

Shape	Steel[1]	Rank	B, D (mm)	t (mm)	B/t D/t	Concrete	N/N_0	Number of specimens
	400	FA	210	5.80	35	Fc40	0.4	4
		FC		4.50	47	Fc90		
	590	FA	210	8.83	23	Fc40	0.4	8[2]
		FC		5.95	35	Fc90	variable	
	780	FA	180	9.45	19	Fc40	0.4	8[3]
		FC		6.66	27	Fc90	variable	
	400	FA	240	4.70	51	Fc40	0.4	2
		FC		-	-	Fc90		
	590	FA	240	9.00	27	Fc40	0.4	6
		FC		4.52	53	Fc90	variable	
	780	FA	160	9.12	17	Fc40	0.4	5
		FC		4.76	34	Fc90	variable	

[1] Nominal tensile strength of steel, $\mathbf{S}_u$, in MPa.

[2] Two specimens among eight are subjected to biaxial bending.

[3] One specimen among eight is subjected to biaxial bending.

Table 1.5 Test Program of Beam-to-Column Connections

Connection type	Tube shape	Diaphragm type	Steel[1]	Concrete	Panel Section	B/t D/t	N/N_0	Number of specimens
		Through	590	Fc40 Fc90	-250x4.5	55	0.2	3[2]
			780				0.2	1
		Outer	590				0.2	1
		Ring	590	Fc40 Fc90	-280x4.5	60	0.2	2
			780				0.2	1
		Through	590	Fc90	-160x3.0	55	variable	2[3]
					-180x3.0	60		1

[1] Nominal tensile strength of steel, S_u, in MPa.

[2] One specimen among three is a three-dimensional beam-to-column connection specimen.

[3] One of the two specimens was loaded constant axial force in spite of exterior joint.

Table 2.1 Results of Axial Compressive Tests of Steel Tubes Used for CFT Specimens

*	Specimen	D,B (mm)	t (mm)	D/t or B/t	σ_{sy} (MPa)	σ_{scy} (MPa)	σ_{su} (MPa)	ε_{su} (%)
1	CC4-A-0	149	2.96	50.2	283	308	340	1.21
2	CC4-C-0	301	2.96	102	283	279	284	0.46
3	CC4-D-0	450	2.96	152	283	-	273	0.28
4	CC6-A-0	122	4.54	26.8	579	576	636	1.79
5	CC6-C-0	238	4.54	52.5	579	507	531	0.65
6	CC6-D-0	360	4.54	79.3	579	525	548	0.60
7	CC8-A-0	108	6.47	16.6	835	853	940	1.73
8	CC8-C-0	222	6.47	34.3	835	843	875	0.74
9	CC8-D-0	336	6.47	52.0	835	823	863	1.22
10	CR4-A-0	149	4.38	33.9	262	287	300	0.50
11	CR4-C-0	215	4.38	49.0	262	-	227	0.22
12	CR4-D-0	323	4.38	73.8	262	-	157	0.14
13	CR6-A-0	144	6.36	22.7	618	632	651	1.01
14	CR6-C-0	211	6.36	33.2	618	-	587	0.28
15	CR6-D-0	318	6.36	50.0	618	-	413	0.32
16	CR8-A-0	120	6.47	18.5	835	848	908	1.37
17	CR8-C-0	175	6.47	27.0	835	-	799	0.50
18	CR8-D-0	265	6.47	40.9	835	-	555	0.59
19	CR4-A-0-2	211	5.84	36.1	294	315	324	0.39
20	CR4-C-0-2	211	4.50	46.9	277	-	263	0.24
21	CR6-A-0-2	210	8.83	23.8	536	540	635	0.98
22	CR6-C-0-2	204	5.95	34.3	540	-	504	0.35
23	CR8-A-0-2	180	9.45	19.0	825	656	913	1.33
24	CR8-C-0-2	180	6.60	27.3	824	-	799	0.50
25	CR4-A-0-2'	137	5.84	23.5	294	334	381	1.68
26	CR4-C-0-2'	100	4.50	22.2	277	328	364	1.82
27	CR6-A-0-2'	150	8.83	17.0	536	572	727	2.53
28	CR6-C-0-2'	102	5.95	17.1	540	605	772	2.74
29	CR8-A-0-2'	155	9.45	16.4	825	820	927	2.18
30	CR8-C-0-2'	102	6.60	15.5	824	802	941	2.81

D, B : Diameter or width of steel tube, t : wall-thickness of steel tube,

σ_{sy} : yield stress of steel tube obtained by tensile test,

σ_{scy} : yield stress of steel tube obtained by the stub column test,

σ_{su} : maximum stress of steel tube obtained by the stub column test, ε_{su} : axial strain at σ_{su}

*19~30 : specimens for the second phase tests

```
C  C  4 - A - 4 - 1
                    └─┬─┘ Identifying Number for Specimens
                         with Same Parameters
               └──── Planed Strength of Concrete
                     (0: Hollow Steel Tube, 2 : 20MPa, 4 : 40MPa, 8 : 80MPa, 9 : 90MPa)
           └──────── Class of Steel Tube Corresponding to the Local Buckling Stress
       └──────────── Tensile Stress of Steel Tube (4 : 400MPa, 6 : 590MPa, 8 : 780MPa)
    └─────────────── Tube Shape (C : circular, R : rectangular)
 └────────────────── Loading Condition (C : centrally compression)
```
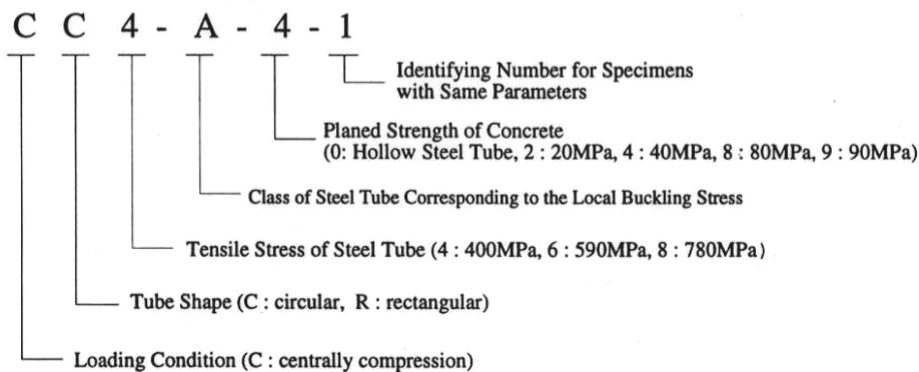
Table 2.2(a) Experimental Variables and Test Results (Circular CFT)

	Specimen	D (mm)	t (mm)	σ_{sy} (MPa)	f_c' (MPa)	D/t	α_c	r_U	N_{exp} (kN)	N_{exp}/N_0
1	CC4-A-2	149	2.96	308	25.4	50.4	0.075	0.96	941	1.16
2	CC4-A-4-1	149	2.96	308	40.5	50.3	0.075	0.96	1064	1.02
3	CC4-A-4-2	149	2.96	308	40.5	50.4	0.075	0.96	1080	1.03
4	CC4-A-8	149	2.96	308	77.0	50.5	0.075	0.96	1781	1.11
5	CC4-C-2	301	2.96	279	25.4	101.5	0.137	0.88	2382	1.04
6	CC4-C-4-1	300	2.96	279	41.1	101.4	0.137	0.88	3277	1.01
7	CC4-C-4-2	300	2.96	279	41.1	101.4	0.137	0.88	3152	0.97
8	CC4-C-8	301	2.96	279	80.3	101.5	0.137	0.88	5540	0.99
9	CC4-D-2	450	2.96	279	25.4	152.0	0.206	0.84	4415	0.99
10	CC4-D-4-1	450	2.96	279	41.1	152.0	0.206	0.84	6870	1.05
11	CC4-D-4-2	450	2.96	279	41.1	152.0	0.206	0.84	6985	1.07
12	CC4-D-8	450	2.96	279	85.1	152.0	0.206	0.84	11665	0.95
13	CC6-A-2	122	4.54	576	25.4	26.9	0.075	0.98	1509	1.24
14	CC6-A-4-1	122	4.54	576	40.5	26.8	0.075	0.98	1657	1.22
15	CC6-A-4-2	122	4.54	576	40.5	26.8	0.075	0.98	1663	1.22
16	CC6-A-8	122	4.54	576	77.0	26.8	0.075	0.98	2100	1.23
17	CC6-C-2	239	4.54	507	25.4	52.5	0.129	0.91	3035	1.15
18	CC6-C-4-1	238	4.54	507	40.5	52.5	0.129	0.91	3583	1.12
19	CC6-C-4-2	238	4.54	507	40.5	52.4	0.129	0.91	3647	1.14
20	CC6-C-8	238	4.54	507	77.0	52.4	0.129	0.91	5578	1.22
21	CC6-D-2	361	4.54	525	25.4	79.4	0.202	0.87	5633	1.17
22	CC6-D-4-1	361	4.54	525	41.1	79.4	0.202	0.87	7260	1.19
23	CC6-D-4-2	360	4.54	525	41.1	79.3	0.202	0.87	7045	1.15
24	CC6-D-8	360	4.54	525	85.1	79.4	0.202	0.87	11505	1.17
25	CC8-A-2	108	6.47	853	25.4	16.7	0.069	1.00	2275	1.17
26	CC8-A-4-1	109	6.47	853	40.5	16.8	0.069	1.00	2446	1.19
27	CC8-A-4-2	108	6.47	853	40.5	16.7	0.069	1.00	2402	1.17
28	CC8-A-8	108	6.47	853	77.0	16.7	0.069	1.00	2713	1.17
29	CC8-C-2	222	6.47	843	25.4	34.3	0.140	0.92	4964	1.10
30	CC8-C-4-1	222	6.47	843	40.5	34.3	0.141	0.92	5638	1.13
31	CC8-C-4-2	222	6.47	843	40.5	34.3	0.140	0.92	5714	1.15
32	CC8-C-8	222	6.47	843	77.0	34.4	0.141	0.92	7304	1.19
33	CC8-D-2	337	6.47	823	25.4	52.1	0.208	0.87	8475	1.15
34	CC8-D-4-1	337	6.47	823	41.1	52.0	0.208	0.87	9668	1.14
35	CC8-D-4-2	337	6.47	823	41.1	52.0	0.208	0.87	9835	1.16
36	CC8-D-8	337	6.47	823	85.1	52.0	0.208	0.87	13776	1.18
	mean	254	4.66	555	46.7	62.8	0.138	0.92	4961	1.13
	max	450	6.47	853	85.1	152.0	0.208	1.00	13776	1.24
	min	108	2.96	279	25.4	16.7	0.069	0.84	941	0.95

D : Diameter of steel tube, t : wall-thickness of steel tube, σ_{sy} : yield stress of steel tube,

f_c': strength of concrete cylinder, D/t : diameter-to-wall-thickness ratio, α_c : normalized D/t ratio,

r_U : scale effect factor, N_{exp} : maximun axial load, N_0 : nominal squash load

Table 2.2(b) Experimental Variables and Test Results (Square CFT)

*	Specimen	B (mm)	t (mm)	σ_{sy} (MPa)	f_c'(MPa)	B/t	$\sqrt{\alpha_s}$	r_U	N_{exp} (kN)	N_{exp}/N_0
1	CR4-A-2	148	4.38	262	25.4	33.9	1.21	0.95	1153	1.04
2	CR4-A-4-1	148	4.38	262	40.5	33.8	1.21	0.95	1414	1.02
3	CR4-A-4-2	148	4.38	262	40.5	33.8	1.21	0.95	1402	1.01
4	CR4-A-8	148	4.38	262	77.0	33.8	1.21	0.95	2108	1.03
5	CR4-C-2	215	4.38	262	25.4	49.1	1.75	0.91	1777	0.92
6	CR4-C-4-1	215	4.38	262	41.1	49.1	1.75	0.91	2424	0.96
7	CR4-C-4-2	215	4.38	262	41.1	49.0	1.75	0.91	2393	0.95
8	CR4-C-8	215	4.38	262	80.3	49.0	1.75	0.91	3837	0.95
9	CR4-D-2	323	4.38	262	25.4	73.7	2.63	0.85	3367	0.94
10	CR4-D-4-1	323	4.38	262	41.1	73.7	2.63	0.85	4950	1.01
11	CR4-D-4-2	323	4.38	262	41.1	73.7	2.63	0.85	4830	0.99
12	CR4-D-8	324	4.38	262	80.3	73.9	2.63	0.85	7481	0.91
13	CR6-A-2	144	6.36	618	25.4	22.7	1.24	0.96	2572	1.04
14	CR6-A-4-1	144	6.36	618	40.5	22.7	1.24	0.96	2808	1.03
15	CR6-A-4-2	144	6.36	618	40.5	22.7	1.24	0.96	2765	1.02
16	CR6-A-8	144	6.36	618	77.0	22.6	1.24	0.96	3399	1.03
17	CR6-C-2	211	6.36	618	25.4	33.1	1.82	0.91	3920	0.98
18	CR6-C-4-1	211	6.36	618	40.5	33.2	1.82	0.91	4428	0.97
19	CR6-C-4-2	211	6.36	618	40.5	33.1	1.82	0.91	4484	0.99
20	CR6-C-8	211	6.36	618	77.0	33.1	1.81	0.91	5758	0.99
21	CR6-D-2	319	6.36	618	25.4	50.1	2.75	0.85	6320	0.92
22	CR6-D-4-1	319	6.36	618	41.1	50.1	2.74	0.85	7780	0.96
23	CR6-D-4-2	318	6.36	618	41.1	50.0	2.74	0.85	7473	0.93
24	CR6-D-8	319	6.36	618	85.1	50.1	2.74	0.85	10357	0.89
25	CR8-A-2	120	6.47	835	25.4	18.5	1.18	0.97	2819	1.09
26	CR8-A-4-1	120	6.47	835	40.5	18.6	1.18	0.97	2957	1.07
27	CR8-A-4-2	120	6.47	835	40.5	18.6	1.18	0.97	2961	1.07
28	CR8-A-8	119	6.47	835	77.0	18.4	1.17	0.97	3318	1.06
29	CR8-C-2	175	6.47	835	25.4	27.0	1.72	0.94	4210	1.02
30	CR8-C-4-1	175	6.47	835	40.5	27.0	1.72	0.94	4493	1.00
31	CR8-C-4-2	175	6.47	835	40.5	27.0	1.72	0.94	4542	1.01
32	CR8-C-8	175	6.47	835	77.0	27.0	1.72	0.94	5366	1.00
33	CR8-D-2	265	6.47	835	25.4	40.9	2.60	0.88	6546	0.96
34	CR8-D-4-1	264	6.47	835	41.1	40.8	2.60	0.88	7117	0.93
35	CR8-D-4-2	265	6.47	835	41.1	40.9	2.60	0.88	7172	0.93
36	CR8-D-8	265	6.47	835	80.3	40.9	2.61	0.88	8990	0.91
37	CR4-A-4-3	210	5.48	294	39.1	38.3	1.45	0.91	3183	1.18
38	CR4-A-9	211	5.48	294	91.1	38.5	1.45	0.91	4773	1.04
39	CR4-C-4-3	210	4.50	277	39.1	46.7	1.71	0.91	2713	1.11
40	CR4-C-9	211	4.50	277	91.1	46.9	1.72	0.91	4371	1.00
41	CR6-A-4-3	211	8.83	536	39.1	23.9	1.22	0.91	5898	1.19
42	CR6-A-9	211	8.83	536	91.1	23.9	1.22	0.91	7008	1.04
43	CR6-C-4-3	204	5.95	540	39.1	34.3	1.76	0.91	4026	1.07
44	CR6-C-9	204	5.95	540	91.1	34.3	1.76	0.91	5303	0.96
45	CR8-A-4-3	180	9.45	825	39.1	19.0	1.21	0.91	6803	1.15
46	CR8-A-9	180	9.45	825	91.1	19.0	1.21	0.94	7402	1.03
47	CR8-C-4-3	180	6.60	824	39.1	27.3	1.72	0.94	5028	1.09
48	CR8-C-9	180	6.60	824	91.1	27.3	1.72	0.94	5873	0.98
	mean	210	6.00	566	51.1	37.0	1.79	0.91	4626	1.01
	max	324	9.45	835	91.1	73.9	2.75	0.97	10357	1.19
	min	119	4.38	262	25.4	18.4	1.17	0.85	1153	0.89

B : width of steel tube, t : wall-thickness of steel tube, σ_{sy} : yield stress of steel tube,

f_c' : strength of concrete cylinder, B/t : width-to-wall-thickness ratio, $\sqrt{\alpha_s}$: normalized B/t ratio,

$_cr_U$: scale effect factor, N_{exp} : maximun axial load, N_0 : nominal squash load

*37~48 : specimens for the second phase tests

Table 2.3 Specific Values for the Stress vs. Strain Models for Concrete

	Original	Circular CFT	Square CFT
$X=$	$\dfrac{\varepsilon_c}{\varepsilon_{cco}}$	$\dfrac{\varepsilon_c}{\varepsilon_{cco}}$	$\dfrac{\varepsilon_c}{\varepsilon_{co}}$
$Y=$	$\dfrac{\sigma_c}{\sigma_{ccB}}$	$\dfrac{\sigma_c}{\sigma_{ccB}}$	$\dfrac{\sigma_c}{\sigma_{cp}}$
$V=$	$\dfrac{E_c \cdot \varepsilon_{cco}}{\sigma_{ccB}}$	$\dfrac{E_c \cdot \varepsilon_{cco}}{\sigma_{ccB}}$	$\dfrac{E_c \cdot \varepsilon_{co}}{\sigma_{cp}}$
$\sigma_{re}=$	$\dfrac{2t^2(B-t)\sigma_{sy}}{b^3}$	$\dfrac{k}{k_e}\sigma_r$	$\dfrac{2t^2(B-t)\sigma_{sy}}{b^3}$
$\dfrac{\sigma_{ccB}}{\sigma_{cp}}=K=$	$1+k_e\dfrac{\sigma_{re}}{\sigma_{cp}}$	$1+0.032\dfrac{\sigma_{sy}}{\sigma_{cp}}$	1

$$W=1.50-17.1\times 10^{-3}\sigma_{cp}+2.39\sqrt{\sigma_{re}}$$

$$E_c=\left(6.90+3.32\sqrt{\sigma_{cp}}\right)\times 10^3$$

$$\varepsilon_{co}=0.94\left(\sigma_{cp}\right)^{1/4}\times 10^{-3}$$

$$\dfrac{\varepsilon_{cco}}{\varepsilon_{co}}=\begin{cases}1.0+4.7(K-1) & K\le 1.5 \\ 3.35+20(K-1.5) & K>1.5\end{cases}$$

$$\sigma_{cp}=\gamma_u\cdot f_c' \qquad \gamma_u=1.67D_c^{-0.112}$$

$$k=4.1,\ k_e=23,\ \sigma_r=0.0079\sigma_{sy}$$

Notations:

B : Outside width of steel tube

b : Inner width of steel tube

D : Outside diameter of steel tube

t : Thickness of steel tube wall

E_c : Young's modulus of elasticity concrete (in MPa)

ε_{co} : Strain at maximum stress of plain concrete

ε_{cco} : Strain at maximum stress of confined concrete

σ_{cp} : Compressive strength of concrete (in MPa)

σ_{ccB} : Strength of confined concrete (in MPa)

σ_{sy} : Yield stress of steel tube (in MPa)

Table 2.4 Specific Values for the Stress vs. Strain Models for Steel Tube in Square CFT Columns

	Type-1	Type-2	Type-3
	$\sqrt{\alpha_s} \le 1.54$	$1.54 < \sqrt{\alpha_s} < 2.03$	$2.03 \le \sqrt{\alpha_s}$
$\sigma_{sB} =$	$\sigma_{sy} \cdot S_1$	σ_{sy}	$\sigma_{sy} \cdot S_3$
$\varepsilon_{sB} =$	$\left(6.06\dfrac{1}{\alpha_s^2} - 0.801\dfrac{1}{\alpha_s} + 1.10\right)\cdot\varepsilon_{sy}$	ε_{sy}	σ_{sB}/E_s
$\varepsilon_{sE} =$	ε_{sy}	ε_{sy}	σ_{sB}/E_s

$$\frac{\left(\varepsilon_{sT} - \varepsilon_{sB}\right)}{\varepsilon_{sE}} = 3.59, \quad \sigma_{sT} = 1.19 - 0.207\sqrt{\alpha_s}$$

Table 3.1(a) Summary of Eccentrically Loaded Stub Columnn Specimens (Circular Tubes)

specimen	D (mm)	t (mm)	D/t	σ_{sy} (MPa)	fc' (MPa)	N/N_o	Loading condition
EC4- A-4-035	150		50.7		39.9	0.35	
EC4- A-4-06						0.59	
EC4-C-2-035					24.5	0.34	
EC4-C-2-06						0.59	
EC4-C-4-03						0.30	
EC4-C-4-04	300	2.96	101.4	283	39.9	0.40	
EC4-C-4-06						0.61	
EC4-C-8-045					77.6	0.45	
EC4-C-8-06						0.60	
EC4-D-4-04	450		152.0		39.9	0.40	
EC4-D-4-06						0.60	
EC6-A-4-02	122		26.9		39.9	0.20	
EC6-A-4-06						0.60	
EC6-C-2-03					24.5	0.30	
EC6-C-2-06						0.60	
EC6-C-4-025						0.25	
EC6-C-4-03	239	4.54	52.6	579	39.9	0.30	Fig. 3.2(a)
EC6-C-4-06						0.60	
EC6-C-8-03					77.6	0.30	
EC6-C-8-06						0.60	
EC6-D-4-03	360		79.3		39.9	0.30	
EC6-D-4-06						0.60	
EC8-A-4-015	108		16.7		39.9	0.15	
EC8-A-4-06						0.60	
EC8-C-2-06					24.5	0.60	
EC8-C-2-08						0.80	
EC8-C-4-015						0.15	
EC8-C-4-03	222	6.47	34.3	835	39.9	0.30	
EC8-C-4-06						0.60	
EC8-C-8-06					77.6	0.60	
EC8-C-8-07						0.70	
EC8-D-4-015	336		51.9		39.9	0.15	
EC8-D-4-045						0.45	

Note:
D = diameter of steel tube
t = wall thickness of steel tube
σ_{sy} = yield strength of steel (yield strength was obtained by 0.2% offset.)
fc' = cylinder strength of concrete
N = applied axial force
N_o = nominal squash load

Eccentric axial loading
Circular or Rectangular section
Nominal tensile strength of steel tube: 4 - 400MPa, 6 - 590MPa, 8 - 780MPa
Rank of D/t (B/t) ratio concerning deformation capacity of hollow steel tube: Rank-FA, FC, FD
Design compressive strength of concrete: 2 - 20MPa, 4 - 40MPa, 8 - 80MPa
Axial force ratio   19 - N/N_o = 0.19

Table 3.1(b) Summary of Eccentrically Loaded Stub Column Specimens (Square Tubes)

Specimen	B (mm)	t (mm)	B/t	σ_{sy} (MPa)	fc' (MPa)	N/N_o	Loading condition
ER4- A-4-19	149	4.38	33.9	262	41.1	0.19	Fig. 3.2(b)
ER4- A-4-57	148		33.9			0.57	
ER4-C-2-25	215		49.1		25.4	0.25	
ER4-C-2-56	214		48.9			0.56	
ER4-C-4-21	215		49.2		41.1	0.21	
ER4-C-4-38			49.0			0.38	
ER4-C-4-51						0.51	
ER4-C-8-33	214		48.9		80.3	0.33	
ER4-C-8-46	215		49.0			0.46	
ER4-D-4-27	323		73.7		41.1	0.27	
ER4-D-4-60						0.60	
ER6- A-4-22	144	6.36	22.7	618	41.1	0.22	Fig. 3.2(c)
ER6- A-4-61						0.61	
ER6-C-2-25	211		33.2		25.4	0.25	Fig. 3.2(c)
ER6-C-2-58			33.1			0.58	
ER6-C-4-18	210		33.0		41.1	0.18	Fig. 3.2(b)
ER6-C-4-44			33.1			0.44	
ER6-C-4-57	209		32.9			0.57	
ER6-C-8-24	210		33.1		80.3	0.24	
ER6-C-8-54			33.0			0.54	
ER6-D-4-23	319		50.2		41.1	0.23	
ER6-D-4-47			50.1			0.47	
ER8- A-4-08	121	6.47	18.7	835	40.5	0.08	Fig. 3.2(c)
ER8-C-2-38	175		27.0		25.4	0.38	
ER8-C-2-57			27.1			0.57	
ER8-C-4-24			27.0		40.5	0.24	
ER8-C-4-38			27.1			0.38	
ER8-C-4-57	176		27.2			0.57	
ER8-C-8-39			27.3		77.0	0.39	
ER8-C-8-58	175		27.1			0.58	
ER8-D-4-40	265		40.9		40.5	0.40	
ER8-D-4-60						0.60	

Note: B = width of steel tube

t = wall thickness of steel tube

σ_{sy} = yield strength of steel (yield strength was obtained by 0.2% offset.)

fc' = cylinder strength of concrete

N = applied axial force

N_o = nominal squash load

Eccentric axial loading

Circular or Rectangular section

Nominal tensile strength of steel tube: 4 - 400MPa, 6 - 590MPa, 8 - 780MPa

Rank of D/t (B/t) ratio concerning deformation capacity of hollow steel tube: Rank-FA, FC, FD

Design compressive strength of concrete: 2 - 20MPa, 4 - 40MPa, 8 - 80MPa

Axial force ratio   19 - $N/N_o = 0.19$

Table 3.2(a) Material Properties of Structural Steel Tubes (Circular Tubes)

	t (mm)	σ_{sy} (MPa)	σ_{st} (MPa)	σ_{sy}/σ_{st}	E_s (GPa)	ε (%)
400MPa	2.96	283	408	0.693	224	29.1
590MPa	4.54	579	646	0.895	228	15.2
780MPa	6.47	834	879	0.949	218	10.1

Note: σ_{st} = tensile strength, E_s = Modulus of elasticity, ε = Elongation

Table 3.2(b) Material Properties of Structural Steel Tubes (Square Tubes)

	t (mm)	σ_{sy} (MPa)	σ_{st} (MPa)	σ_{sy}/σ_{st}	E_s (GPa)	ε (%)
400MPa	4.38	262	411	0.637	214	32.5
590MPa	6.36	618	673	0.918	219	15.1
780MPa	6.47	834	879	0.949	218	10.1

Table 3.3(a) Material Properties of Concrete (Circular Tubes)

F_c	fc' (MPa)	E_c (GPa)	ε_B (%)
20MPa	25.4	25.4	0.206
40MPa	40.7	32.1	0.220
80MPa	78.1 - 85.1	36.3 - 38.5	0.281 - 0.288

Note:　fc' = compressive Strength, E_c = modulus of elasticity
ε_B = strain at the compressive strength

Table 3.3(b) Material Properties of Concrete (Square Tubes)

F_c	fc' (MPa)	E_c (GPa)	ε_B (%)
20MPa	25.4	25.1 - 26.0	0.205 - 0.207
40MPa	40.5 - 41.1	29.3 - 33.4	0.219 - 0.223
80MPa	77.0 - 80.3	35.9 - 37.3	0.280 - 0.304

Table 3.4(a) Experimental and Analytical Results (Circular Tubes)

Specimen	M_u of test (kN m)	$M_{cal.1}$ (kN m)	$M_{cal.2}$ (kN m)	$M_{cal.3}$ (kN m)	$\dfrac{M_u}{M_{cal.1}}$	$\dfrac{M_u}{M_{cal.2}}$	$\dfrac{M_u}{M_{cal.3}}$
EC4-A-4-035	32.0	28.0	27.6	29.9	1.14	1.16	1.07
EC4-A-4-06	36.5	23.4	22.7	25.1	1.14	1.18	1.06
EC4-C-2-035	128.3	125.9	119.0	128.9	1.02	1.08	1.00
EC4-C-2-06	109.7	108.2	93.8	104.2	1.01	1.17	1.05
EC4-C-4-03	150.0	155.4	147.4	157.0	0.97	1.02	0.96
EC4-C-4-04	156.6	158.2	146.6	154.9	0.99	1.07	1.01
EC4-C-4-06	130.5	138.8	116.4	122.5	0.94	1.12	1.07
EC4-C-8-045	194.1	237.8	215.1	218.3	0.82	0.90	0.89
EC4-C-8-06	160.8	218.8	181.6	173.7	0.74	0.89	0.93
EC4-D-4-04	409.7	457.5	406.1	425.2	0.90	1.01	0.96
EC4-D-4-06	346.8	414.1	312.1	316.5	0.84	1.11	1.10
EC6-A-4-02	(46.9)	40.8	40.8	46.4	1.15	1.15	1.01
EC6-A-4-06	42.2	28.6	28.4	37.3	1.48	1.49	1.13
EC6-C-2-03	(156.9)	164.8	161.4	185.1	0.95	0.97	0.85
EC6-C-2-06	132.3	121.1	114.2	149.1	1.09	1.16	0.89
EC6-C-4-025	(173.8)	184.4	180.4	197.3	-	-	-
EC6-C-4-03	(177.6)	183.2	178.2	195.2	0.97	1.00	0.91
EC6-C-4-06	155.4	140.3	129.6	153.7	1.11	1.20	1.01
EC6-C-8-03	217.3	222.6	215.6	229.3	0.98	1.01	0.95
EC6-C-8-06	178.2	182.6	165.1	175.8	0.98	1.08	1.01
EC6-D-4-03	(460.5)	474.5	451.8	488.8	-	-	-
EC6-D-4-06	399.6	379.3	322.6	369.0	1.05	1.24	1.08
EC8-A-4-015	(48.2)	58.0	58.0	65.1	-	-	-
EC8-A-4-06	53.8	37.3	37.4	50.4	1.44	1.44	1.07
EC8-C-2-06	(219.8)	176.8	171.9	236.3	1.24	1.28	0.93
EC8-C-2-08	149.3	96.3	90.0	170.9	1.55	1.66	0.87
EC8-C-4-015	301.7	280.8	278.2	314.9	1.07	1.08	0.96
EC8-C-4-03	282.3	269.5	265.5	306.5	1.05	1.06	0.92
EC8-C-4-06	261.3	192.2	184.2	247.2	1.36	1.42	1.06
EC8-C-8-06	(267.0)	230.2	216.3	254.3	-	-	-
EC8-C-8-07	262.0	184.9	168.0	207.5	1.42	1.56	1.26
EC8-D-4-015	(604.1)	695.9	682.9	761.5	-	-	-
EC8-D-4-045	648.1	618.3	582.9	685.3	1.05	1.11	0.95

The values in (——) and ( ) mean the experimental ultimate moment of specimens failed in cracking in welded portion, before and after the value of ϕD reaching 2.5%, respectively.

$M_{cal.1}$ = theoretical ultimate moment (cylinder strength was used as concrete strength)

$M_{cal.2}$ = theoretical ultimate moment (scale effect on concrete strength was considered)

$M_{cal.3}$ = analytical ultimate moment by the fiber analysis

Table 3.4(b) Experimental and Analytical Results (Square Tubes)

Specimen	M_u of test (kN m)	$M_{cal.1}$ (kN m)	$M_{cal.2}$ (kN m)	$M_{cal.3}$ (kN m)	$\dfrac{M_u}{M_{cal.1}}$	$\dfrac{M_u}{M_{cal.2}}$	$\dfrac{M_u}{M_{cal.3}}$
ER4-A-4-19	53.9	48.2	47.7	50.3	1.12	1.13	1.07
ER4-A-4-57	38.9	40.5	38.6	38.6	0.96	1.01	1.01
ER4-C-2-25	101.4	101.9	99.4	99.4	1.00	1.02	1.02
ER4-C-2-56	69.0	83.3	76.4	67.9	0.83	0.90	1.02
ER4-C-4-21	115.4	115.7	113.0	114.5	1.00	1.02	1.01
ER4-C-4-38	103.2	118.0	112.4	108.2	0.87	0.92	0.95
ER4-C-4-51	83.0	109.3	101.0	87.4	0.76	0.82	0.95
ER4-C-8-33	146.3	160.0	153.1	151.0	0.91	0.96	0.97
ER4-C-8-46	121.4	159.0	147.6	133.7	0.76	0.82	0.91
ER4-D-4-27	296.8	322.2	305.0	285.4	0.92	0.97	1.04
ER4-D-4-60	200.9	283.8	226.6	184.2	0.71	0.89	1.09
ER6-A-4-22	124.0	119.9	119.3	124.8	1.03	1.04	0.99
ER6-A-4-61	83.7	75.5	73.5	79.6	1.11	1.14	1.05
ER6-C-2-25	253.0	256.9	253.5	240.5	0.99	1.00	1.06
ER6-C-2-58	145.7	175.5	166.5	142.9	0.83	0.88	1.02
ER6-C-4-18	(257.4)	279.1	275.4	268.1	-	-	-
ER6-C-4-44	214.2	244.1	235.4	207.3	0.88	0.91	1.03
ER6-C-4-57	164.3	203.9	192.1	161.6	0.81	0.86	1.02
ER6-C-8-24	(299.4)	316.6	309.8	301.9	0.95	0.97	0.99
ER6-C-8-54	206.3	263.5	245.3	206.2	0.78	0.84	1.00
ER6-D-4-23	(592.9)	711.9	688.6	587.2	-	-	-
ER6-D-4-47	407.7	632.7	581.8	400.3	0.64	0.70	1.02
ER8-A-4-08	(103.0)	102.6	110.0	113.0	-	-	-
ER8-C-2-38	(203.0)	205.1	203.0	172.0	0.99	1.00	1.18
ER8-C-2-57	157.9	143.5	139.7	114.4	1.10	1.13	1.38
ER8-C-4-24	(211.8)	240.4	238.3	222.2	-	-	-
ER8-C-4-38	(212.8)	214.9	210.7	181.9	0.99	1.01	1.17
ER8-C-4-57	153.0	157.7	151.5	121.4	0.97	1.01	1.26
ER8-C-8-39	(235.4)	245.2	240.2	210.2	0.96	0.98	1.12
ER8-C-8-58	182.4	190.0	180.6	140.3	0.96	1.01	1.30
ER8-D-4-40	446.2	544.1	531.2	362.8	0.82	0.84	1.23
ER8-D-4-60	319.7	415.2	394.7	236.8	0.77	0.81	1.35

The values in (——) and (　　) mean the experimental ultimate moment of specimens failed in cracking in welded portion, before and after the maximum moment, respectively.
$M_{cal.1}$ = theoretical ultimate moment (cylinder strength was used as concrete strength)
$M_{cal.2}$ = theoretical ultimate moment (scale effect on concrete strength was considered)
$M_{cal.3}$ = analytical ultimate moment by the fiber analysis

Table 4.1 Summary of Beam-Column Specimens

Specimen	Section Shape	Steel Strength S_u (MPa)	Depth D (mm)	Thickness t (mm)	Concrete Strength F_c (MPa)	Axial Load	
SC4-A-4-C		400	240	4.5	40		
SC4-A-9-C					90		
SC6-A-4-C				9.0	40	$0.4N_o$	
SC6-A-9-C					90		
SC6-A-9-V		590	240			$0.7N_o$	$-0.3N_{so}$
SC6-C-4-C	Circular			4.5	40	$0.4N_o$	
SC6-C-9-C					90		
SC6-C-9-V						$0.7N_o$	$-0.3N_{so}$
SC8-A-4-C				9.0	40	$0.4N_o$	
SC8-A-9-C		780	160				
SC8-A-9-V					90	$0.7N_o$	$-0.3N_{so}$
SC8-C-9-C				4.5		$0.4N_o$	
SC8-C-9-V						$0.7N_o$	$-0.3N_{so}$
SR4-A-4-C				6.0	40		
SR4-A-9-C		400	210		90		
SR4-C-4-C				4.5	40	$0.4N_o$	
SR4-C-9-C					90		
SR6-A-4-C				9.0	40		
SR6-A-9-C					90		
SR6-A-9-V		590	210			$0.7N_o$	$-0.3N_{so}$
SR6-C-4-C	Square			6.0	40	$0.4N_o$	
SR6-C-9-C					90		
SR6-C-9-V						$0.7N_o$	$-0.3N_{so}$
SR8-A-4-C				9.0	40	$0.4N_o$	
SR8-A-9-C					90		
SR8-A-9-V		780	180			$0.7N_o$	$-0.3N_{so}$
SR8-C-4-C				6.0	40	$0.4N_o$	
SR8-C-9-C					90		
SR8-C-9-V						$0.7N_o$	$-0.3N_{so}$

Specimen	Section Shape	Steel Strength S_u (MPa)	Depth D (mm)	Thickness t (mm)	Concrete Strength F_c (MPa)	Axial Load	Loading Angle
SR6-A-9-C-45		590	210	9.0			45°
SR6-C-9-C-45				6.0	90	$0.4N_o$	
SR8-A-9-C-45	Square	780	180	9.0			
SR8-A-9-C-22.5							22.5°

$\underline{S}$ $\underline{R}$ $\underline{6}$-$\underline{A}$-$\underline{9}$-$\underline{C}$-$\underline{45}$

D Column Depth (Diameter)
t Thickness of Steel Tube

Beam-Column test
Shape of Section, R-Square section, C-Circular section
Steel Strength, 4-400, 6-590, 8-780(MPa)
Width (Diameter)-to-thickness ratio, A-FA Class, C-FC Class
Concrete Strength, 4-Fc40, 9-Fc90
Axial Load Ratio C-Constant(0.4No), V-Variable(0.7No -0.3Nso
Loading Angle, 45-45degree, 22.5-22.5degree

Table 4.2 Material Properties of Structural Steel Tubes

Section Shape	Steel Strength s_u	Thickness	Coupon Test				Comp. Yield Strength s_{yc}
			Yield Strength s_y	Tensile Strength s_t	Yield Ratio s_y/s_t	u	
Circular	400	4.71	284	449	0.633	24.7	338
	590	4.52	504	662	0.761	23.6	530
		9.00	482	618	0.780	24.0	508
	780	4.76	771	788	0.979	10.0	785
		9.12	820	833	0.984	11.7	806
Square	400	4.50	276	412	0.669	29.0	326
		5.84	295	434	0.679	29.0	323
	590	5.95	540	669	0.808	12.9	609
		8.83	537	673	0.797	14.1	588
	780	6.66	824	851	0.968	11.0	805
		9.45	825	865	0.954	11.9	837

Table 4.3 Material Properties of Concrete

Design Strength F_c	Cylinder Strength fc'		Young's Modulus c		Poisson's Ratio		Tensile Strength	
40	35.5	42.4	31.3	33.8	0.18	0.23	3.12	3.26
90	84.5	94.5	36.2	38.6	0.21	0.24	4.85	5.01

Table 4.4 Summary of Test Results

Specimen	D or B ( )	t ( )	D/t or B/t	α or β	σ_{scy} ( )	f_c' ( )	$\frac{N}{N_o}$ or $\frac{N}{N_{so}}$	N_{ue} ( )	M_{ue} ( )	M_{uc} ( )	$\frac{M_{ue}}{M_{uc}}$	M_{ua} ( )	$\frac{M_{ue}}{M_{ua}}$
SC4-A-4-C	241	4.70	51.3	0.08	338	39.2	0.37	1034	173	128	1.35	176	0.98
SC4-A-9-C	238		50.6			88.2	0.38	1784	202	174	1.16	201	1.00
SC6-A-4-C			26.7			35.5	0.38	1809	371	255	1.45	387	0.96
SC6-A-9-C	241	9.00	26.8	0.07	508	84.4		2567	422	313	1.35	408	1.03
SC6-A-9-V			26.7			91.7	0.67	4682	274	223	1.23	310	0.88
							(-0.28)	-947	-323	-234	1.38	-239	1.35
SC6-C-4-C	238		52.6			35.5	0.45	1462	220	151	1.45	225	0.98
SC6-C-9-C	240	4.52	53.1	0.14	530	84.4	0.39	2086	254	218	1.16	266	0.95
SC6-C-9-V	241		53.2			91.7	0.68	3874	153	168	0.91	203	0.75
							(-0.27)	-491	-185	-132	1.40	-131	1.41
SC8-A-4-C						35.5	0.41	1612	245	153	1.60	223	1.10
SC8-A-9-C	161	9.12	17.7	0.07	806			1988	261	175	1.49	233	1.12
SC8-A-9-V						93.9	0.71	3457	173	109	1.59	145	1.19
							(-0.30)	-1026	-147	-156	0.94	-163	0.90
SC8-C-9-C	160		33.6				0.39	1347	151	112	1.35	143	1.06
SC8-C-9-V	159	4.76	33.4	0.12	785	93.9	0.69	2359	110	75	1.48	96	1.15
							(-0.29)	-513	-82	-84	0.97	-83	0.99
SR4-A-4-C	210	5.80	36.2	1.37	323	39.2	0.40	1162	187	145	1.29	183	1.02
SR4-A-9-C						88.2	0.39	1895	225	197	1.14	222	1.01
SR4-C-4-C	210	4.50	46.7	1.71	326	39.2	0.40	1021	151	128	1.18	146	1.03
SR4-C-9-C	209		46.4	1.70		88.2		1791	202	177	1.14	185	1.09
SR6-A-4-C	211		23.9	1.22		39.3	0.38	1959	373	306	1.22	387	0.96
SR6-A-9-C		8.83			588	88.3		2649	402	363	1.11	423	0.95
SR6-A-9-V	210		23.8	1.21		91.7	0.70	4880	259	243	1.07	246	1.05
							(-0.29)	-1070	-302	-276	1.09	-306	0.99
SR6-C-4-C	211		35.5	1.82		39.3	0.38	1545	263	244	1.08	271	0.97
SR6-C-9-C	210	5.95	35.3	1.81	609	93.7		2368	295	303	0.97	314	0.94
SR6-C-9-V	212		35.6	1.82		91.7	0.69	4326	163	217	0.75	151	1.08
							(-0.30)	-769	-226	-209	1.08	-230	0.98
SR8-A-4-C	178			1.19		42.3	0.43	2576	345	275	1.25	344	1.00
SR8-A-9-C	179	9.45	18.9	1.20	837		0.42	3077	377	322	1.17	375	1.01
SR8-A-9-V	178			1.19		94.5	0.72	5294	217	182	1.19	205	1.06
							(-0.32)	-1569	-280	-278	1.01	-291	0.96
SR8-C-4-C				1.70		42.3	0.42	2003	240	217	1.11	252	0.95
SR8-C-9-C	180	6.66	27.0		805		0.41	2540	264	262	1.01	287	0.92
SR8-C-9-V				1.71		94.5	0.71	4437	146	149	0.98	139	1.05
							(-0.31)	1142	-210	-202	1.04	-220	0.95
SR6-A-9-C-45	210	8.83	23.8	1.21	588	88.3	0.38	2644	374	343	1.09	418	0.89
SR6-C-9-C-45	211	5.95	35.5	1.82	609	88.3	0.39	2358	270	284	0.95	295	0.92
SR8-A-9-C-45	181	9.45	19.2	1.21	837	91.7	0.40	2965	371	326	1.14	392	0.95
SR8-A-9-C-22.5	180		19.0	1.20	837	84.4	0.39	2782	390	324	1.20	390	1.00

$\alpha = B/t\sqrt{\sigma_{sc}/E_s}$, $\beta = (D/t)\cdot\left(\sigma_{sc}/E_s\right)$, Es: Young's Modulus of Steel

Table 5.1 Summary of Beam-to-Column Connection Specimens

Specimen	Rectangular Tube							Circular Tube			
	R1	R2	R3	R4	R6	R5	R5'	C1	C2	C3	C4
Shape of Specimen	plain			solid	plain			plain			plain
Nominal Tensile Strength of Steel Tube S_u (MPa)	590	590	780	590	590	590	590	590	590	780	590
Design Concrete Strength F_c (MPa)	90	40	90	90	90	90	90	90	40	90	90
Beam section (mm)	H-250x250x9x12					H-160x160 x12x16		H-250x250x9x12			H-160x160 x12x16
Beam length(mm)	3000			3500		1000		2500		3000	1000
Column section(mm)	-250x12					-160x9		-280x12		-280 x9	-180x9
Column length(mm)	3000			3050		2000		3000			2000
Panel section(mm)	-250x4.5					-160x3		-280x4.5			-180x3
Panel $_pD_s/_pt$	55.6					53.3		62.2			60.0
Panel $_pD_s/_Bd$	1.05					1.11		1.18			1.25
Diaphragm	continuing to beam flanges							continuing to beam flanges			
Axial force ratio	Com. 0.2 $_pN_o$					Com. 0.67 $_pN_o$ Tens. 0.3 $_pN_{so}$	Com. 0.2 $_pN_o$	Com. 0.2 $_pN_o$			Com. 0.67 $_pN_o$ Tens. 0.3 $_pN_{so}$

exterior column :   interior column :

Table 5.2 Material Properties of Panel Zone Steel and Filled Concrete

Specimen		Rectangular Tube						Circular Tube			
		R1	R2	R3	R4	R6	R5,R5'	C1	C2	C3	C4
Steel Panel	Thickness $_pt$ (mm)	4.58	4.58	4.72	4.58	4.58	3.08	4.64	4.64	4.78	3.09
	Diameter $_pD_s$ (mm)	248.3	249.5	251.4	237.3	251.5	161.5	280.5	280.0	280.0	179.8
	Young's modulus E_s (kN/mm²)	207	207	204	203	207	207	204	204	204	203
	Yield point $_pS_{sy}$ (MPa)	492	492	756	442	492	513	439	439	730	448
	Max. Strength $_pS_{st}$ (MPa)	656	656	809	616	656	658	641	641	805	640
	Elongation (%)	23.4	23.4	18.6	34.4	23.4	23.7	24.0	24.0	16.8	23.9
Filled Concrete	Young's Modulus E_c (kN/mm²)	43.90	35.80	42.22	42.22	44.6	41.36	42.88	34.28	41.1	41.36
	Poisson's ratio u	0.253	0.217	0.242	0.242	0.255	0.229	0.238	0.207	0.244	0.229
	Comp. Strength f_c' (MPa)	109.7	54.4	102.5	102.5	97.7	99.6	98.4	49.1	94.2	99.6

Table 5.3 (a) Test Results of Rectangular Tube Specimens

Specimen		R1	R2	R3	R4	R5	R5'	R6
experiment	eKf $(x10^3 kN/rad)$	16.90	14.12	15.42	11.70	5.80	5.13	10.04
	$eQpyo(kN)$	113	90.6	186	68.8	40.2	37.5	138
	$eQpy(kN)$	140	106	213	102	53.6	49.5	167
	$eQm+(kN)$	226	175	251	188	85.8	90.9	224.6
	$eQm-(kN)$	-216	-171	-251	-186	-88.4	-95.5	-223.3
calculation	cKf $(x10^3 kN/rad)$	15.3	14.72	15.03	14.50	5.62 -3.05	5.60 -3.05	12.29
	$cQpa(kN)$	129	105	153	121	46.5	46.5	120
	$cQpu(kN)$	155	126	186	144	55.8	55.8	144
	$cQca(kN)$	326	294	748	504	80.0	142	232
	$cQby(kN)$	243	243	390.2	241	195	194	201
	$cQdy(kN)$	395	395	662	259	222	222	339
$eQpy+/cQpa$		1.09	1.01	1.39	0.84	1.15	1.06	1.39
$eQm+/cQpu$		1.45	1.39	1.35	1.31	1.53	1.62	1.56
$eQm-/cQpu$		-1.39	-1.36	-1.35	-1.29	-1.58	-1.71	-1.55

Table 5.3 (b) Test Results of Circular Tube Specimens

Specimen		C1	C2	C3	C4
experiment	eKf $(x10^3 kN/rad)$	15.96	16.16	13.98	5.45
	$eQpyo(kN)$	191	136	170	36.7
	$eQpy(kN)$	208	171	194	46.6
	$eQm+(kN)$	284	228	277	92.6
	$eQm-(kN)$	-281	-224	-272	-94.0
calculation	cKf $(x10^3 kN/rad)$	19.88	19.05	14.71	5.73 -3.18
	$cQpa(kN)$	130	107	139	41.9
	$cQpu(kN)$	156	128	167	50.5
	$cQca(kN)$	268	240	358	62.0
	$cQby(kN)$	295	295	406	99.0
	$cQdy(kN)$	238	238	343	??
$eQpy+/cQpa$		1.60	1.60	1.40	1.11
$eQm+/cQpu$		1.82	1.78	1.66	1.83
$eQm-/cQpu$		-1.80	1.75	1.63	-1.86

e: experiment   c: calculation K_f :elastic stiffness

$eQpyo$: equivalent to first yield of shear panel $eQpy$: equivalent to yield of shear panel

$cQpa$: equivalent to short term allowable shear strength of shear panel by AIJ-SRC Standards

$cQpu$: equivalent to ultimate shear strength of panel by AIJ-SRC Standards

$eQm+$: maximum strength in positive loading cycle

$eQm-$: maximum strength in negative loading cycle

$cQca$: equivalent to short term allowable strength of column

$cQby$: equivalent to yield strength of steel beam

$cQdy$: equivalent to yield strength of diaphragm

Table 5.4 Virtual Specimens for Numerical Simulation

	Imaginary Specimen	Column Depth Dc (mm)	Beam Depth H (mm)	H/Dc	Concrete Strength fc' (MPa)	Steel Yield Point s_{sy} (MPa)	D'[1]
Rectangular Column	R3-150	238	357	1.5	102.5	756	1.42
	R3-075	238	179	0.75	102.5	756	1.42
	R3-125	238	298	1.25	102.5	756	1.42
	R3-C300	238	238	1	29.4	756	2.67
Circular Column	C3-150	268	402	1.5	94.2	730	1.86
	C3-075	268	201	0.75	94.2	730	1.86
	C3-125	268	335	1.25	94.2	730	1.86
	C3-C300	268	238	0.89	29.4	730	2.97

[1] D': Coefficient of Declivity in Concrete Stress-Strain Softening Region in Sakino's Model

Table 5.5 Results of Numerical Simulation

	Specimen	H/Dc	D'	fc' (MPa)	s_{sy} (MPa)	Qp - max (kN)	cQp - max (kN)	sQp - max (kN)	cQp - max/($Ac \times fc'$)
Rectangular Column	R3-150	1.5	1.42	102.5	756.0	2510	1574	986	0.27
	R3-075	0.75	1.42	102.5	756.0	2839	1869	1037	0.32
	R3-125	1.25	1.42	102.5	756.0	2611	1676	1012	0.29
	R3-C300	1	2.67	29.4	756.0	1780	639	1192	0.38
	R1	1	1.04	109.7	492	2344	1757	697	0.28
	R2	1	1.99	54.4	492	1721	1073	685	0.35
	R3	1	1.42	102.5	756.0	2670	1727	1107	0.30
Circular Column	C3-150	1.5	1.86	94.2	730	2648	1713	942	0.32
	C3-075	0.75	1.86	94.2	730	3049	2003	1112	0.38
	C3-125	1.25	1.86	94.2	730	2743	1774	1019	0.33
	C3-C300	0.89	2.97	29.4	730	1995	774	1253	0.47
	C1	0.89	1.39	98.4	439	2363	1910	545	0.34
	C2	0.89	2.23	49.1	439	1855	1214	671	0.44
	C3	0.89	1.86	94.2	730	2950	1974	1024	0.37

Table 6.1 Characteristic Parameters of Concrete Stress Block for Circular CFT Section

$$\alpha'\beta' = A(X_n,K) - B(X_n,K)\frac{\sigma_{ccB}}{42} \qquad \frac{\beta'}{2} = C(X_n,K) - D(X_n,K)\frac{\sigma_{ccB}}{42}$$

$$A(X_n,K) = \frac{0.723 + 0.061K}{0.112 + X_n}X_n \qquad C(X_n,K) = (0.476 + 0.051K)(1 - 0.132X_n^2) \qquad X_n = \frac{X}{D_c}$$

$$B(X_n,K) = \frac{0.048K^{-2.0}}{0.072K^{-1.5} + X_n}X_n \qquad D(X_n,K) = 0.017\left[1 - (0.024 + 0.187K)X_n^2\right] \qquad K = \frac{\sigma_{ccB}}{r_{cu} \cdot f_c'}$$

Table 6.2 Characteristic Parameters of Concrete Stress Block

for Square CFT Section

$$k_1 = 0.831 - 0.076\left(\frac{\sigma_{cp}}{41.2}\right), \quad k_2 = 0.429 - 0.010\left(\frac{\sigma_{cp}}{41.2}\right)$$

$$\sigma_{cp} = 0.85f_c'$$

$$f_c' = \text{cylinder strength of concrete} (MPa)$$

Table 6.3 Relationships Between Ductility Grades and Limit Rotation Angles of Beam-Columns

Ductility Grades	Limit Rotation Angle R_u(%)
FA	$2.0 \leq R_u$
FB	$1.5 \leq R_u < 2.0$
FC	$1.0 \leq R_u < 1.5$
FD	$R_u < 1.0$

Table 6.4 Summary of Database on Stiffness Degrading Ratio ay

	Circular CFT		Square CFT	
	US-Japan	Others	US-Japan	Others
Number of Date	13	45	33	108
D/t （B/t）	17.7~53.2	20.4~77.0	18.9~46.7	15.6~70.0
$\boldsymbol{s}_{sy}$ [MPa]	284~819	283~549	276~824	194~642
fc' [MPa]	35.5~93.9	28.0~84.9	39.2~94.5	20.0~101.7
N/N_0	0.39~0.70	0.0~0.71	0.40~0.72	0.0~0.83
a/D （a/B）	3.0	1.75~5.2	3.0	1.5~5.67

Table 7.1 Investigation Items and Material Properties of Each Theme Structure

Theme structure	10-story frame		24-story frame		40-story frame	
	CFT-10	S-10	CFT-24	S-24	CFT-40	S-40
Type of column	CFT	S	CFT	S	CFT	S
Elastic stress analysis	○	○	○	○	○	○
Elastic dynamic analysis	○	○	○	○	○	○
Push-over analysis	○	○	○	○	○	○
Elasto-plastic dynamic analysis	-	-	○	○	-	-
Steel yield strength(Mpa)	325	325	325	325	325	325
Concrete strength(Mpa)	36	-	72	-	72	-

Table 7.2 Design Loads

	Gravity load			Seismic load	
	Dead load (N/m^2)	Live load (N/m^2)		Story	Base shear coefficient
		For vertical	For seismic		
Roof	5190	1270	590	10-story frame	0.20
Office	2940	1760	780	24-story frame	0.12
				40-story frame	0.10

Table 7.3 Gravity and Seismic Loads of 40-Story Frames

W   : Gravity load of each story (MN)   C   : Shear coefficient in each story

W/A : Gravity load per unit floor area (kN/m^2)   Q   : Shear force in each story (MN)

ΣW   : Total Gravity load supported by the story (MN)

FL	CFT-40					S-40				
	W	W/A	ΣW	C	Q	W	W/A	ΣW	C	Q
40	11.2	8.3	12.5	0.480	6.0	9.6	7.1	11.8	0.469	5.5
30	11.5	8.5	125.1	0.204	25.5	10.1	7.5	109.5	0.205	22.5
20	11.8	8.7	241.5	0.155	37.4	10.4	7.7	212.1	0.156	33.0
10	12.0	8.9	360.6	0.123	44.5	10.7	7.9	318.3	0.124	39.4
2	12.2	9.0	470.0	0.100	47.0	11.1	8.2	417.7	0.100	41.8

Table 7.4 List of Members for 40-Story Frames

	Beam list for CFT-40		Beam list for S-40	
Story	B1	B2	B1	B2
R-34F	BH-800x250x16x28	BH-800x250x16x28	BH-800x250x16x28	BH-800x250x16x28
33-26F	BH-900x300x16x36	BH-900x300x16x36	BH-900x300x16x36	BH-900x300x16x36
25-2F	BH-900x400x16x36	BH-900x400x16x36	BH-900x400x16x36	BH-900x400x16x36
Story	G1	G2	G1	G2
R-34F	BH-800x300x16x28	BH-800x300x16x28	BH-800x300x16x28	BH-800x300x16x28
33-26F	BH-900x350x16x36	BH-900x350x16x36	BH-900x350x16x36	BH-900x350x16x36
25-2F	BH-900x400x16x40	BH-900x400x16x40	BH-900x400x16x40	BH-900x400x16x40

	Column list for CFT-40			Column list for S-40		
Story	C1	C2	C3	C1	C2	C3
40-33F	φ900x19	φ900x19	φ900x19	φ900x25	φ900x25	φ900x25
32-25F	φ900x22	φ900x22	φ900x22	φ900x32	φ900x32	φ900x32
24-17F	φ900x25	φ900x25	φ900x25	φ900x36	φ900x36	φ900x36
16-9F	φ900x28	φ900x50	φ900x40	φ900x40	φ900x60	φ900x50
8-1F	φ900x32	φ900x70	φ900x60	φ900x45	φ900x90	φ900x70

Table 7.5 Input Seismic Ground Motions for 24-Story Frames

	EL CENTRO (NS)	TAFT (EW)	HACHINOHE (NS)
Maximum velocity (cm/sec)	25 , 50	25 , 50	25 , 50
Maximum acceleration (cm/sec^2)	255.4 , 510.8	248.4 , 496.7	165.1 , 330.1
Duration time (sec)	53.76	54.40	36.00
Time interval (sec)	0.02	0.02	0.01
	0.01 or 0.005 seconds for calculation		

Table 7.6 Hysteresis Models for 24-Story Frames

	Classification	Hysteresis models	Points of changing stiffness
Columns	CFT	Normal tri-linear	$M_1=M_y$, $M_2=M_p$
	S	Normal bi-linear	$M_1=M_p$
Beams	S	Normal bi-linear	$M_1=M_p$

where : M_1 : 1st point M_2 : 2nd point
M_y : yield moment under the existing axial load
M_p : full plastic moment under the existing axial load

Table 7.7 Weight and Stiffness of 40-Story Frames

Story	Type	Section	For unit column			For story		
			Weight (kN)	E·A (kN)	E·I (kN·cm^2)	Weight (MN)	Shear stiffness X (kN/cm)	Shear stiffness Y (kN/cm)
33	CFT	φ900x19	68.8	3.13E+7	2.00E+10	11.2	1.07E+4	1.03E+4
	S	φ900x25	21.2	1.41E+7	1.35E+10	9.7	8.33E+3	8.11E+3
	CFT/S		3.25	2.21	1.48	1.16	1.29	1.27
25	CFT	φ900x22	70.6	3.27E+7	2.13E+10	11.5	1.63E+4	1.55E+4
	S	φ900x32	26.9	1.80E+7	1.69E+10	10.1	1.33E+4	1.28E+4
	CFT/S		2.63	1.82	1.26	1.14	1.23	1.21
17	CFT	φ900x25	72.3	3.41E+7	2.25E+10	11.8	2.04E+4	1.91E+4
	S	φ900x36	30.1	2.01E+7	1.88E+10	10.4	1.76E+4	1.66E+4
	CFT/S		2.40	1.69	1.20	1.13	1.16	1.15
9	CFT	φ900x28	74.1	3.54E+7	2.38E+10	12.0	2.44E+4	2.26E+4
	S	φ900x40	33.2	2.22E+7	2.06E+10	10.7	2.24E+4	2.08E+4
	CFT/S		2.23	1.59	1.15	1.12	1.09	1.09
1	CFT	φ900x32	76.3	3.72E+7	2.54E+10	12.2	3.32E+4	3.26E+4
	S	φ900x45	37.2	2.49E+7	2.28E+10	11.1	3.11E+4	3.06E+4
	CFT/S		2.05	1.50	1.11	1.10	1.07	1.07

EA : axial stiffness   EI : bending stiffness

Table 7.8 Story Drift of 40-Story Frames

Story	CFT X (cm)	CFT Y (cm)	S X (cm)	S Y (cm)	CFT/S X	CFT/S Y
40	1.13	1.16	1.36	1.37	0.83	0.84
30	1.77	1.84	1.95	2.00	0.91	0.92
20	1.91	2.02	1.99	2.09	0.96	0.97
10	1.84	1.99	1.79	1.92	1.03	1.03
1	1.41	1.44	1.34	1.36	1.05	1.06

Table 7.9 First Natural Period

Stories	Type	Tx (sec)	Ty (sec)
10	CFT	1.37	1.42
	S	1.39	1.43
	CFT/S	0.99	0.99
24	CFT	2.64	2.71
	S	2.70	2.75
	CFT/S	0.98	0.98
40	CFT	3.73	3.80
	S	3.72	3.80
	CFT/S	1.00	1.00

Table 7.10 Absorbed Energy

Story	Type	Ex (MJ)	Ey (MJ)
9th	CFT	1.87	1.79
	S	1.76	1.66
	CFT/S	1.06	1.08
2nd	CFT	2.15	2.10
	S	2.08	2.03
	CFT/S	1.04	1.04

Table 7.11 Results of Response Analyses

		CFT	S
Maximum story shear coefficients	EL CENTRO	0.191	0.208
	TAFT	0.171	0.180
	HACHINOHE	0.173	0.182
Maximum overturning moment ($\times 10^5$ kN·m)	EL CENTRO	4.38	4.25
	TAFT	3.42	3.18
	HACHINOHE	4.50	4.42
Maximum story drift angle	EL CENTRO	1/100	1/109
	TAFT	1/167	1/165
	HACHINOHE	1/100	1/102

Table 7.12 Cost Estimation of CFT and Steel Frames

Stories	Type	Amount of steel (t)	Amount of concrete (m³)	Cost
10	CFT	1283	454	¥336,640,000
	S	1414	0	¥353,500,000
	CFT/S	0.91	-	0.95
24	CFT	4186	1379	¥1,094,765,000
	S	4653	0	¥1,163,250,000
	CFT/S	0.90	-	0.94
40	CFT	9148	2905	¥2,388,675,000
	S	10221	0	¥2,555,250,000
	CFT/S	0.90	-	0.93
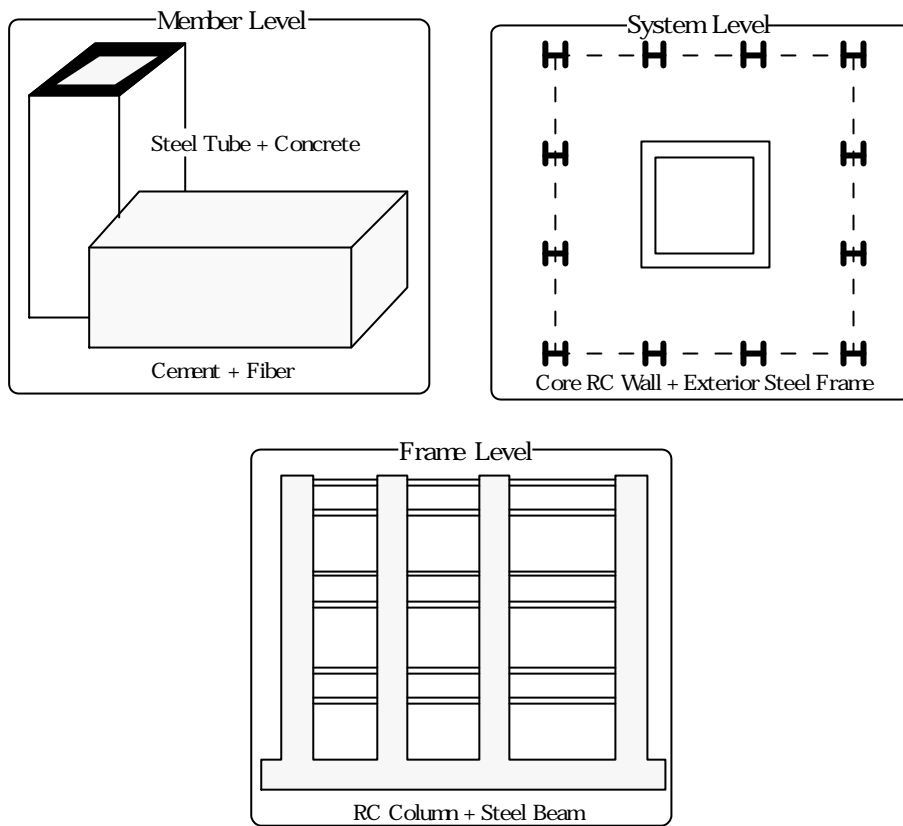
Figure 1.1 Classification of Composite and Hybrid Structures

Figure 1.2 Typical CFT Column System and Concrete Filling
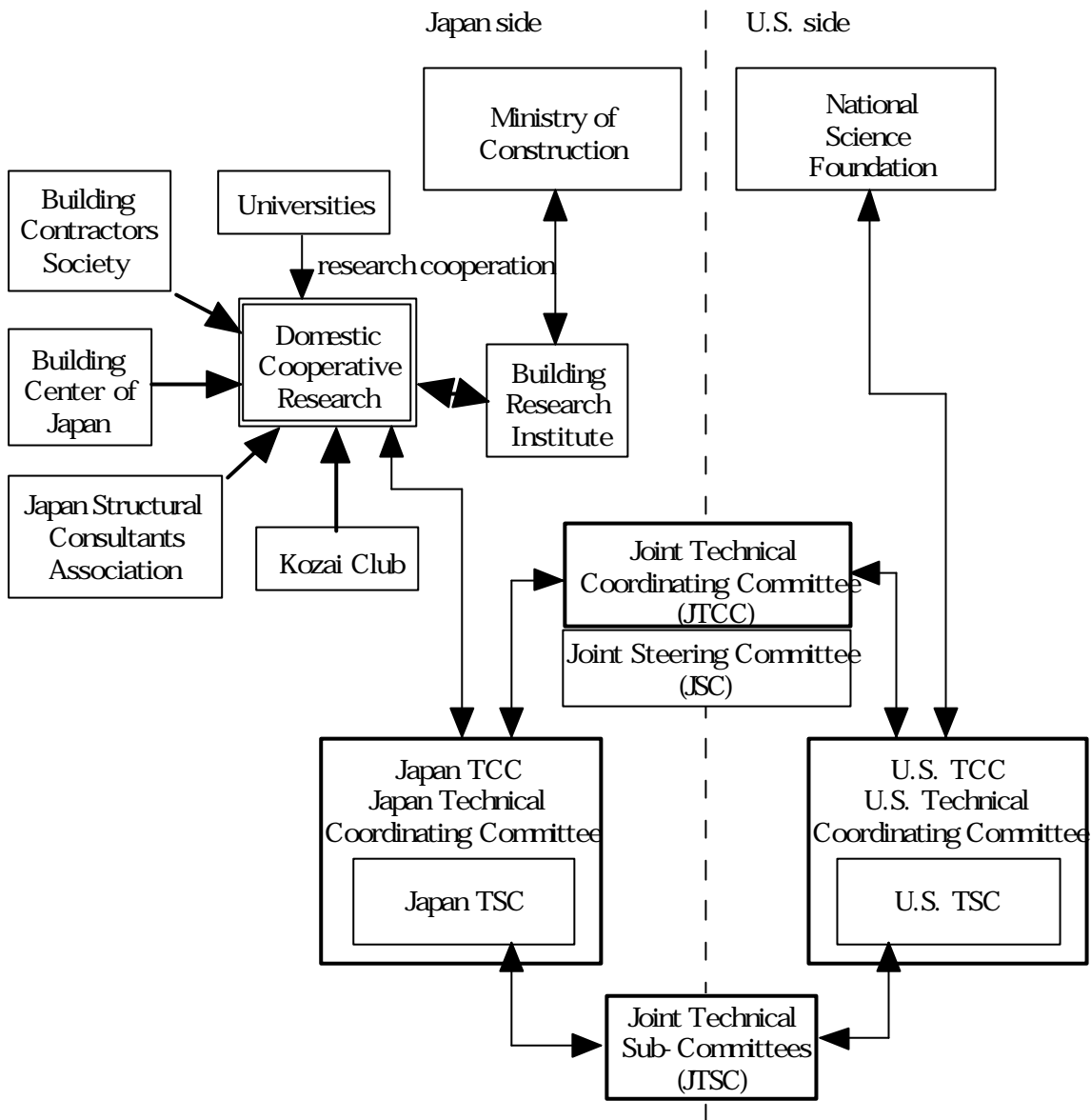
Figure 1.3 Overall Research Operation System of the US -Japan Cooperative Research Program on Composite and Hybrid Structures
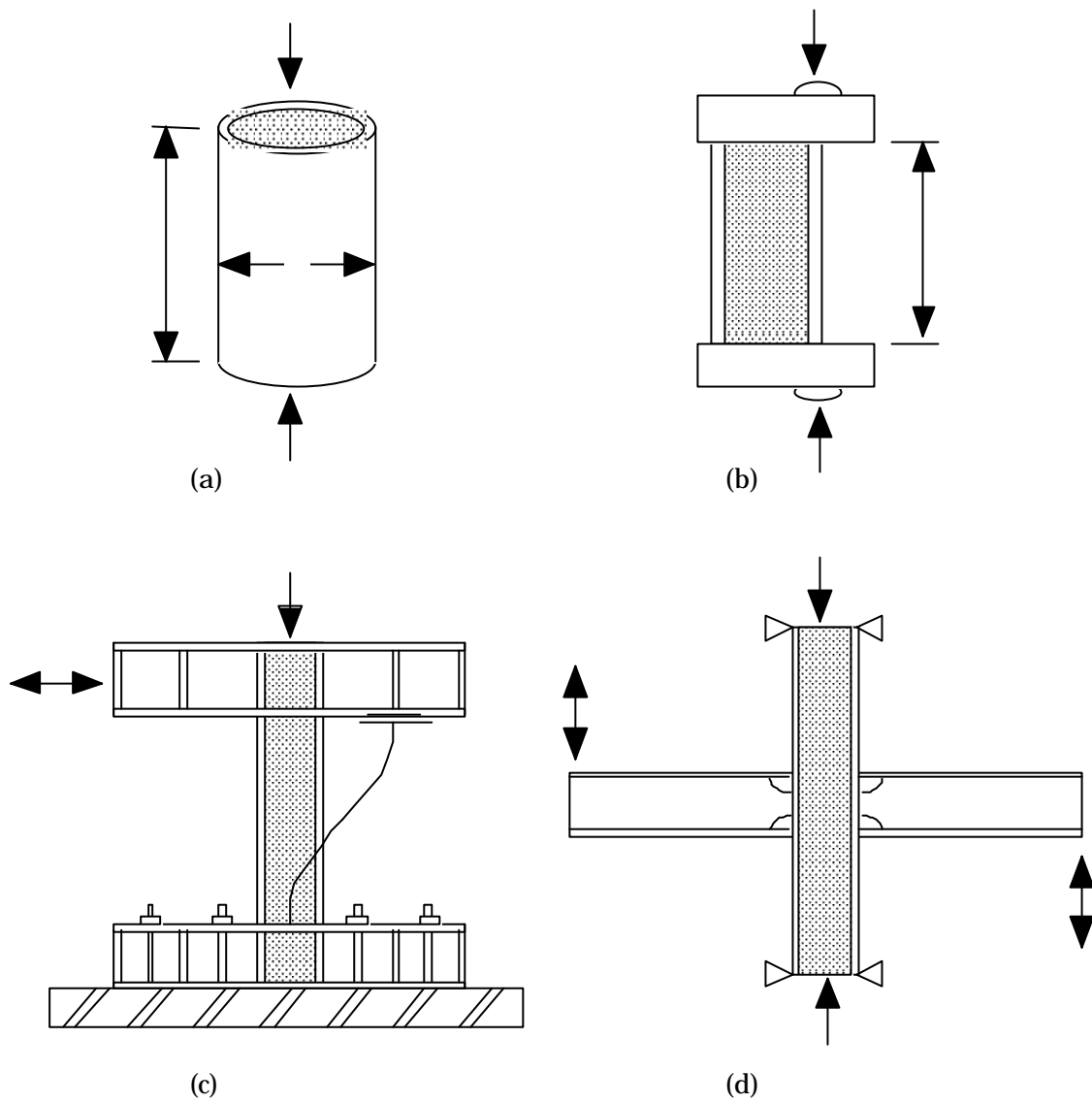
Figure 1.4 Element Tests on CFT Column System
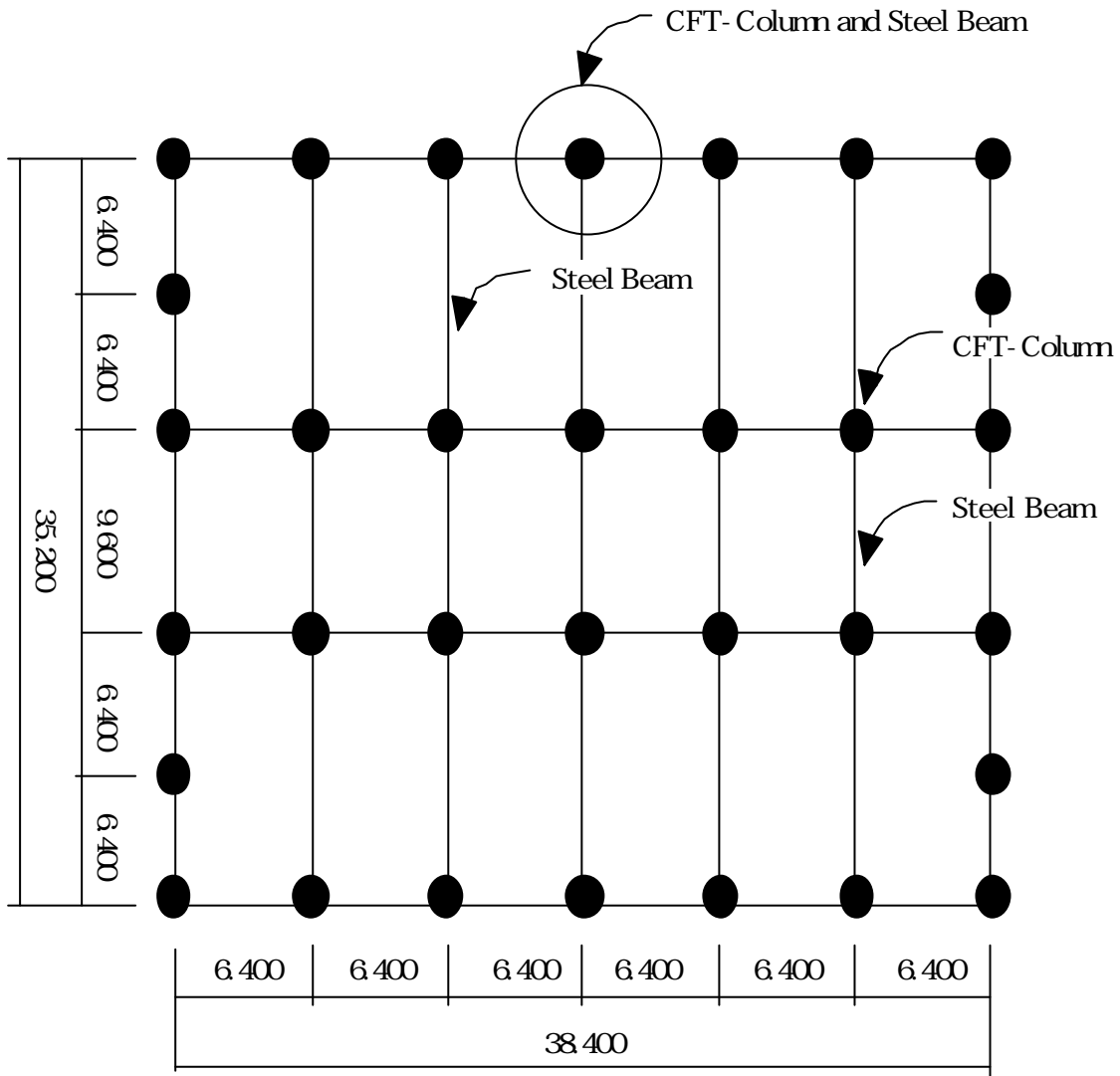
Figure 1.5 Key Plan of CFT Theme Structure
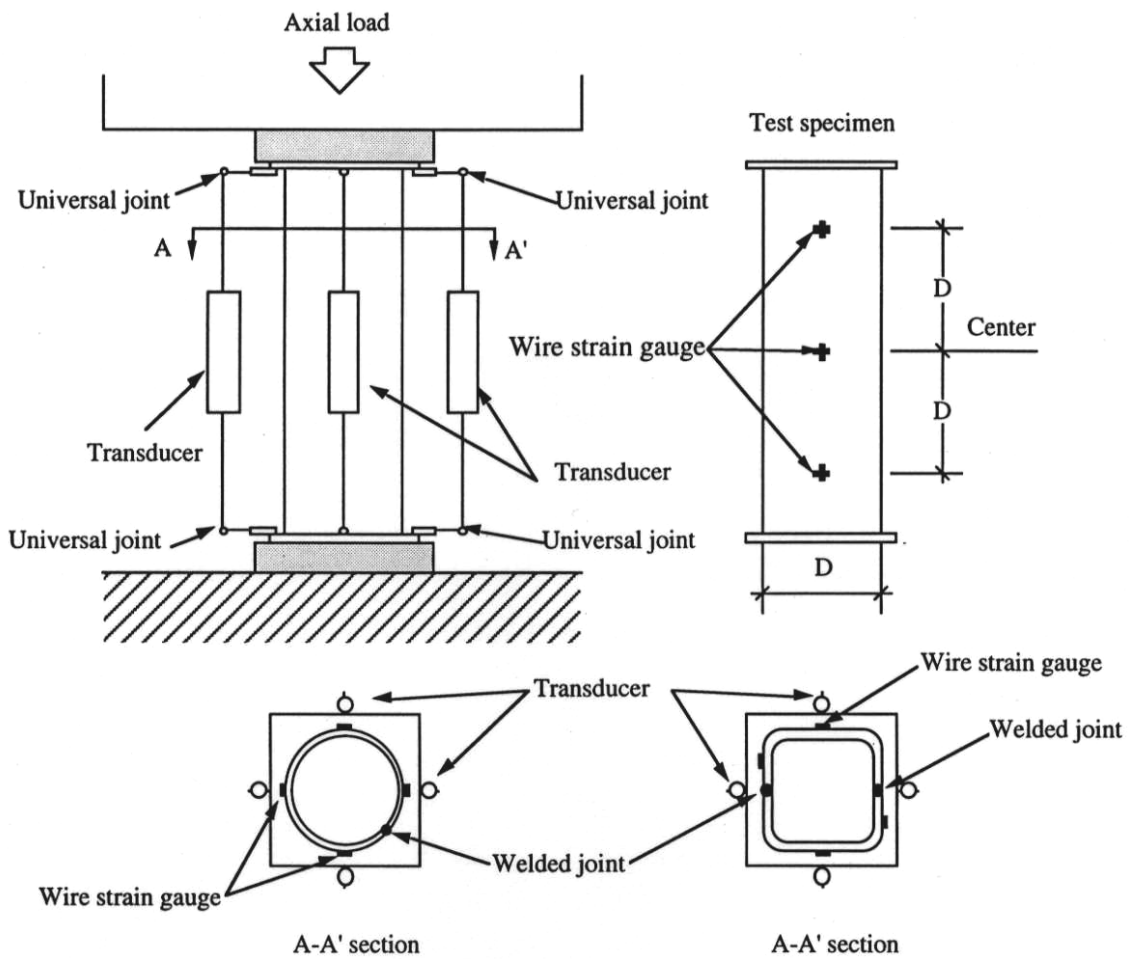
Figure 2.1 Test Setup Used for Centrally Loaded Stub Columns
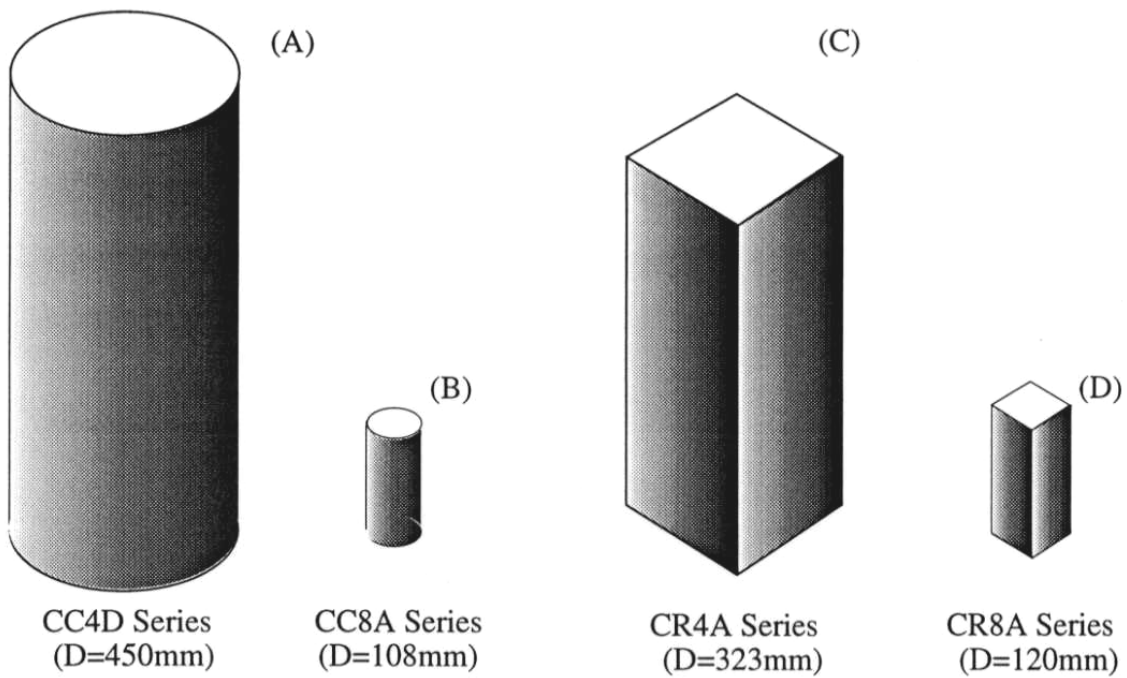
Figure 2.2 Sizes of Specimens
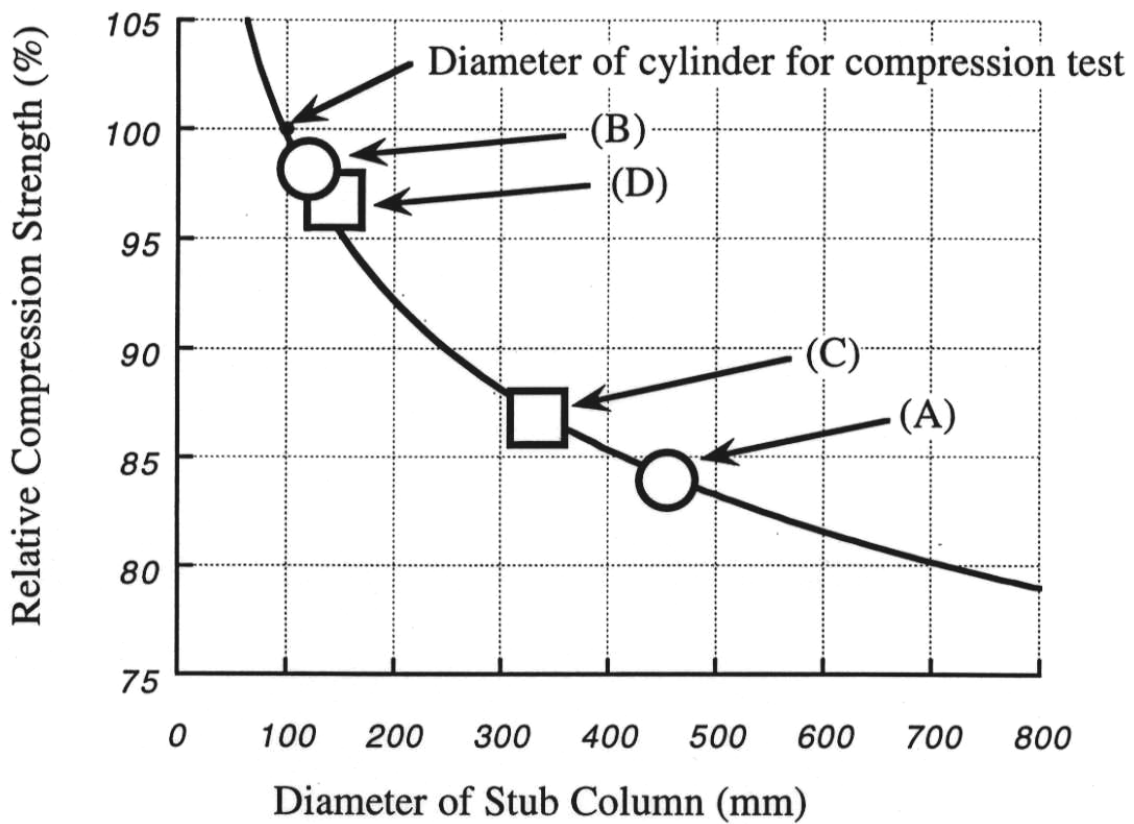
Figure 2.3 Scale Effect on Compressive Strengths of Circular Plain Concrete Columns
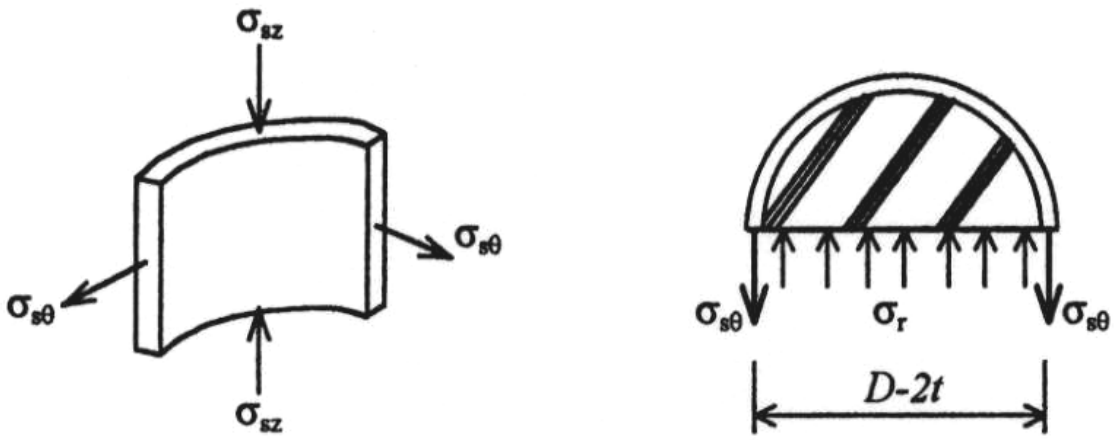
Figure 2.4 Stress States of Steel Tube and Concrete
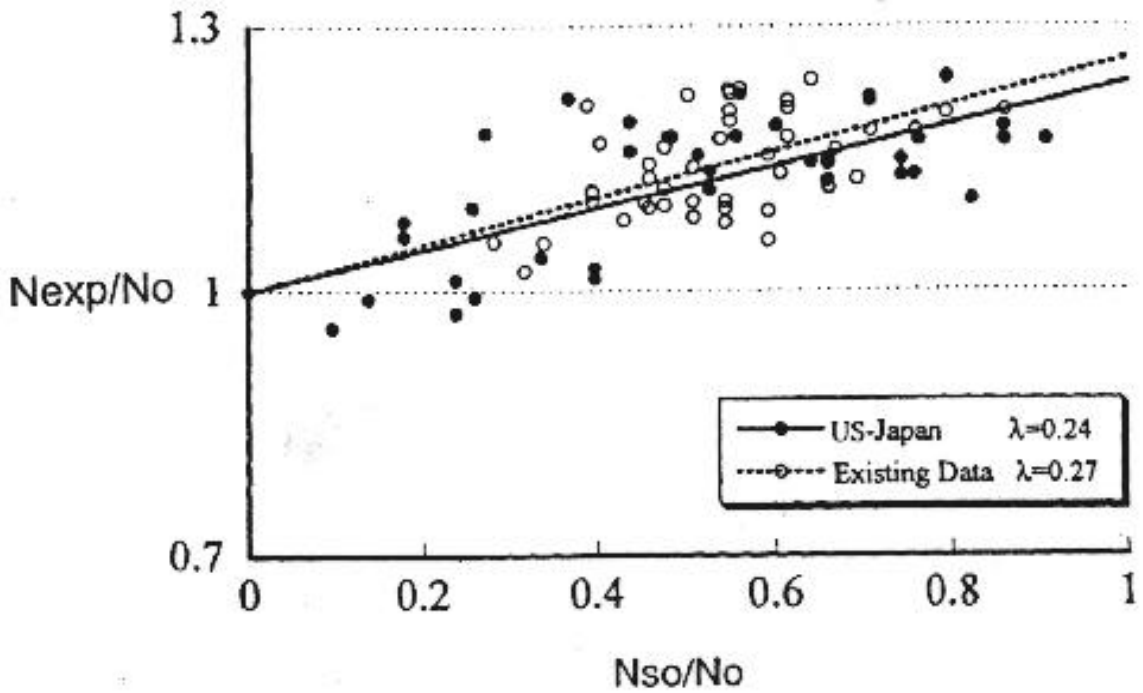
Figure 2.5 Experimental Axial Compressive Strengths of Circular CFT Columns
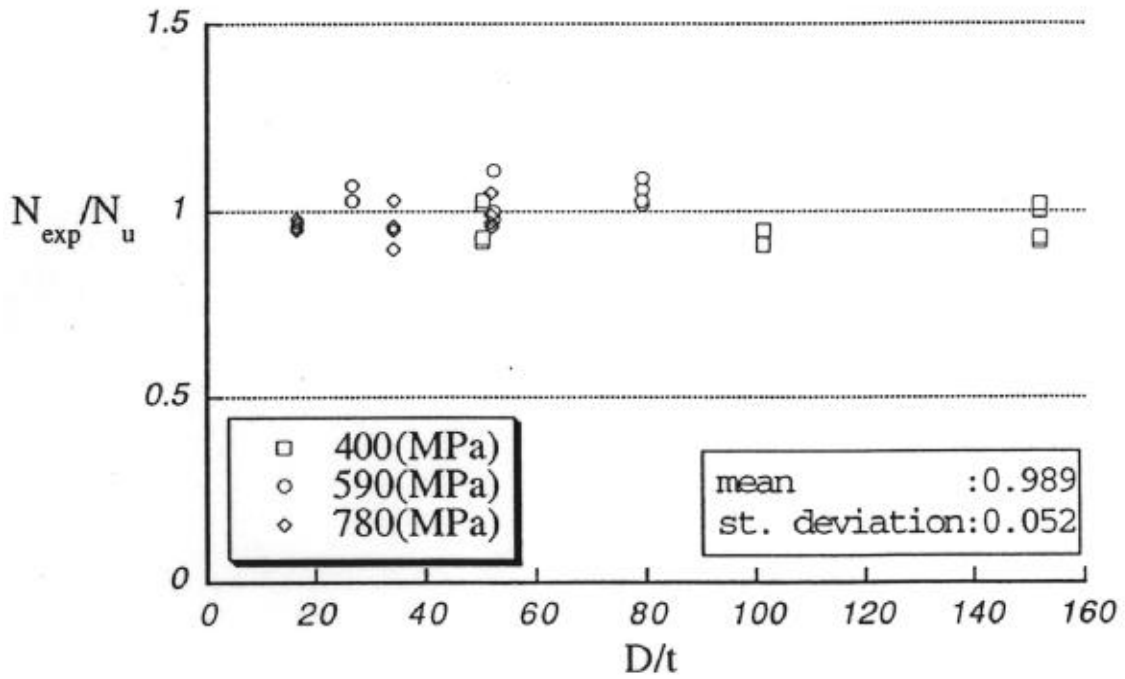
Figure 2.6 Comparisons Between Experimental and Calculated Strengths (Circular CFT Columns)

$$\sqrt{\alpha_s} = \frac{B}{t}\sqrt{\frac{\sigma_{sy}}{E_s}}$$
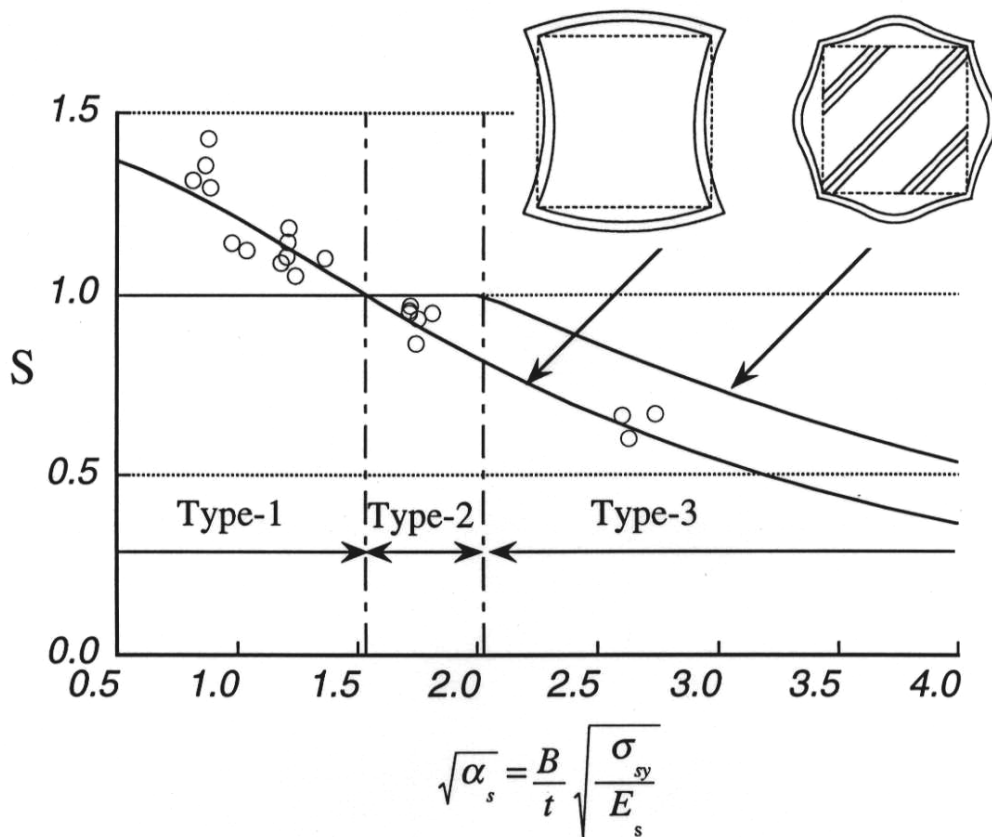
Figure 2.7 Compressive Strength Factors of Hollow Square Steel Tubes
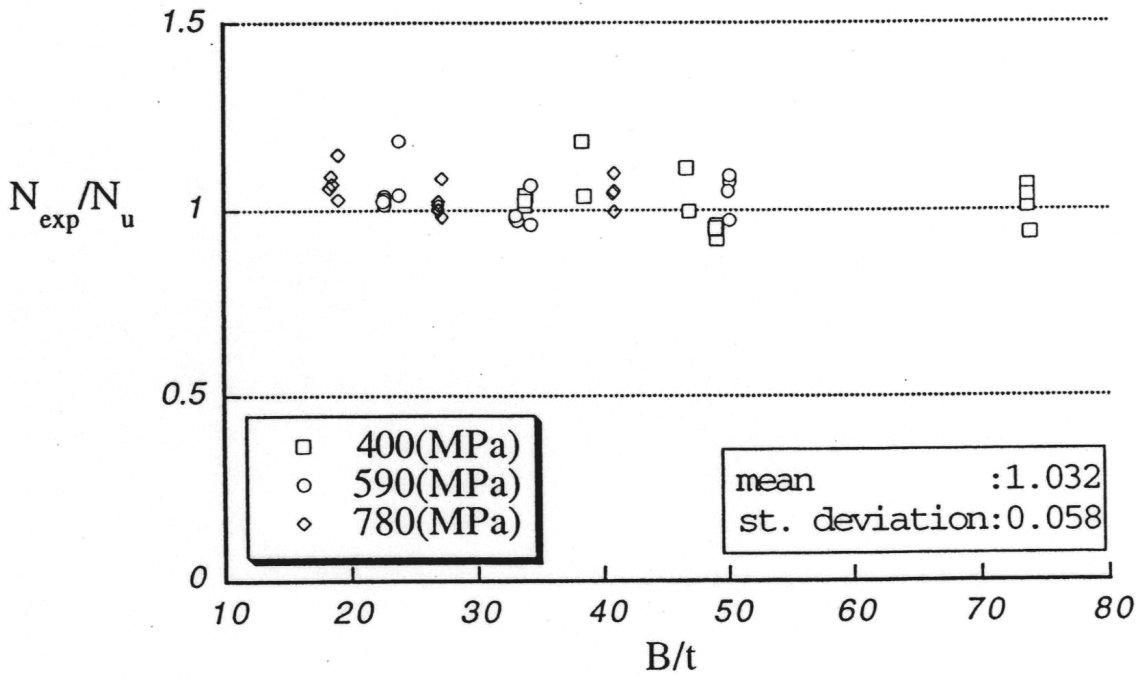
Figure 2.8 Comparisons Between Experimental and Calculated Strengths (Square CFT Columns)
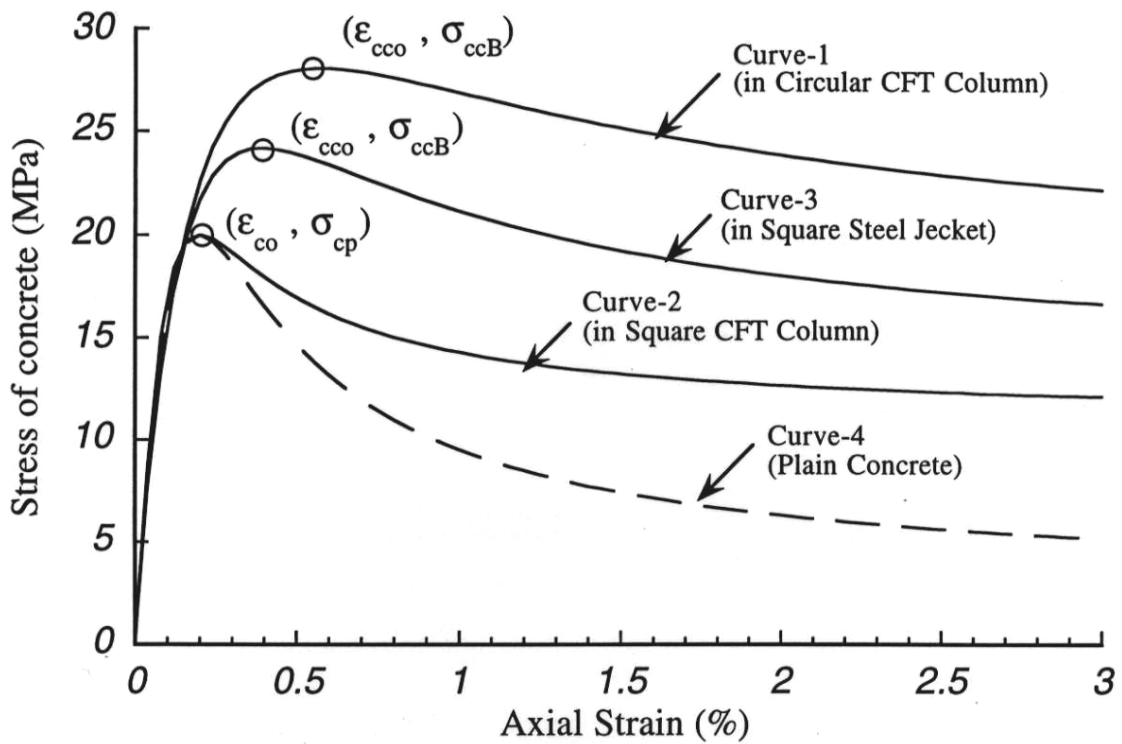
Figure 2.9 Stress vs. Strain Models for Concrete in CFT Column
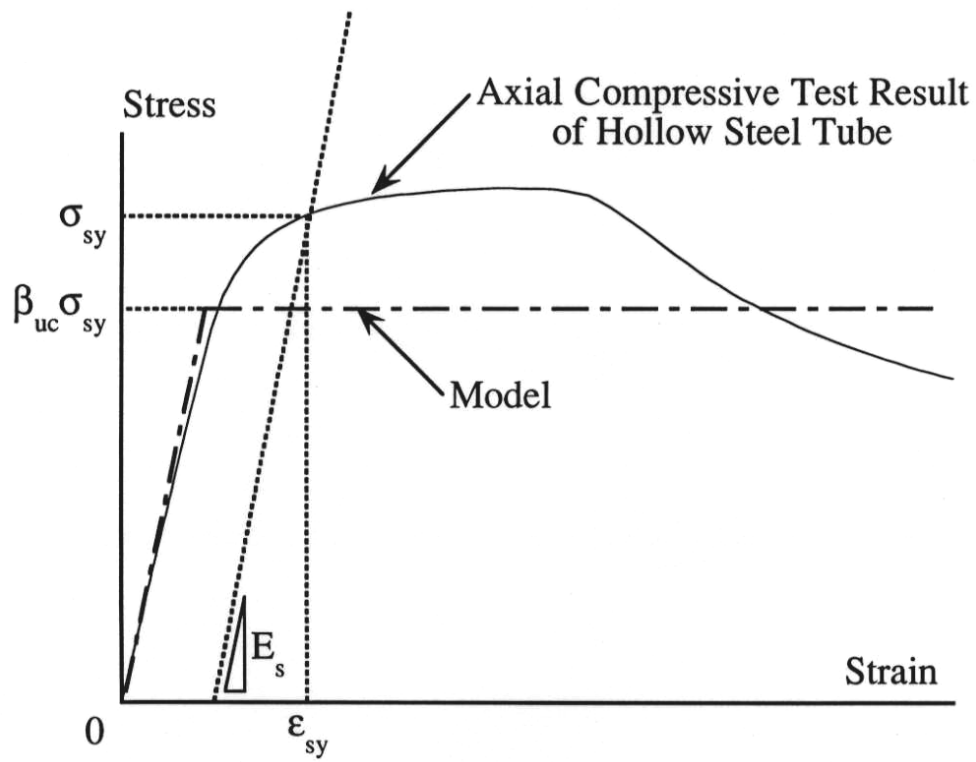
Figure 2.10 Stress vs. Strain Model for Steel Tube in Circular CFT Column
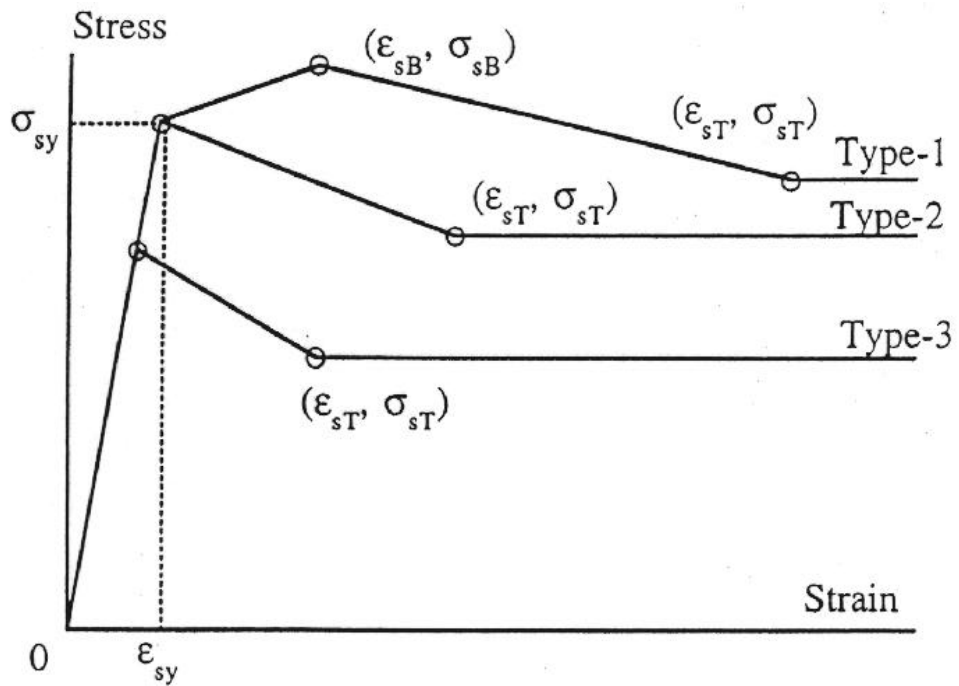
Figure 2.11 Stress vs. Strain Models for Steel Tube in Square CFT Column
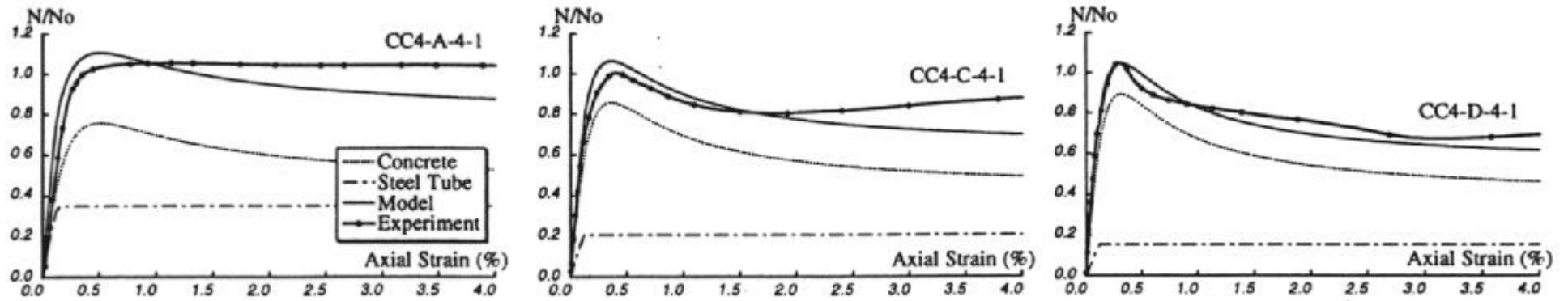
(a) CC4-A, C, D-4   Circular CFT Columns
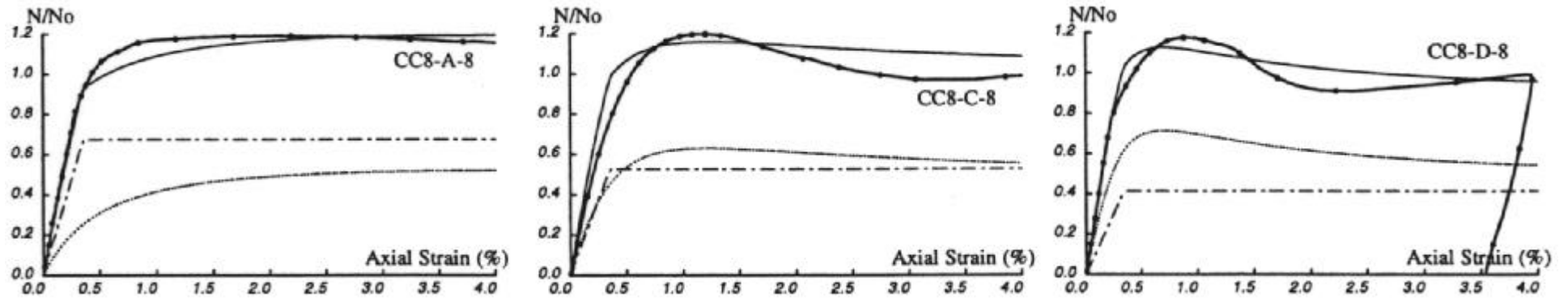
(b) CC8-A, C, D-8   Circular CFT Columns

Figure 2.12 Comparisons Between Experimental Results and Proposed Models
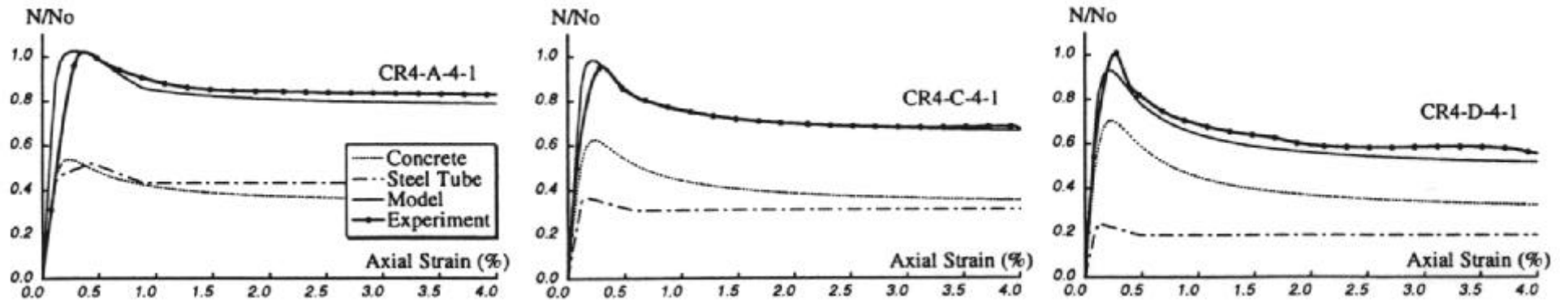
(a) CR4-A, C, D-4   Square CFT Columns
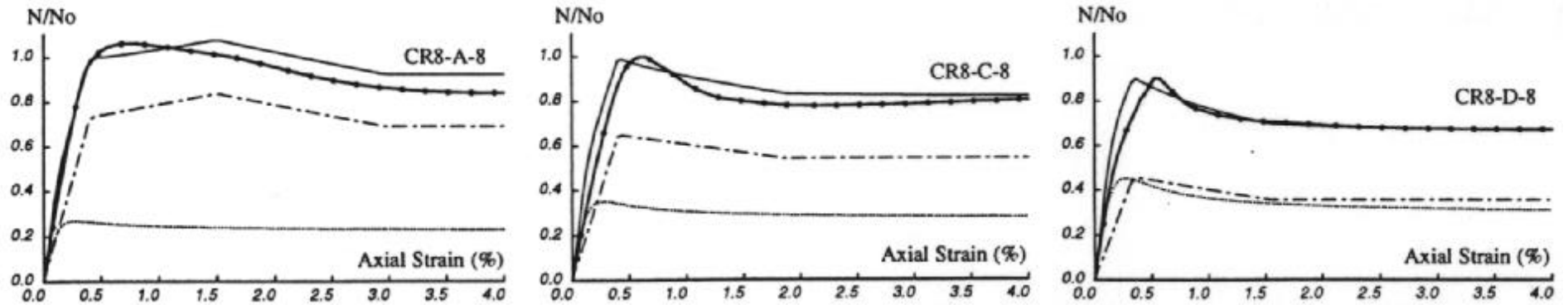
(b) CR8-A, C, D-8   Square CFT Columns

Figure 2.13 Comparisons Between Experimental Results and Proposed Models
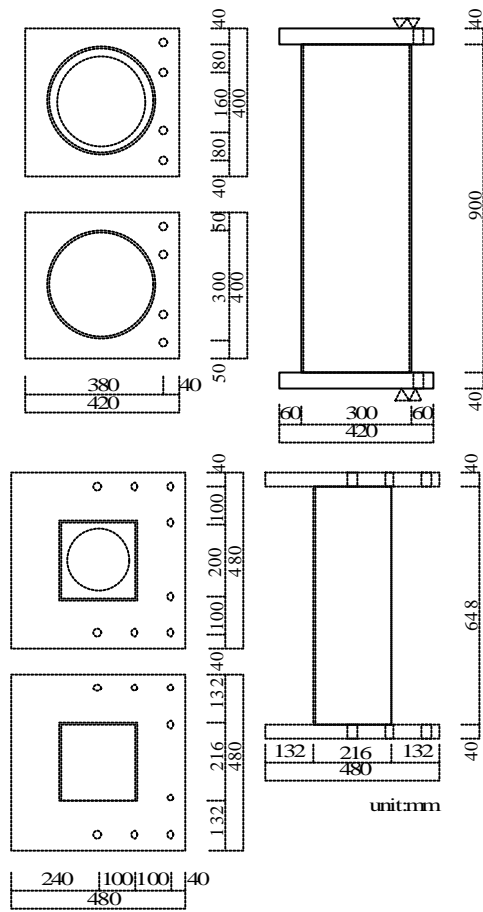
Figure 3.1 Dimensions of Eccentrically Loaded Stub Columns
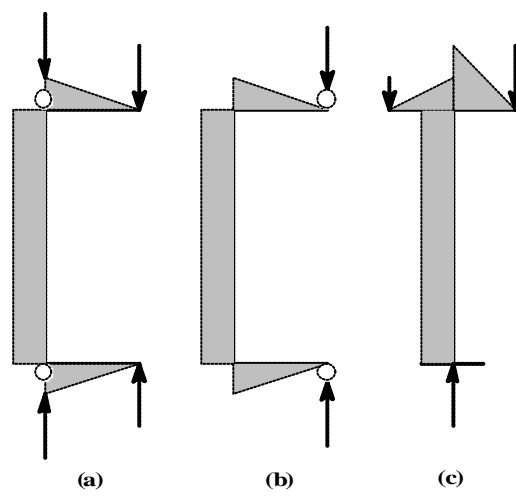
Figure 3.2 Loading Condition of Eccentrically Loaded Stub Columns
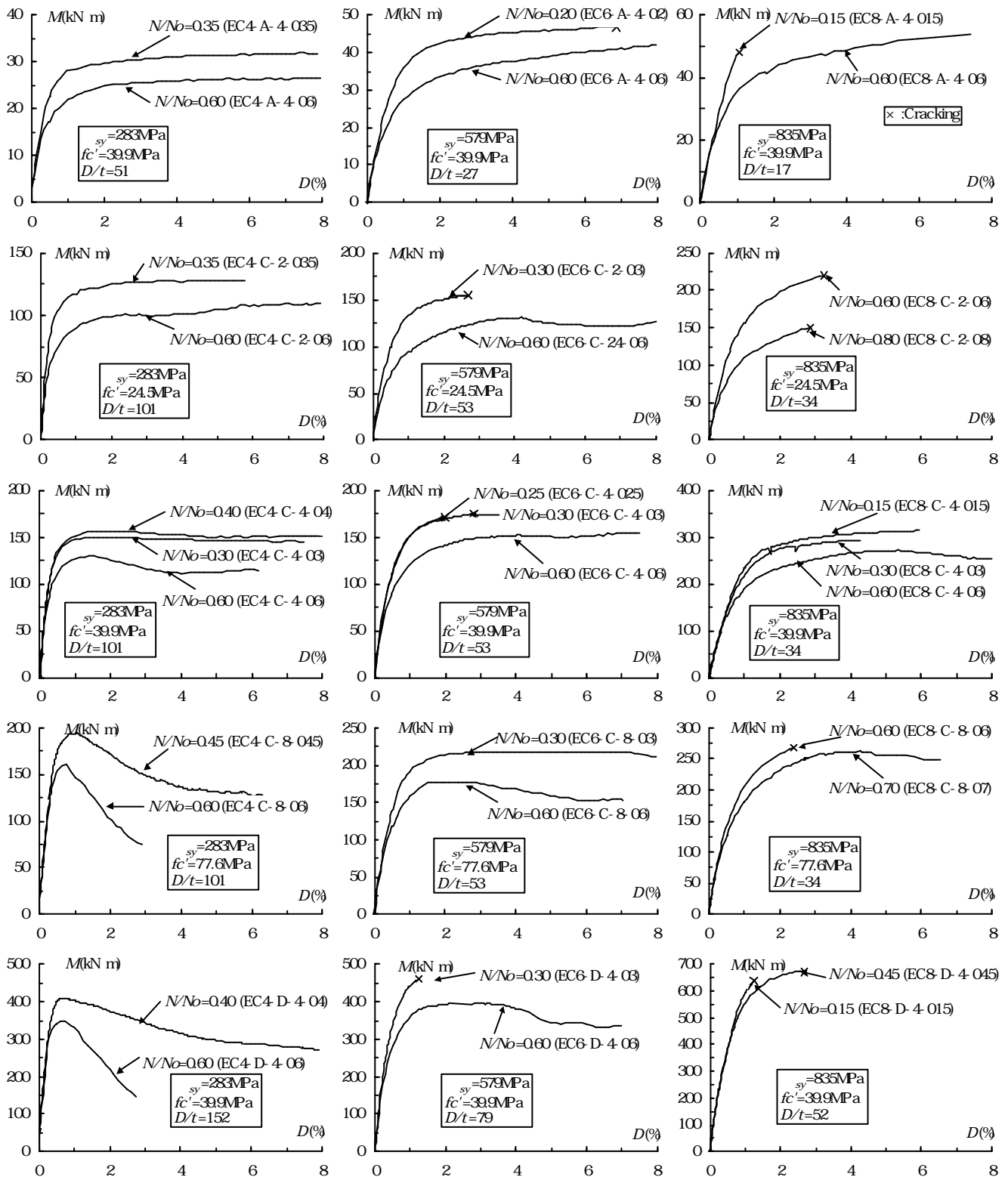
Figure 3.3(a) Moment vs. Curvature Relations (Circular Specimens)
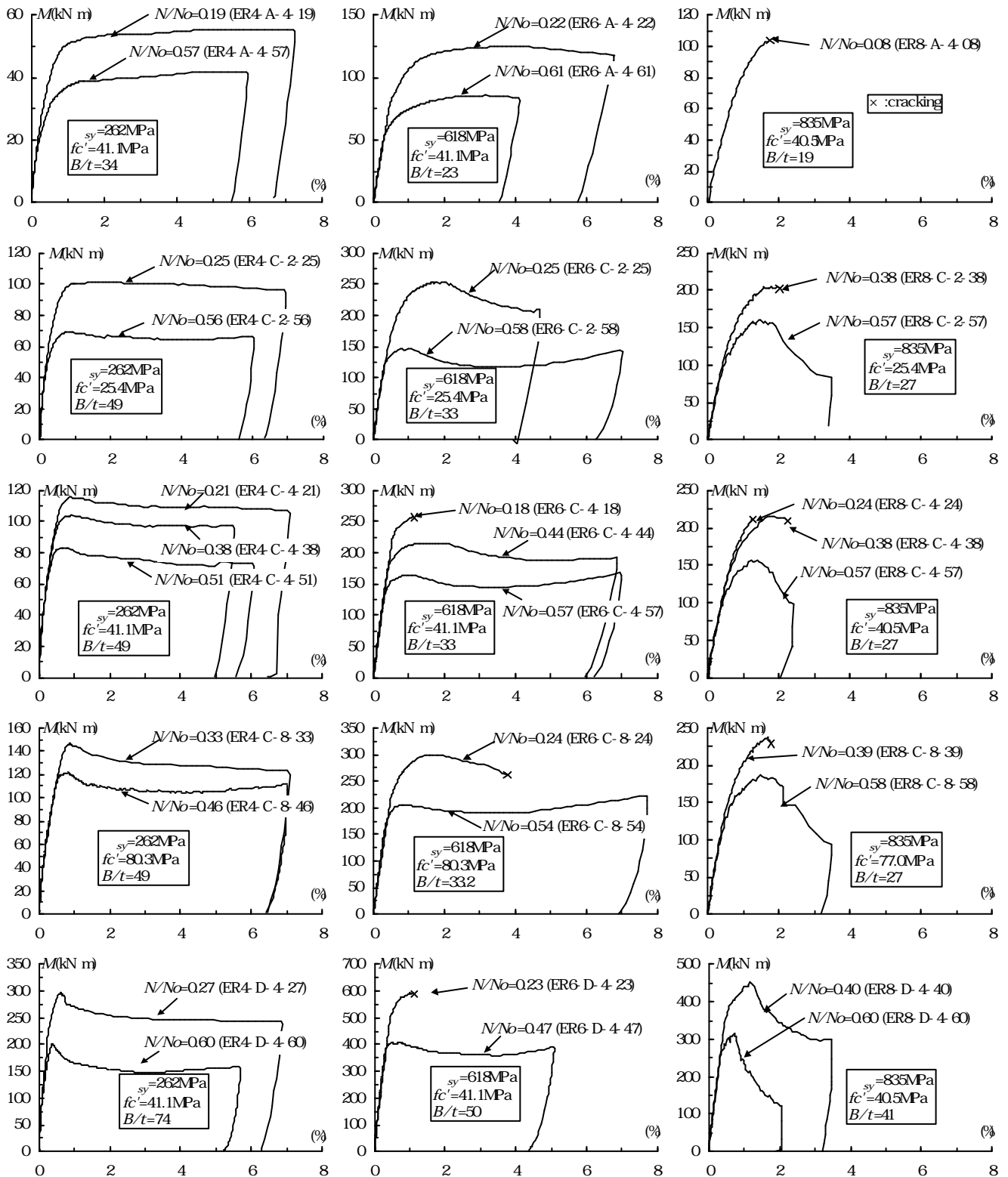
Figure 3.3(b) Moment vs. Curvature Relations (Square Specimens)
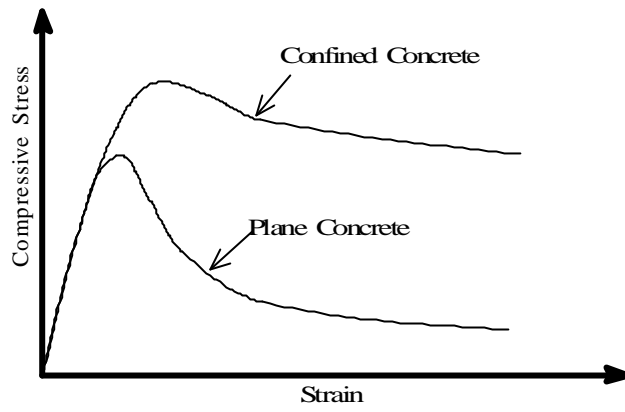
(a) Circular Section
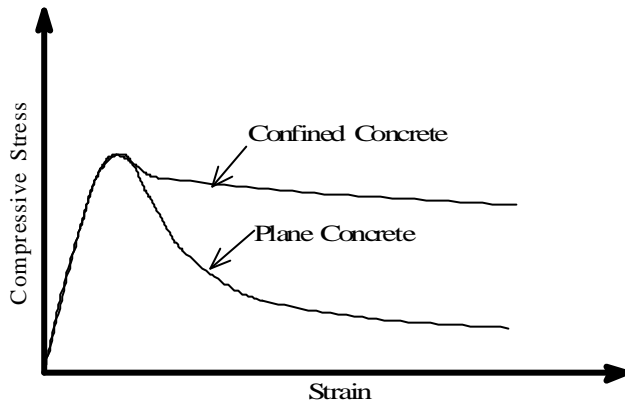
(b)Square Section

Figure 3.4 Stress vs. Strain Relations of Filled Concrete
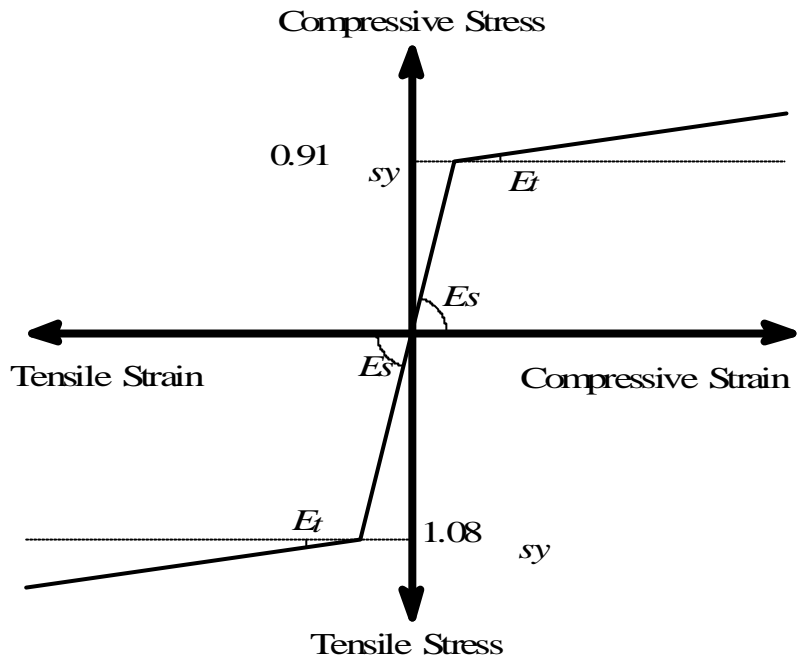
(a) Circular Tube
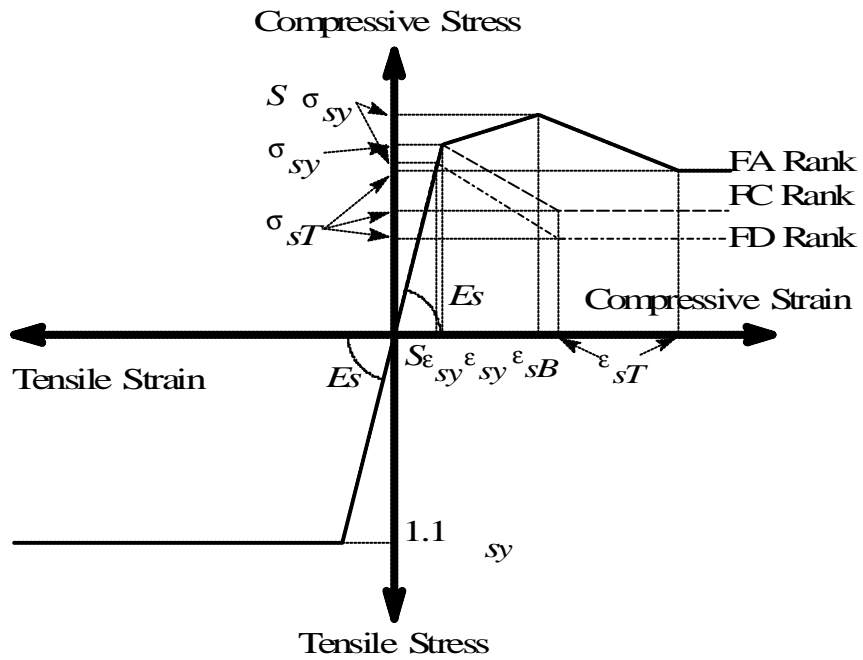
(b) Square Tube

Figure 3.5 Stress vs. Strain Relations of Steel Tube
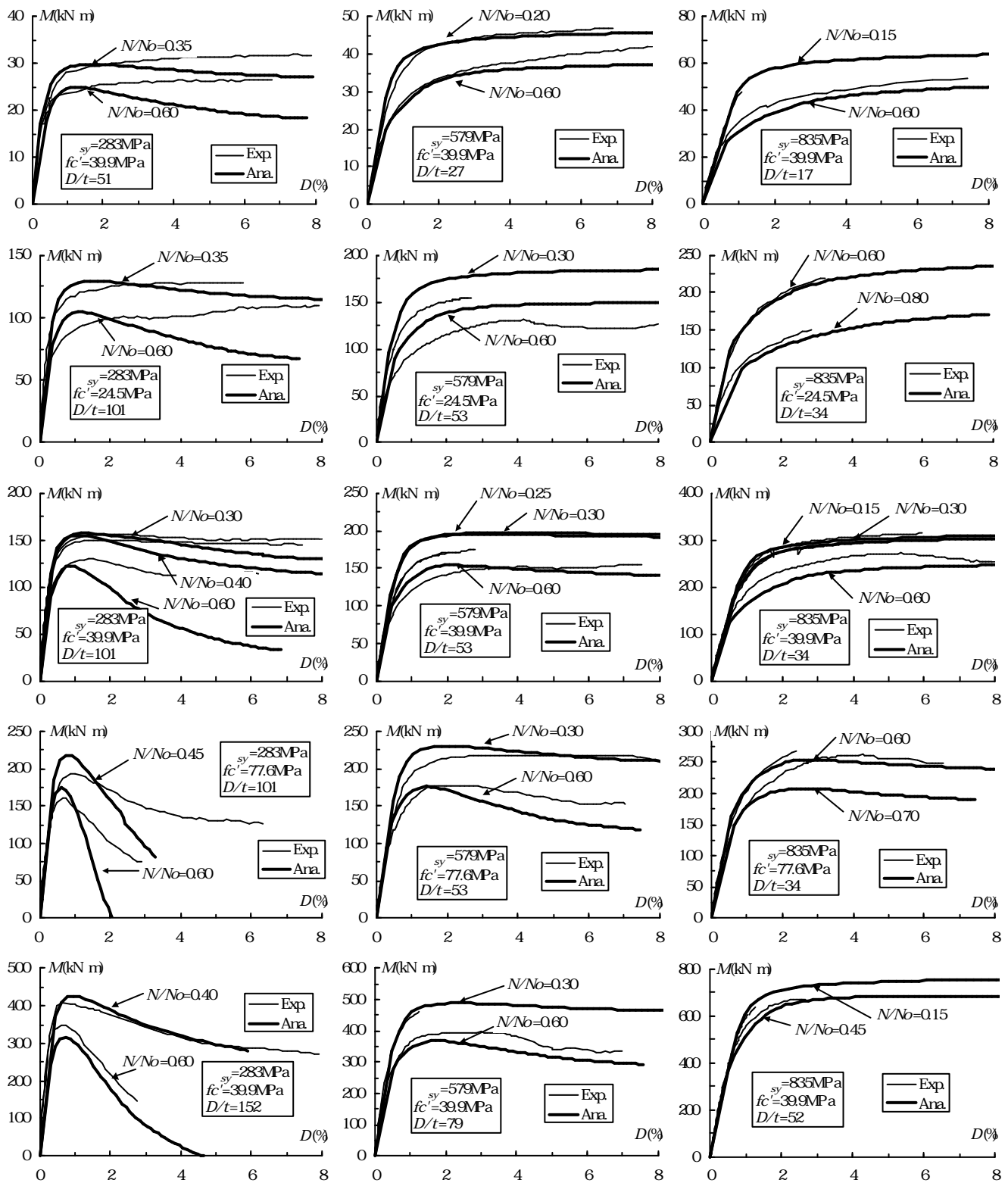
Figure 3.6(a) Comparisons Between Experimental and Analytical Results (Circular Tubes)
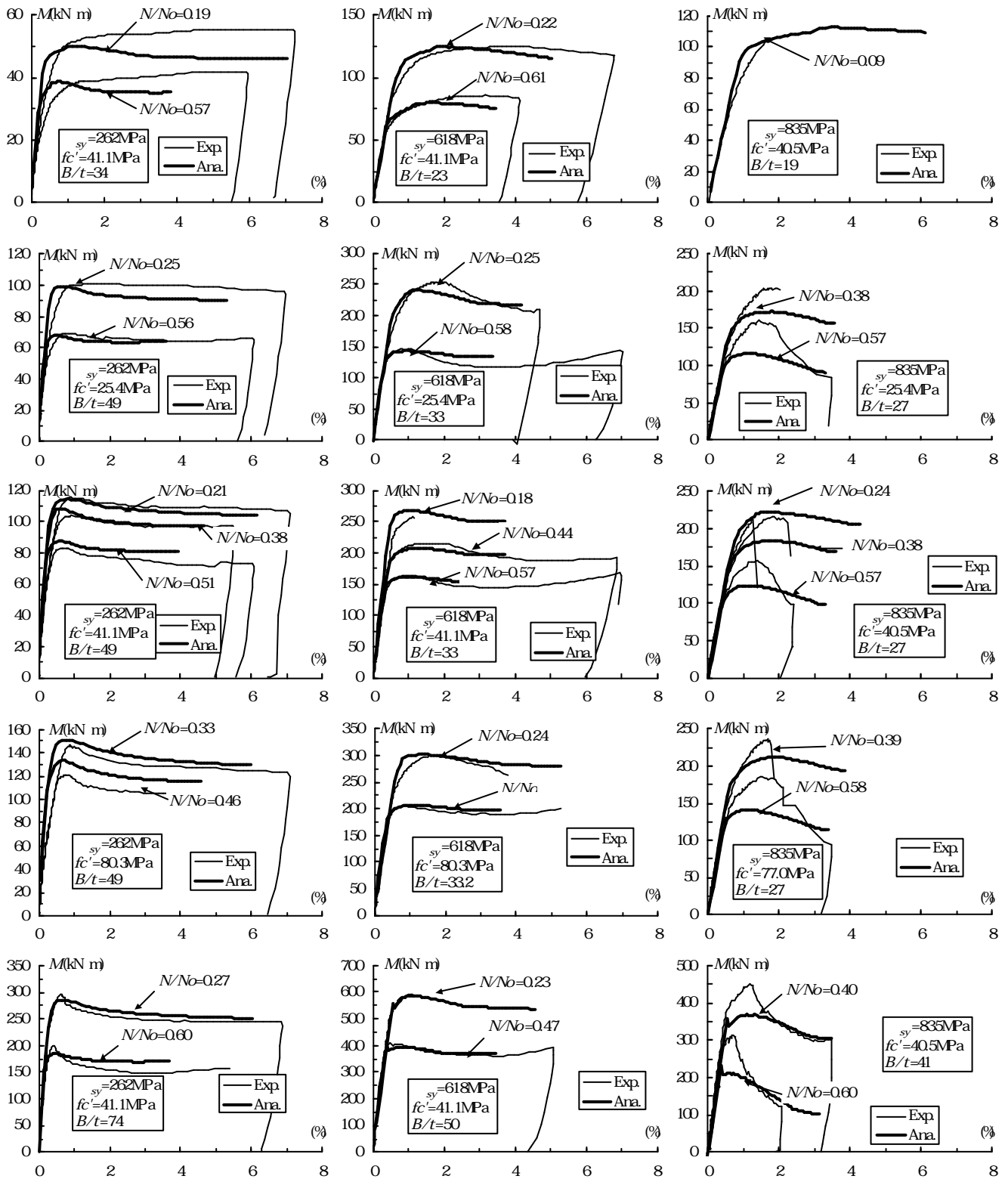
Figure 3.6(b) Comparisons Between Experimental and Analytical Results (Square Tubes)
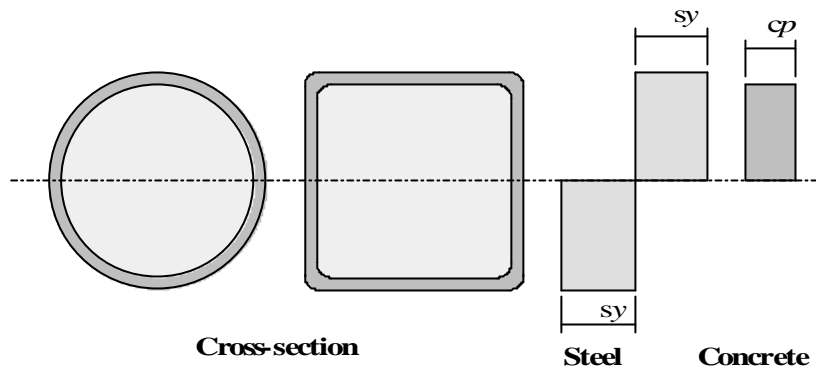
Figure 3.7 Assumed Stress Blocks
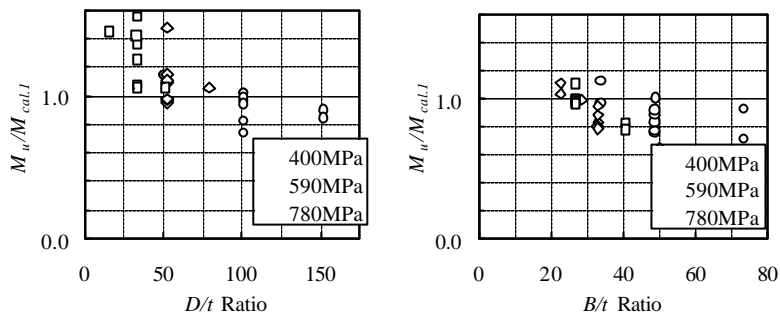
(a) Circular Tube   **(b) Square Tube**
Figure 3.8 Values of $M_u/M_{cal.1}$
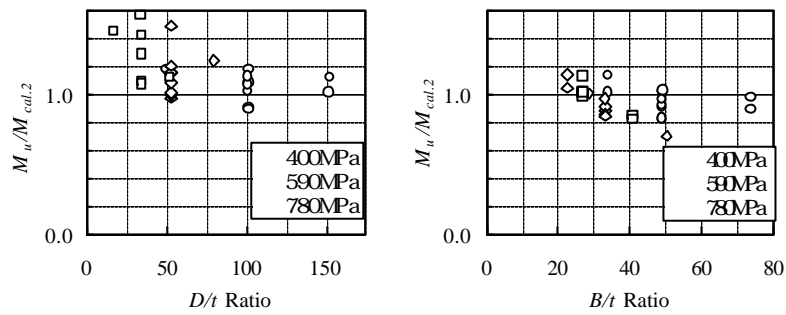
(a) Circular Tube   **(b) Square Tube**
Figure 3.9 Values of $M_u/M_{cal.2}$
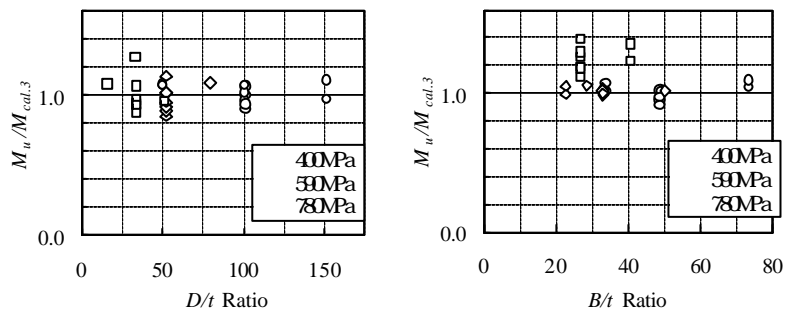
(a) Circular Tube   **(b) Square Tube**
Figure 3.10 Values of $M_u/M_{cal.3}$
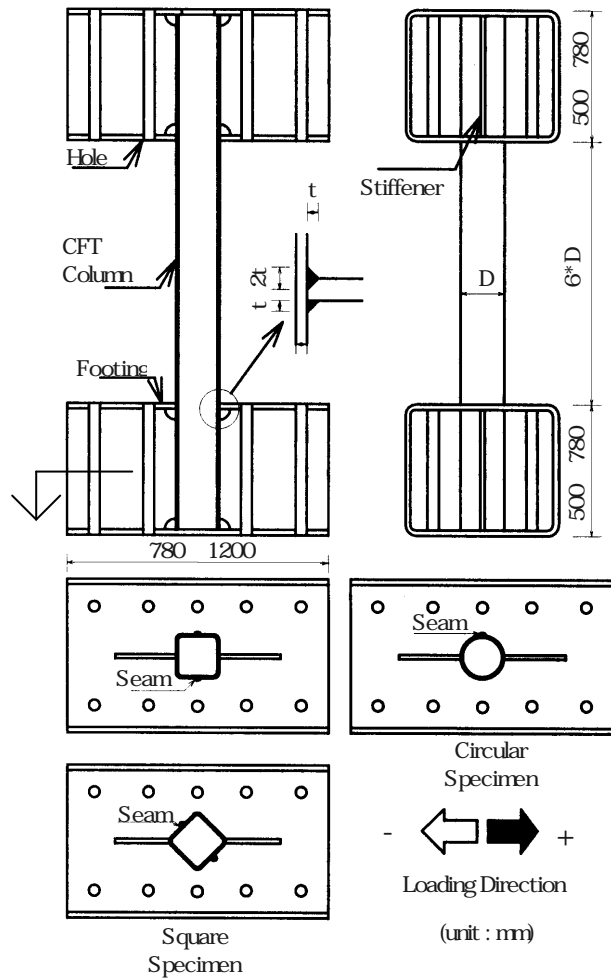
Figure 4.1 Details of Beam-Column Specimens

(a) Test Setup
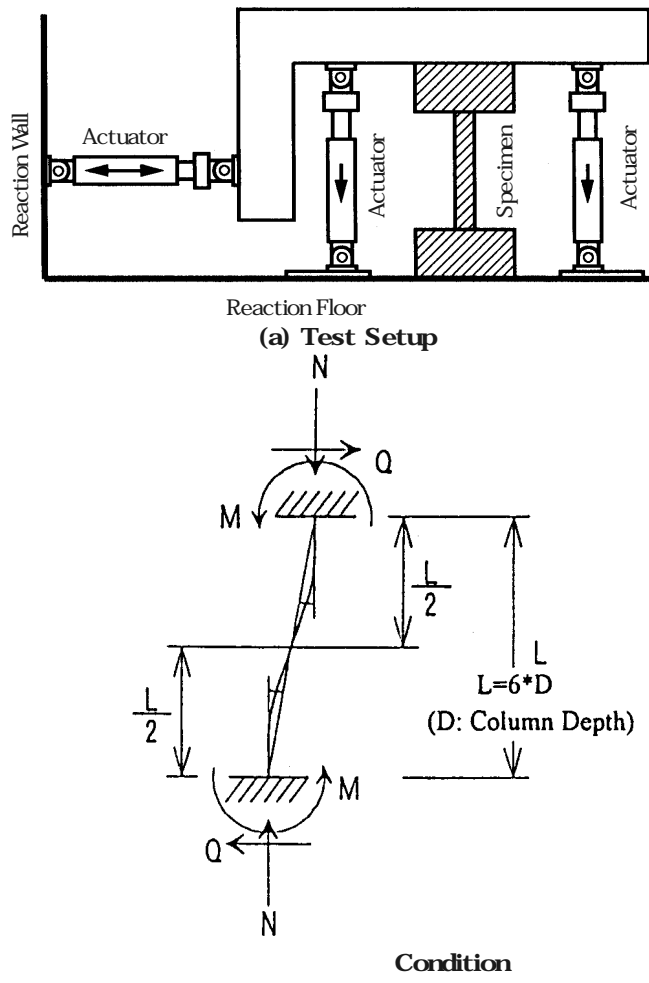
Condition

Figure 4.2 Test Setup and Loading Condition for Beam-Column Specimens
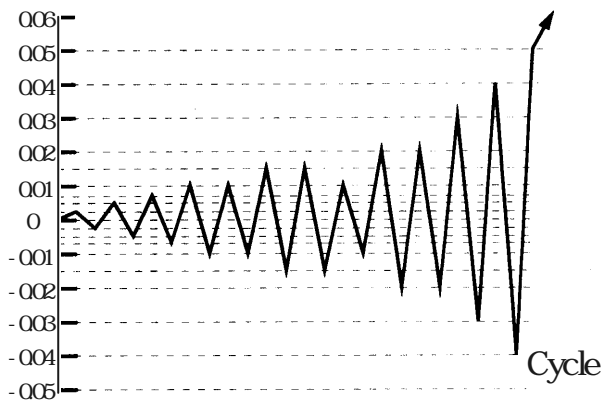
Figure 4.3 Loading History for Beam-Column Specimens
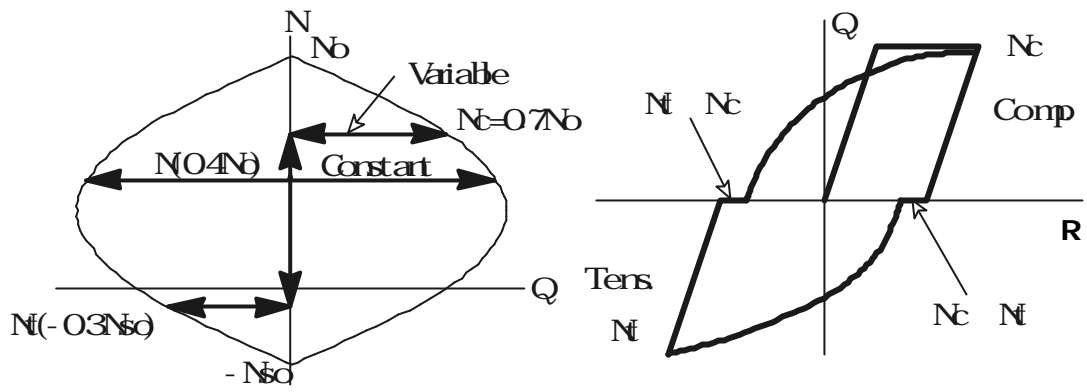
Figure 4.4 Rules for Axial Force Loading in Beam-Column Tests
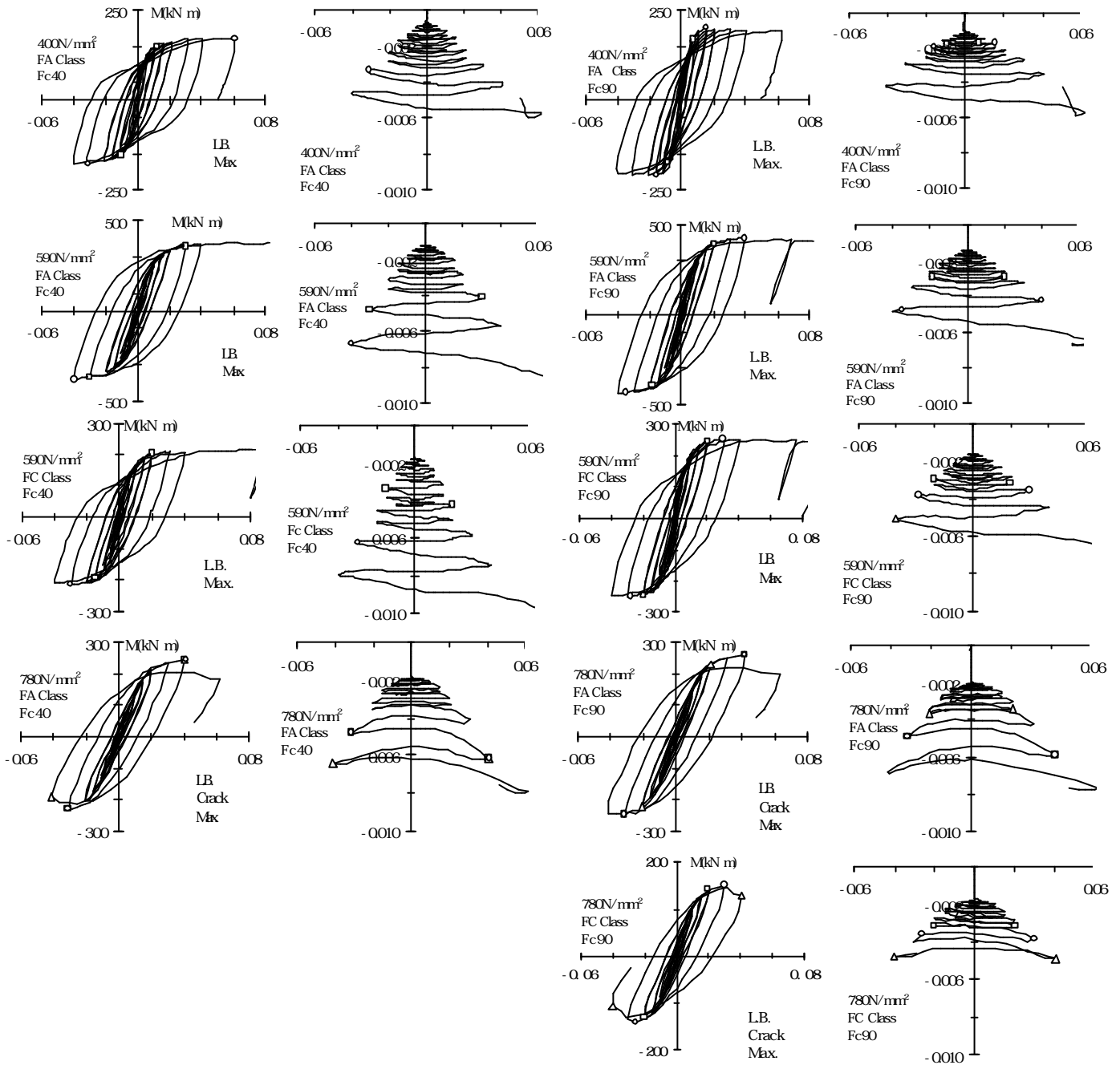
Figure 4.5 Test Results of Circular Interior Beam-Column Specimens
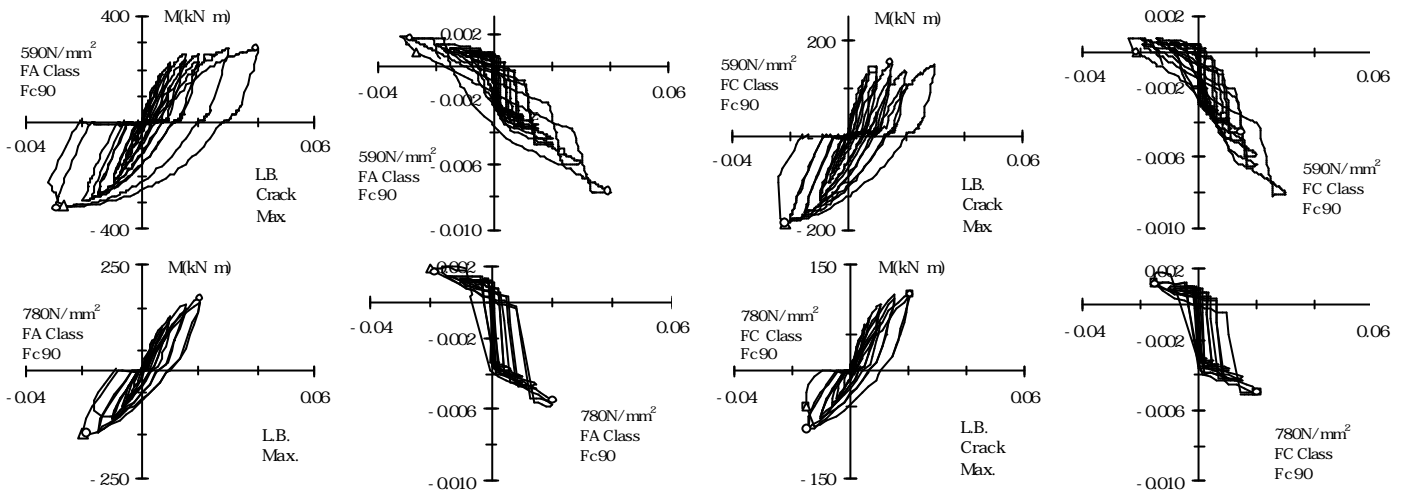
Figure 4.6 Test Results of Circular Exterior Beam-Column Specimens
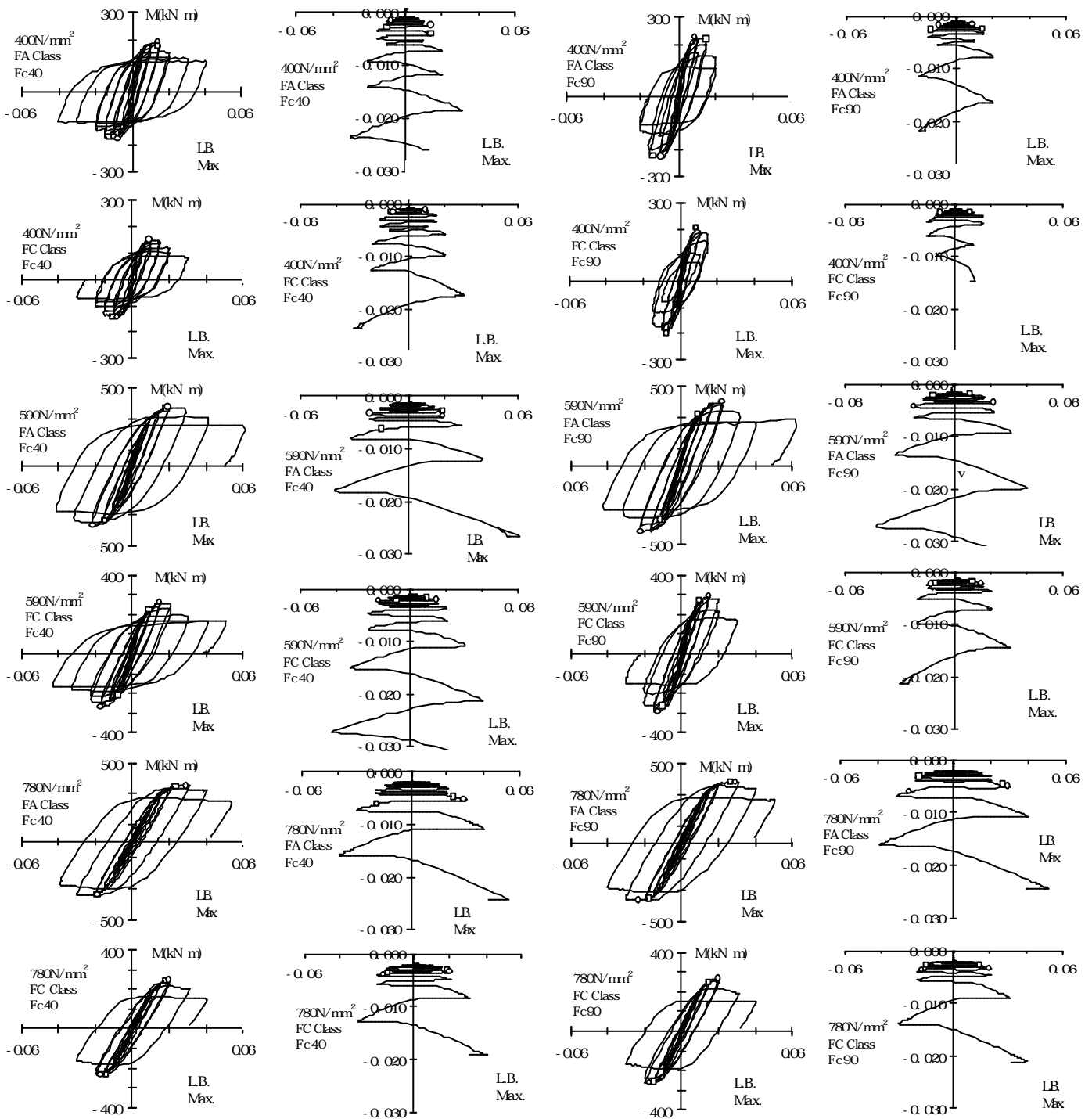
Figure 4.7 Test Results of Square Interior Beam-Column Specimens
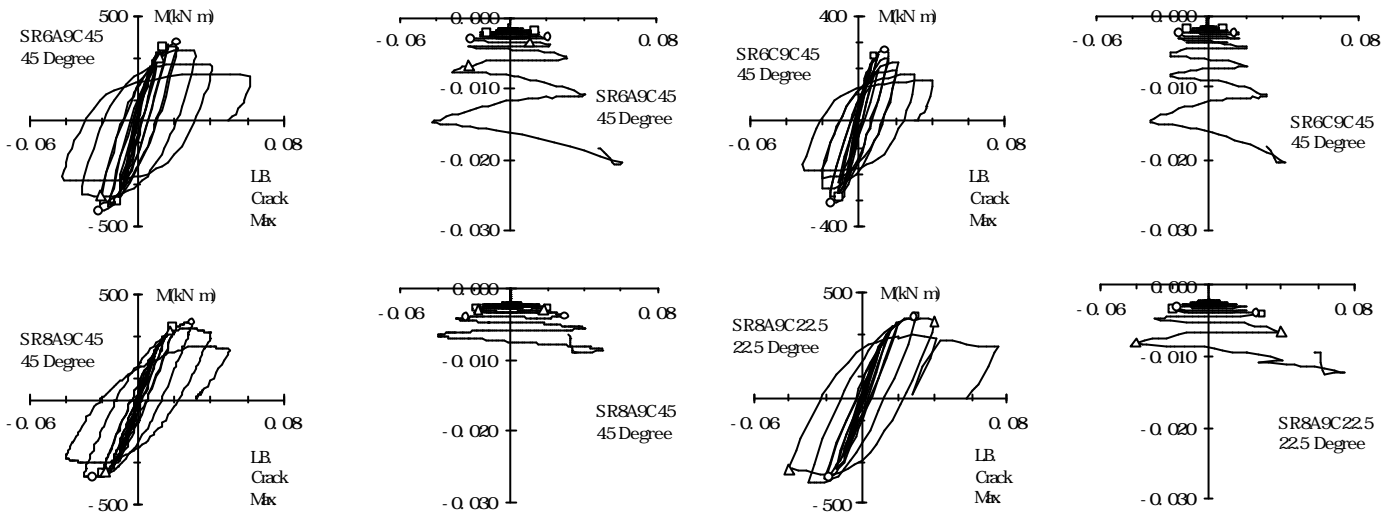
Figure 4.8 Test Results of Square Interior Beam-Column Specimens Subjected to Biaxial Bending
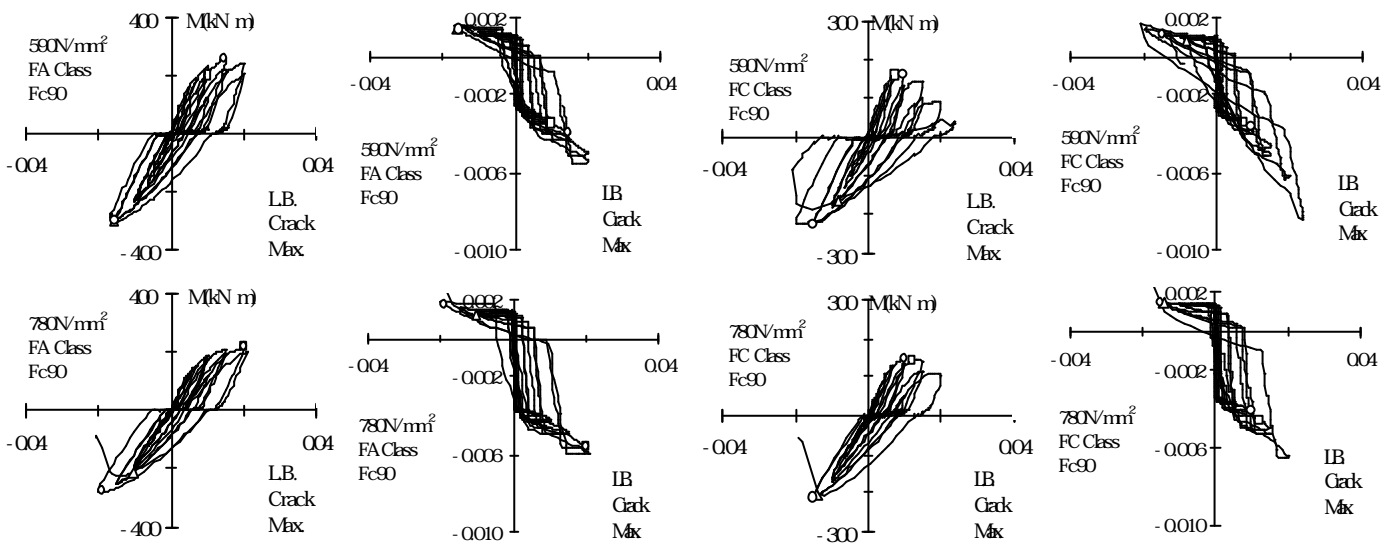
Figure 4.9 Test Results of Square Exterior Beam-Column Specimens
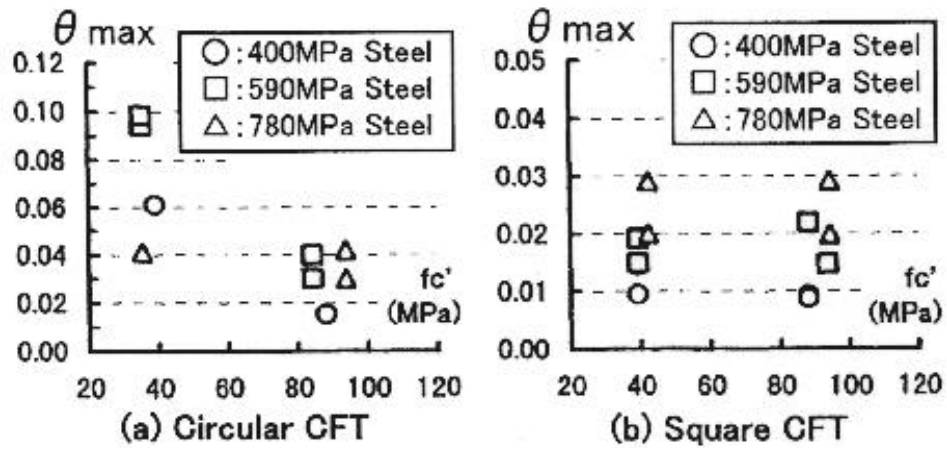
Figure 4.10 Effect of Material Strength on Ductility
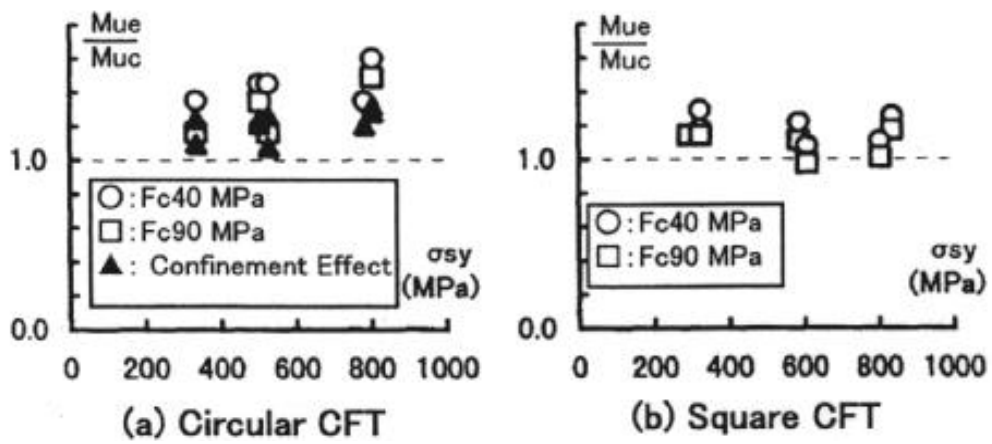
Figure 4.11 Effect of Material Strength on Enhancement in Flexural Strength
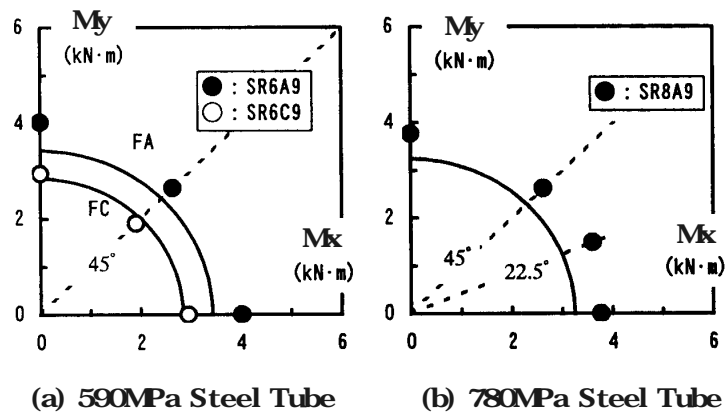
Figure 4.12 Effect of Loading Direction on Flexural Strength

(a) Column Model

(b) Curvature
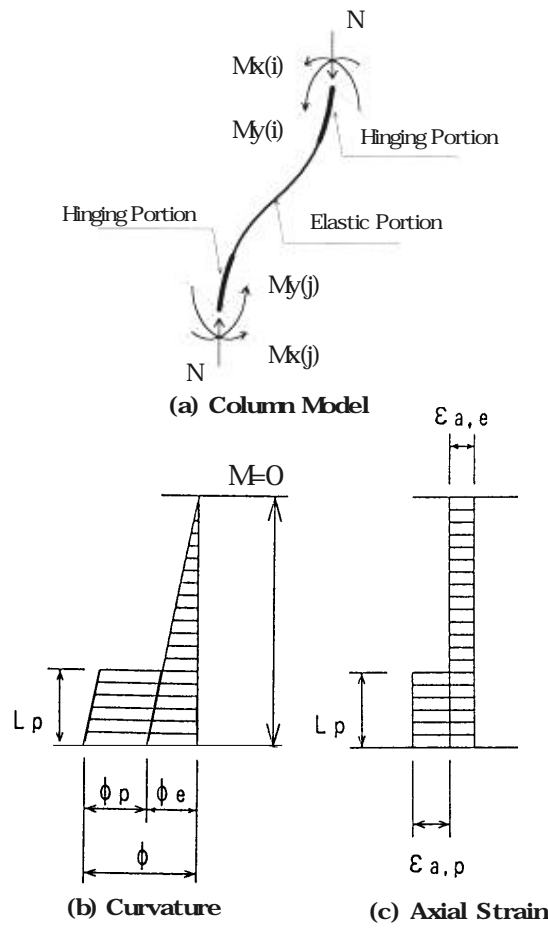
(c) Axial Strain

Figure 4.13 Model of Beam-Column, and Assumed Curvature and Axial Strain Distributions

(a) Square CFT   **(b) Circular CFT**
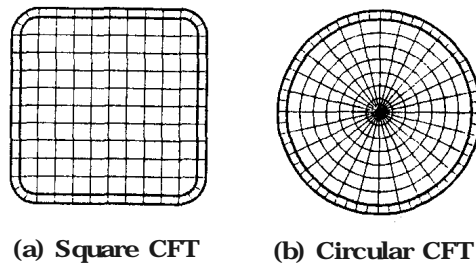
Figure 4.14 Analytical Fiber Elements at the Critical Sections of Square and Circular CFT

(a) Concrete   **(b) Steel Tube**
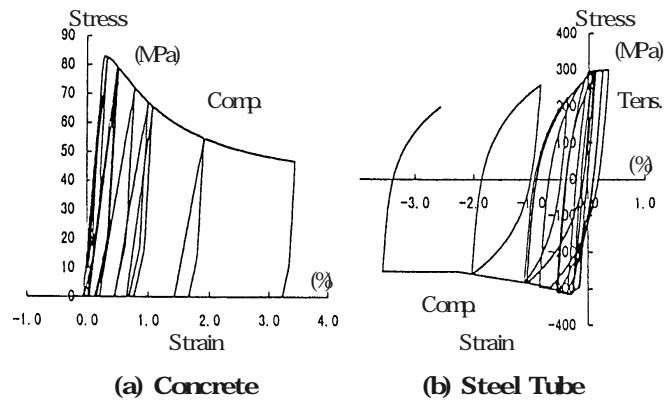
Figure 4.15 Typical Stress vs. Strain Relationships of Concrete and Steel Tube
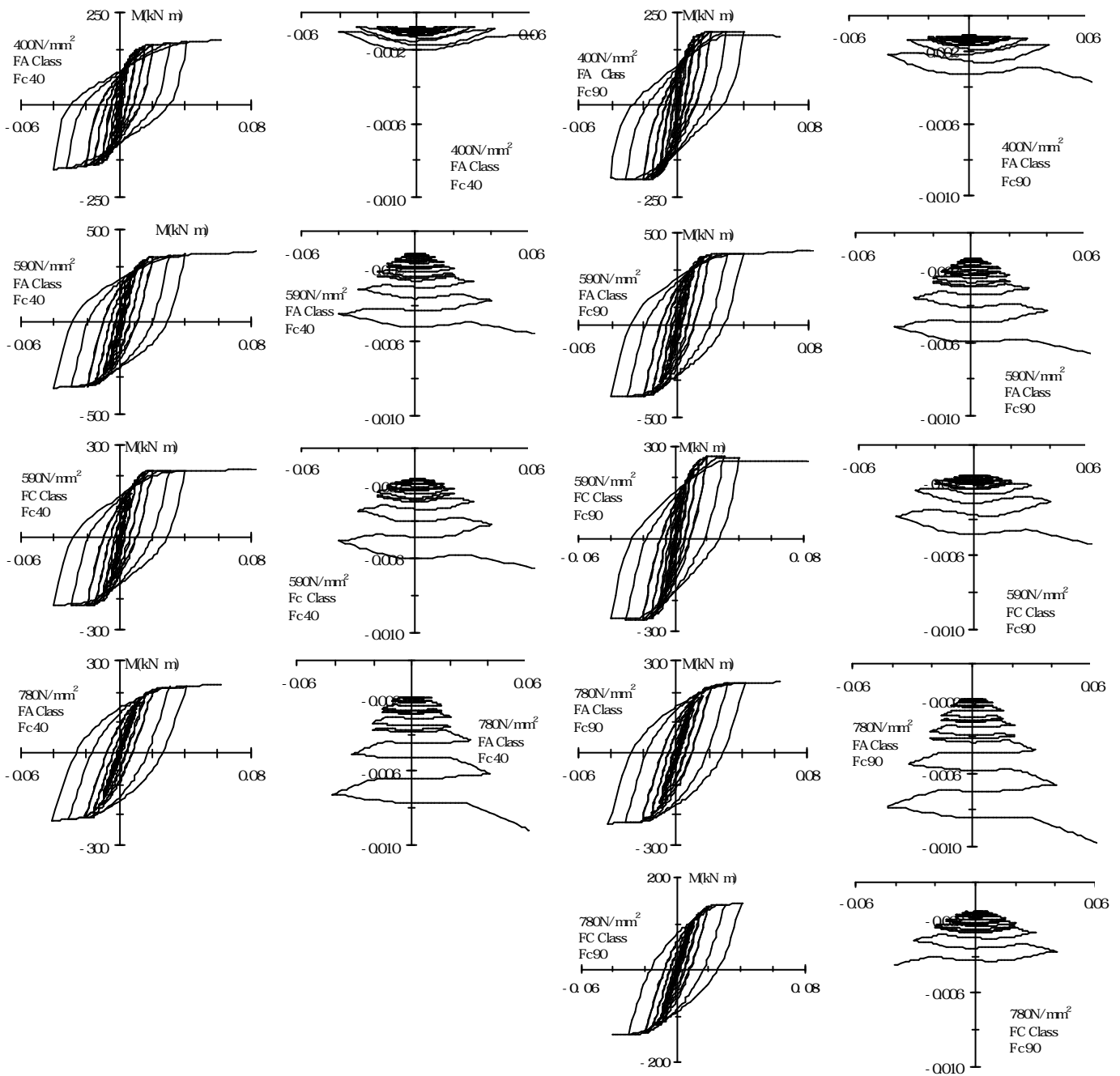
Figure 4.16 Analytical Results of Circular Interior Beam-Column Specimens
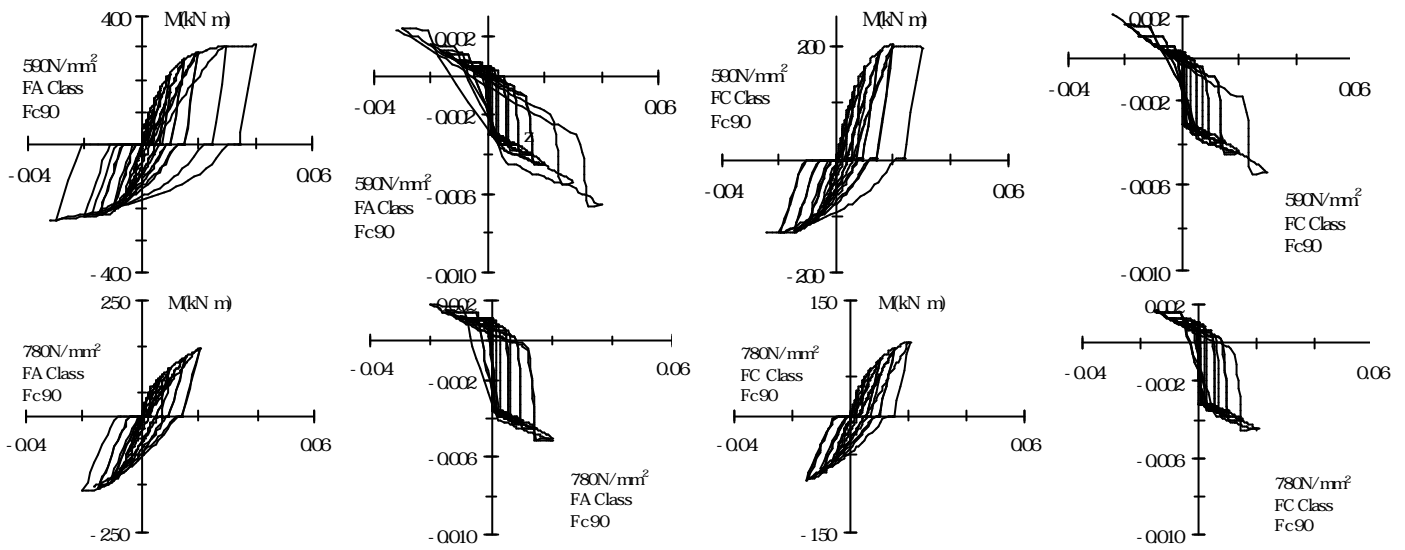
Figure 4.17 Analytical Results of Circular Exterior Beam-Column Specimens
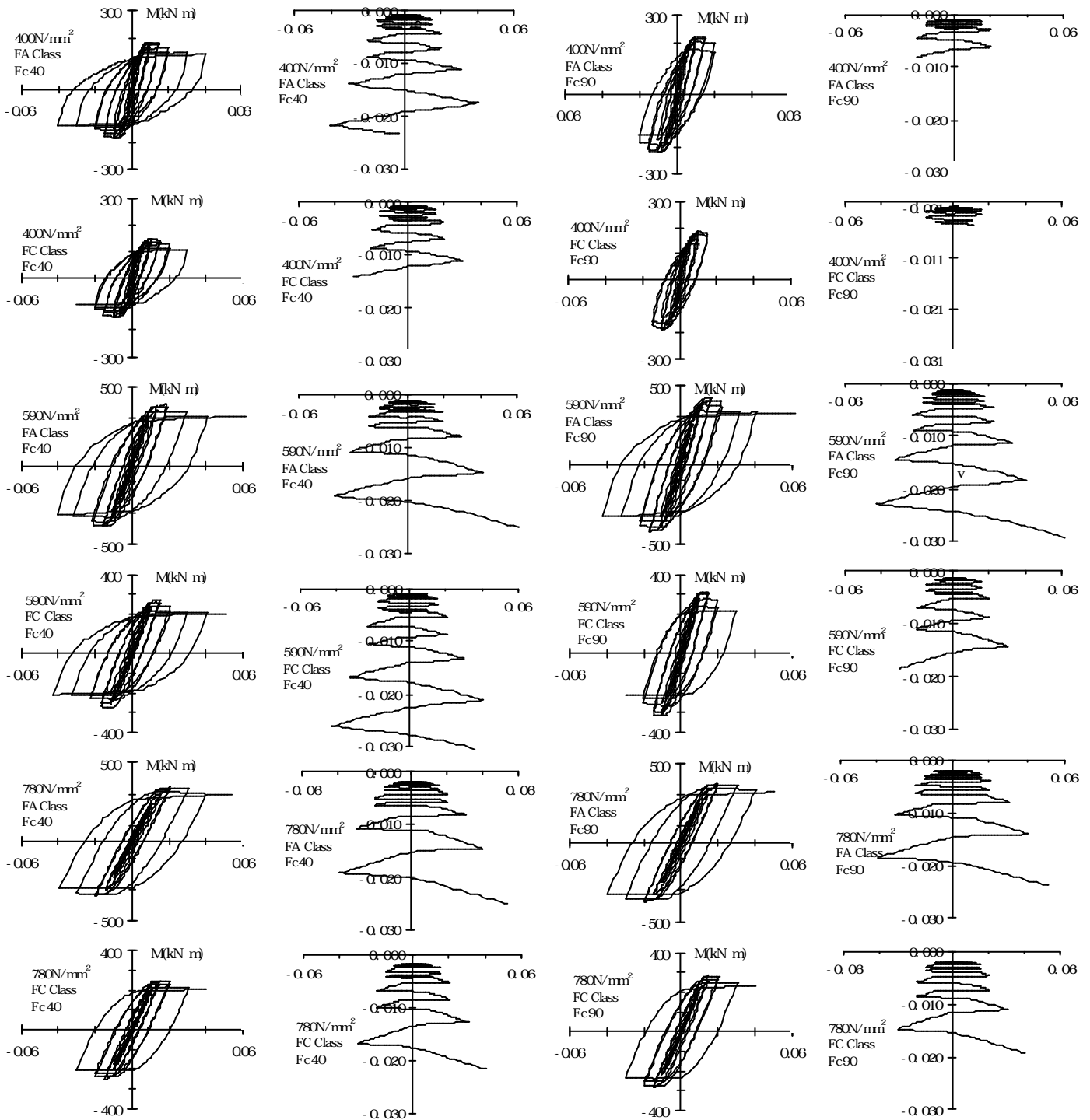
Figure 4.18 Analytical Results of Square Interior Beam-Column Specimens
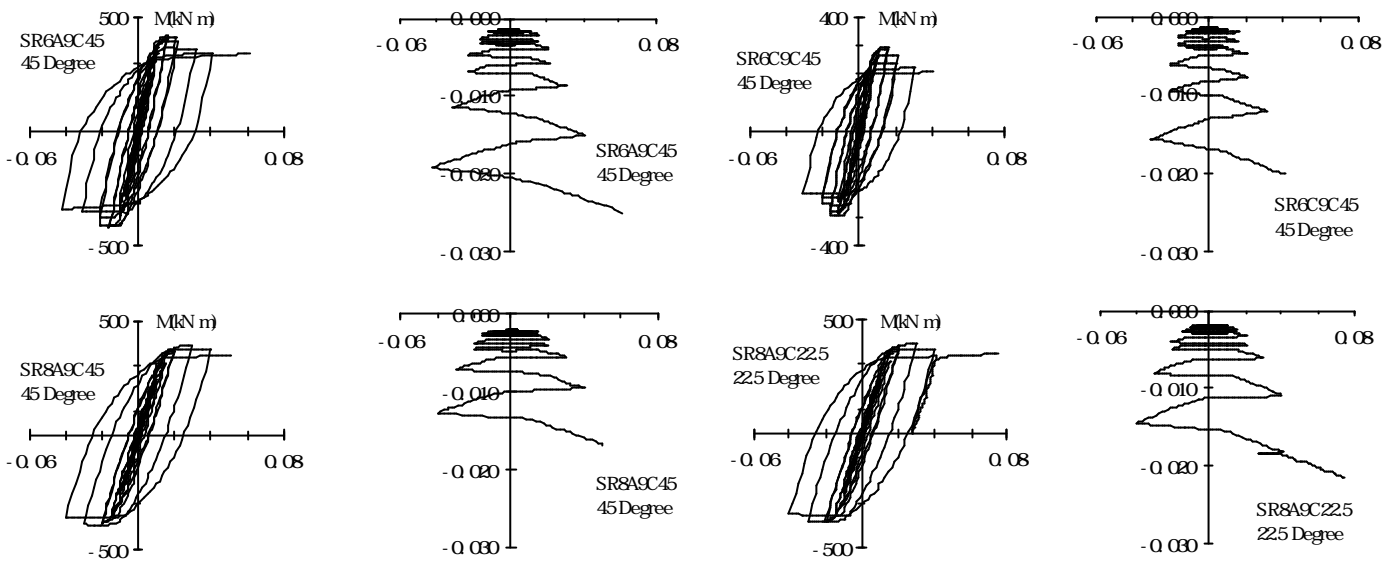
Figure 4.19 Analytical Results of Square Interior Beam-Column Specimens Subjected to Biaxial Bending
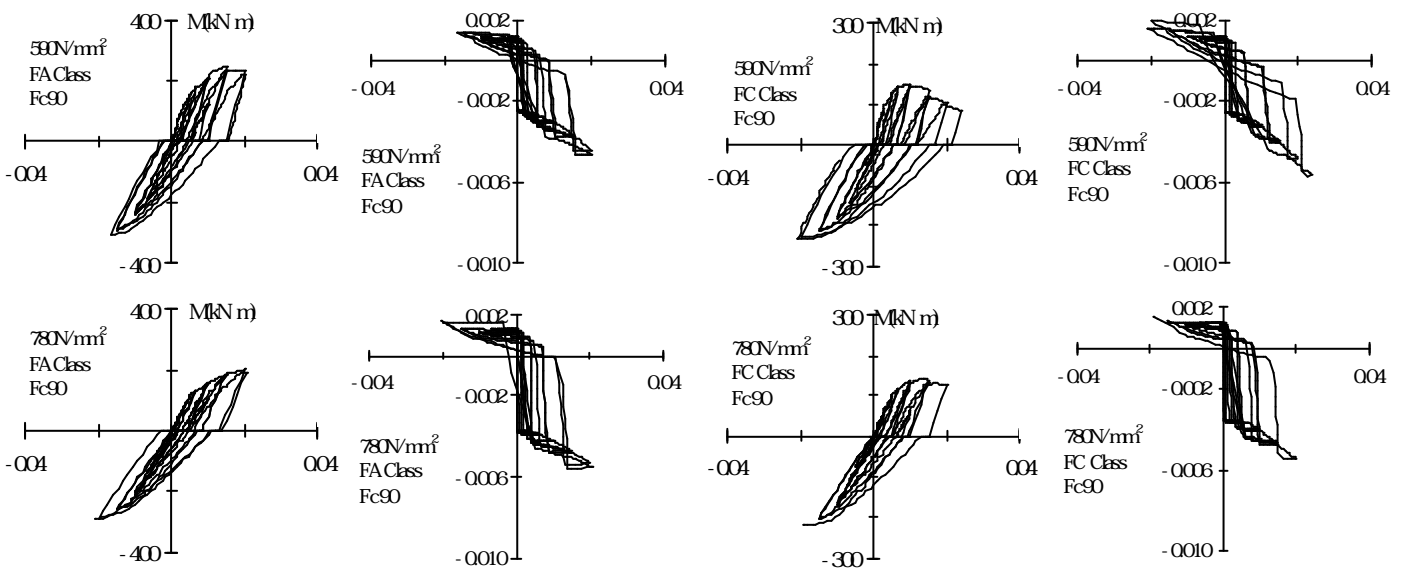
Figure 4.20 Analytical Results of Square Exterior Beam-Column Specimens

(a) SPECIMEN: R1, R2, R3

(b) SPECIMEN: R4

(c) SPECIMEN: R5

(d) SPECIMEN: R6

(e) SPECIMEN: C1, C2, C3
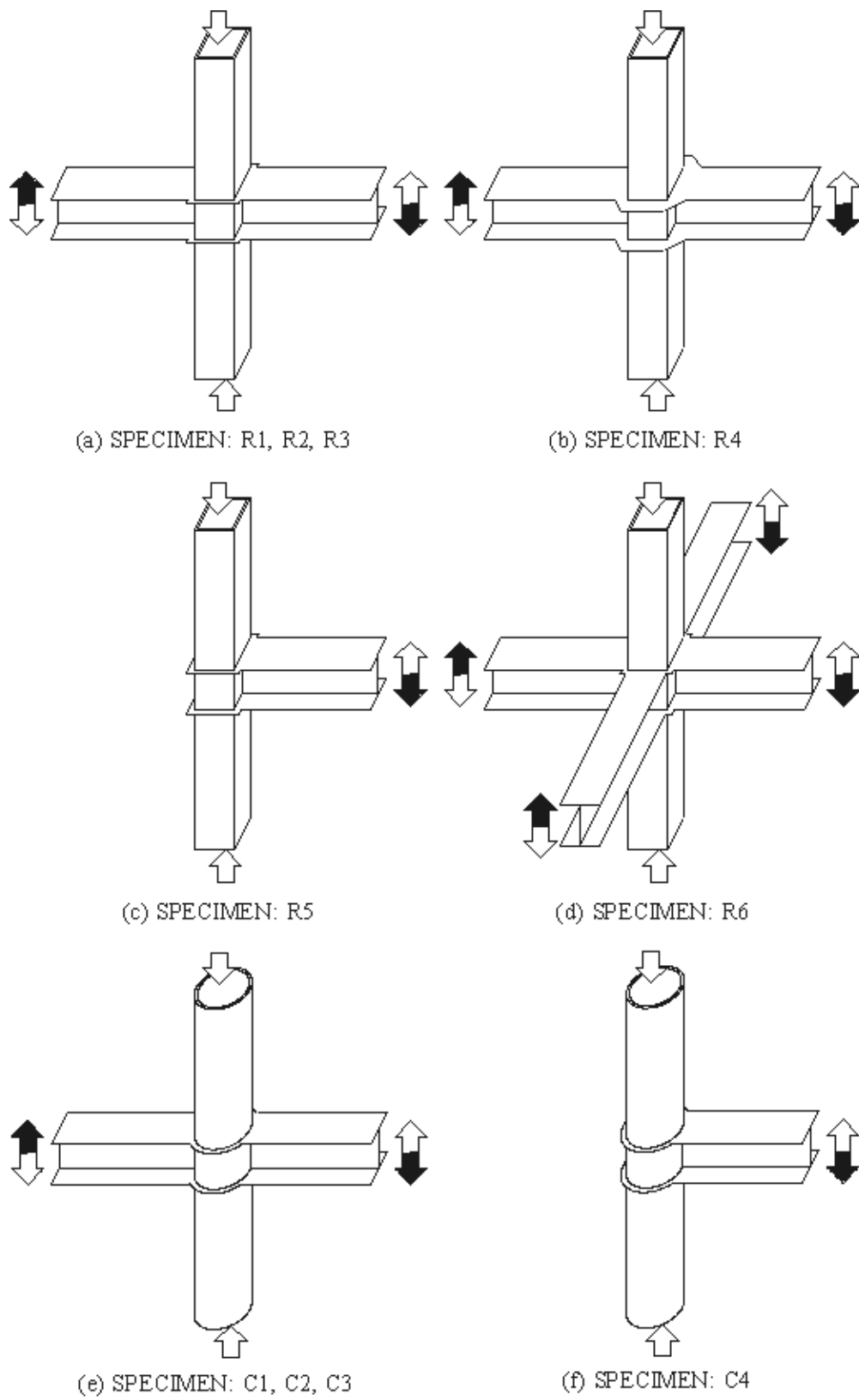
(f) SPECIMEN: C4

Figure 5.1 Shapes of Specimens
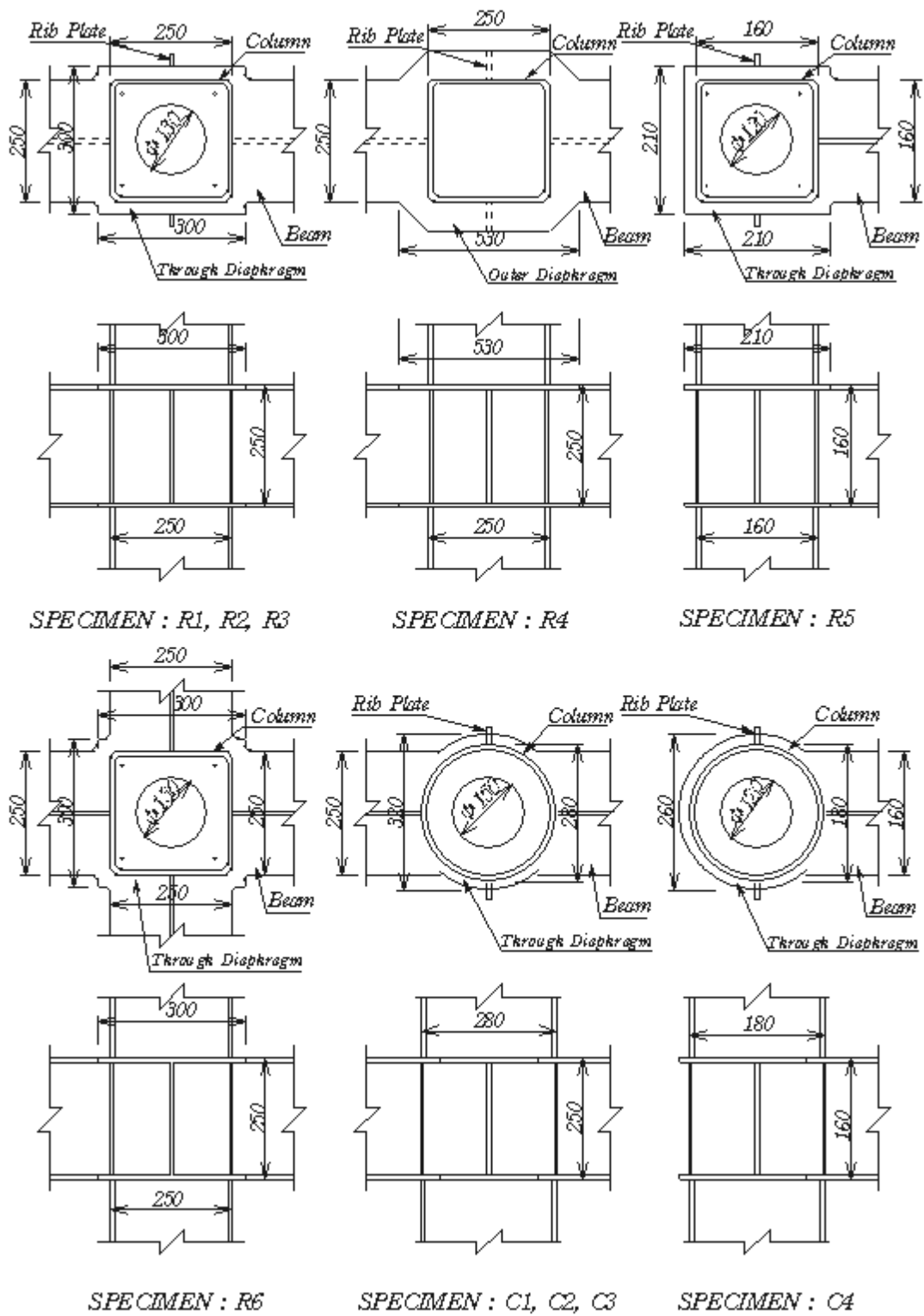
Figure 5.2 Details of Panel Zone
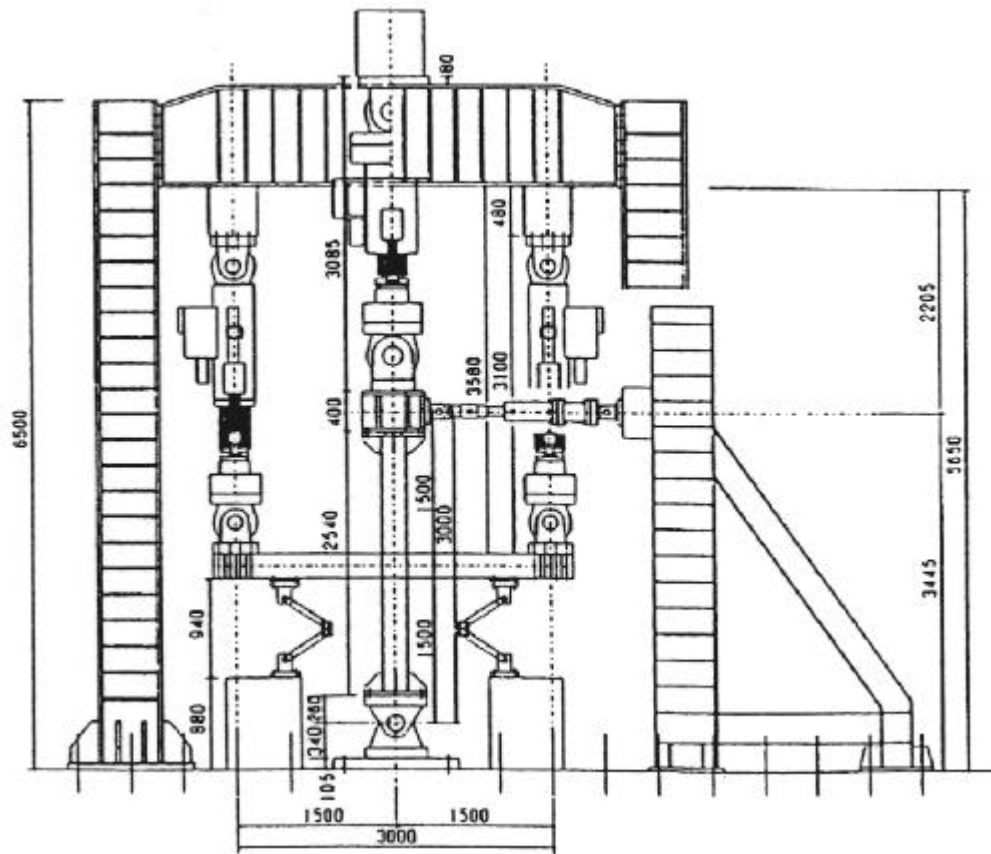
Figure 5.3 Test Setup for Specimens R1 and R2
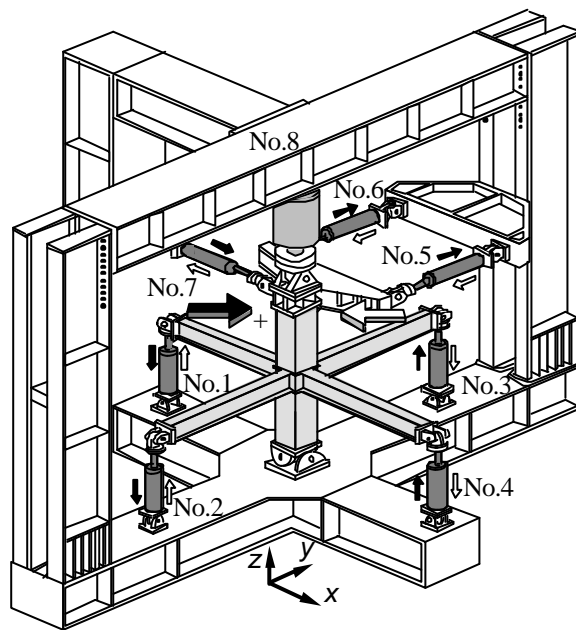
Figure 5.4 Test Setup for Specimen R6
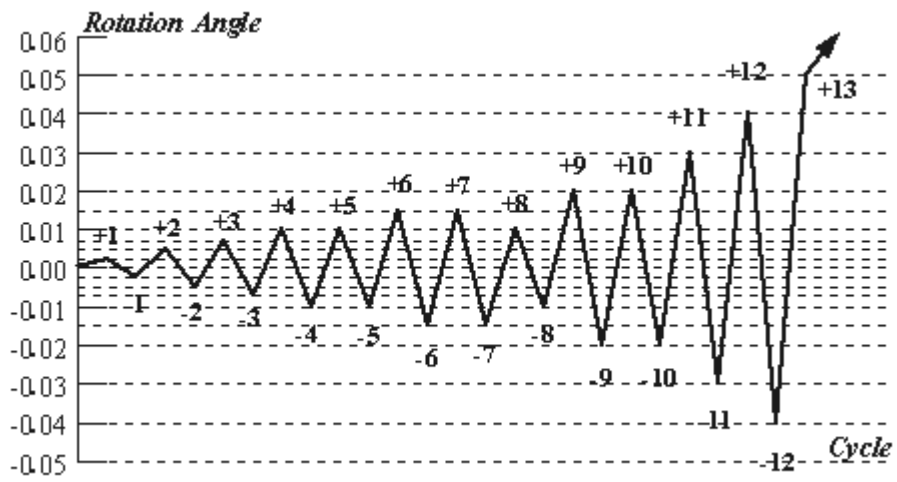
Figure 5.5 Loading History for Beam-to-Column Specimens
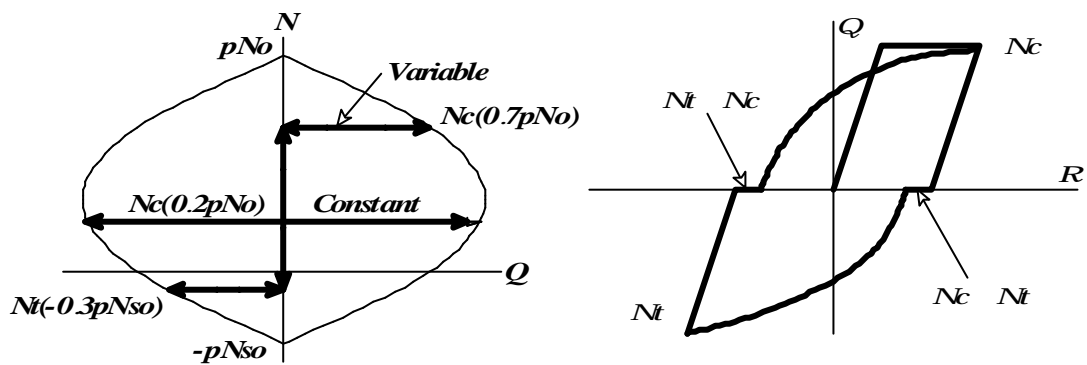
Figure 5.6 Rules for Axial Force Loading for Beam-to-Column Specimens
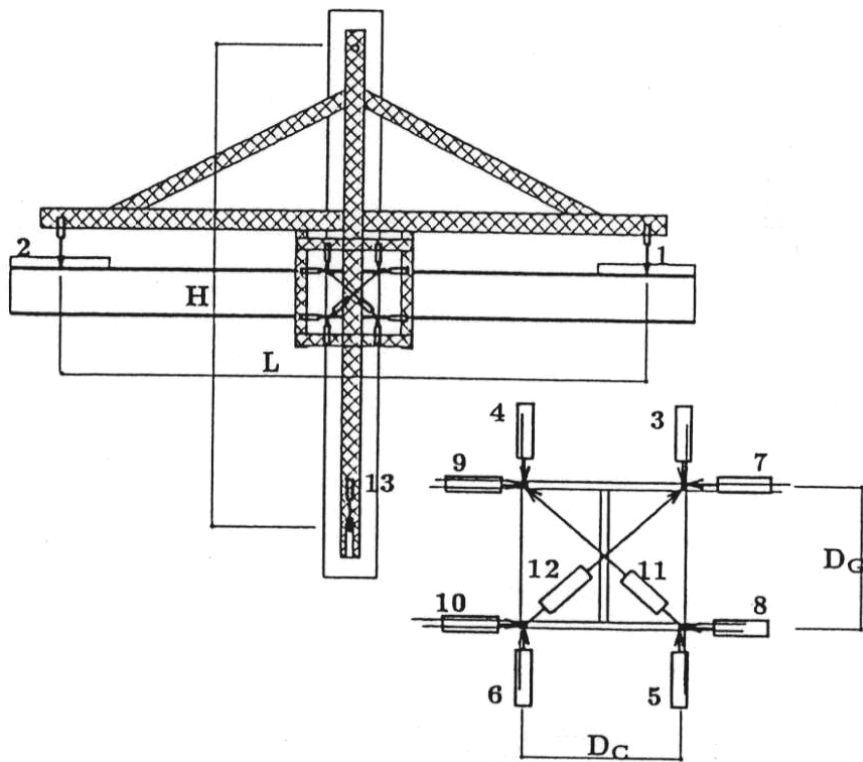
**Figure 5.7 Instruments for Measurements of Story Drift
and Displacement of Panel Zone**
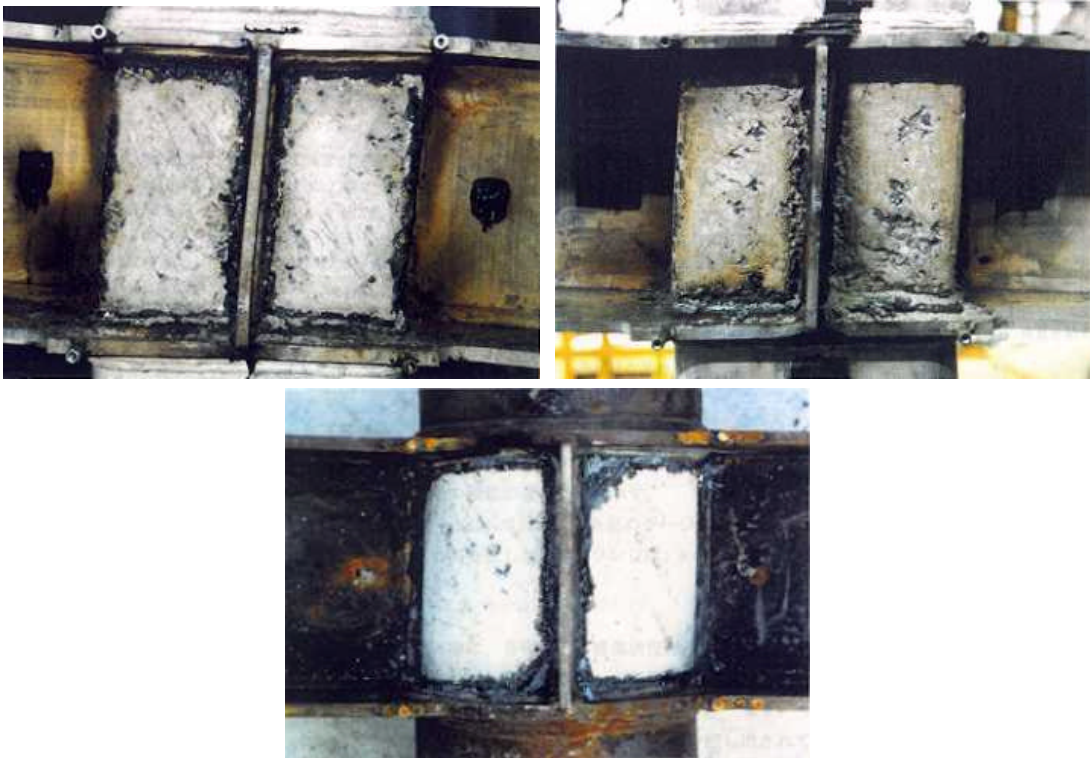
Figure 5.8 Crack Patterns of Filled Concrete in Panel Zone
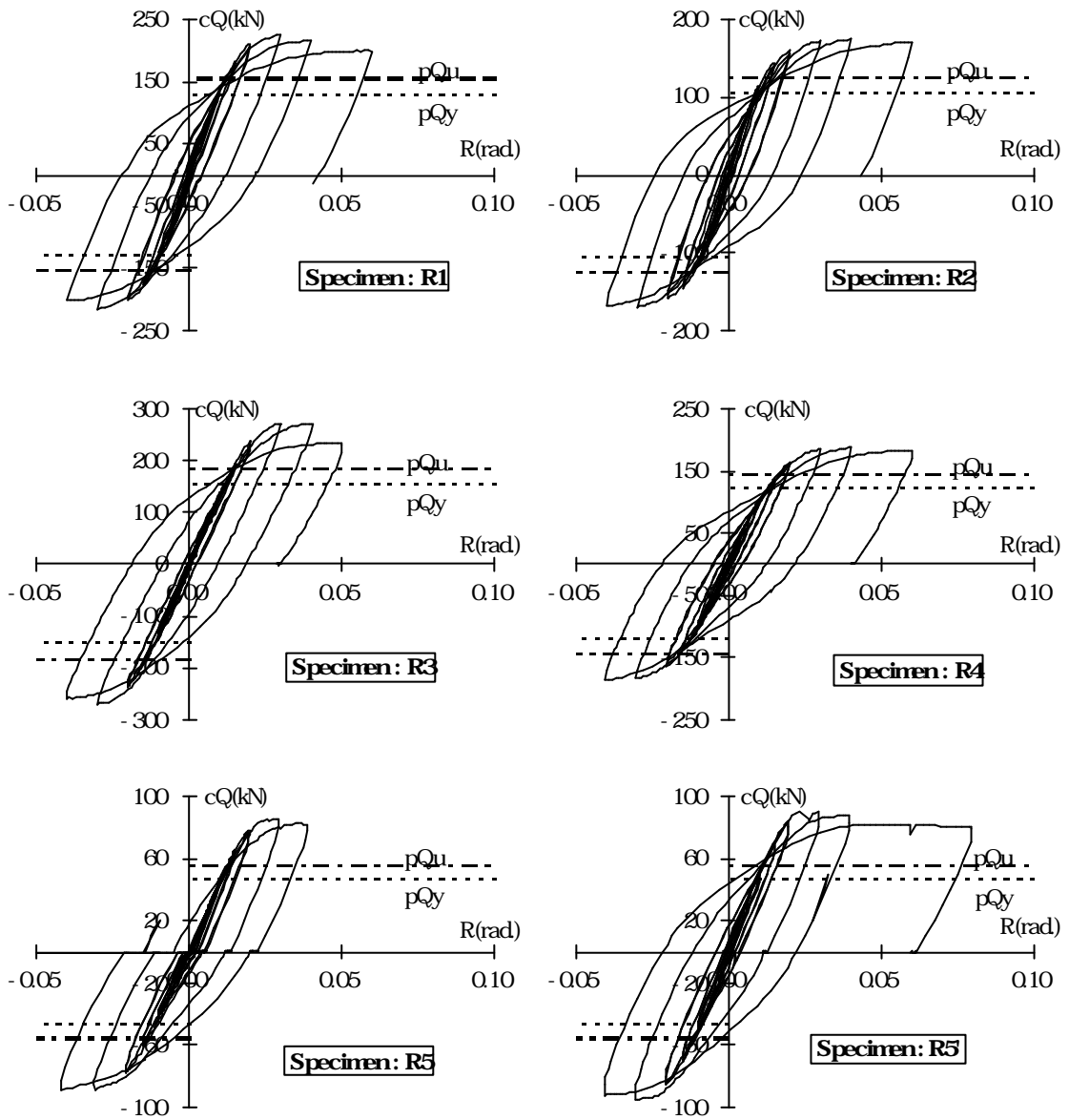
Figure 5.9(a) Story Shear vs. Story Drift Angle Relations of Rectangular Specimens

- 133 -
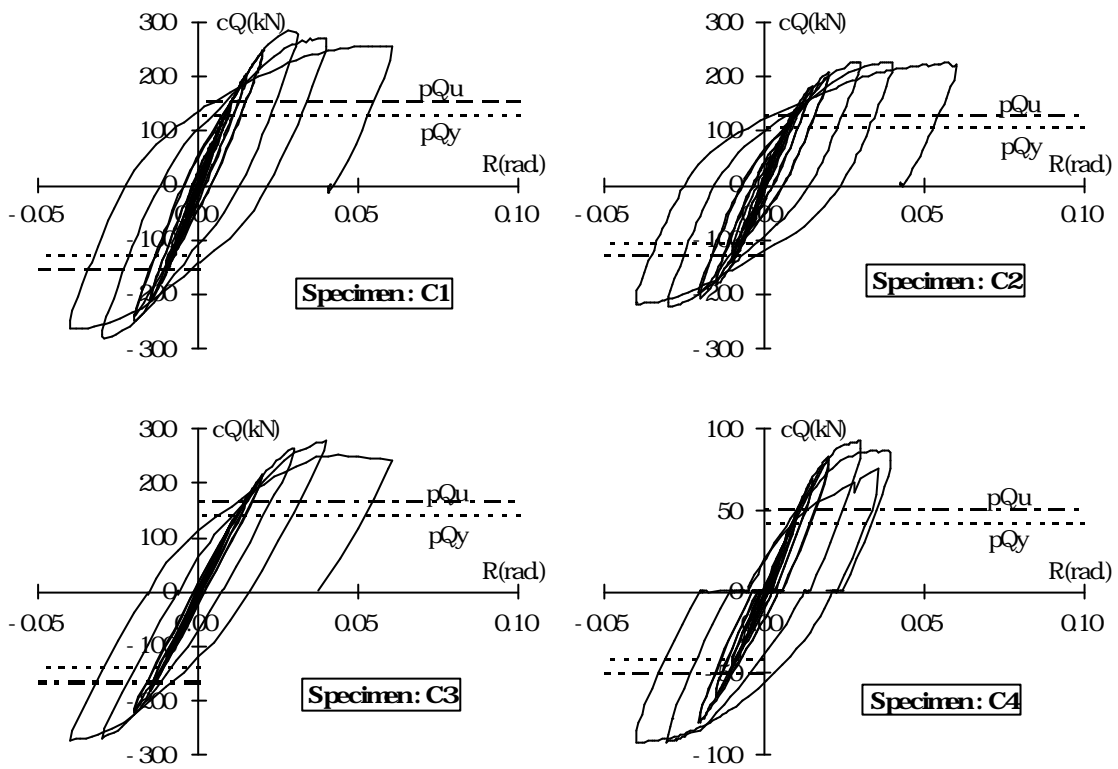
Figure 5.9(b) Story Shear vs. Story Drift Angle Relations of Circular Specimens

- 134 -

SPECIMEN: R1   **SPECIMEN: R2**   **SPECIMEN: R3**
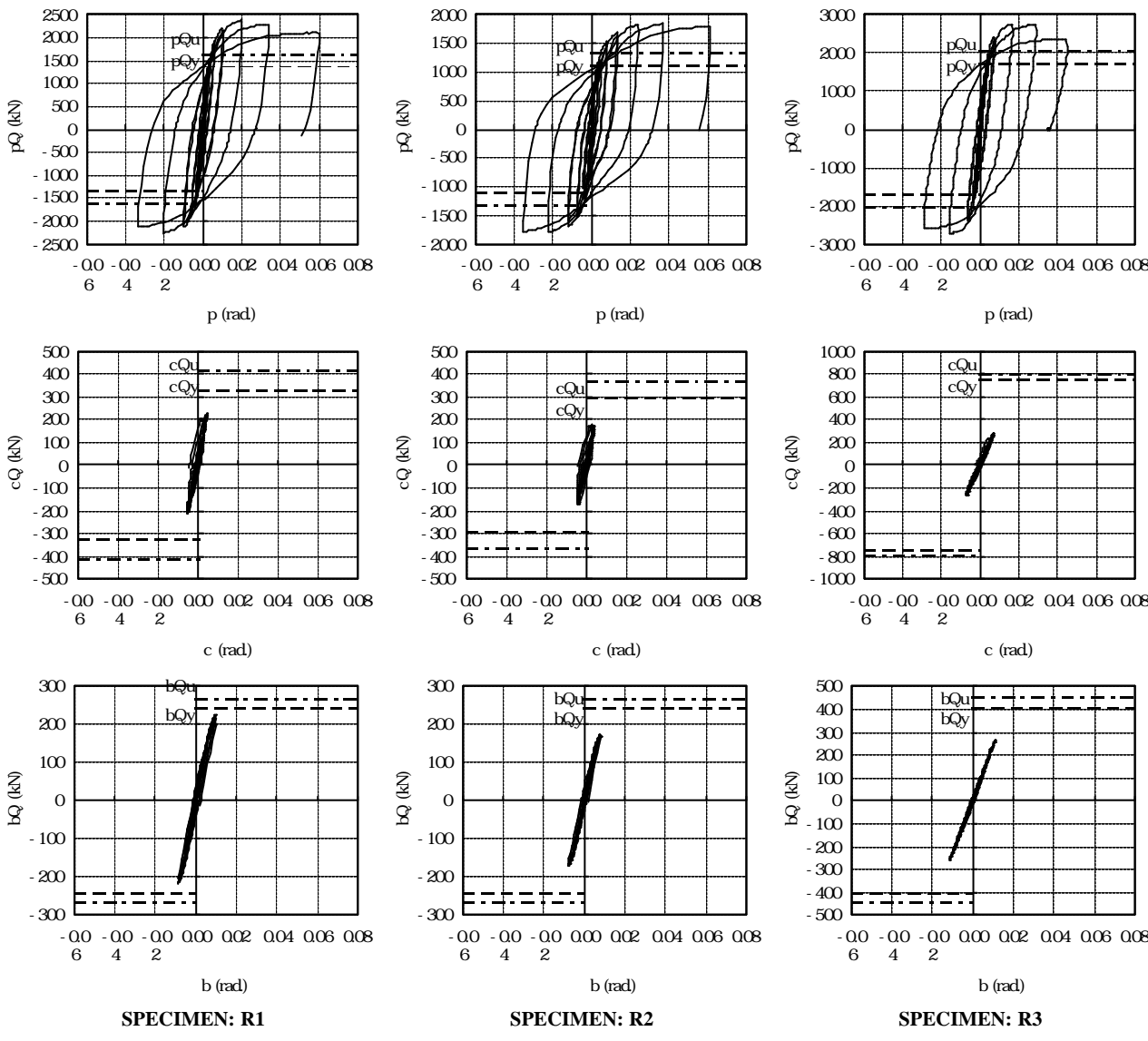
Figure 5.10(a) Hysteresis Curves of Panel Zone, Column and Beam of Rectangular Specimens

(continue)
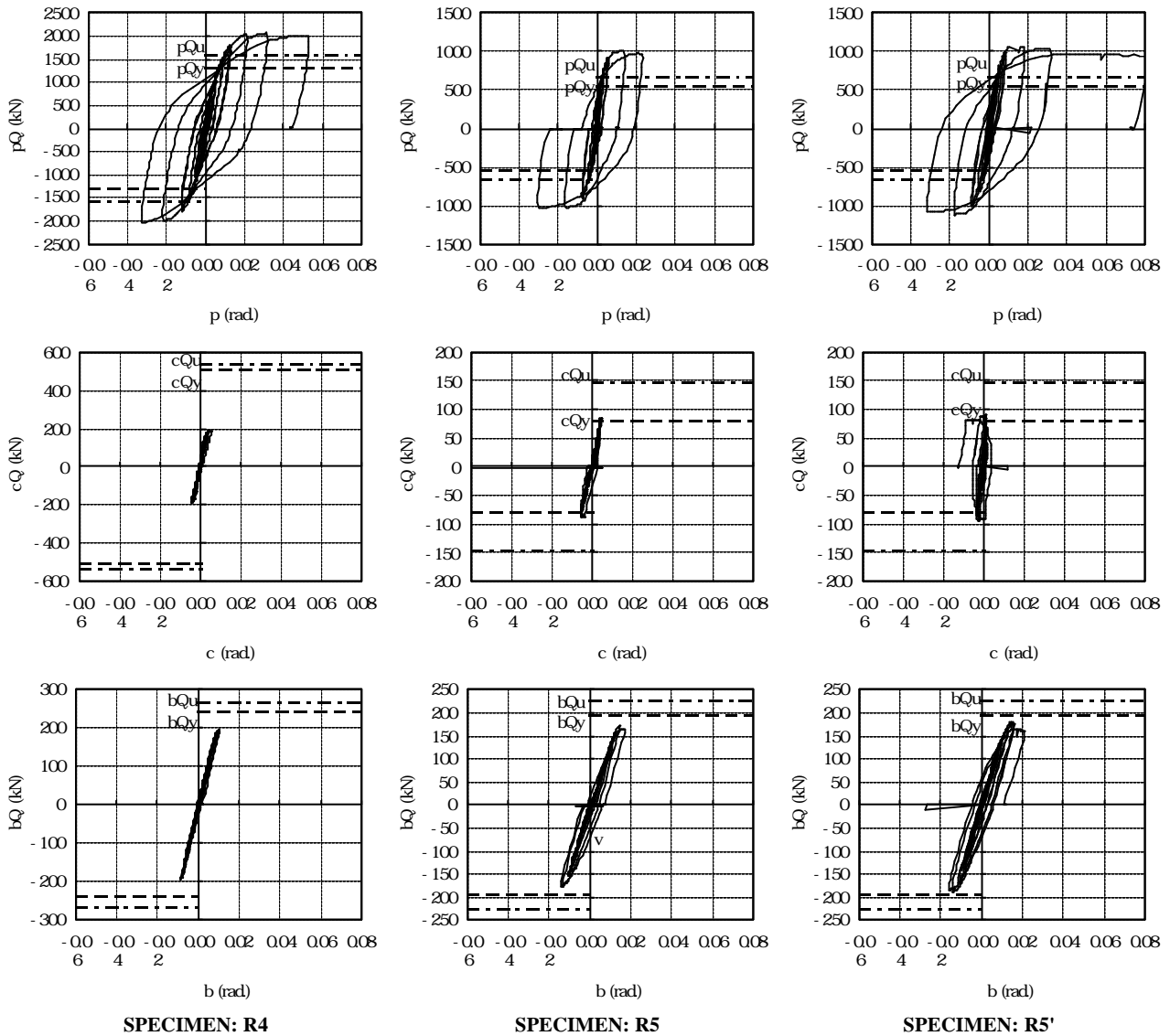
Figure 5.10(a) Hysteresis Curves of Panel Zone, Column and Beam of Rectangular Specimens
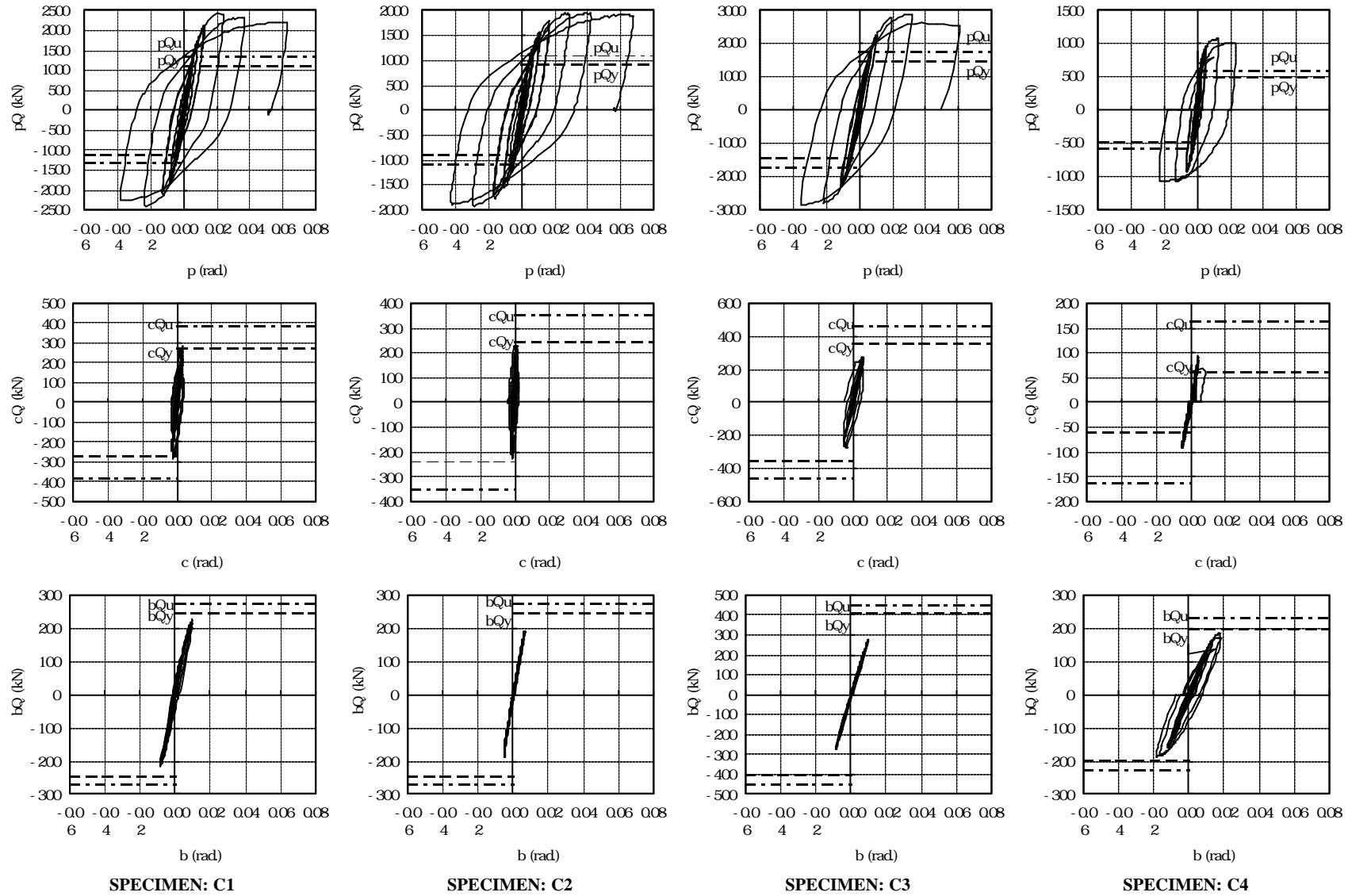
Figure 5.10 (b) Hysteresis Curves of Panel Zone, Column and Beam of Circular Specimens
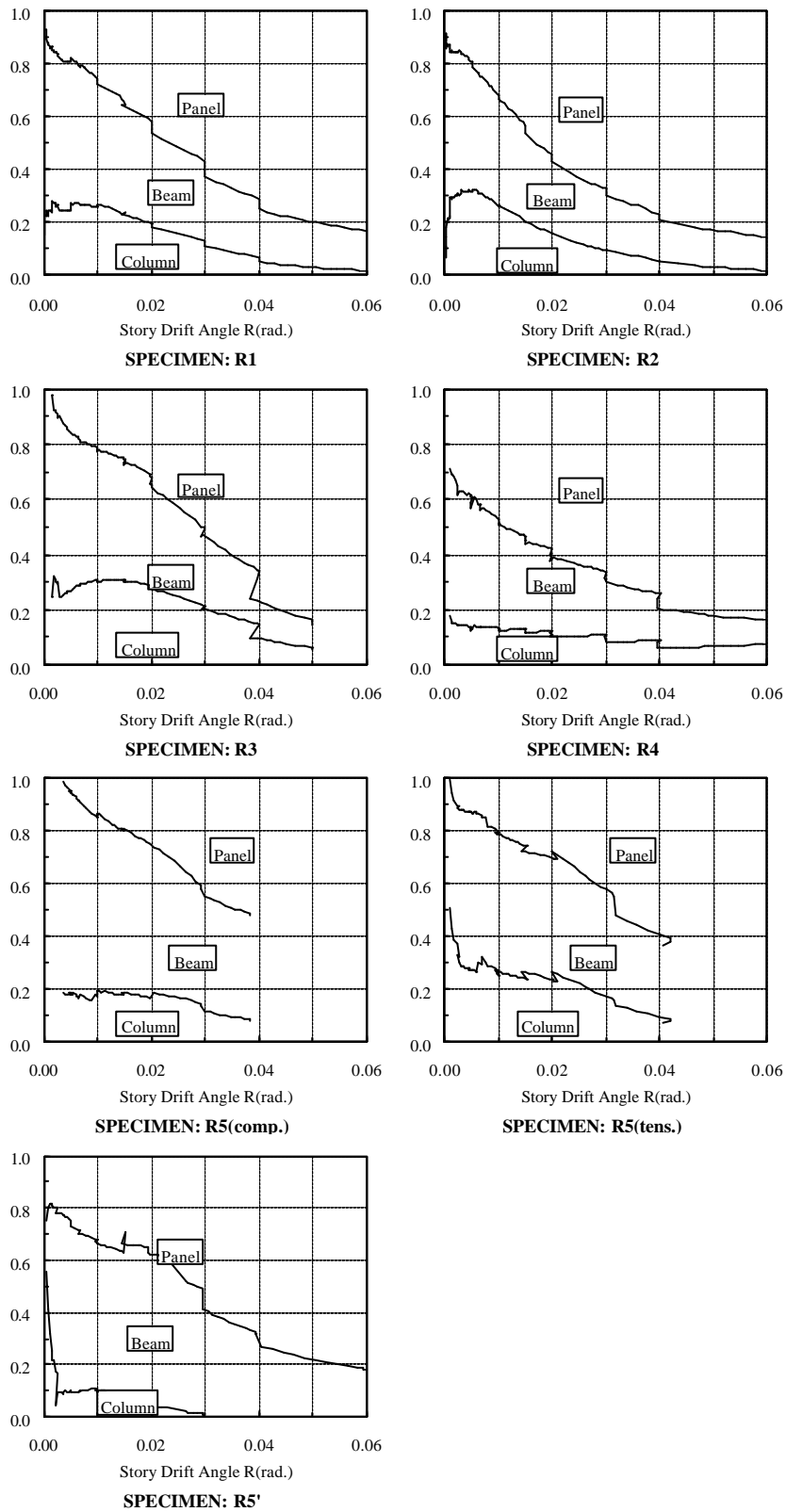
Figure 5.11(a) Contribution of Deformation of Panel Zone, Beam and Column

to Overall Story Drift in Rectangular Specimens
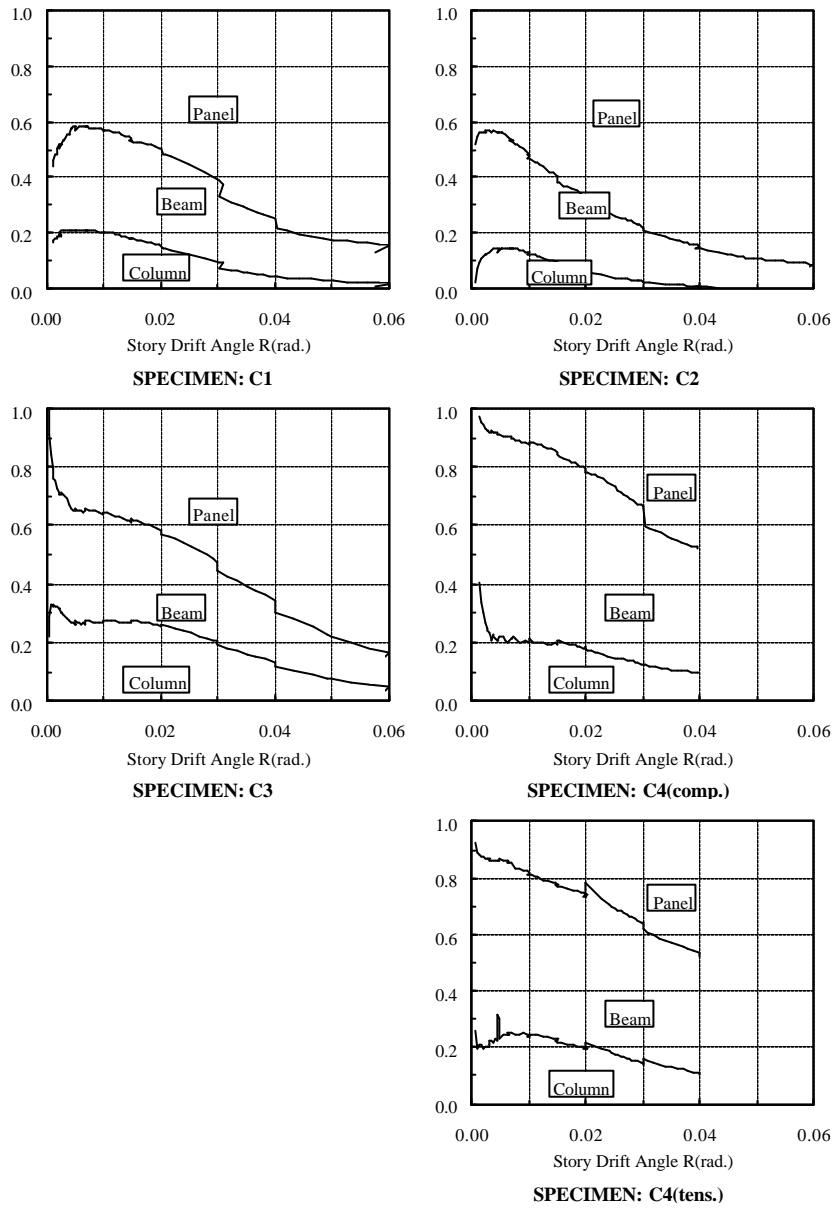
Figure 5.11(b) Contribution of Deformation of Panel Zone, Beam and Column to Overall Story Drift in Circular Specimens
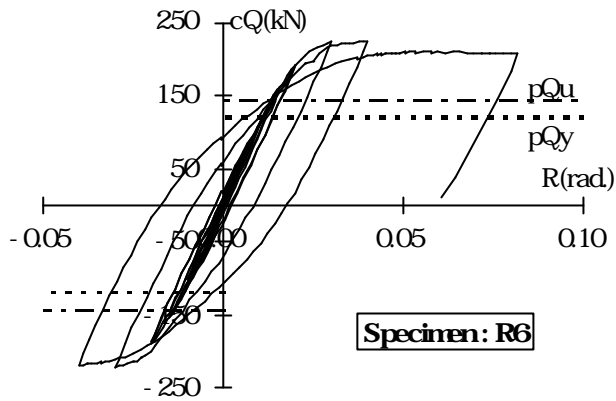
Figure 5.12 Story Shear vs. Story Drift Angle Relation

of Three Dimensional Specimen R6

X-direction　　　　　　　　**Y-direction**
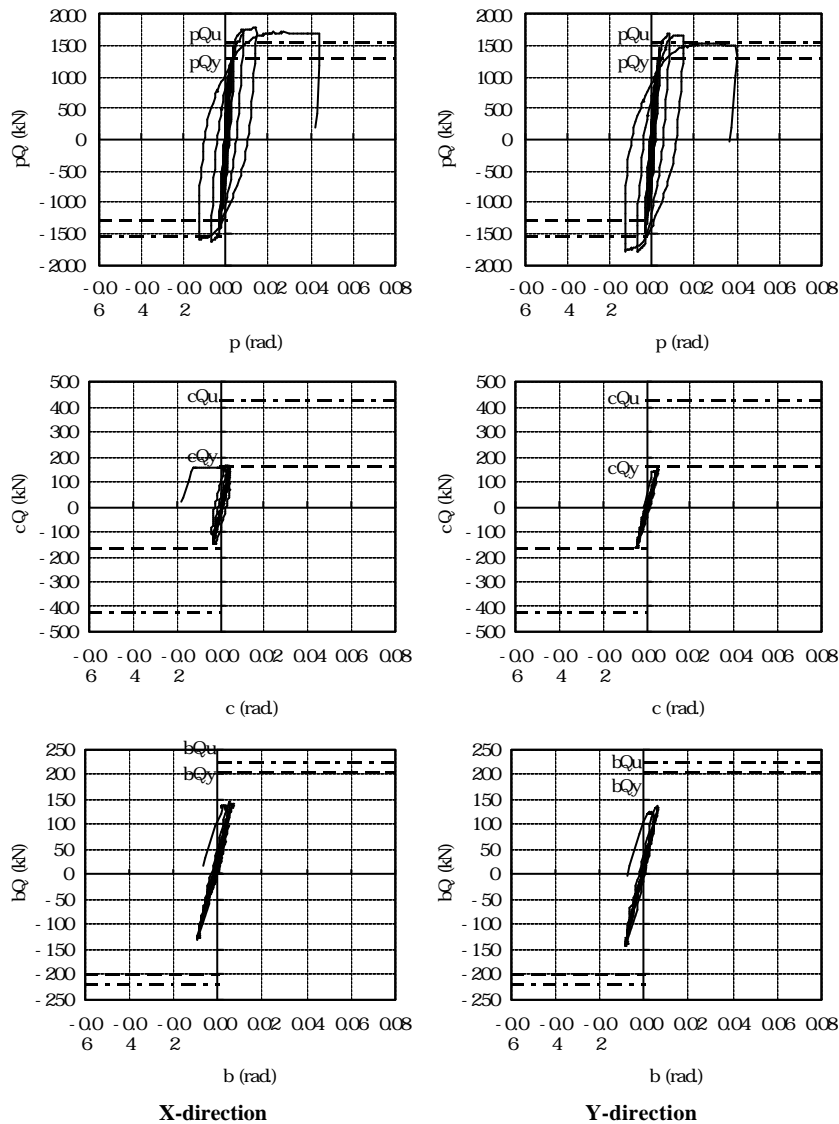
Figure 5.13 Hysteresis Curves of Panel Zone, Column and Beam

of Three Dimensional Specimen R6

X-direction

Y-direction
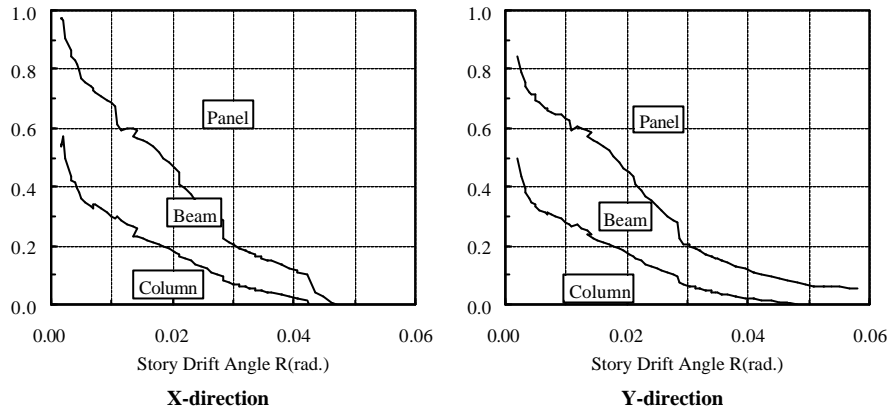
Figure 5.14 Contribution of Deformation of Panel Zone, Beam and Column

to Overall Story Drift in Rectangular Specimens

(a) Effect of Material Strength

(b) Effect of Axial Load

(c) Effect of Diaphragm Type

(d) Effect of Loading Direction
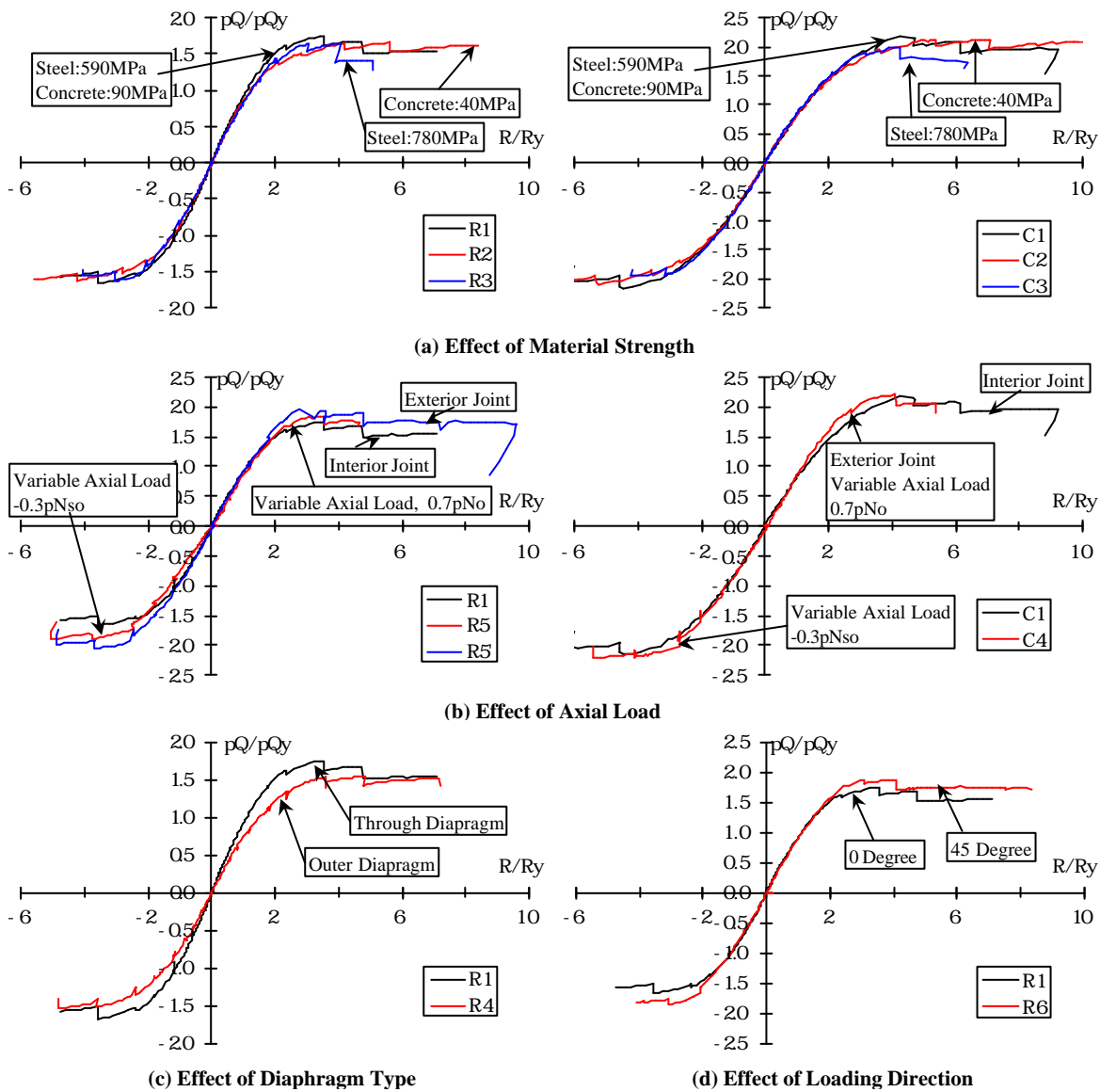
Figure 5.15 Normalized Shear Force of Panel Zone vs.

Normalized Story Drift A ngle Relations
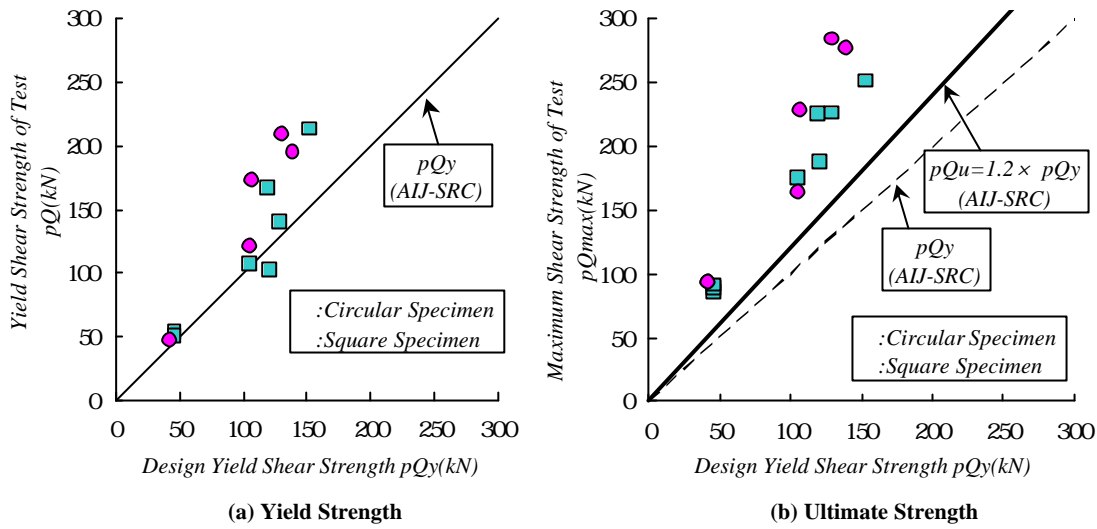
Figure 5.16 Yield and Ultimate Shear Strengths of Panel Zone

of Two Dimensional Specimens
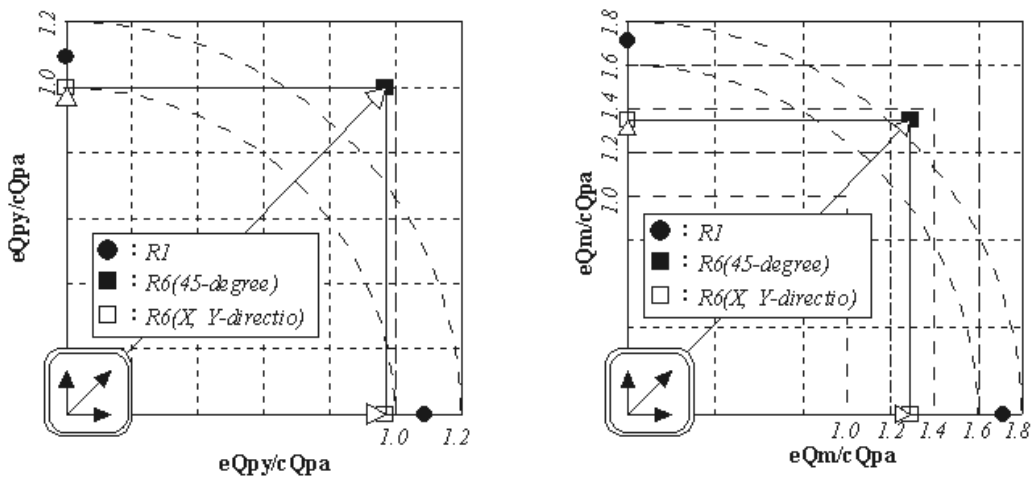
Figure 5.17 Yield and Ultimate Shear Strengths of Panel Zone

of Three Dimensional Specimen
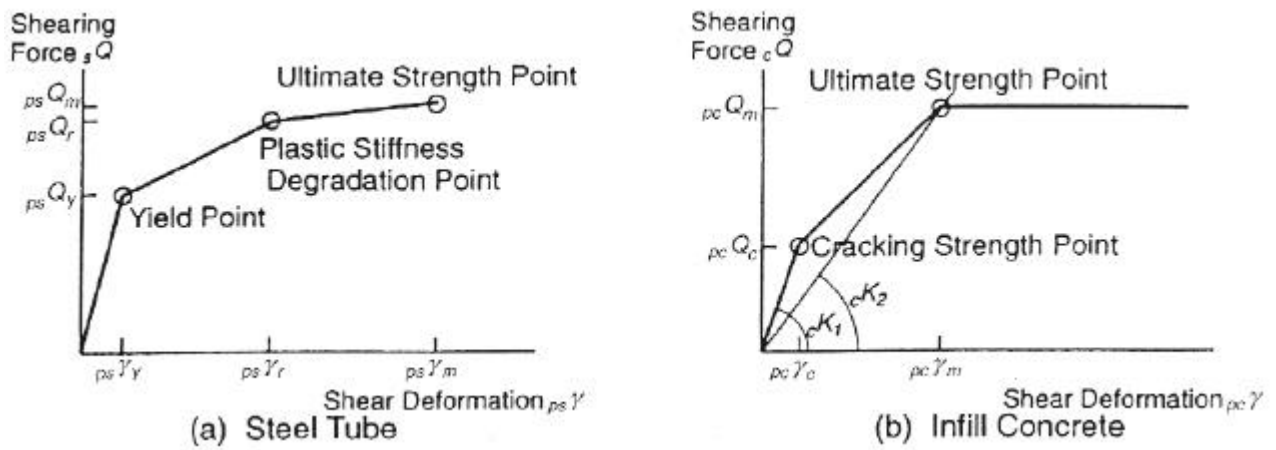
Figure 5.18 Assumed Tri-Linear Skelton Curves for Steel and Filled Concrete in Panel Zone
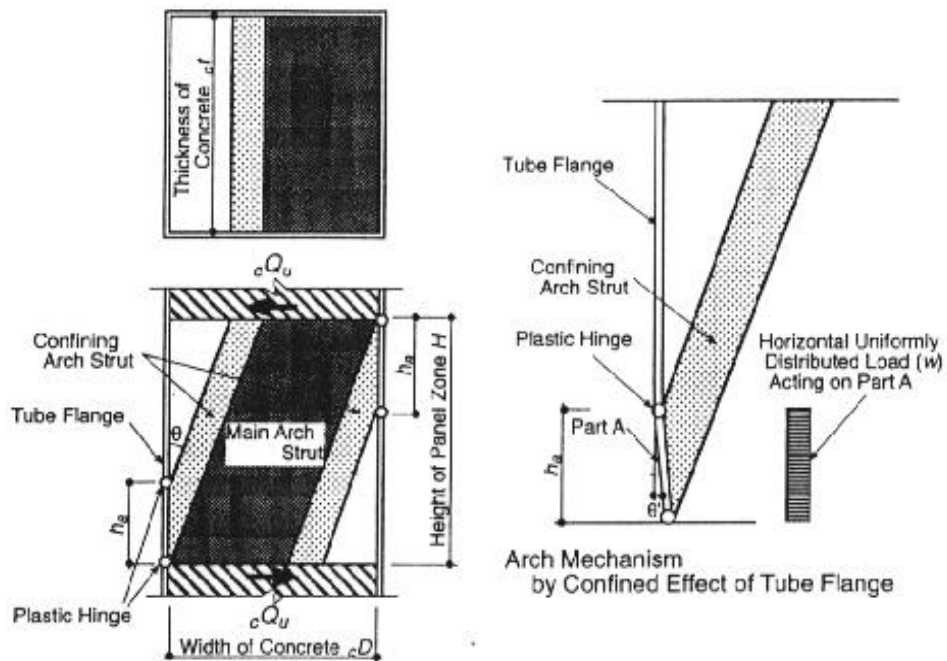
Figure 5.19 Arch Mechanisms in Panel Zone
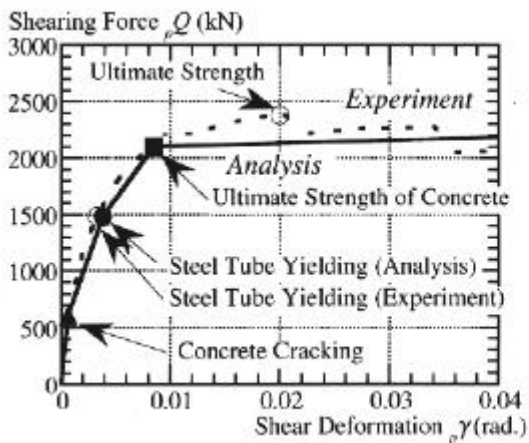
(a) Specimen R1
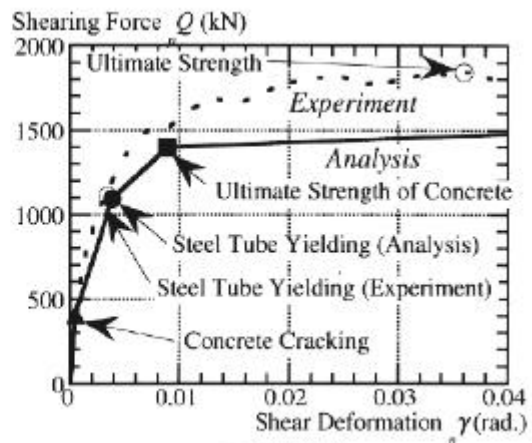
(b) Specimen R2
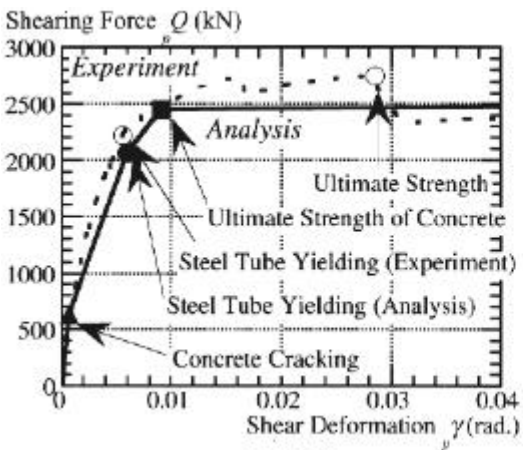
(c) Specimen R3
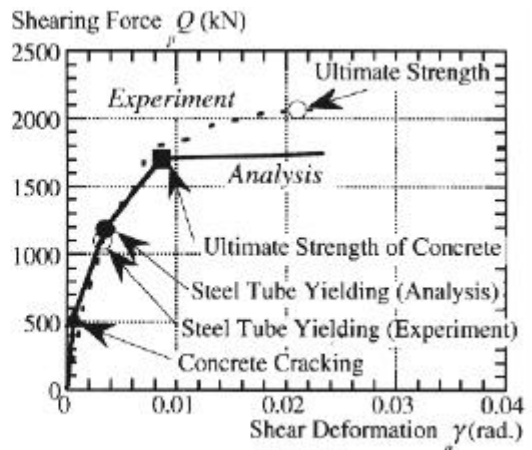
(d) Specimen R4
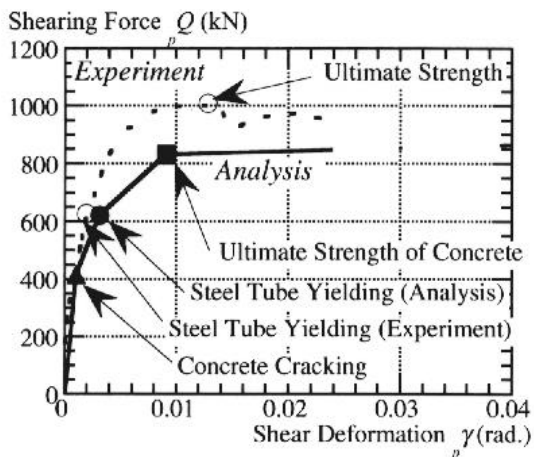
(e) Specimen R5 (Compressive Column Axial Force) (f) Specimen R5 (Tensile Column Axial Force)
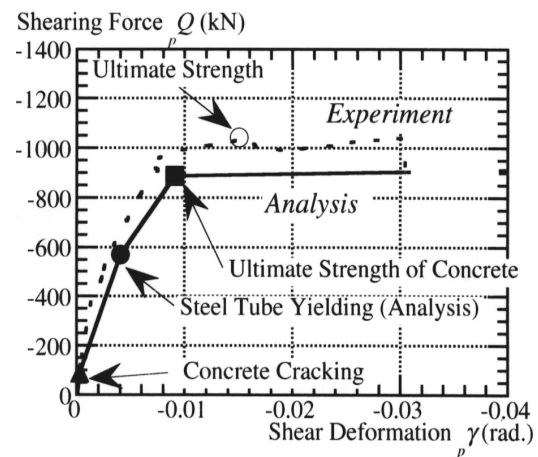
Figure 5.20 Comparisons of Calculated and Experimental Skeleton Curves
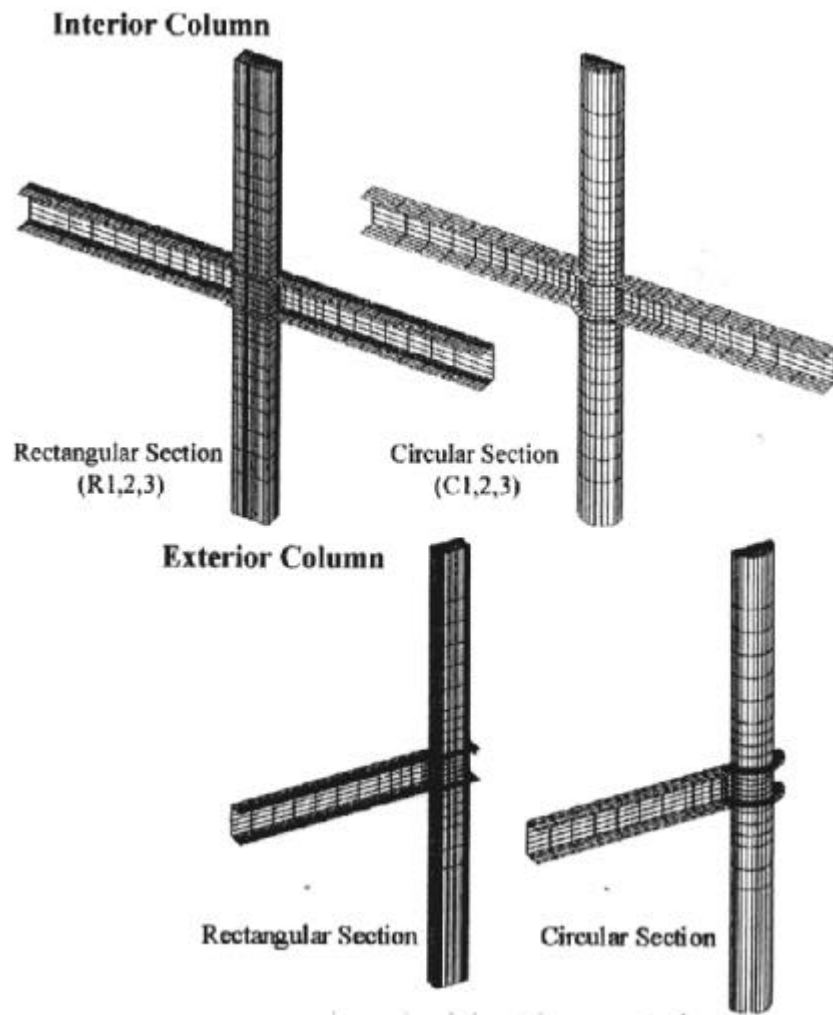
Figure 5.21 Analytical Meshes for Finite Element Method
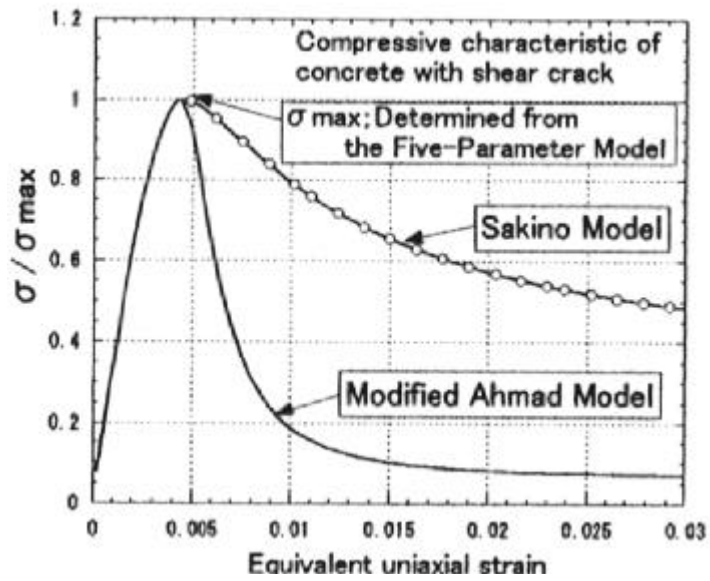
Figure 5.22 Stress vs. Strain Relationships of Concrete

1) Exterior Specimens
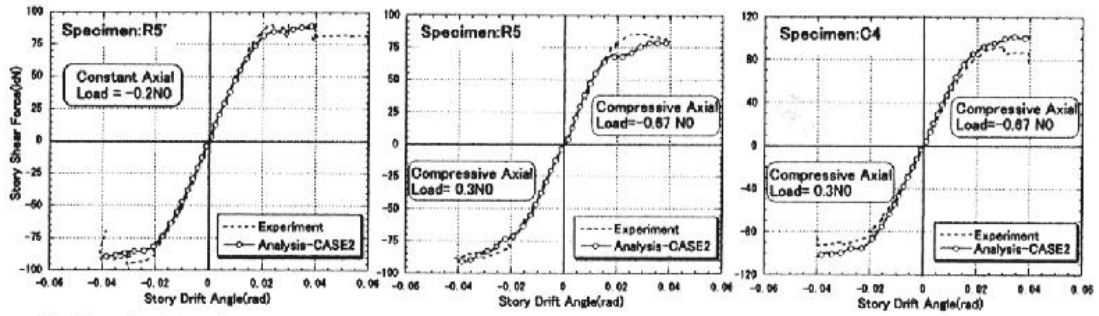
2) Interior Specimens
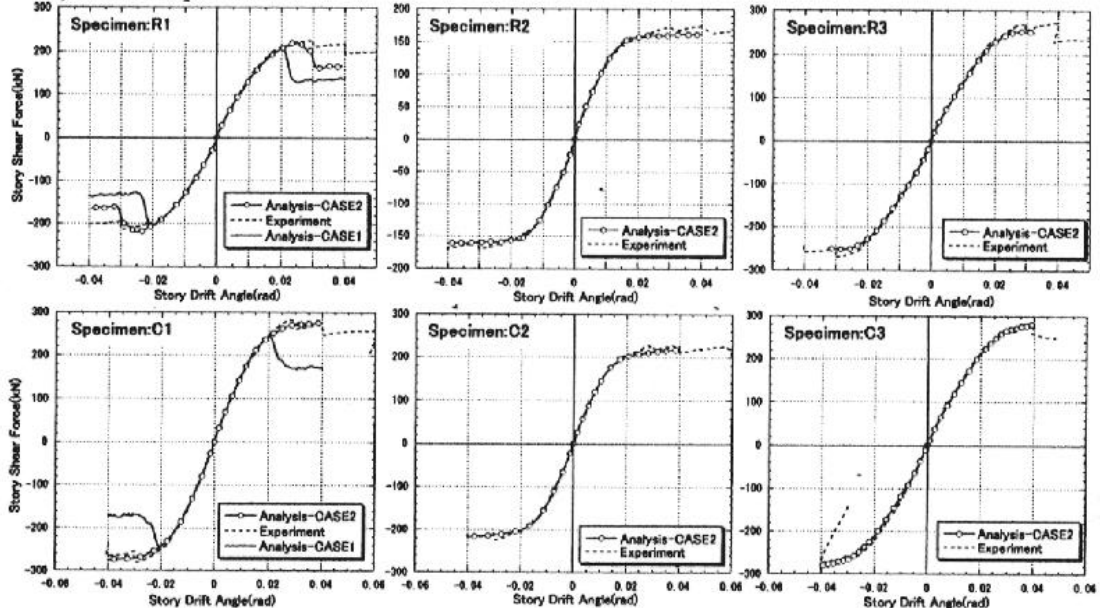
Figure 5.23 Story Shear Force vs. Story Drift Angle Relationships of Beam-to-Column Connection Specimens
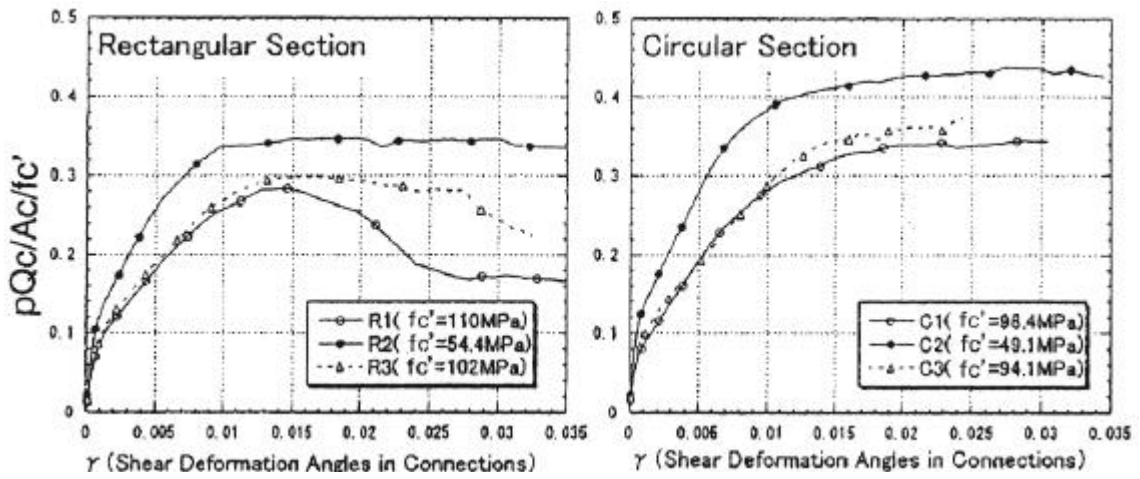
Figure 5.24 $pQc / Ac / fc'$ - g **Relationships**
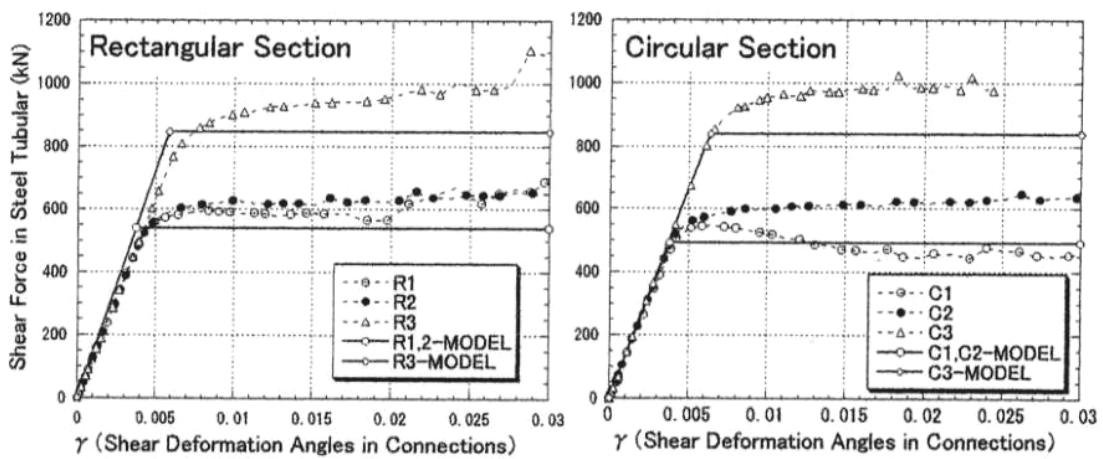
Figure 5.25 pQs - g **Relationships**

Rectangular Section (R1) Specimen   Circular Section (C1) Specimen
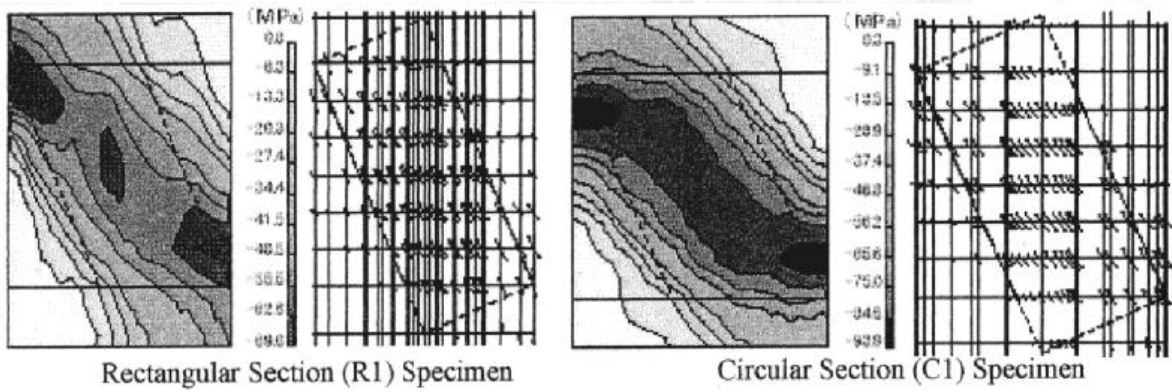
Figure 5.26 Contour and Flow of Principal Compressive Concrete Stress in Panel Zones
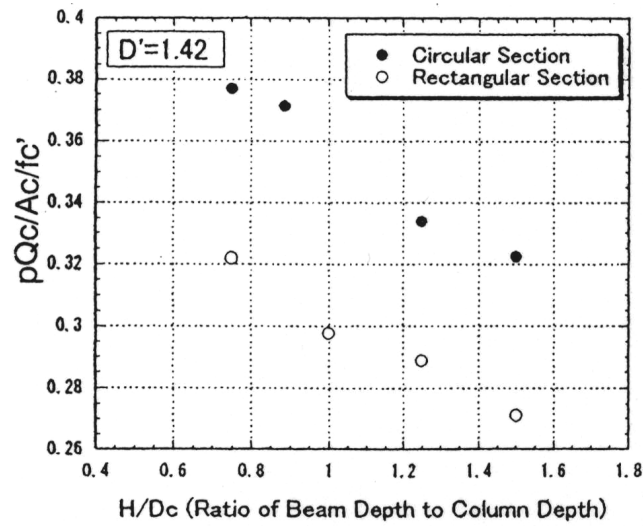
Figure 5.27 $pQc\,/\,Ac\,/\,fc'{-}H\,/\,Dc$ **Relationships**
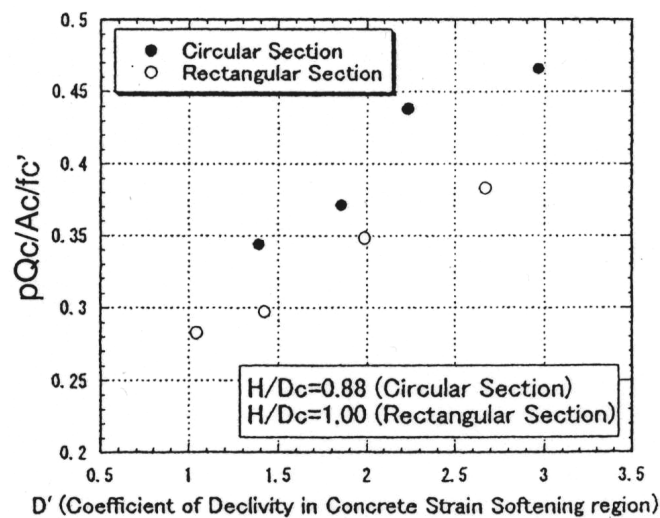
Figure 5.28 $pQc\,/\,Ac\,/\,fc'{-}H\,/\,D^{'}$ **Relationships**
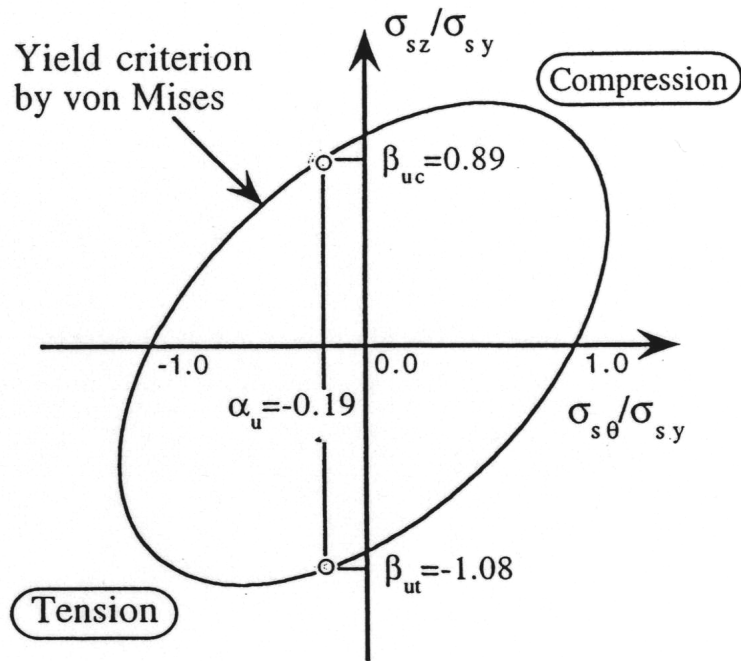
Figure 6.1 Biaxial Stress State of Steel Tube under Yielding
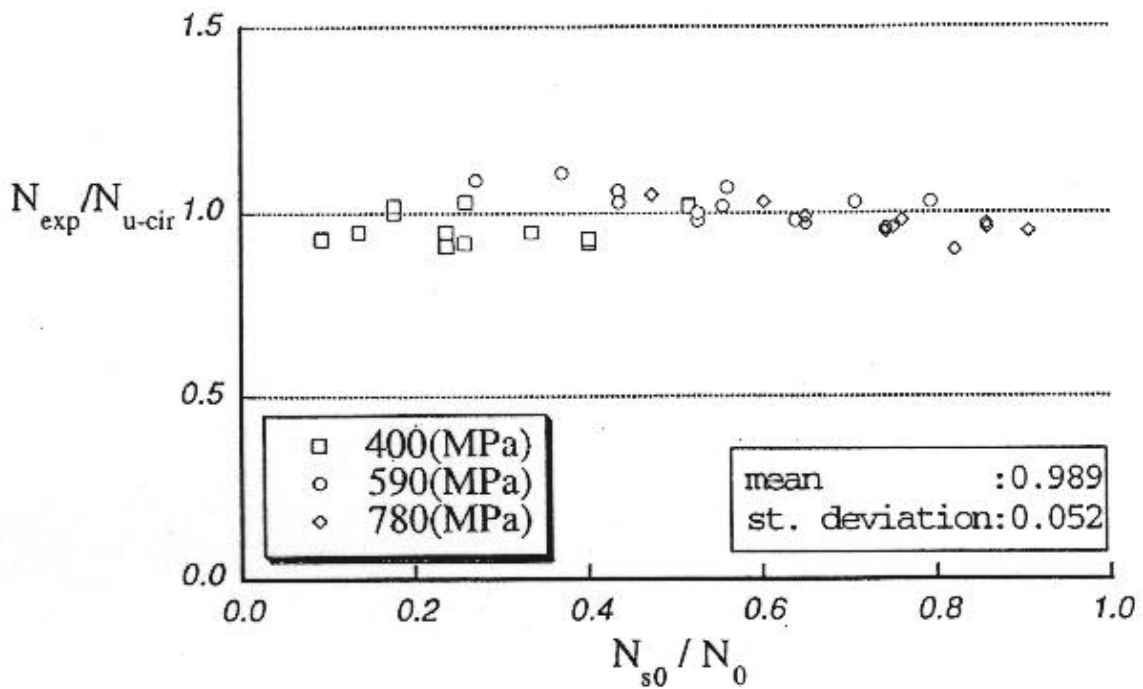
(a) Specimens of US-Japan Research Program
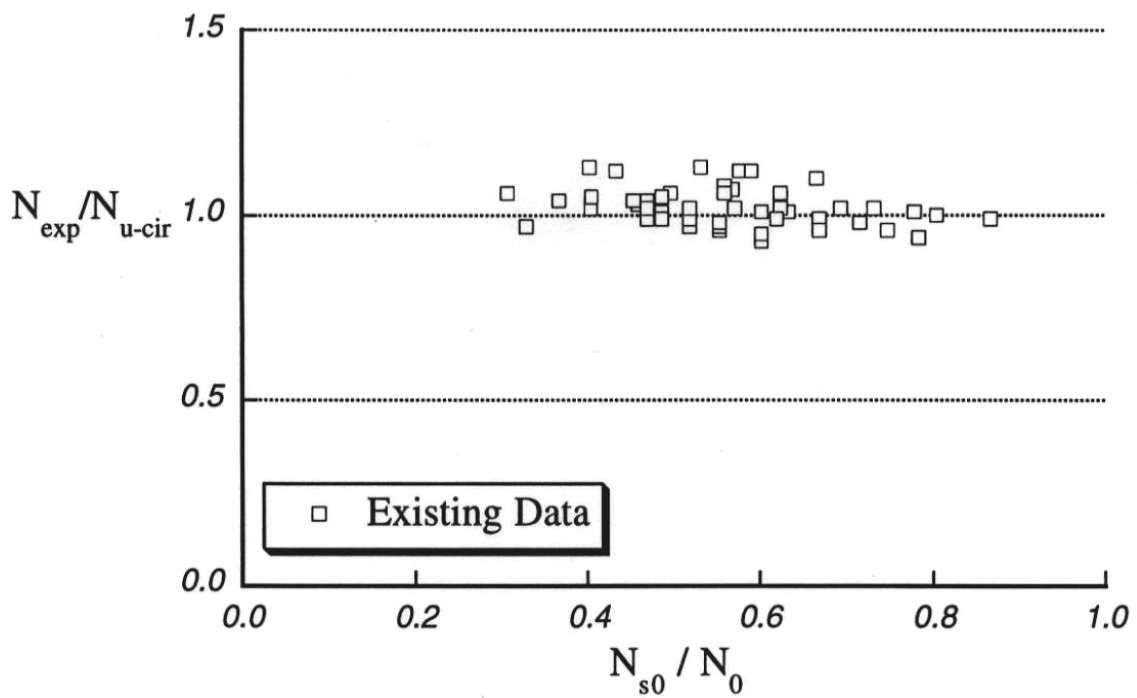
(b) Specimens in Database Collected from the Proceedings of AIJ Annual Meetings

Figure 6.2 Comparisons Between Calculated Ultimate Axial Loads and Experimental Ones of Circular Columns
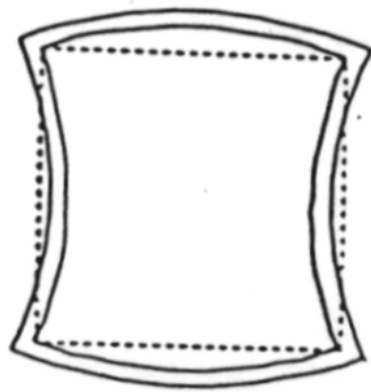
(a) Hollow Steel Tube   (b) Concrete Filled Steel Tube

Figure 6.3 Local Bucking Modes of Square Steel Tube
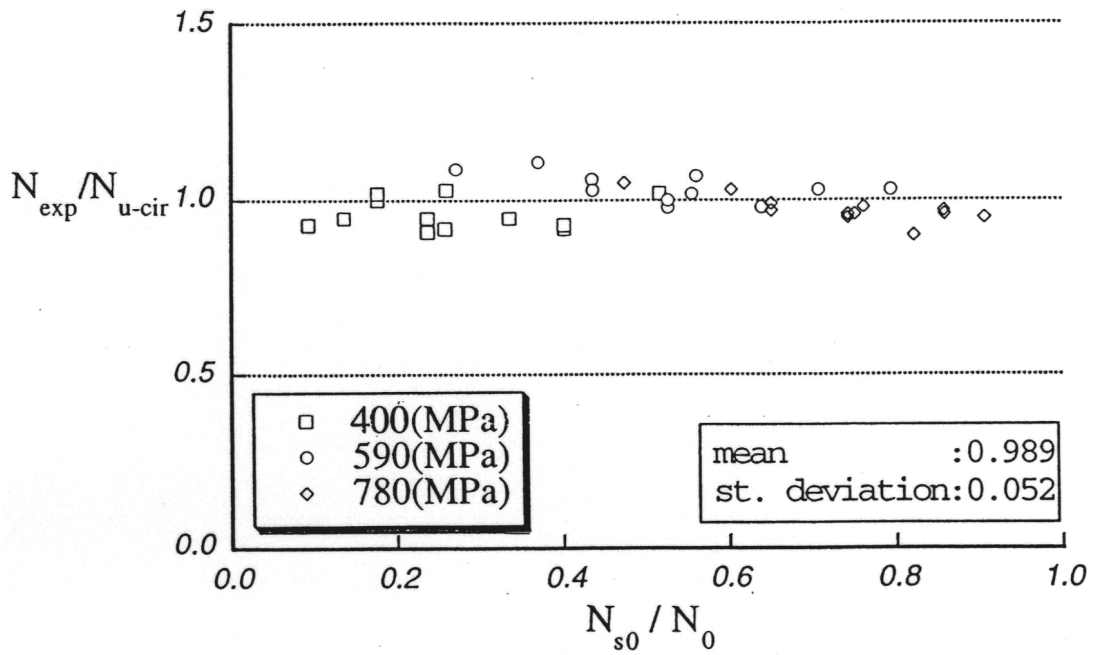
(a) Specimens of US-Japan Research Program
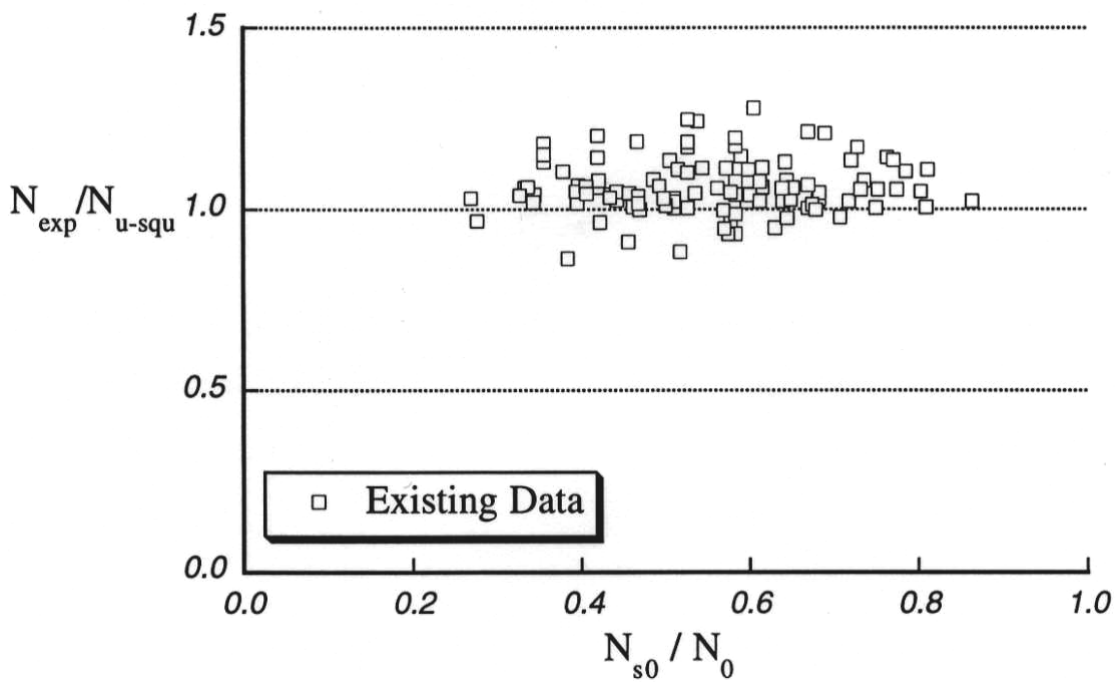
(b) Specimens in Database Collected from the Proceedings of AIJ Annual Meetings

Figure 6.4 Comparisons Between Calculated Ultimate Axial Loads

and Experimental Ones of Square Columns
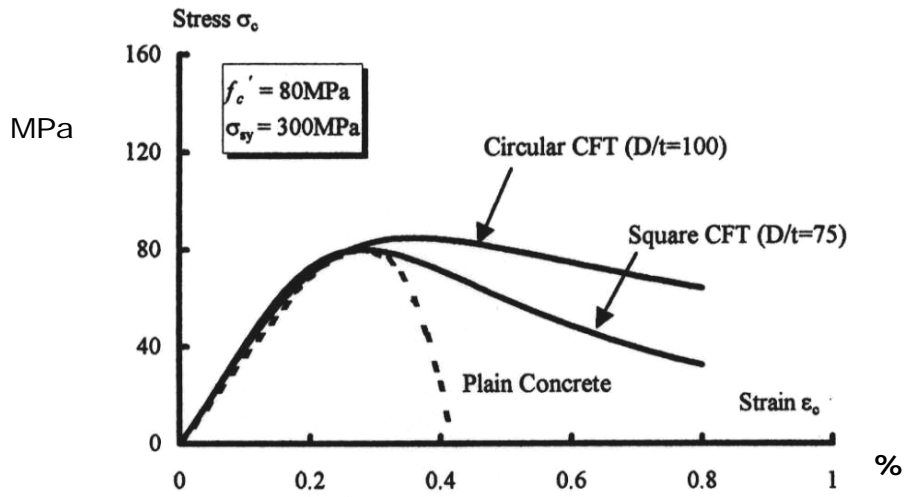
Figure 6.5 Stress vs. Strain Curves for Plain and Confined Concrete
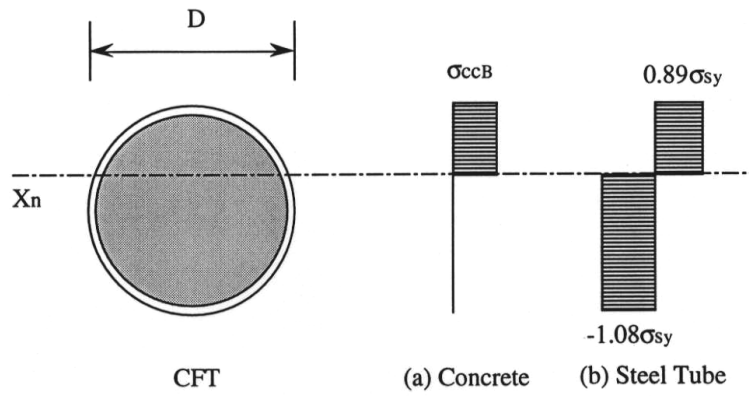
Figure 6.6 Stress Blocks for Concrete and Steel in Circular CFT Section

(Prescribed in the AIJ -CFT Recommendations [6.1])
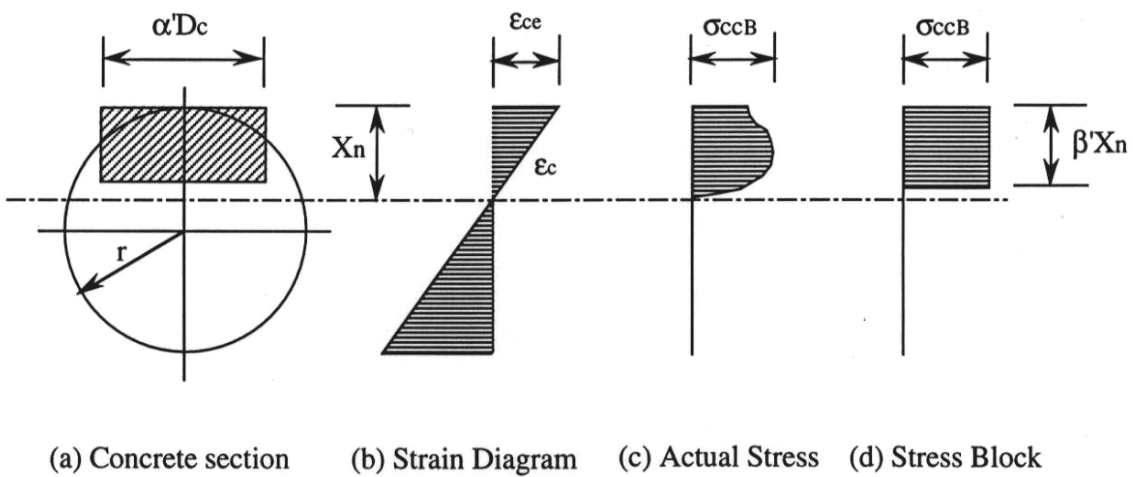
Figure 6.7 Stress Blocks for Concrete in Circular CFT Section

(Proposed by Sun and Sakino [6.9])

- 153 -
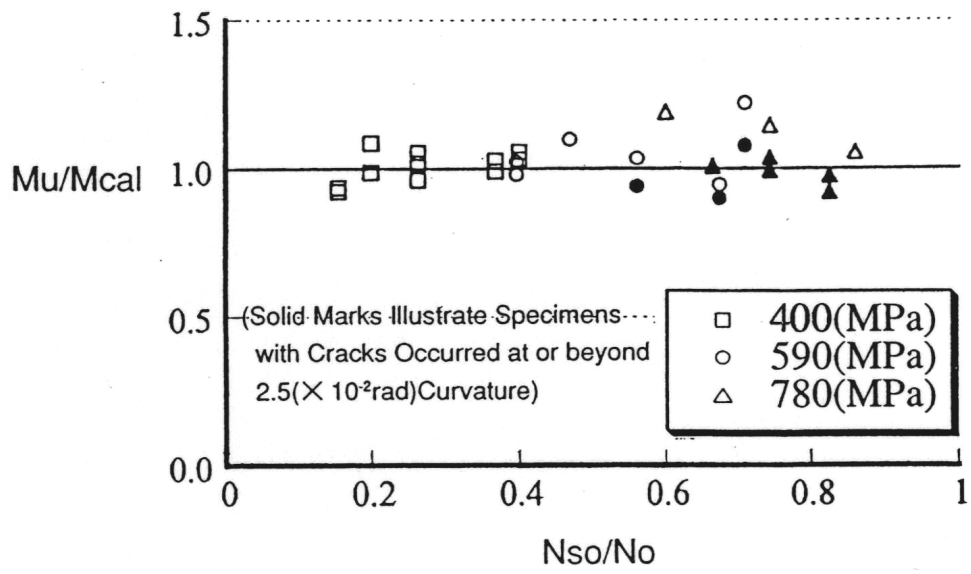
Figure 6.8 Comparisons Between Calculated Ultimate Flexural Strengths and Experimental Ones of Circular Columns
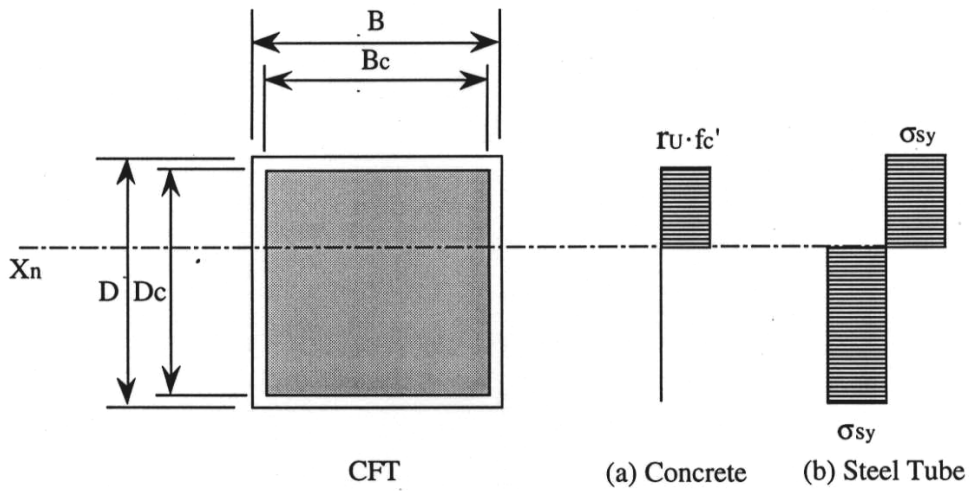
Figure 6.9 Stress Blocks for Concrete and Steel in Square CFT Section

(Prescribed in the AIJ -CFT Recommendations [6.1])
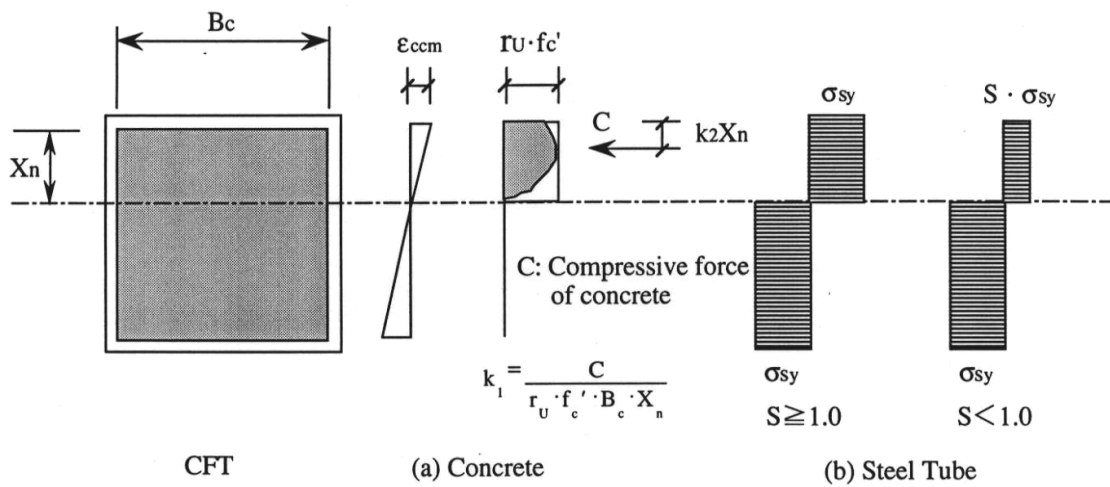
Figure 6.10 Proposed Stress Blocks for Concrete and Steel in Square CFT Section with High

Strength Concrete and / or Thin Steel Tube Wall
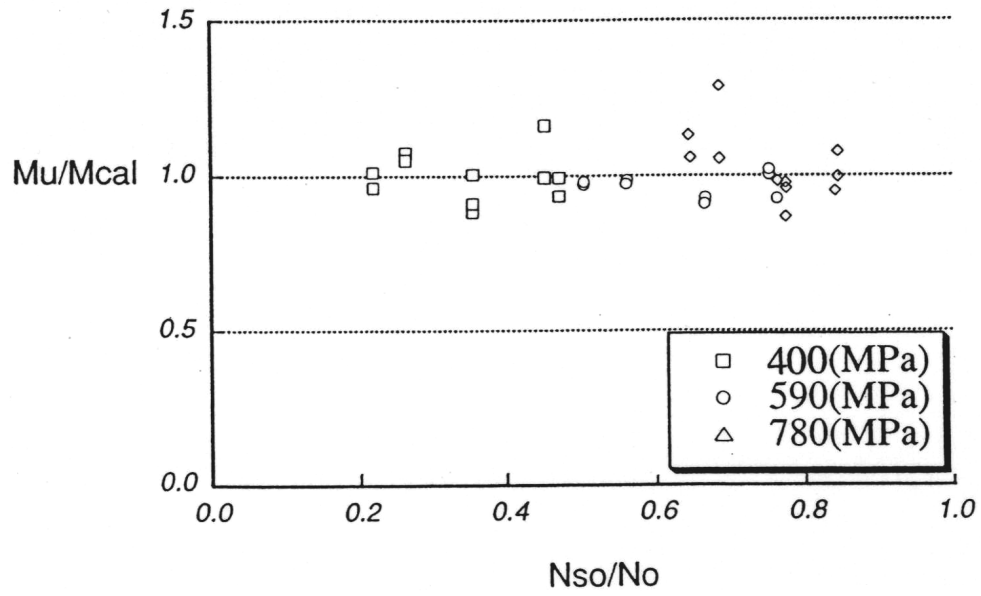
Figure 6.11 Comparisons Between Calculated Ultimate Flexural Strengths and Experimental Ones of Square Columns
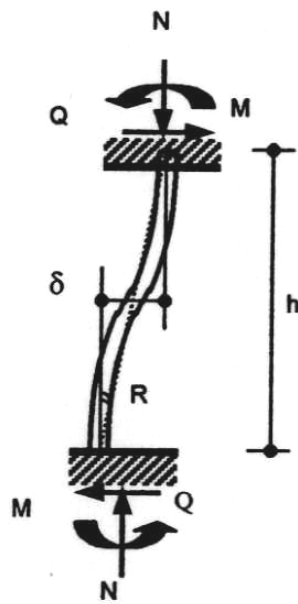
Figure 6.12 Beam-Column Under Combined Forces
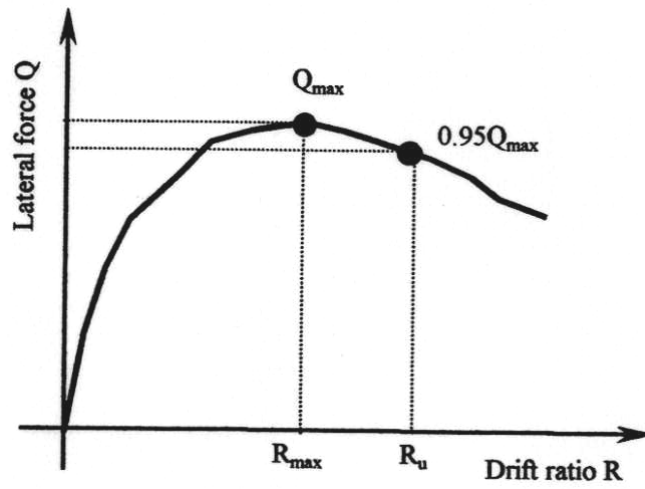
Figure 6.13 Definition of Limit Rotation Angle
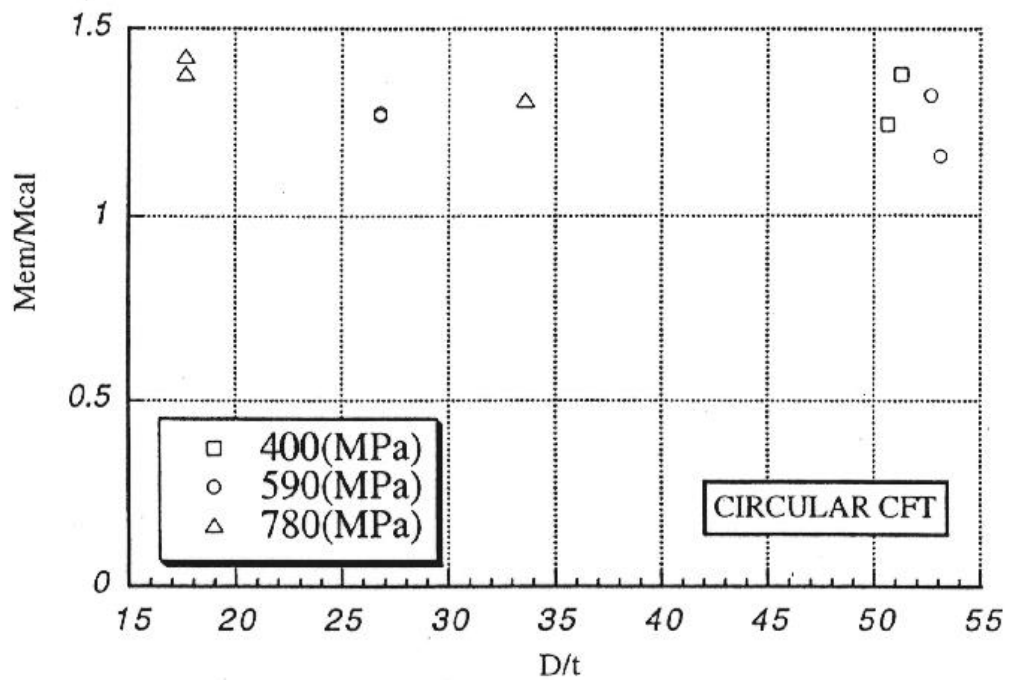
(a) Circular Columns
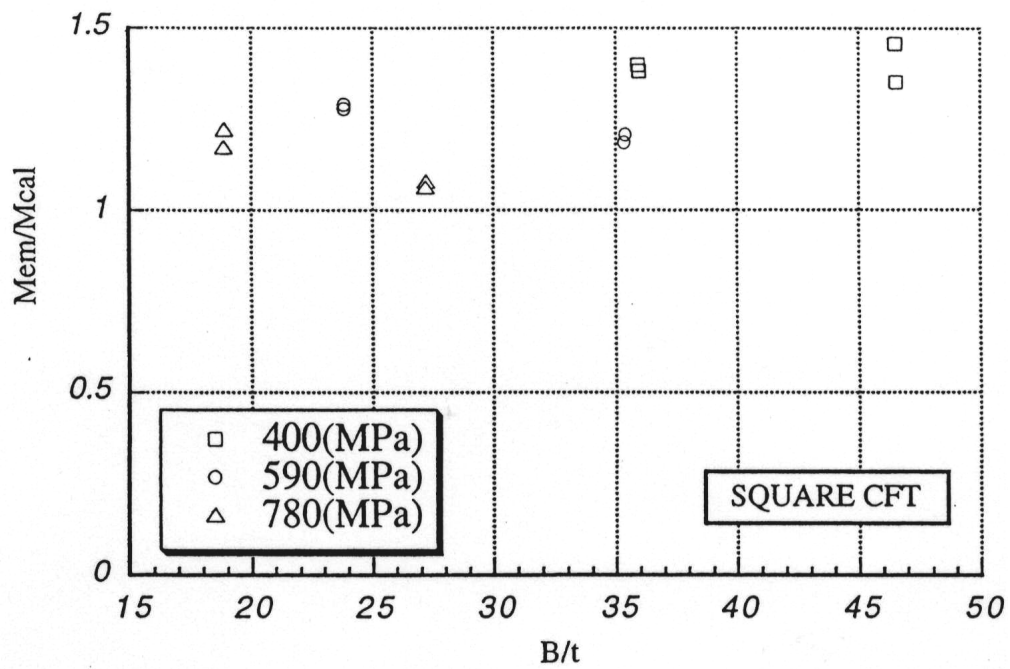
(b) Square Columns

Figure 6.14 Comparisons Between Calculated Ultimate Flexural Strengths and Experimental Ones
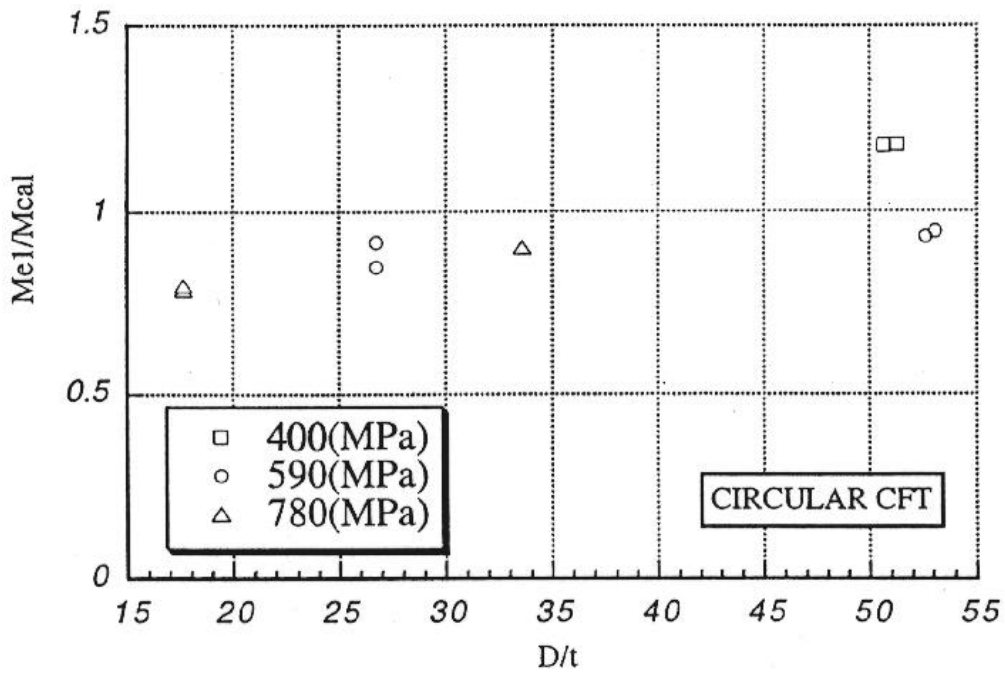
(a) Circular Columns
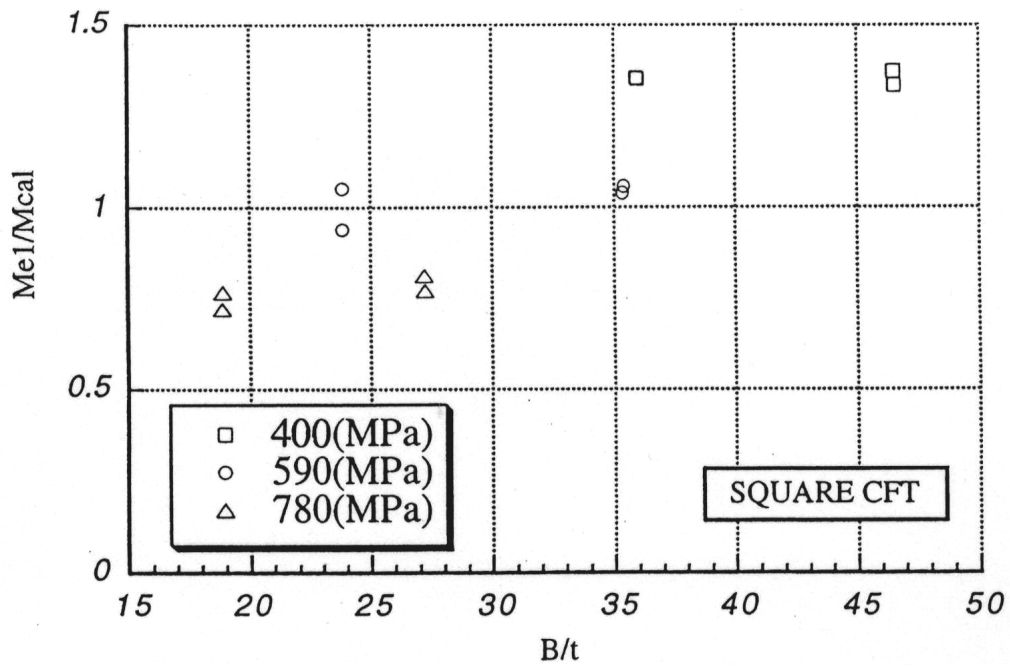
(b) Square Columns

Figure 6.15 Comparisons Between Calculated Ultimate Flexural Strengths and Experimental Ones Attained within Rotation Angle Limitation of 0.01 radian

- 159 -
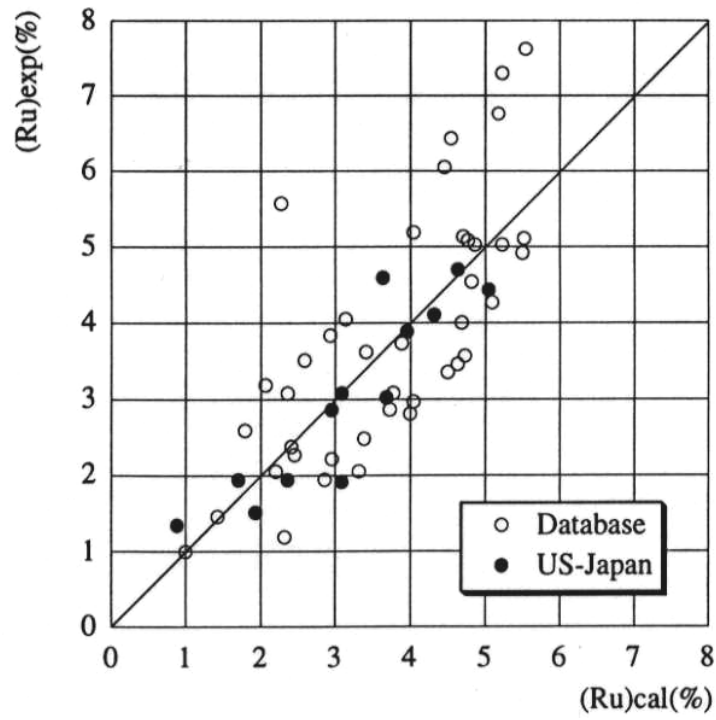
Figure 6.16 Comparison Between Predicted Limit Rotation and Experimental One (Circular Columns)
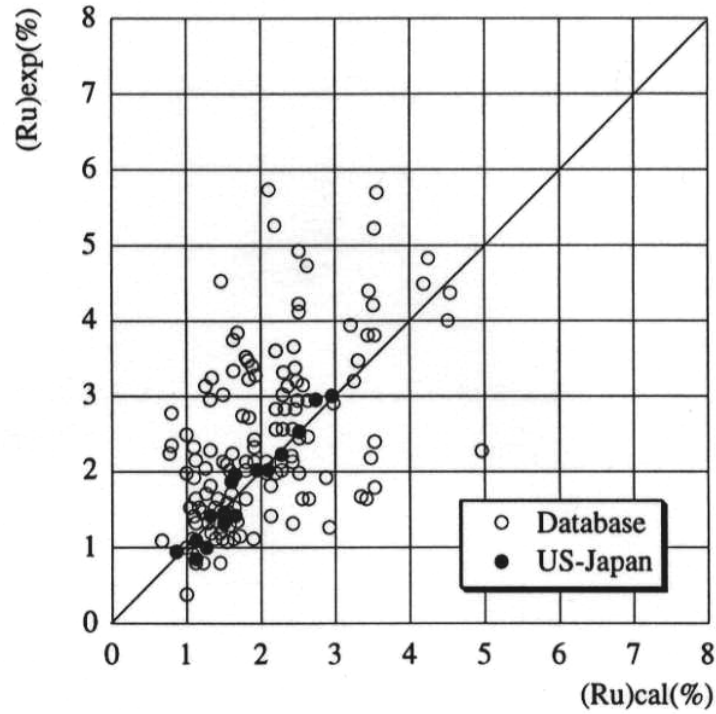
Figure 6.17 Comparison Between Predicted Limit Rotation and Experimental One (Square Columns)
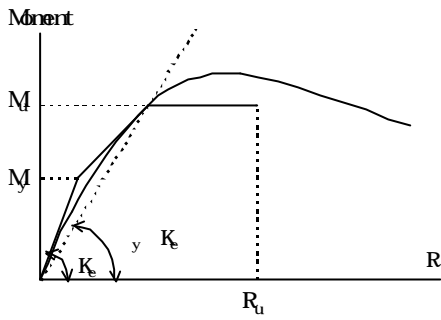
Figure 6.18 Tri-linear Skeleton Model
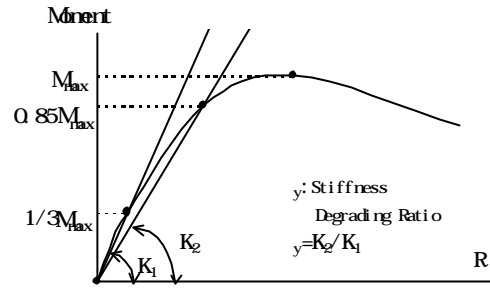
Figure 6.19 Definition of Experimental ay
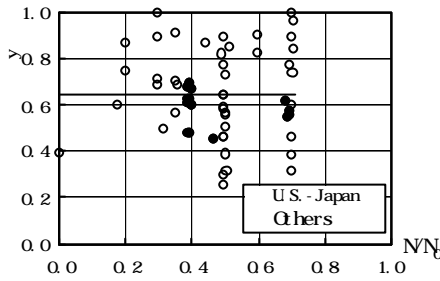
Figure 6.20 Effect of N/No on ay
(Circular CFT)

Figure 6.21 Effect of N/No on ay
(Square CFT)

(a) Circular CFT
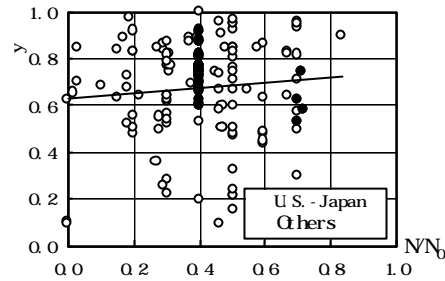
(b) Square CFT
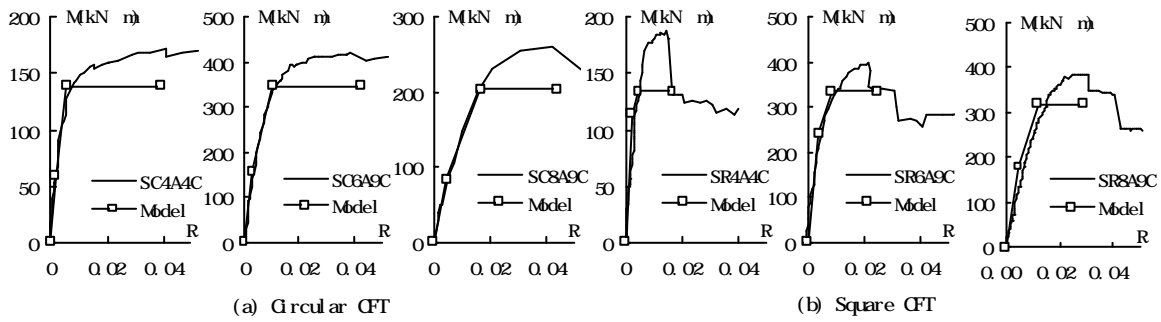
Figure 6.22 Comparisons Between Tri-linear Skeleton Model and Experimental Results

(a) Circular CFT

(b) Square CFT
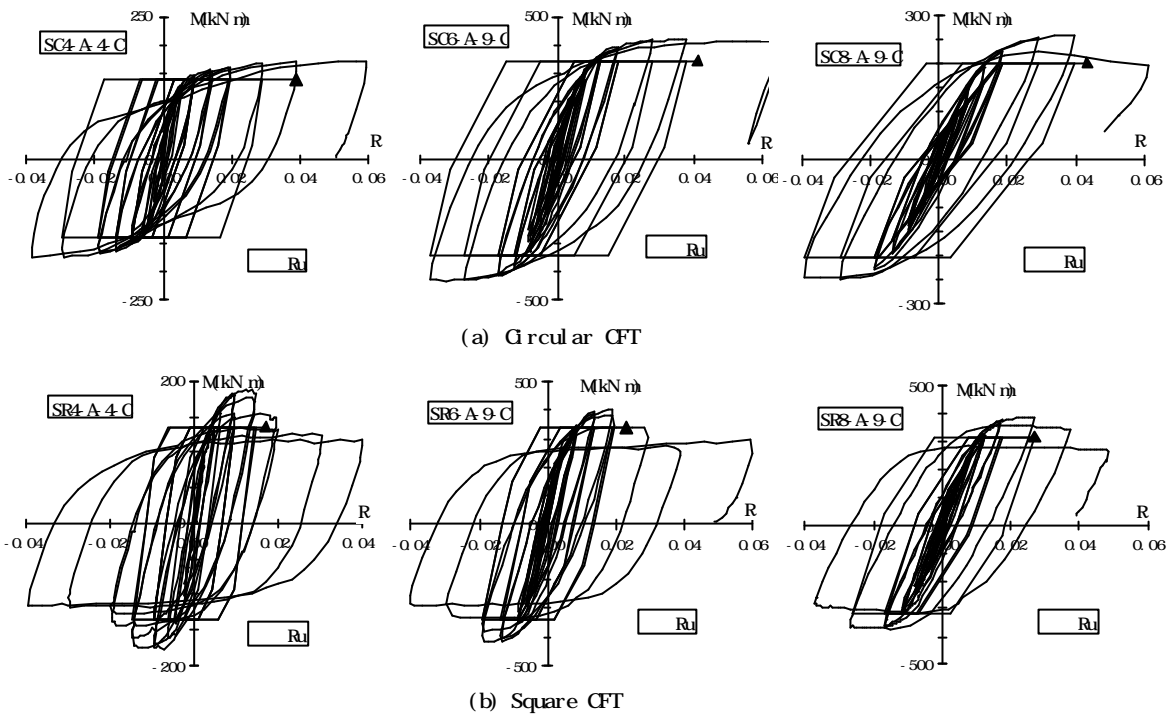
Figure 6.23 Comparisons Between Normal Tri-linear Hysteretic Model and Experimental Results
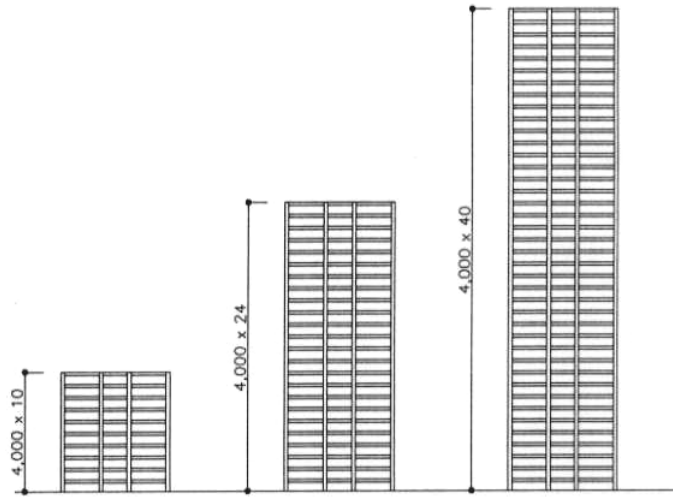
Figure 7.1 Elevations of Theme Structures
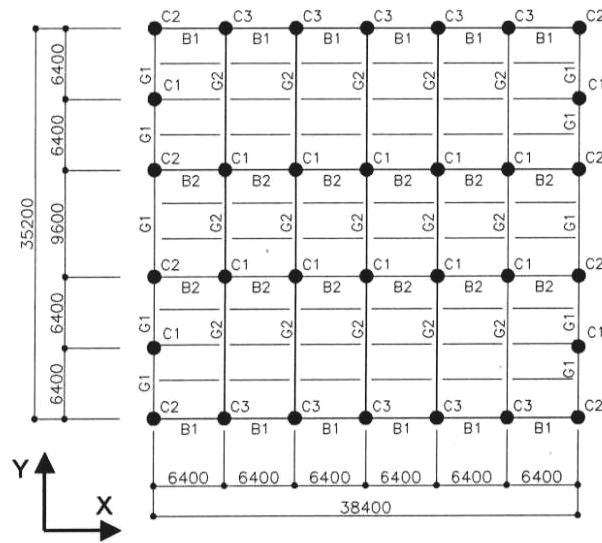
Figure 7.2 Floor Plan of Theme Structures
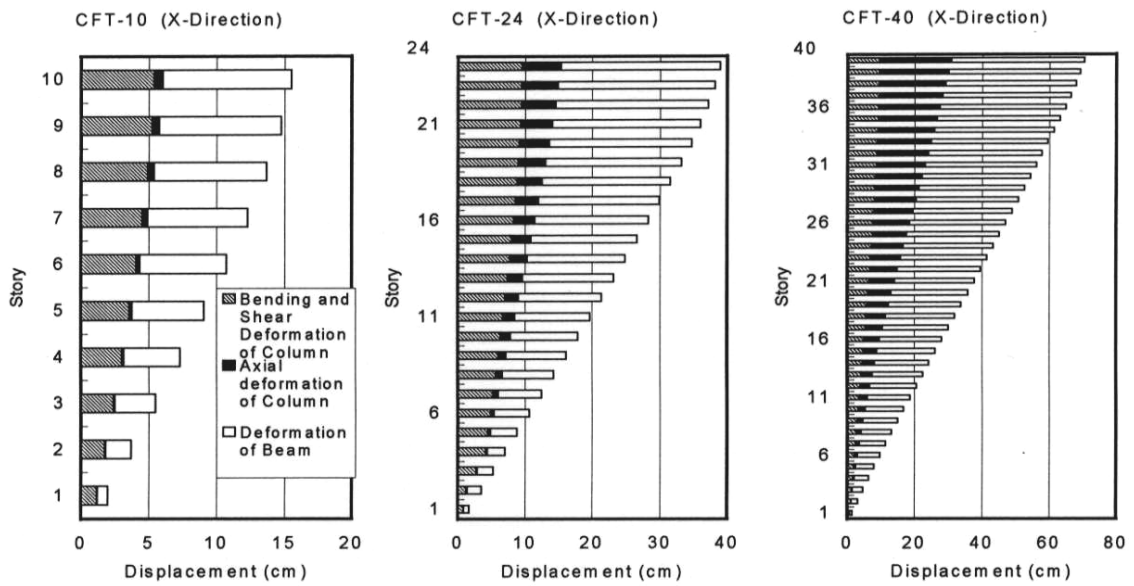
Figure 7.3 Story Displacements Caused by Beam and Column Deformations
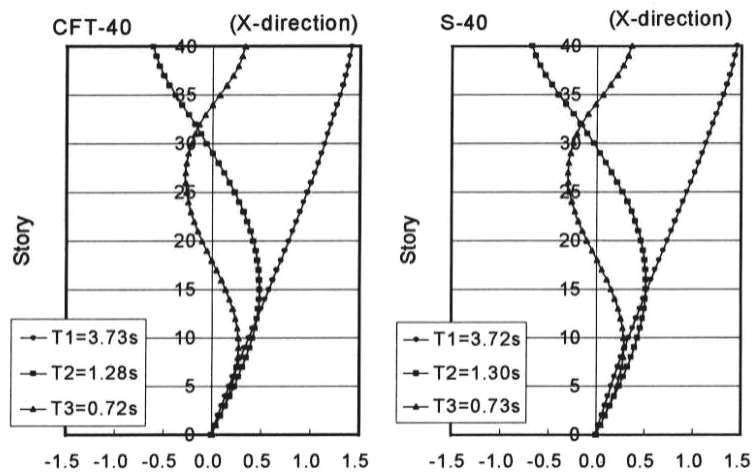
Figure 7.4 Vibrational Mode Shapes
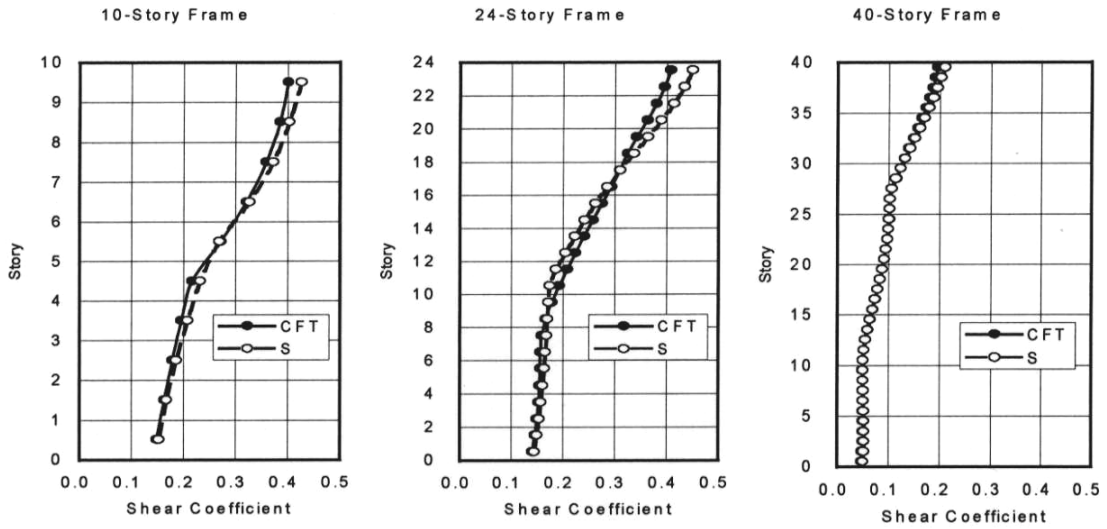
Figure 7.5 Maximum Responses of Shear Coefficients

(El Centro NS : 25cm/sec)
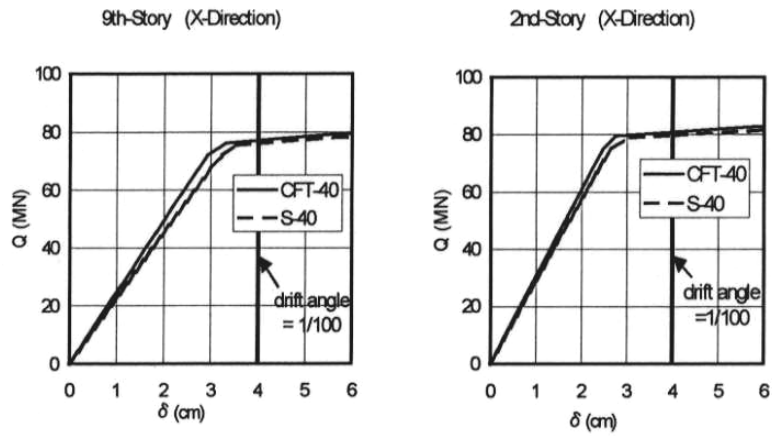
Figure 7.6 Q - d **Relations of 40-Story Frames**

(a) Shear Coefficient   (b) Overturning Moment   (c) Story Drift
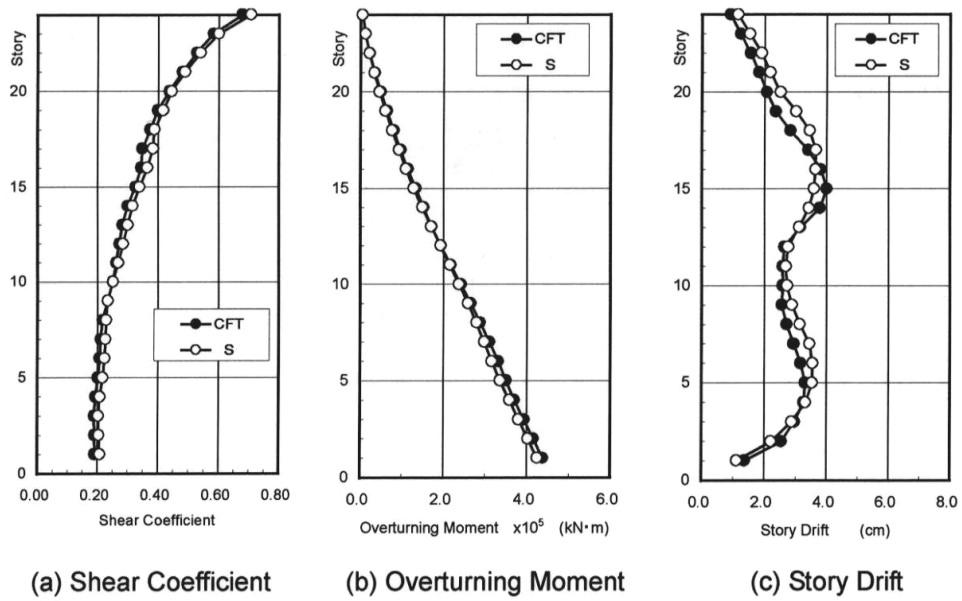
Figure 7.7 Maximum Responses of Shear Coefficients, Overturning Moments and Story Drifts
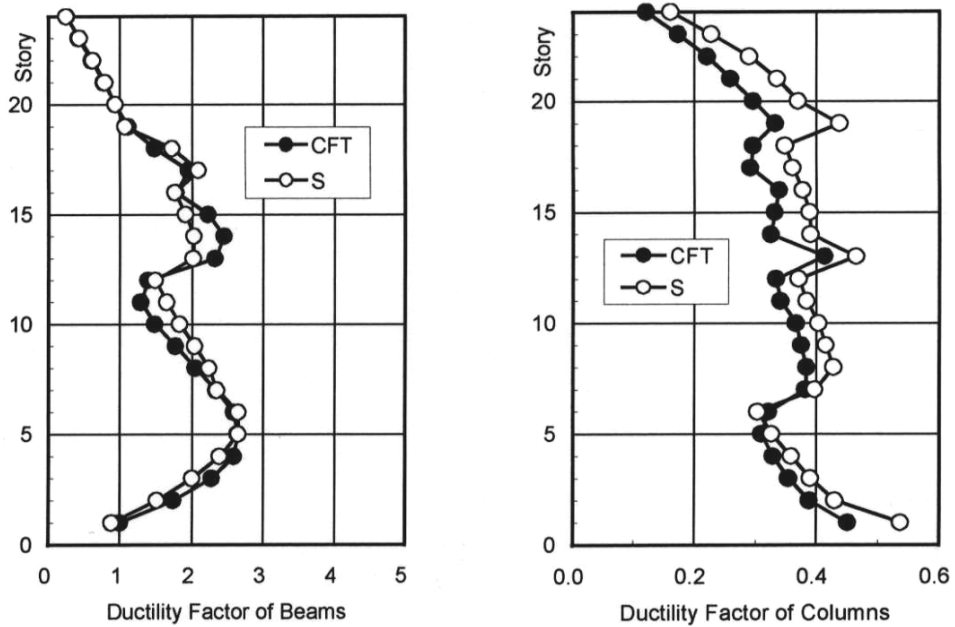
Figure 7.8 Maximum Responses of Ductility Factors of Beams and Columns

(HACHINOHE : 50cm/sec)
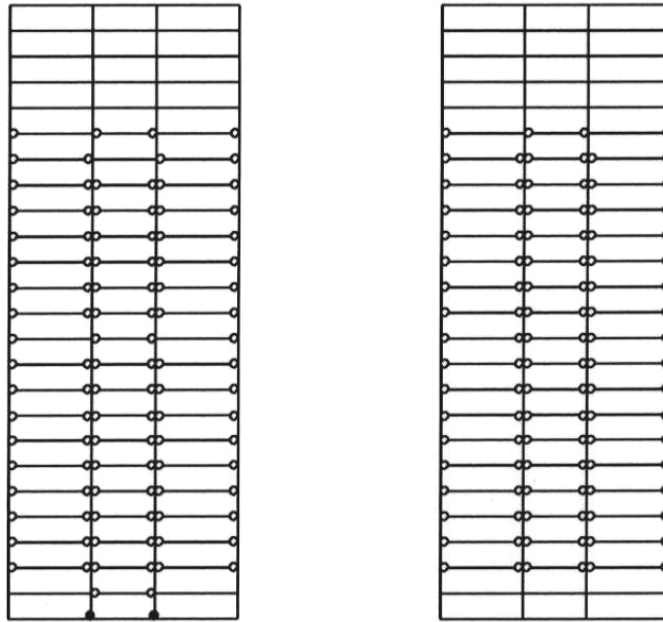
○ : plastic hinge   ● : yielding

              CFT system   Steel system

Figure 7.9 Formation of Plastic Hinges in Beams and Columns
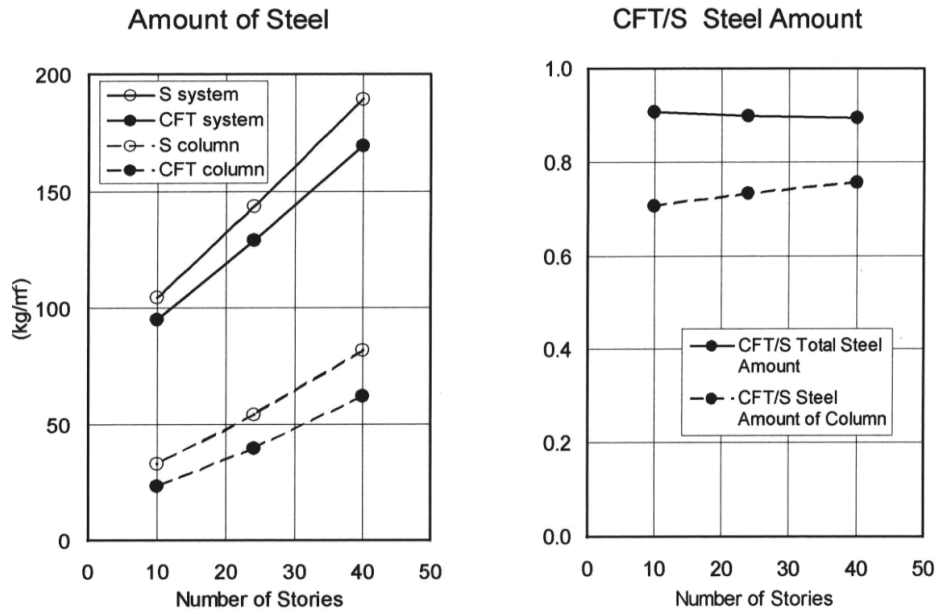
Figure 7.10 Comparison of Steel Amount Between CFT and Steel Frames

APPENDIX

The list of the technical papers written in English is shown below, which includes the papers on concrete-filled structural steel tube column system together with those on new materials, elements and systems, reinforced concrete column and structural steel beam systems, and reinforced concrete and steel reinforced concrete wall systems .

***** *Fiscal Year of 1993* *****

[1]-1993

Hiroyuki Yamanouchi, Stephen A. Mahin, Subhash C. Goel and Isao Nishiyama

U.S.-Japan Cooperative Earthquake Research Program on Composite and Hybrid Structures

Proceedings of the 25th Joint Meeting of U.S.-Japan Panel on Wind and Seismic Effects, UJNR, Gaithersburg, USA, pp.585-591, May 17-20, 1993

***** *Fiscal Year of 1995* *****

[1]-1995

Isao Nishiyama and Hiroyuki Yamanouchi

U.S.-Japan Cooperative Earthquake Engineering Research Program on Composite and Hybrid Structures - Research Plan and its Progress -

Proceedings of the 27th Joint Meeting of U.S.-Japan Panel on Wind and Seismic Effects, UJNR, Tsukuba, Japan, pp.333-343, May 16-19, 1995

[2]-1995

Kabeyasawa, T. , Ohkubo, T. and Nakamura, Y.

Tests and Analyses of Reinforced Concrete Shear Walls in Hybrid Structures

Pacific Conference on Earthquake Engineering, Australia, Vol.2, pp.145-154, November 20-22, 1995

***** *Fiscal Year of 1996* *****

[1]-1996

Shosuke Morino, Kenji Sakino, Akiyoshi Mukai and Kenzo Yoshioka

U.S.-Japan Cooperative Earthquake Research Program on CFT Column Systems

Proceedings of 5th International Colloquium on Stability of Metal Structures, SSRC, April 1996

[2]-1996

Subhash C. Goel and Isao Nishiyama

U.S.-Japan Cooperative Earthquake Engineering Research Program on Composite and Hybrid Structures - Research Progress and Current Status -

Proceedings of the 28th Joint Meeting of U.S.-Japan Panel on Wind and Seismic Effects, UJNR, Gaithersburg, USA, pp.319-325, May 14-17, 1996

[3]-1996

Chen Lian, Sanada Y. and Kabeyasawa T.

3-Dimensional Analysis of Hybrid Wall System - Static and Earthquake Response Analysis

Transactions of the Japan Concrete Institute, Vol. 18, pp. 213-220, 1996

[4]-1996

Hiroshi Kuramoto

Seismic Resistance of Through Column Type Connections for Composite RCS Systems

11th World Conference on Earthquake Engineering (11WCEE), Acapulco, Mexico, June 23-28, 1996

[5]-1996

Makoto Kato, Ken-ichi Sugaya and Norikazu Nagatsuka

Optimum Moment Distribution between Shear Walls and Boundary Beams of Coupled Shear Wall with Flange Walls

11th World Conference on Earthquake Engineering (11WCEE), Acapulco, Mexico, June 23-28, 1996

[6]-1996

T. Kabeyasawa, T. Ohkubo and Y. Nakamura

Tests and Analyses of Hybrid Wall Systems

11th World Conference on Earthquake Engineering (11WCEE), Acapulco, Mexico, June 23-28, 1996

[7]-1996

S. Morino

U.S.-Japan Cooperative Earthquake Research Program on Composite and Hybrid Structures

The 2nd International Symposium on Civil Infrastructure Systems, Hong Kong/China, December 9-12, 1996

***** Fiscal Year of 1997 *****

[1]-1997

H. Kuramoto and H. Noguchi

An Overview of Japanese Research on RCS Systems

ASCE Structures Congress XV, Portland, Oregon, pp.716-720, April 13-16, 1997

[2]-1997

H. Noguchi and K. Kim

Analysis of Beam-Column Joints in Hybrid Structures

ASCE Structures Congress XV, Portland, Oregon, pp.726-730, April 13-16, 1997

[3]-1997

M. Teshigawara

An Overview of Japanese Research on Hybrid Wall Systems

ASCE Structures Congress XV, Portland, Oregon, pp.1096-1100, April 13-16, 1997

[4]-1997

S. Morino, K. Sakino, A. Mukai and K. Yoshioka

Experimental Studies on CFT Column Systems - U.S.-Japan Cooperative Earthquake Research Program

ASCE Structures Congress XV, Portland, Oregon, pp.1106-1110, April 13-16, 1997

[5]-1997

Isao Nishiyama and Hiroyuki Yamanouchi

U.S.-Japan Cooperative Earthquake Engineering Research Program on Composite and Hybrid Structures - Japan Side Progress -

Proceedings of the 29th Joint Meeting of U.S.-Japan Panel on Wind and Seismic Effects, UJNR, Tsukuba, Japan, pp.473-478, May 13-16, 1997

[6]-1997

Nobuhiro Araki, Yasuhiro Matsuzaki, Katsuhiko Nakano, Takahiro Kataoka and Hiroshi Fukuyama

Shear Capacity of Retrofitted RC Members with Continuous Fiber Sheets

Proceedings of the Third International Symposium on Non-Metallic (FRP) Reinforcement for Concrete Structures (FRPRCS-3), Sapporo, Japan, Vol.1, pp515-522, 1997-10

[7]-1997

Takahiro Kataoka, Nobuhiro Araki, Katsuhiko Nakano, Yasuhiro Matsuzaki and Hiroshi Fukuyama

Ductility of Retrofitted RC Columns with Continuous Fiber Sheets

Proceedings of the Third International Symposium on Non-Metallic (FRP) Reinforcement for Concrete Structures (FRPRCS-3), Sapporo, Japan, Vol.1, pp547　554, 1997-10

***** *Fiscal Year of 1998* *****

[1]-1998

Isao Nishiyama, Hiroyuki Yamanouchi and Hisahiro Hiraishi

U.S.-Japan Cooperative Earthquake Engineering Research Program on Composite and Hybrid Structures - Current Status of Japan Side Research -

Proceedings of the 30th Joint Meeting of U.S.-Japan Panel on Wind and Seismic Effects, UJNR, Gaithersburg, USA, pp.443-451, May 12-15, 1998 (Wind and Seismic Effects, NIST SP 931, Issued August 1998)

[2]-1998

S. Morino

An Overview of U.S.-Japan Cooperative Earthquake Research Program on CFT Column Systems

Structural Engineers World Congress, Paper Reference T169-1, San Francisco, USA July 19-23, 1998 (Structural Engineering World Wide 1998)

[3]-1998

K. Sakino, T. Ninakawa, H. Nakahara and S. Morino

Experimental Studies and Design Recommendations on Concrete Filled Steel Tubular Columns -US-Japan Cooperative Earthquake Research Program-

Structural Engineers World Congress, Paper Reference T169-3, San Francisco, USA July 19-23, 1998 (Structural Engineering World Wide 1998)

[4]-1998

I. Nishiyama, H. Itadani and K. Sugihiro

Bi-directional Seismic Response of Reinforced Concrete Column and Structural Steel Beam Subassemblages

Structural Engineers World Congress, Paper Reference T177-2, San Francisco, USA July 19-23, 1998 (Structural Engineering World Wide 1998)

[5]-1998

H. Noguchi and K. Kim

Shear Strength of Beam-to-column Connections in RCS System

Structural Engineers World Congress, Paper Reference T177-3, San Francisco, USA July 19-23, 1998 (Structural Engineering World Wide 1998)

[6]-1998

V. C. Li, H. Fukuyama and A. Mikame

Development of Ductile Engineered Cementitious Composite Elements for Seismic Structural Applications

Structural Engineers World Congress, Paper Reference T177-5, San Francisco, USA July 19-23, 1998 (Structural Engineering World Wide 1998)

[7]-1998

T. Kabeyasawa and Y. Nakamura

Displacement-based Design of Hybrid Core Wall System

Structural Engineers World Congress, Paper Reference T186-1, San Francisco, USA July 19-23, 1998 (Structural Engineering World Wide 1998)

[8]-1998

M. Teshigawara, K. Sugaya, M. Kato and Y. Matsushima

Seismic Test on 12-story Coupled Shear Wall with Flange Walls

Structural Engineers World Congress, Paper Reference T186-4, San Francisco, USA July 19-23, 1998 (Structural Engineering World Wide 1998)

[9]-1998

M. Teshigawara, K. Sugaya, M. Kato and Y. Matsushima

Energy Absorption Mechanism and the Fluctuation of Shear Force in the Coupled Shear Walls

Structural Engineers World Congress, Paper Reference T186-5, San Francisco, USA July 19-23, 1998 (Structural Engineering World Wide 1998)

[10]-1998

K. Sakino, E. Inai and H. Nakahara

Tests and Analysis on Elasto-Plastic Behavior of CFT Beam-Columns - U.S.-Japan Cooperative earthquake Research Program -

Proceedings of Fifth Pacific Structural Steel Conference, Edited by Dong-Il Chang, Hyo-Nam Cho, Chung-Bang Yun and Sang-Dae Kim, Seoul, Korea, Vol. 2, pp. 901-906, October 13-16, 1998

[11]-1998

R. Kanno and G. G. Deierlein

Bearing Strength of Joints between Steel Beams and Reinforced Concrete Columns

Proceedings of Fifth Pacific Structural Steel Conference, Edited by Dong-Il Chang, Hyo-Nam Cho, Chung-Bang

Yun and Sang-Dae Kim, Seoul, Korea, Vo l. 2, pp. 919-924, October 13-16, 1998

[12]-1998

Isao Nishiyama

An Overview of U.S.-Japan Cooperative Earthquake Research Program on Composite and Hybrid Structures

Proceedings of Fifth Pacific Structural Steel Conference, Edited by Dong-Il Chang, Hyo-Nam Cho, Chung-Bang Yun and Sang-Dae Kim, Seoul, Korea, Vol. 2, pp. 925-930, October 13-16, 1998

[13]-1998

H. Nakahara and K. Sakino

Axial Compressive and Uniform Bending Tests of High Strength Concrete Filled Square Steel Tubular Columns

Proceedings of Fifth Pacific Structural Steel Conference, Edited by Dong-Il Chang, Hyo-Nam Cho, Chung-Bang Yun and Sang-Dae Kim, Seoul, Korea, Vol. 2, pp. 943-948, October 13-16, 1998

[14]-1998

J. Kawaguchi, S. Morino, J. Shirai and E. Tatsuta

Database and Structural Characteristics of CFT Beam-Columns

Proceedings of Fifth Pacific Structural Steel Conference, Edited by Dong-Il Chang, Hyo-Nam Cho, Chung-Bang Yun and Sang-Dae Kim, Seoul, Korea, Vol. 2, pp. 955-960, October 13-16, 1998

[15]-1998

Hiroshi Kuramoto and Isao Nishiyama

Equivalent Damping Factor of Composite RCS Frames

1998 ACI Fall Convention, Westin Century Plaza, Los Angeles, USA, October 25-30, 1998

[16]-1998

Hiroyuki Yamanouchi, Isao Nishiyama and Jun Kobayashi

Development and Usage of Composite and Hybrid Structures (CHS) Based on Performance

ACI SP-174 - Hybrid and Composite Structures, 1998

***** *Fiscal Year of 1999* *****

[1]-1999

Isao Nishiyama, Hiroyuki Yamanouchi and Hisahiro Hiraishi

U.S.-Japan Cooperative Earthquake Engineering Research Program on Composite and Hybrid Structures - Japanese Side Research Accomplishments-

Proceedings of the 31th Joint Meeting of U.S.-Japan Panel on Wind and Seismic Effects, UJNR, Tsukuba, Japan, pp.422-430, May 11-14, 1999

[2]-1999

H. Fukuyama, Y. Matsuzaki, K. Nakano and Y. Sato

Structural Performance of Beam Elements with PVA -ECC

Proceedings of the Third International RILEM Workshop on High Performance Fiber Reinforced Cement Composites (HPFRCCS-3), Mainz, Germany, Edited by H. W. Reinhardt and A. E. Naaman, RILEM Proceedings PRO6, RILEM Publications S.A.R.L., pp.531-541, 1999-5

[3]-1999

Hiroshi Fukuyama, Yukihiro Sato, Victor C. Li, Yasuhiro Matsuzaki and Hirozo Mihashi

Ductile Engineered Cementitious Composite Elements for Seismic Structural Application

12th World Conference on Earthquake Engineering (12WCEE), Auckland, New Zealand, January 30 - February 4, 2000

[4]-1999

Yasuhiro Matsuzaki, Shigeru Fujii, Hiroshi Fukuyama and Katsuhiko Nakano

Seismic Retrofit using Continuous Fiber Sheets

12th World Conference on Earthquake Engineering (12WCEE), Auckland, New Zealand, January 30 - February 4, 2000

[5]-1999

Nozomu Baba and Yasushi Nishimura

Seismic Behavior of RC Column - S beam Moment Frames

12th World Conference on Earthquake Engineering (12WCEE), Auckland, New Zealand, January 30 - February 4, 2000

[6]-1999

Subhash C. Goel, Atsuo Tanaka, Hiroyuki Yamanouchi and Hiroshi Fukuyama

Experimental Study on the Performance of the RC Research on New Materials, Elements and Systems

12th World Conference on Earthquake Engineering (12WCEE), Auckland, New Zealand, January 30 - February 4, 2000

[7]-1999

Charles W. Roeder and Shosuke Morino

Research on CFT Column Systems

12th World Conference on Earthquake Engineering (12WCEE), Auckland, New Zealand, January 30 - February 4, 2000

[8]-1999

John W. Wallace and Akira Wada

Hybrid Wall Systems: US-Japan Research

12th World Conference on Earthquake Engineering (12WCEE), Auckland, New Zealand, January 30 - February 4, 2000

[9]-1999

Gregory G. Deierlein and Noguchi Hiroshi

Research on RC/SRC Column Systems

12th World Conference on Earthquake Engineering (12WCEE), Auckland, New Zealand, January 30 - February 4, 2000

[10]-1999

Yoshiyuki Matsushima, Masaomi Teshigawara, Ken-ichi Sugaya and Makoto Kato

Seismic Performance Evaluation Method for a Building with Centre Core Reinforced Concrete Walls and

Exterior Steel Frame

12th World Conference on Earthquake Engineering (12WCEE), Auckland, New Zealand, January 30 - February 4, 2000

[11]-1999

Isao Nishiyama, Hidehiko Itadani, Kunio Sugihiro and Hiroshi Kuramoto

Bi-Directional Behavior of Interior-, Exterior-, and Corner-Joints of RCS System

12th World Conference on Earthquake Engineering (12WCEE), Auckland, New Zealand, January 30 - February 4, 2000

[12]-1999

Shao-Hua Chen and Toshimi Kabeyasawa

Modelling of Reinforced Concrete Shear Wall for Nonlinear Analysis

12th World Conference on Earthquake Engineering (12WCEE), Auckland, New Zealand, January 30 - February 4, 2000

[13]-1999

Hiroyuki Nakahara and Kenji Sakino

Flexural Behavior of Concrete Filled Square Steel Tubular Beam-Columns

12th World Conference on Earthquake Engineering (12WCEE), Auckland, New Zealand, January 30 - February 4, 2000

[14]-1999

Hiroyoshi Tokinoya, Akiyoshi Mukai, Kenzo Yoshioka, Toshiyuki Fukumoto, Takashi Noguchi, Yoshiyuki Murata and Yoshinari Tanaka

Earthquake Resistance Behavior of CFT Columns

12th World Conference on Earthquake Engineering (12WCEE), Auckland, New Zealand, January 30 - February 4, 2000

[15]-1999

Ken-ichi Sugaya, Makoto Kato, Yoshiyuki Matsushima and Masaomi Teshigawara

Experimental Study on Carrying Shear Force Ratio of 12-Story Coupled Shear Walls

12th World Conference on Earthquake Engineering (12WCEE), Auckland, New Zealand, January 30 - February 4, 2000

[16]-1999

Toshiaki Fujimoto, Eiichi Inai, Makoto Kai, Koji Mori, Osamu Mori and Isao Nishiyama

Behavior of Beam-To-Column Connection of CFT Column System

12th World Conference on Earthquake Engineering (12WCEE), Auckland, New Zealand, January 30 - February 4, 2000

[17]-1999

Makoto Kato, Yoshiyuki Matsushima, Ken-ichi Sugaya and Masaomi Teshigawara

Seismic Energy Dissipation System of 12-Story Coupled Shear Walls

12th World Conference on Earthquake Engineering (12WCEE), Auckland, New Zealand, January 30 - February

4, 2000

[18]-1999

Subhash C. Goel, Hiroyuki Yamanouchi and Isao Nishiyama

U.S.-Japan Cooperative Earthquake Research Program on Composite and Hybrid Structures: An Overview

Proceedings of the Sixth ASCCS International Conference on Steel-Concrete Composite Structures, Edited by Y. Xiao and S. A. Mahin, Los Angeles, California, USA, Vol. 1, pp. 23-34, March 22-24, 2000

[19]-1999

Mizuaki Uchikoshi, Yukio Hayashi and Shosuke Morino

Merits of CFT Column System - Results of Trial Design of Theme Structures

Proceedings of the Sixth ASCCS International Conference on Steel-Concrete Composite Structures, Edited by Y. Xiao and S. A. Mahin, Los Angeles, California, USA, Vol. 1, pp. 135-142, March 22-24, 2000

[20]-1999

Hiroyuki Nakahara and Kenji Sakino

Practical Analysis for High-Strength CFT Columns Under Eccentric Compression

Proceedings of the Sixth ASCCS International Conference on Steel-Concrete Composite Structures, Edited by Y. Xiao and S. A. Mahin, Los Angeles, California, USA, Vol. 1, pp. 441-448, March 22-24, 2000

[21]-1999

Kenji Sakino and Hiroyuki Nakahara

Flexural Capacities of Concrete Filled Square Steel Tubular Beam-Columns with High Strength Concrete

Proceedings of the Sixth ASCCS International Conference on Steel-Concrete Composite Structures, Edited by Y. Xiao and S. A. Mahin, Los Angeles, California, USA, Vol. 1, pp. 473-480, March 22-24, 2000

[22]-1999

Shosuke Morino

Recent Development on CFT Column Systems - US-Japan Cooperative Earthquake Research Program

Proceedings of the Sixth ASCCS International Conference on Steel-Concrete Composite Structures, Edited by Y. Xiao and S. A. Mahin, Los Angeles, California, USA, Vol. 1, pp. 531-538, March 22-24, 2000

[23]-1999

Toshiaki Fujimoto, Eiichi Inai, Hiroyoshi Tokinoya, Makoto Kai, Koji Mori, Osamu Mori and Isao Nishiyama

Behavior of Beam-to-Column Connection of CFT Column System under Seismic Force

Proceedings of the Sixth ASCCS International Conference on Steel-Concrete Composite Structures, Edited by Y. Xiao and S. A. Mahin, Los Angeles, California, USA, Vol. 1, pp. 557-564, March 22-24, 2000

[24]-1999

Toshiyuki Fukumoto and Koji Morita

Elasto-Plastic Behavior of Steel Beam to Square Concrete Filled Steel Tube (CFT) Column Connections

Proceedings of the Sixth ASCCS International Conference on Steel-Concrete Composite Structures, Edited by Y. Xiao and S. A. Mahin, Los Angeles, California, USA, Vol. 1, pp. 565-572, March 22-24, 2000

[25]-1999

Eiichi Inai, Takashi Noguchi, Osamu Mori and Toshiaki Fujimoto

Deformation Capacity and Hysteresis Model of Concrete Filled Steel Tubular Beam-Columns

Proceedings of the Sixth ASCCS International Conference on Steel-Concrete Composite Structures, Edited by Y. Xiao and S. A. Mahin, Los Angeles, California, USA, Vol. 1, pp. 605-612, March 22-24, 2000

[26]-1999

Nozomu Baba and Yasushi Nishimura

Stress Transfer on Through Beam Type Steel Beam - Reinforced Concrete Column Joints

Proceedings of the Sixth ASCCS International Conference on Steel-Concrete Composite Structures, Edited by Y. Xiao and S. A. Mahin, Los Angeles, California, USA, Vol. 2, pp. 753-760, March 22-24, 2000

[27]-1999

Subhash Goel, Atsuo Tanaka, Hiroyuki Yamanouchi and Hiroshi Fukuyama

Research on New Materials, Elements and Systems: An Overview

Proceedings of the Sixth ASCCS International Conference on Steel-Concrete Composite Structures, Edited by Y. Xiao and S. A. Mahin, Los Angeles, California, USA, Vol. 2, pp. 961-968, March 22-24, 2000

[28]-1999

H. Fukuyama, Y. Matsuzaki, Y. Sato and H. Suwada

Structural Performance of Engineered Cementitious Composite Elements

Proceedings of the Sixth ASCCS International Conference on Steel-Concrete Composite Structures, Edited by Y. Xiao and S. A. Mahin, Los Angeles, California, USA, Vol. 2, pp. 969-976, March 22-24, 2000

[29]-1999

K. Kobayashi, Y. Matsuzaki, H. Fukuyama, S. Hakuto, T. Toritani and H. Kumagai

Performance Evaluation of RC Elements with Ultra Light Weight Concrete

Proceedings of the Sixth ASCCS International Conference on Steel-Concrete Composite Structures, Edited by Y. Xiao and S. A. Mahin, Los Angeles, California, USA, Vol. 2, pp. 977-984, March 22-24, 2000

[30]-1999

Hiroshi Noguchi and Kazuhiro Uchida

FEM Analysis of Hybrid Structural Frames with R/C Columns and Steel Beams

Proceedings of the Sixth ASCCS International Conference on Steel-Concrete Composite Structures, Edited by Y. Xiao and S. A. Mahin, Los Angeles, California, USA, Vol. 2, pp. 1099-1106, March 22-24, 2000

[31]-1999

Kenji Yonezawa and Kenzo Yoshioka

Three Dimensional Finite Element Analysis on CFT Column - Steel Beam Joints

Proceedings of the Sixth ASCCS International Conference on Steel-Concrete Composite Structures, Edited by Y. Xiao and S. A. Mahin, Los Angeles, California, USA, Vol. 2, pp. 1123-1130, March 22-24, 2000

[32]-1999

Hiroshi Kuramoto, Isao Nishiyama and Hiroshi Noguchi

Outline of Japanese Design Guidelines for Composite RCS Buildings

Proceedings of the Sixth ASCCS International Conference on Steel-Concrete Composite Structures, Edited by Y. Xiao and S. A. Mahin, Los Angeles, California, USA, Vol. 2, pp. 1183-1190, March 22-24, 2000